

Analysis of the Pharmacokinetics and Metabolism of Skepinone-L in different Animal Species and Humans by LC-MS/MS

Dissertation

der Mathematisch-Naturwissenschaftlichen Fakultät
der Eberhard Karls Universität Tübingen
zur Erlangung des Grades eines
Doktors der Naturwissenschaften
(Dr. rer. nat.)

vorgelegt von
Eva Döring
aus Dresden

Tübingen
2024

Gedruckt mit Genehmigung der Mathematisch-Naturwissenschaftlichen Fakultät der Eberhard Karls Universität Tübingen.

Tag der mündlichen Qualifikation:	31.10.2024
Dekan:	Prof. Dr. Thilo Stehle
1. Berichterstatter:	Prof. Dr. Stefan Laufer
2. Berichterstatter:	Prof. Dr. Michael Lämmerhofer

Statement

The present work was performed from 01.03.2014 to 31.12.2018 under the supervision of Prof. Dr. Stefan Laufer at the Department of Pharmaceutical and Medicinal Chemistry, Institute of Pharmaceutical Sciences, Eberhard Karls University of Tübingen, Germany.

Acknowledgement

Without the support of all my friends, direct and indirect colleagues, the successful completion of this thesis would not have been possible.

In particular, I would like to express my gratitude to:

... **Prof. Dr. Stefan Laufer**, for the preparation of the initial review of this thesis, for entrusting me with this interesting topic, for the provision of resources and equipment, for the excellent supervision during the doctorate and for your endless patience and constant encouragement following the practical phase.

... **Prof. Dr. Michael Lämmerhofer**, for the preparation of the secondary review and for the opportunity to participate in the ASAC summer school.

... **Dr. Wolfgang Albrecht**, for the mediation of this work as well as the constant advice, support and scientific discourse.

... **Dr. Thomas Mürdter** and **Prof. Dr. Matthias Schwab** for the elaborate synthesis of the Skepinone-L glucuronides.

... **Dr. Michael Burnett**, **Dr. Ramona Rudalska** and **Dr. Daniel Dauch** for the realisation of the *in vivo* experiments in mice.

... the 8th-semester team, **Dr. Silke Bauer**, **Dr. Ida D'Orazio**, **Jakub Kubiak**, **Gernot-Sebastian Businger** and **Dr. Juliander Reiner** for their great help with subject-specific questions, correction marathons and for almost all the time ensuring a good mood.

... **Katharina Bauer**, for always having an open door, giving the right advice and an 'Ohren-lang-ziehen' at the right time. Of course, the numerous delicious cakes and great conversations have not been forgotten.

... **Gerd Helms**, for the endless support with any computer-, university-, coffee machine- and everyday-problem as well as broadening my musical horizon.

... **Daniela Müller**, for your priceless help in the form of candy, teasing and good, loud music in the lab, which helped me to defy the bumpy start.

... **Dr. Raimund Nieß**, for the tireless support and assistance in the daily lab business and for always having an open ear. Even during unplanned adventures such as the 'master key' and the 'Suche nach Passierschein A 38', you were a reliable partner in crime.

... **Dr. Adrian Sievers-Engler** and **Mike Kaupert** for their support and instruction in the 'blue boxes' as well as the daily check 'haschs hie gmacht ?!' and the general loosening up of everyday life with conversations that nobody else understood either in terms of content or language.

... **Mark Kudolo**, for the great support in the lab, the reliable continuation of my tasks and the mental encouragement when Murphy was very active again, unforgotten here the 'aquarium'. I would also like to thank you for taking the time to proofread this work in addition to your numerous tasks.

... **Dr. Ida D'Orazio**, for the lift from Stuttgart to the university, the unforgettable 'Ida-moments', the numerous past and future perfect dinner events and for the great friendship that has developed from the hustle and bustle.

... **Dr. Michael Juchum**, for the exhilarating lectures in the coffee room, as well as the calm and open-minded help with any synthesis questions. I thank you and your wife, **Dr. Christina Juchum**, for taking time out of your busy schedules to proofread this work intensively and constructively. I would also like to thank you for your sincere friendship, which connects our families in a unique way.

... **Dr. Dirk Flötgen**, for the synthesis of the Sorafenib metabolites, the amusing commentary on my weeks of work with the separating funnel as well as for the tireless, constructive and detailed proofreading. I would also like to thank you for your friendship and the associated lunches in the coffee room plus all past and future activities with our families.

... to the remaining current and former members of the Laufer Working Group, for the pleasant working atmosphere, as well as all Wahlpflichtfach-, Bachelor's and Master's students who have contributed to this work and the unforgettable time in this research group.

... to my family, especially **Karin Döring** and **Gudrun Schöne**, for being my safe harbour during this exciting, thrilling and sometimes nerve-wracking journey. Your unconditional belief in me and your support wherever possible have always given me the strength to carry on.

... to my husband **Stefan Michael Sättele**, for your constant support, love, understanding, sacrifice and always the right encouragement at the right moment, sometimes as a word or as a glass of wine. I thank you that no matter how bumpy the road was, you were and are always by my side.

... and last but not least, I want to thank a special person, for the endless encouragement, the dedicated commitment and also the one or other strong but important push in the right direction.

Dedicated to Lorange und Alastair

'Remember to look up at the stars
and not down at your feet. (..) Be curious.
And however difficult life may seem,
there is always something you can do and succeed at.'

– Stephen William Hawking

Table of Contents

Abstract	V
Zusammenfassung der Dissertation	VI
Abbreviations	VII
List of Tables	X
List of Figures	XIII
1. Introduction	1
1.1. Pharmaceutical Research and Development	1
1.2. Principles of Pharmacokinetics	2
1.2.1. Pharmacokinetic Model Conceptions	3
1.2.2. Major Pharmacokinetic Parameters	5
1.2.3. Absorption	6
1.2.4. Distribution	7
1.2.5. Metabolism	7
1.2.6. Excretion	10
1.3. Enzyme Kinetics	11
1.4. Drug Interactions	12
1.4.1. Enzyme Inhibition	12
1.4.2. Allosteric Regulation	13
1.4.3. Drug-Drug Interactions	13
1.5. Instrumental Analytic	14
1.5.1. Electrospray Ionisation Mass Spectrometry	14
1.5.2. Quadrupole Mass Analyser	15
1.6. Hepatocellular Carcinoma	16
1.7. Protein Kinase Inhibitors	17
1.7.1. Sorafenib	18
1.7.2. Skepinone-L	20
1.8. Combinatorial Treatment with Skepinone-L and Sorafenib	21
2. Aim of the Work	23
3. Results and Discussion	25
3.1. Development of the Analytical Method	25
3.1.1. Description of the Developed Method	26
3.2. Validation of the Analytical Method	30

3.2.1. Selectivity of the Analytical Method	30
3.2.2. Sensitivity of the Analytical Method	34
3.2.3. Linearity of Skepinone-L and Sorafenib Determination	35
3.2.4. Accuracy and Precision of the Analytical Method.....	36
3.2.5. Reproducibility and Carry-Over	38
3.2.6. Stability of Skepinone-L and Sorafenib in Plasma.....	40
3.2.7. Analytical Quality Assurance	43
3.3. Pharmacokinetic Studies of Skepinone-L <i>in vivo</i>	44
3.3.1. Preliminary Pharmacokinetic Study of Skepinone-L in Mice	45
3.3.2. Bioavailability Study of Skepinone-L in Dogs	51
3.3.3. Pharmacokinetic Studies of Skepinone-L and Sorafenib in Rats	57
3.3.4. Pharmacokinetic Study of Skepinone-L and Sorafenib in Monkeys	90
3.3.5. Summary and Discussion of the Preclinical Pharmacokinetic Studies of Skepinone-L in Mice, Rats, Dogs and Monkeys	94
3.4. Plasma Protein Binding of Skepinone-L <i>in vitro</i>	97
3.5. Metabolic Conversion of Skepinone-L <i>in vitro</i>	100
3.5.1. Biotransformation of Skepinone-L in Liver Microsomes	101
3.5.2. Biotransformation of Sorafenib in the Presence of Skepinone-L in Liver Microsomes	124
3.5.3. Glucuronidation of Skepinone-L in Recombinant Isoenzymes	151
3.5.4. Summary and Discussion of <i>in vitro</i> Metabolism Studies of Skepinone-L....	164
3.6. Excretion of Skepinone-L <i>in vivo</i>	171
3.6.1. Skepinone-L and its Glucuronides in Mouse Faeces	172
4. Conclusion	175
4.1. Synopsis of Results	178
4.1.1. Pharmacokinetic behaviour of Skepinone-L <i>in vivo</i>	178
4.1.2. Pharmacokinetic behaviour of Sorafenib <i>in vivo</i>	179
4.1.3. Metabolic Stability and Transformation of Skepinone-L <i>in vitro</i>	180
4.1.4. Influence of Skepinone-L on the Metabolic Stability and Transformation of Sorafenib <i>in vitro</i>	181
4.2. Outlook	183
4.3. Summary	183
5. Material and Methods	185
5.1. Material	185

5.1.1. Biological Material	185
5.1.2. Chemicals and Reagents	185
5.1.3. Test and Reference Compounds.....	186
5.1.4. Consumables.....	190
5.1.5. Apparatus	190
5.2. Methods.....	190
5.2.1. Descriptive Statistic	190
5.2.2. Method Validation of Skepinone-L and Sorafenib in Plasma	191
5.2.3. Pharmacokinetic Studies of Skepinone-L <i>in vivo</i>	195
5.2.4. Pharmacokinetic Data Analysis	200
5.2.5. Pharmacokinetic Model Assessment.....	202
5.2.6. Determination of Plasma Protein Binding of Skepinone-L.....	202
5.2.7. Metabolism and Biotransformation <i>in vitro</i>	204
5.2.8. Incubations with Recombinant UGTs	213
5.2.9. p38 α -Mitogen-Activated Protein Kinase Assay	216
5.2.10. Extraction of Skepinone-L from Mouse Faeces	217
6. List of Publications	219
7. Appendix	221
7.1. Primary Calibration Lines during Method Validation.....	221
7.2. Plasma Concentrations of Skepinone-L and Sorafenib <i>in vivo</i>	222
7.3. Calibration Lines during Kinetic Analysis of Skepinone-L Glucuronidation ..	229
8. Bibliography.....	232

Abstract

The available therapeutic options for hepatocellular carcinoma (HCC) are quite limited and rapidly exhausted e.g., to acquired resistance. This explains the urgent need for new therapeutic approaches. In the mouse model, it was possible to overcome resistance to the multikinase inhibitor Sorafenib (SRF) by inhibiting p38 α -mitogen-activated protein kinase (MAPK). As Skepinone-L (SKL) is a highly potent inhibitor of p38 α MAPK with outstanding selectivity, a combined therapy of SKL with SRF represents a promising approach to HCC therapy.

Poor pharmacokinetic properties are one of the main reasons for the termination of clinical trials prior to market approval. The failure of a new therapy during the clinical trial causes very high costs and loss of time. To mitigate this risk, a comprehensive elucidation of the pharmacokinetic profile of SKL in different preclinical animal species was performed in this thesis. Despite distinct species-specific differences, most of the obtained parameters show that SKL exhibits very favourable pharmacokinetic properties *in vivo*. Co-administration with SRF resulted in increased plasma levels with improved absorption and elimination profiles. In contrast, SRF exposure appeared to be reduced in the presence of SKL. Incubated with human microsomes, SKL is metabolically degraded especially by conjugation with glucuronic acid. The three formed reaction products were identified as primary oxygen-bound (pO), secondary oxygen-bound (sO) and nitrogen-bound (N) glucuronide and the responsible enzymes determined. Interestingly, N-glucuronide formation was not observed in any animal species. Co-incubation with SRF results in a concentration-dependent decrease in the formation of pO- and sO-glucuronide. In contrast, the formation of N-glucuronide seems to be induced by SRF. Metabolically unchanged SKL is mainly excreted via faeces while the glucuronides presumably leave the organism by renal elimination. Regarding the pharmacokinetics and biotransformation of SKL as well as the interaction of SKL with SRF, the obtained results in the present work show promising properties for the clinical development of the intended combinatorial therapy of HCC with both kinase inhibitors SKL and SRF.

Zusammenfassung der Dissertation

Die verfügbaren Therapiemöglichkeiten des hepatozellulären Karzinoms (HCC) sind stark limitiert und aufgrund erworbener Resistenzen zudem schnell ausgeschöpft. Dies begründet den dringenden Bedarf an neuen Therapieansätzen. Im Mausmodell war es möglich die erworbene Resistenz gegen den Multikinaseinhibitor Sorafenib (SRF) durch Hemmung der p38 α -mitogen-aktivierten Proteinkinase (MAPK) zu überwinden. Da Skepinone-L (SKL) ein hochpotenter Inhibitor der p38 α MAPK mit herausragender Selektivität ist, stellt die Kombinationstherapie von SKL mit SRF einen vielversprechenden Ansatz zur HCC-Therapie dar.

Mangelhafte pharmakokinetische Eigenschaften sind einer der Hauptgründe für den Abbruch klinischer Studien vor der Marktzulassung. Das Scheitern einer neuen Therapie während der klinischen Studie bedeutet einen sehr hohen Kosten- und Zeitverlust. Um dies zu vermeiden, erfolgte die umfassende Aufklärung des pharmakokinetischen Profils von SKL in verschiedenen präklinischen Tierspezies. Trotz deutlicher speziesspezifischer Unterschiede zeigen die erhaltenen Parameter mehrheitlich, dass SKL sehr gute pharmakokinetische Eigenschaften *in vivo* besitzt. Die zeitgleiche Verabreichung mit SRF resultierte in höheren Plasmaspiegeln mit günstigerem Absorptions- sowie Eliminationsverlauf. Dagegen schien die SRF-Exposition in Gegenwart von SKL vermindert. In Inkubationen mit humanen Mikrosomen wird SKL nahezu ausschließlich per Konjugation mit Glucuronsäure metabolisch degradiert. Die drei entstehenden Reaktionsprodukte konnten als primär-Sauerstoffgebunden (pO), sekundär-Sauerstoffgebunden (sO) und als Stickstoffgebundenes (N) Glucuronid identifiziert werden. Zudem konnten die jeweils verantwortlichen Enzyme ermittelt werden. Interessanterweise wird das N-Glucuronid in keiner Tierspezies gebildet. Die Co-Inkubation mit SRF resultiert konzentrationsabhängig überwiegend in verminderter Bildung des pO- und sO-Glucuronides. Dagegen scheint die Bildung des N-Glucuronides durch SRF induziert. Unverändertes SKL wird hauptsächlich über den Fäzes ausgeschieden, während die Glucuronide vermutlich auf renalem Wege den Organismus verlassen.

Hinsichtlich der Pharmakokinetik und Biotransformation von SKL sowie der Wechselwirkung von SKL mit SRF zeigen die in der vorliegenden Arbeit erzielten Ergebnisse vielversprechende Eigenschaften für die klinische Entwicklung der angestrebten kombinatorischen Therapie von HCC.

Abbreviations

1,2-PG	1,2-propylene glycol
ACN	acetonitrile
ADME	absorption, distribution, metabolism, excretion
API	active pharmaceutical ingredient
AUC	area under the curve
AUMC	area under the moment curve
BSA	bovine serum albumin
CA	compartmental analysis
Cl	whole body clearance
Cl _{int}	intrinsic clearance
CMLM	cynomolgus monkey liver microsomes
conc.	concentration
CV	coefficient of variation
CYP	cytochrome P450
D	applied dose
DA	dual activity
DCF	diclofenac
DDI	drug-drug interaction
DES	N-desmethyl sorafenib
DLM	dog liver microsomes
DMSO	dimethyl sulfoxide
e.g.	exempli gratia; for example
ELISA	enzyme-linked immunosorbent assay
EMA	European Medicines Agency
eq	equation
ESI	electrospray ionisation
f	female
F	bioavailability
f _b	fraction bound
f _u	fraction unbound
fig	figure
G6P	glucose-6-phosphate
G6PDH	glucose-6- phosphate dehydrogenase
GIT	gastrointestinal tract
H ₂ O	water
HCC	hepatocellular carcinoma
HLM	human liver microsomes
HOM	N-hydroxymethyl sorafenib
HR	hydrophobic region
HTMC	hydroxytrifluoromethylcoumarin
i.e.	id est; that is to say

i.v.	intravenous
IC ₅₀	mean inhibitory concentration
ICH	The International Council for Harmonisation of Technical Requirements for Pharmaceuticals for Human Use
ISTD	internal standard
IUPAC	International Union of Pure and Applied Chemistry
K _m	Michaelis-Menten constant
LC	liquid chromatography
LM	liver microsomes
LOD	limit of detection
LOQ	limit of quantification
m	male
M	molarity
MAPK	mitogen-activated protein kinase
min	minute
mL	milliliter
MLM	mouse liver microsomes
MRM	multiple reaction monitoring
MS	mass spectrometry
MS/MS	tandem MS
N-Glc	nitrogen-linked SKL-glucuronide
N/A	not available
N/D	not detected
NADPH	nicotinamide adenine dinucleotide phosphate
NCA	non-compartmental analysis
NCE	new chemical entity
nM	nanomolar
NMP	N-methyl-2-pyrrolidone
NOX	sorafenib N-oxide
p.o.	per oral
PAR	peak area ratio
PDGFR	platelet-derived growth factor receptor
PEG400	polyethylene glycol 400
Ph1	phase I metabolism
Ph2	phase II metabolism
PK	pharmacokinetic
pO-Glc	primary oxygen-linked SKL-glucuronide
QC	quality control
RGF	Regorafenib
RLM	rat liver microsomes
rpm	rounds per minute
s	second
s.d.	single dose
SKL	Skepinone-L

sO-Glc	secondary oxygen-linked SKL-glucuronide
SRF	Sorafenib
SRF-N-Glc	Sorafenib nitrogen-linked glucuronide
SS	stock solution
tab	table
TFP	trifluoperazine
TFP-N-Glc	trifluoperazine nitrogen-linked glucuronide
Tris-HCl	Tris(hydroxymethyl)aminomethane hydrochloride
UDPGA	uridine diphosphate glucuronic acid
UGT	uridine 5'-diphospho-glucuronosyltransferase
US	ultra sonic
V	Volt
V_{max}	maximum reaction velocity
V_{ss}	volume of distribution at steady state
VEGFR	vascular endothelial growth factor receptor
WSS	weighted sum of squares
μL	microlitre
μM	micromolar

List of Tables

Tab. 1: Calculated limits of detection and quantification in ng/mL for the determination of SKL and SRF in rat, dog, monkey and human plasma	35
Tab. 2: Summarized results of the linearity of SKL and SRF determined in rat, dog and human plasma	36
Tab. 3: Intra-day and inter-day accuracy and precision of SKL and SRF in rat plasma	37
Tab. 4: Intra-day and inter-day accuracy and precision of SKL and SRF in dog plasma	37
Tab. 5: Intra-day and inter-day accuracy and precision of SKL and SRF in human plasma	38
Tab. 6: Evaluation of SKL and SRF reproducibility in rat plasma	39
Tab. 7: Evaluation of SKL reproducibility in dog plasma	39
Tab. 8: Evaluation of SKL and SRF reproducibility in human plasma	40
Tab. 9: Stability analysis of SKL and SRF in rat plasma	42
Tab. 10: Stability analysis of SKL in dog plasma	42
Tab. 11: Stability analysis of SKL and SRF in human plasma	43
Tab. 12: Overview of selected species, test items and route of administration to investigate the PK profile of SKL <i>in vivo</i>	44
Tab. 13: Pharmacokinetic parameters for SKL derived from NCA of mean plasma concentration vs. time profiles in male mice after intravenous bolus injection	46
Tab. 14: Pharmacokinetic parameters for SKL derived from NCA of mean plasma concentration vs. time profiles in male mice after oral administration	47
Tab. 15: Pharmacokinetic parameters for SKL derived from NCA of individual plasma concentration vs. time curves in female mice	48
Tab. 16: Pharmacokinetic parameters for SKL	49
Tab. 17: Calculated pharmacokinetic parameters for SKL	51
Tab. 18: Pharmacokinetic parameters for SKL derived from NCA of individual plasma concentration vs. time curves in male and female beagle dogs	52
Tab. 19: Pharmacokinetic parameters for SKL derived from NCA of individual plasma concentration vs. time curves in male and female beagle dogs	53
Tab. 20: Pharmacokinetic parameters for SKL from individual plasma concentration vs. time curves in male and female beagle dogs after single oral administration	54
Tab. 21: Pharmacokinetic parameters for SKL determined by compartmental analysis of mean plasma concentration vs. time profiles	55
Tab. 22: Overview of the treatment groups during pharmacokinetic studies of SKL	58
Tab. 23: Pharmacokinetic parameters for SKL determined by NCA from individual plasma concentration vs. time curves in male rats	60
Tab. 24: Pharmacokinetic parameters for SKL calculated by NCA	60
Tab. 25: Pharmacokinetic parameters for SKL derived by NCA	61
Tab. 26: Pharmacokinetic parameters for SKL derived by NCA	62
Tab. 27: Pharmacokinetic parameters for SKL derived by NCA	63
Tab. 28: Pharmacokinetic parameters for SKL derived by NCA	64
Tab. 29: Overview of treatment groups during the PK studies of SKL in rats part II	66
Tab. 30: Pharmacokinetic parameters for SKL derived by NCA	67
Tab. 31: Pharmacokinetic parameters for SKL derived by NCA	68
Tab. 32: Pharmacokinetic parameters for SKL derived by NCA	70
Tab. 33: Pharmacokinetic parameters for SKL derived by NCA	72
Tab. 34: Pharmacokinetic parameters for SKL derived by NCA from individual plasma concentration vs. time curves in male and female rats	74
Tab. 35: Pharmacokinetic parameters for SRF derived by NCA	78
Tab. 36: Pharmacokinetic parameters for SRF derived by NCA from individual plasma concentration vs. time curves in male and female rats	79
Tab. 37: Pharmacokinetic parameters for SRF derived by NCA	80
Tab. 38: Pharmacokinetic parameters for SRF derived by NCA	82
Tab. 39: Pharmacokinetic parameter for SRF derived by NCA	83

Tab. 40: Overview of mean C _{max} of SKL and SRF in male and female rats	89
Tab. 41: Pharmacokinetic parameters for SKL derived by NCA o.....	92
Tab. 42: Pharmacokinetic parameter for SRF derived from NCA of individual plasma concentration vs. time curves in male and female cynomolgus monkeys	93
Tab. 43: Fraction bound (f _b) to plasma proteins.....	98
Tab. 44: Metabolic stability of SKL <i>in vitro</i> after 120 min incubation by addressing microsomal CYPs of human, rat, mouse, dog and monkey LMs	102
Tab. 45: Metabolic stability <i>in vitro</i> of SKL after 120 min incubation by addressing microsomal CYPs of human and rat LMs.....	103
Tab. 46: Percentage of formed SKL Ph1 metabolites	104
Tab. 47: Percentage of formed SKL Ph1 metabolites after 120 min incubation in the presence of SRF.....	107
Tab. 48: Metabolic stability of SKL <i>in vitro</i> after 120 min incubation by addressing microsomal UGTs of human, rat, mouse, dog and monkey LMs	108
Tab. 49: Percentages of formed SKL Ph2 metabolites.....	110
Tab. 50: Percentages of formed pO-Glc, sO-Glc and N-Glc after 120 min incubation in the presence of SRF	112
Tab. 51: Metabolic stability of 10 µM SKL after 120 min incubation by co-activation of microsomal CYPs and UGTs of human, rat, mouse, dog and monkey LMs	114
Tab. 52: Percentages of formed SKL Ph2 metabolites.....	114
Tab. 53: Percentage of formed SKL Ph1 metabolites	117
Tab. 54: Percentages of formed pO-Glc, sO-Glc and N-Glc	118
Tab. 55: Metabolic stability of SKL and percentages formed pO-Glc, sO-Glc and N-Glc after 120 min in the presence of SRF	119
Tab. 56: Metabolic stability of TFP and percentages of formed TFP- N-Glc	124
Tab. 57: Percentages of formed oxidative metabolites.....	126
Tab. 58: Percentages of formed SRF-N-glucuronide	129
Tab. 59: Percentages of formed NOX, HOM, DES and SRF-Glc.....	131
Tab. 60: Kinetic parameters of the glucuronidation reaction of SKL.....	150
Tab. 61: Overview of the amount of food.....	172
Tab. 62: Summary of the pharmacokinetic parameters of SKL in mice, dogs and rats following intravenous administration	178
Tab. 63: Summary of the pharmacokinetic parameters of SKL in mice, dogs, rats, monkeys and humans following single oral administration	178
Tab. 64: Summary of the pharmacokinetic parameters of SKL in rats	179
Tab. 65: Summary of the pharmacokinetic parameters of SRF in monkeys	179
Tab. 66: Summary of the pharmacokinetic parameters of SRF in rats.....	179
Tab. 67: Metabolic stability of 10 µM SKL after 120 min incubation	180
Tab. 68: Formation of SKL metabolites after 120 min incubation of 10 µM SKL	180
Tab. 69: Metabolic stability and metabolite formation of SKL.....	181
Tab. 70: Metabolic stability of 10 µM SRF after 120 min incubation.....	181
Tab. 71: Formation of SRF oxidative metabolites after 120 min incubation	182
Tab. 72: Formation of SRF-Glc [%] after 120 min incubation of 10 µM SRF.....	182
Tab. 73: Instrumental parameters for the mass spectral analysis of SKL, SRF and FS112 in dog, rat, monkey and human plasma using MRM-mode.	191
Tab. 74: Initial weight and preparation of SKL, SRF and FS112 stock solutions	193
Tab. 75: Preparation of SKL/SRF calibration standards in rat plasma.	193
Tab. 76: Preparation of SKL/SRF quality control samples.	193
Tab. 77: Initial weight and preparation of SKL and FS112 stock solutions.....	193
Tab. 78: Preparation of SKL calibration standards in dog plasma.....	194
Tab. 79: Preparation of SKL quality control samples.....	194
Tab. 80: Initial weight and preparation of SKL, SRF and FS112 stock solutions	194
Tab. 81: Preparation of SKL/SRF calibration standards in human plasma.	194
Tab. 82: Preparation of SKL/SRF quality control samples	195
Tab. 83: Treatment summary of C57BL/6 mice with SKL.....	196

Tab. 84: Treatment summary of beagle dogs with SKL.....	196
Tab. 85: Summary of treatment of Sprague Dawley rats with SKL	196
Tab. 86: Summary of treatment of Sprague Dawley rats with SKL and SRF	196
Tab. 87: Summary of treatment of cynomolgus monkeys with SKL and SRF	196
Tab. 88: Instrumental parameters for the mass spectral analysis of SKL and FS694 in mouse plasma applying MRM-mode.	198
Tab. 89: Instrumental parameters for the mass spectral analysis using MRM	204
Tab. 90: Overview of purchased and for <i>in vitro</i> metabolism studies of SKL and SRF applied liver microsomes	205
Tab. 91: Characteristic CYP content and UGT activity of applied LMs	205
Tab. 92: Composition of the Ph1 incubation assays.....	206
Tab. 93: Instrumental parameters for the mass spectral analysis	207
Tab. 94: Instrumental parameters for the mass spectral analysis using MRM	207
Tab. 95: Composition of Ph2 incubation assay	208
Tab. 96: Instrumental parameters for the mass spectral analysis	209
Tab. 97: Instrumental parameters for the mass spectral analysis of N-methyl-SKL, FS352, FS332	210
Tab. 98: Instrumental parameters for the mass spectral analysis	210
Tab. 99: Composition of mixture parts A and B for the dual-activity assay	211
Tab. 100: Instrumental parameters for the mass spectral analysis using MRM to analyse RGF, TFP and TFP-Glc.....	212
Tab. 101: Concentrations of SKL, liver microsomal protein content of each species and incubation time applied to determine K_m and V_{max}	213
Tab. 102: Overview of purchased and for <i>in vitro</i> glucuronidation studies of SKL applied UGT isoforms	214
Tab. 103: Composition of glucuronidation reaction mixture.....	215
Tab. 104: Instrumental parameters for the mass spectral analysis using MRM	216
Tab. 105: Individual and mean concentrations of SKL in mouse plasma	222
Tab. 106: Individual and mean concentrations of SKL in mouse plasma	223
Tab. 107: Individual concentrations of SKL in plasma of beagle dogs	223
Tab. 108: Individual concentrations of SKL in dog plasma.....	223
Tab. 109: Individual concentrations of SKL in dog plasma.....	223
Tab. 110: Individual and mean concentrations of SKL in rat plasma.....	224
Tab. 111: Individual and mean concentrations of SKL in rat plasma.....	224
Tab. 112: Individual and mean concentrations of SKL in rat plasma.....	224
Tab. 113: Individual and mean concentrations of SKL in rat plasma.....	224
Tab. 114: Individual and mean concentrations of SKL in rat plasma.....	225
Tab. 115: Individual and mean concentrations of SKL in rat plasma.....	225
Tab. 116: Individual and mean concentrations of SKL in rat plasma.....	225
Tab. 117: Individual and mean concentrations of SKL in rat plasma.....	225
Tab. 118: Individual and mean concentrations of SKL in rat plasma.....	226
Tab. 119: Individual and mean concentrations of SKL in rat plasma.....	226
Tab. 120: Individual and mean concentrations of SRF in rat plasma	226
Tab. 121: Individual and mean concentrations of SRF in rat plasma	226
Tab. 122: Individual and mean concentrations of SRF in rat plasma	227
Tab. 123: Individual and mean concentrations of SRF in rat plasma	227
Tab. 124: Individual concentrations of SKL and SRF in rat plasma	227
Tab. 125: Individual concentrations of SKL and SRF in rat plasma	227
Tab. 126: Individual concentrations of SKL and SRF in rat plasma	228
Tab. 127: Individual concentrations of SKL and SRF in rat plasma	228
Tab. 128: Individual concentrations of SKL and SRF in rat plasma	228
Tab. 129: Individual concentrations of SKL and SRF in rat plasma	228
Tab. 130: Individual concentrations of SKL in plasma of cynomolgus monkeys	229
Tab. 131: Individual concentrations of SRF in plasma cynomolgus monkeys.....	229

List of Figures

Fig. 1: Scheme representing the time-consuming and cost-intensive development process from the discovery of the active ingredient to the approved drug.....	2
Fig. 2: Schematic representation of the one- and the two-compartment model	4
Fig. 3: Schematic representation of the oxidation process of the membrane-bound monooxygenase complex	8
Fig. 4: Glucuronic acid transfer of UDPGA to the substrate	9
Fig. 5: Types of reversible enzyme inhibition.....	13
Fig. 6: Schematic representation of the ESI process in positive mode.....	15
Fig. 7: Schematic diagram of a triple quadrupole system.....	16
Fig. 8: Schematic representation of SRF's cellular targets and mechanism of action in tumour cells and endothelial cells	18
Fig. 9: Biotransformation pathway of SRF and its major metabolites NOX, HOM, DES and SRF-N-Glc.	19
Fig. 10: Structure and overview of probe criteria and achievements by SKL	20
Fig. 11: Scheme representing the involvement of p38aMAPK in the RAF-MEK-ERK signalling pathway in SRF sensitivity and resistance in HCC	21
Fig. 12: Comprehensive presentation of the objectives of the thesis	24
Fig. 13: Structures of analyte SKL and internal standard FS112.....	27
Fig. 14: ESI(+) mass spectrum of SKL	27
Fig. 15: Daughter ion mass spectrum of SKL	28
Fig. 16: ESI(+) mass spectrum of SRF	28
Fig. 17: Daughter ion mass spectrum of SRF.....	28
Fig. 18: ESI(+) mass spectrum of ISTD FS112	29
Fig. 19: Daughter ion mass spectrum of ISTD FS112	29
Fig. 20: MRM chromatograms of SKL, SRF and ISTD in rat plasma	31
Fig. 21: MRM chromatograms of SKL and ISTD in dog plasma.....	32
Fig. 22: MRM chromatograms of SKL, SRF and ISTD in monkey plasma	33
Fig. 23: MRM chromatograms of SKL, SRF and ISTD in human plasma.....	34
Fig. 24: Plasma concentration vs. time profile of SKL following cassette dosing	46
Fig. 25: Plasma concentration vs. time profile of SKL following cassette dosing	47
Fig. 26: Individual plasma concentration vs. time curves of SKL in female mice	48
Fig. 27: Two-compartment model plots of SKL in male mice	50
Fig. 28: Individual plasma concentration vs. time curves of SKL in male and female beagle dogs after single i.v. administration	52
Fig. 29: Individual plasma concentration vs. time curves of SKL in male and female beagle dogs after single oral administration	53
Fig. 30: Individual plasma concentration vs. time curves of SKL.....	54
Fig. 31: Two-compartment model plots of SKL.....	56
Fig. 32: Individual plasma concentration vs. time curves of SKL in rats.....	58
Fig. 33: Individual plasma concentration vs. time curves of SKL in rats.....	59
Fig. 34: Individual plasma concentration vs. time curves of SKL.....	67
Fig. 35: Individual plasma concentration vs. time curves of SKL.....	68
Fig. 36: Mean plasma concentration vs. time curves of SKL.....	69
Fig. 37: Individual plasma concentration vs. time curves of SKL.....	71
Fig. 38: Individual plasma concentration vs. time curves of SKL.....	71

Fig. 39: Mean plasma concentration vs. time curves of SKL in male and female rats of treatment group 9	73
Fig. 40: Individual plasma concentration vs. time curves of SKL in male and female rats of treatment group 10	74
Fig. 41: Mean plasma concentration vs. time curves of SKL.....	75
Fig. 42: Individual plasma concentration vs. time curves of SRF in male and female rats of treatment group 7	77
Fig. 43: Individual plasma concentration vs. time curves of SRF	78
Fig. 44: Individual plasma concentration vs. time curves of SRF	80
Fig. 45: Individual plasma concentration vs. time curves of SRF in male and female rats from treatment group 9	81
Fig. 46: Individual plasma concentration vs. time curves of SRF	82
Fig. 47: Mean plasma concentration vs. time curves of SRF	84
Fig. 48: Mean PAR vs. time profiles of SRF phase 1 metabolites	85
Fig. 49: Mean PAR vs. time profiles of SRF phase 1 metabolites in male and female rats from treatment group 10	86
Fig. 50: Individual plasma concentration vs. time curves of SKL in male and female cynomolgus monkeys	91
Fig. 51: Individual plasma concentration vs. time curves of SRF	92
Fig. 52: Proposed structures for Ph1 metabolites of SKL.....	105
Fig. 53: Metabolic stability <i>in vitro</i> of SKL solely and in the presence of SRF	106
Fig. 54: Structures of the primary and secondary oxygen-linked glucuronides as well as the nitrogen-linked glucuronide of SKL.....	109
Fig. 55: Metabolic stability <i>in vitro</i> of SKL solely and in the presence of SRF	111
Fig. 56: Metabolic stability of SKL.....	114
Fig. 57: Percentages of formed pO-Glc, sO-Glc and N-Glc.....	115
Fig. 58: Metabolic stability <i>in vitro</i> of SKL solely and in the presence of SRF	117
Fig. 59: Formation of pO-Glc, sO-Glc and N-Glc in HLM after 120 min	121
Fig. 60: Structures of multi-kinase inhibitors Sorafenib and Regorafenib.....	122
Fig. 61: Formation of pO-Glc, sO-Glc and N-Glc in HLM in the presence of RGF	122
Fig. 62: Structures of trifluoperazine and trifluoperazine-N-glucuronide.....	123
Fig. 63: Metabolic stability <i>in vitro</i> of SRF solely and in the presence of SKL	125
Fig. 64: Metabolic stability <i>in vitro</i> of SRF solely and in the presence of SKL after 120 min incubation by addressing activated microsomal UGTs.....	128
Fig. 65: Metabolic stability <i>in vitro</i> of SRF solely and in the presence of SKL after 120 min incubation by co-activation of microsomal CYPs and UGTs	131
Fig. 66: Mass spectrum of postulated SKL-glucuronides	134
Fig. 67: Chromatograms of intensity over time	134
Fig. 68: LC-MS/MS chromatogram of SKL-glucuronides.....	135
Fig. 69: LC-MS/MS chromatogram of SKL-glucuronides.....	135
Fig. 70: Possible binding sites of SKL for conjugation with glucuronic acid	136
Fig. 71: Structures of SKL derivatives	137
Fig. 72 (Continuation of fig.71): Structures of SKL derivatives.....	138
Fig. 73: LC-MS/MS chromatogram and the related structures of SKL-glucuronides.....	140
Fig. 74: LC-MS/MS chromatogram of sO-Glc, pO-Glc and SKL at 10 μ M.....	141
Fig. 75: Inhibitory activities of pO-Glc and sO-Glc towards p38 α MAP kinase.....	142

Fig. 76: Graphical representation of the binding mode of SKL in the ATP-binding pocket of p38 α MAP kinase.	143
Fig. 77: Graphical representation of the glucuronidation kinetic of SKL in HLM.....	145
Fig. 78: Graphical representation of the glucuronidation kinetic of SKL in RLM.....	146
Fig. 79: Graphical representation of the glucuronidation kinetic of SKL in MLM	147
Fig. 80: Graphical representation of the glucuronidation kinetic of SKL in DLM.....	148
Fig. 81: Graphical representation of the glucuronidation kinetic of SKL in CMLM.....	149
Fig. 82: Formation of the primary SKL-O-glucuronide, the secondary SKL-O-glucuronide and the N-glucuronide <i>in vitro</i>	152
Fig. 83: Summarised results of the structural elucidation of pO-Glc, sO-Glc and postulated N-Glc as well as the respective contributing UGT-isoenzymes	153
Fig. 84: Graphical representation of the glucuronidation kinetic of SKL with rUGT2B7	156
Fig. 85: Graphical representation of the glucuronidation kinetic of SKL with rUGT1A4	157
Fig. 86: Formation of HTMC-Glc <i>in vitro</i> after 60 min incubation.....	159
Fig. 87: Metabolic stability of SKL solely and in the presence of 10 μ M and 40 μ M SRF after 60 min incubation with rUGT2B7	161
Fig. 88: Metabolic stability of SKL solely and in the presence of 10 μ M and 40 μ M SRF after 60 min incubation with rUGT1A1	162
Fig. 89: Metabolic stability of SKL solely and in the presence of 10 μ M and 40 μ M SRF after 60 min incubation with rUGT1A4	163
Fig. 90: Metabolic stability of TFP solely and in the presence of 10 μ M and 40 μ M SRF after 60 min incubation with rUGT1A4	164
Fig. 91: The binding of SRF to the allosteric site of UGT1A4	170
Fig. 92: Mean plasma concentration vs. time profiles of SKL.....	177
Fig. 94: Schematic representation of the obtained results regarding the pharmacokinetic profile of SKL <i>in vitro</i> and <i>in vivo</i> and the influence of SRF.....	184
Fig. 95: Primary calibration line for the determination of SKL in dog plasma	221
Fig. 96: Primary calibration lines for the determination of SKL and SRF in rat plasma	222
Fig. 97: Primary calibration lines for the determination of SKL and SRF in human plasma	222
Fig. 98: Calibration lines for the determination of SKL and its glucuronides pO-Glc and sO-Glc in human LM to determine V_{max} and K_m	229
Fig. 99: Calibration lines for the determination of SKL and its glucuronides pO-Glc and sO-Glc in rat LM to determine V_{max} and K_m	230
Fig. 100: Calibration lines for the determination of SKL and its glucuronides pO-Glc and sO-Glc in mouse LM to determine V_{max} and K_m	230
Fig. 101: Calibration lines for the determination of SKL and its glucuronides pO-Glc and sO-Glc in dog LM to determine V_{max} and K_m	230
Fig. 102: Calibration lines for the determination of SKL and its glucuronides pO-Glc and sO-Glc in monkey LM to determine V_{max} and K_m	231
Fig. 103: Calibration lines for the determination of SKL and its glucuronides pO-Glc and sO-Glc in rUGT1A4 to determine V_{max} and K_m	231
Fig. 104: Calibration lines for the determination of SKL and its glucuronides pO-Glc and sO-Glc in rUGT1A4 to determine V_{max} and K_m	231

1. INTRODUCTION

1.1. Pharmaceutical Research and Development

The *de novo* drug development is a long-term and cost-intensive process which consists of three major stages (Fig. 1). The first stage is described as the drug discovery process. This includes the search for a hit, identification of the target and optimisation of the lead structure for subsequent preclinical studies [1]. The selected candidate molecules must have sufficient biological activity at the disease relevant target structure, adequate safety, and certain physicochemical properties [2]. During the second stage, extensive *in vitro* and *in vivo* tests are conducted on the potential clinical candidate molecules. The preclinical phase serves to clarify the target and the relation to human diseases as well as the reliability of findings. In addition, potency, kinetics, specificity [2] and safety are assessed, the latter in at least one rodent and one non-rodent species [3] to select the clinical compound for future administration to humans. The third stage involves the performance of various clinical trials in different groups of participants [4]. In this stage, adverse effects, side effects, overall safety and efficacy are studied. The market approval is granted to the drug if the corresponding extensive criteria and requirements are fulfilled.

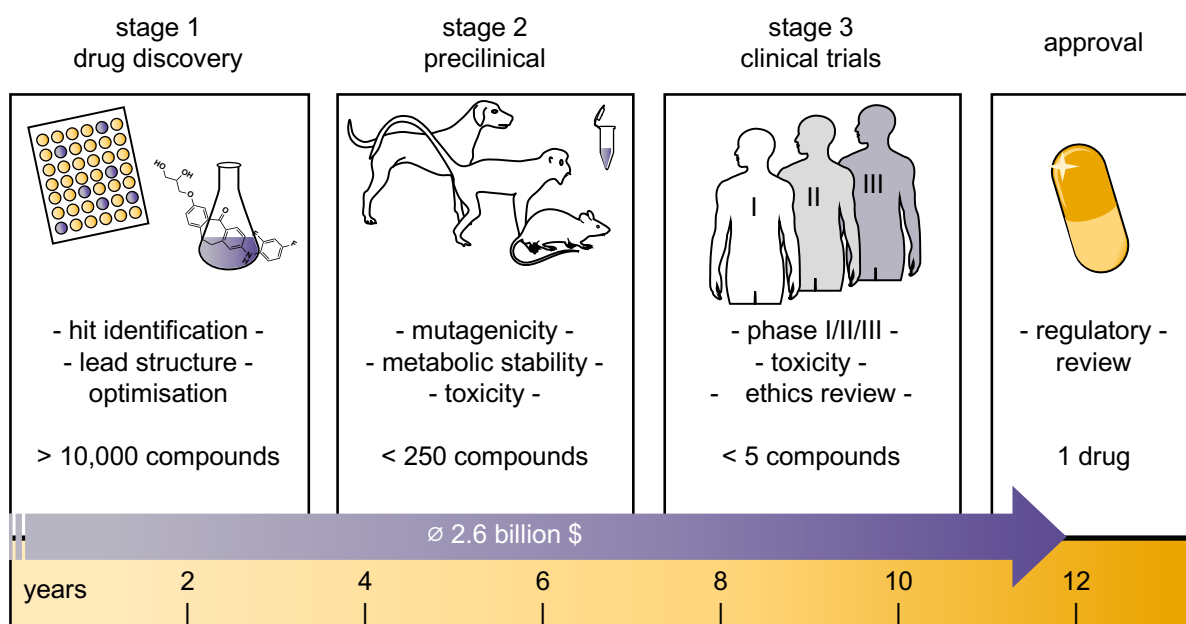


Fig. 1: Scheme representing the time-consuming and cost-intensive development process from the discovery of the active ingredient to the approved drug. Graphic adapted from [2] and [5].

This whole process can take 10 to 15 years from the identification of the lead molecule to market maturity, with a probability of success of less than 1% [6]. The entire development of a new drug costs on average about 2.6 billion dollars. These comprise the preclinical and clinical phases with 1.1 and 1.5 billion dollars respectively [7]. Failure to achieve drug approval thus represents a very high risk due to the extensive time and costs involved. Insufficient characteristics in terms of absorption, distribution, metabolism and excretion (ADME) of the new chemical entity (NCE) represents the major cause for the discontinuation of drug development [8]. To avert this, the pharmacokinetic behaviour of drug candidates is extensively investigated during the preclinical phase, according to the “fail fast, fail early” devise, thus preventing expensive late-stage failures of drug molecules [2].

1.2. Principles of Pharmacokinetics

‘A chemical cannot be a drug, no matter how active nor how specific its action, unless it is also taken appropriately into the body (absorption), distributed to the right parts of the body, metabolized in a way that does not instantly remove its activity, and eliminated in a suitable manner - a compound must get in, move about, hang around, and then get out.’ This definition by J. Hodgson [8] aptly summarises the importance

and fundamental processes of pharmacokinetics. As a part of pharmacology, pharmacokinetic is the study of the time-dependent processes to which a xenobiotic (drug, NCE) is exposed in the organism. It involves the study and characterisation of a drug's absorption (A), distribution (D), metabolic transformation (M) and elimination (E), referred to as ADME [9]. These processes are responsible for the API-concentration at the site of action. Furthermore, pharmacokinetic involves the use of mathematical and biochemical techniques in a physiological and pharmacological context [10].

1.2.1. Pharmacokinetic Model Conceptions

Different model conceptions facilitate the understanding and comparison of summarised data. In addition, they allow certain predictions for experimental designs, dosages and concentrations. The complex structure of the organism and its diverse functions are abstracted or significantly simplified. The body is represented as a system of one or more compartments by the single- or multiple-compartmental model. Usually, these compartments have neither an anatomical nor a physiological meaning [11]. This system is referred to as open because the absorbed drug is eliminated after its distribution, thus leaving the body. The transfer of substances into, out of and between the different compartments is described by rate constants. As early as 1937, compartmental analysis was used by T. Teorell [12]. In pharmacokinetics, compartment models, empirical, physiological and also statistical models are used.

1.2.1.1. Non-Compartmental Analysis

A simple and fast method for describing the pharmacokinetics of an API is the model-independent method, also called non-compartmental analysis (NCA). A linear relationship between the administered dose and the API concentration in the investigated medium is a prerequisite for the application of this statistical model. The pharmacokinetic parameters are calculated based on the determined concentrations, without the entire concentration-time profile being described by a mathematical function [13]. The degree of systemic exposure of a drug is evaluated by estimating the area under the concentration-time curve (AUC) and the moment curve (AUMC) [14]. This method can be used to calculate further important pharmacokinetic

parameters, which will be explained in more detail later. However, since NCA cannot determine an API concentration at any time, this model is not suitable for predicting pharmacokinetic profiles with alterations in dose regimen [11]. This limitation does not account for compartmental analysis (CA).

1.2.1.2. Compartmental Models

Modelling the concentration-time data with a suitable pharmacokinetic compartment model to quantitatively evaluate and predict the *in vivo* fate of a drug is performed by CA, a widely used technique [15]. In the simplest scenario, the entire body is considered as one compartment (Fig. 2a). This model can be described both without absorption after intravenous administration (i.v.) or with absorption described by the rate constant k_a after oral administration (p.o.). Thus, the concentration present in compartment C1 is dependent on the applied or absorbed dose as well as of the compartmental volume. Decrease in concentration in the C1 is directly related to the elimination rate constant k_{10} . However, that highly simplified model is only suitable for relatively few compounds.

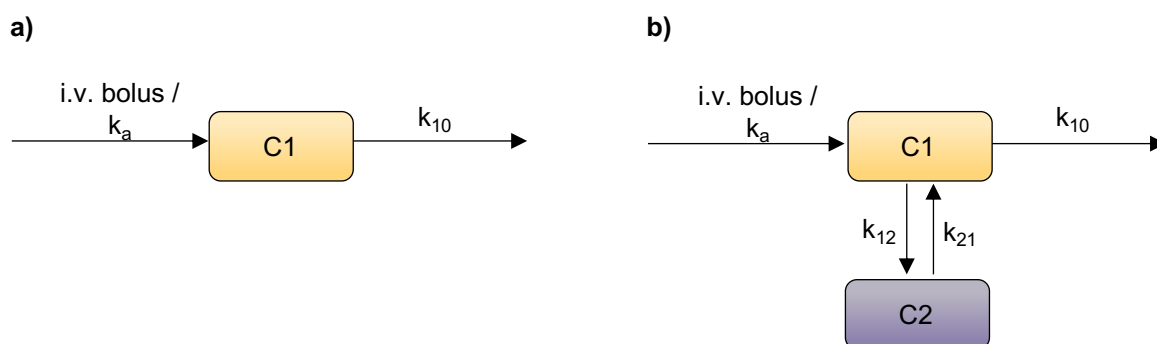


Fig. 2: Schematic representation of the one- (a) and the two-compartment model (b) which distinguishes a central (C1) and a peripheral (C2) compartment. Scheme modified according to [16].

The two-compartment approach (Fig. 2b) is predominantly used to describe the pharmacokinetics of an API. In this model, the drug diffuses between two compartments, the central (C1) and the peripheral (C2) one. C1 represents the organs that quickly reach equilibrium with the blood due to strong perfusion. C2 compartment represents less perfused tissues and other areas of the body. Between these and the systemic circulation, equilibrium occurs much more slowly. The rate constants k_{12} and k_{21} denote the distribution and redistribution of the substance between the compartments C1 and C2. The rate constant of absorption is described by k_a and can

only occur to C_1 , just as the elimination k_{10} can also only occur from C_1 . In addition to the one- and two-compartment models, a variety of complex model concepts exist for a more detailed mathematical description, such as three-compartment models [17], physiologically based pharmacokinetic models [18] and the associated advanced compartmental absorption and transit model [19]. Thus, the selection of the most appropriate model depends on the nature of the data and the purpose of the analysis.

1.2.2. Major Pharmacokinetic Parameters

Using NCA and CA calculations, numerous different pharmacokinetic parameters can be derived from the plasma concentration-time curves. The most relevant ones are described in more detail below.

maximum plasma concentration C_{max}

This parameter represents the highest drug concentration reached in plasma. After extravascular administration, it depends on the rate of absorption and can be determined visually from the plasma concentration-time profile. When determined by NCA, C_{max} corresponds to the highest plasma concentration measured. In CA it is determined by the global maximum of the mathematically fitted function [20]. Since C_{max} cannot be determined experimentally following i.v. administration the initial plasma concentration is determined by extrapolation to time zero (C_0) [11].

time of maximum plasma concentration t_{max}

This parameter reflects the time at which the maximum plasma concentration C_{max} is observed and is considered a measure of drug absorption.

terminal plasma half-life $t_{1/2}$

This parameter corresponds to the time interval in which the drug concentration in plasma has decreased by half. Since $t_{1/2}$ controls the degree of drug accumulation, concentration fluctuations and the time to reach equilibrium, it is particularly relevant for multiple dosing regimens [21].

volume of distribution at steady state V_{ss}

This parameter represents as notional variable the apparent volume into which a drug would be distributed based on the dose administered and the subsequently measured plasma concentrations [22]. Although V_{ss} does not represent an actual physiological volume, it can be used to determine the extent of the distribution of the drug from the plasma into the tissues. For accurate determination of V_{ss} , the drug must be completely absorbed and not eliminated prior to reaching systemic circulation. Therefore, V_{ss} is determined after i.v. administration [11].

total body clearance Cl

This parameter expresses the plasma volume which is totally cleared of a drug per unit of time. Cl represents the sum of renal and non-renal clearance. Formally Cl is defined as the ratio of the rate of drug elimination and the related drug concentration [23]. This means that the administered dose must be completely available, which is almost impossible with extravascular administration. Therefore, Cl is determined after i.v. application [11].

bioavailability F

This parameter describes the percentage of active substance that reaches the systemic circulation unchanged after non-parenteral administration. Based on F , prognoses regarding the optimal dosage of an NCE are possible.

1.2.3. Absorption

The absorption of an API is the basic prerequisite for achieving the desired effect. Oral administration is the most common and preferred route. Thus, the gastrointestinal tract (GIT) is the major site of drug absorption and membrane permeation is required. Solubility and dissolution of the compound in the GIT and the intestinal membrane permeability are key factors of oral drug absorption. The rate and extent of drug absorption is affected by the physicochemical properties of the compound, e.g., solubility, hydrophobicity, ionization and molecular weight [24]. The biological and physicochemical conditions of the GIT also influence the absorption and thus F of an orally administered drug. The entire blood supply of the upper GIT first enters the liver

prior reaching the systemic circulation [25]. Hence, metabolic transformation and thus inactivation can occur during the first liver passage via the so-called first-pass effect, which in turn results in a poor F [26].

1.2.4. Distribution

After reaching the systemic circulation, the API is distributed into the various fluids and tissues of the body to its site of action. Both the initiation and the extent of the therapeutic effect are determined by the distribution. This in turn is influenced by the hemodynamic activity of the tissue, passive diffusion across lipid membranes and the presence of carrier-mediated active transport [27]. In addition, distribution can be limited by binding of the API to plasma proteins. According to the free drug hypothesis only unbound drug passes through membranes and exerts its pharmacological effect at the target site of action [28]. Thus, plasma protein binding can influence V_{ss} and reduce the metabolic transformation of the xenobiotic, thereby increasing $t_{1/2}$ and reducing Cl [29]. Furthermore, binding to plasma proteins may reduce efficacy and require changes in the dosing regimen [30]. However, the fraction bound can also serve as a reservoir that releases the drug to maintain equilibrium after excretion of previously unbound fraction from the body [31].

1.2.5. Metabolism

Metabolic conversion, also termed biotransformation, describes the process by which xenobiotics are enzymatically modified to more hydrophilic compounds to increase their excretability from the body. The liver is the main site for drug biotransformation although many organs contain drug metabolising enzymes. In most cases, the resulting biotransformation products are less active than the parent compound or inactive. However, some metabolites may have enhanced activity or toxic effects [32]. In general, drug metabolism reactions can be divided into phase I (Ph1) and phase II (Ph2) reactions. Modifications in Ph1 involve oxidation, reduction, and hydrolysis reactions. Ph2 conversions include the conjugation of highly polar groups, e.g. glucuronic acid, either sequentially to Ph1 reactions or directly to the parent compound. Pharmacokinetic parameters such as F, Cl and $t_{1/2}$ are influenced by the biotransformation of a drug, which in turn affects its efficacy and toxicology.

1.2.5.1. CYP-mediated Metabolism

The cytochrome P450 (CYP) superfamily is the major group of Ph1 drug-metabolising enzymes [33]. They are responsible for the metabolic degradation of 70-80 % of all drugs in clinical use [34]. CYPs are distributed throughout various tissues and organs whereas the liver and small intestine contribute to the maximum extent to the biotransformation [35]. Based on protein content, CYP3A4 is the most abundant isoform in human liver, followed by CYP2E1 and CYP2C9, with approximately 22.1 %, 15.3 % and 14.6 % of total CYPs, respectively [36]. They are membrane-bound and located in the smooth endoplasmatic reticulum. Their major substrates involve sterols, xenobiotics, fatty acids, eicosanoids and vitamins [37]. The chemical modifications include oxidation, sulphoxidation, aromatic hydroxylation, aliphatic hydroxylation, N-dealkylation, O-dealkylation, and deamination. However, CYP-mediated transformation could lead to cancerogenic or toxic products [38]. CYPs belong to the heme proteins containing heme *b* in their catalytic centre [39]. Since they react almost exclusively as monooxygenases, the CYP-mediated oxidation process leads to the addition of one oxygen atom to the parent compound (Fig 3).

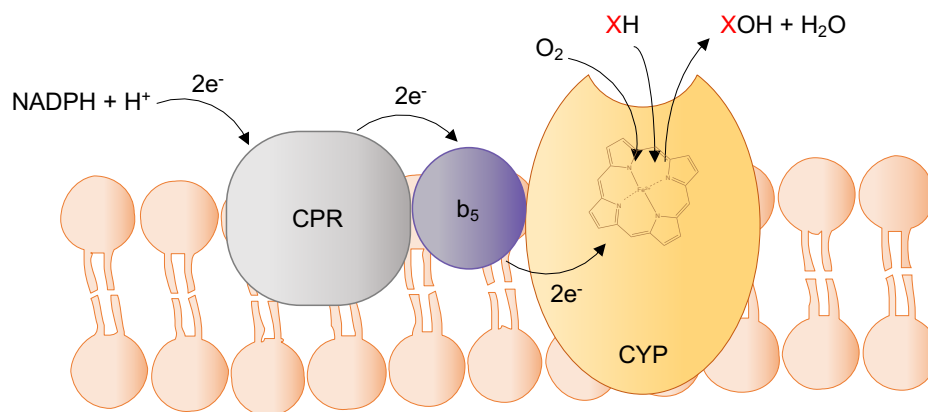


Fig. 3: Schematic representation of the oxidation process of the membrane-bound monooxygenase complex. NADPH-dependent CYP reductase (CPR) and cytochrome b_5 reductase act as electron donor and intermediate electron carrier, respectively, whereby CYP-mediated conversion of the substrate (XH) with oxygen to oxidised metabolite (XOH) and water occurs. Graphic adapted from [40].

The biotransformation reaction requires cofactors such as nicotinamide adenine dinucleotide phosphate (NADPH), NADPH-CYP reductase (CPR) and cytochrome b_5 reductase. Thus, the functional activity of CYPs is affected by these regulators. This leads to inter- and intraindividual variability regarding metabolic transformation as well as elimination of drugs which may result in different responses to treatment [41].

Induction of mRNA expression and associated increase in protein levels leads to enhanced CYP-mediated metabolic degradation and thus lower drug exposure. In contrast, inhibition of CYP enzymes by endogenous and exogenous substances can lead to toxicity, as substrate concentrations in the blood increase dramatically due to lack of degradation [35].

1.2.5.2. UGT-mediated Metabolism

Glucuronidation of human endogenous and exogenous compounds is a major Phase 2 metabolism pathway. It requires the cofactor uridine diphosphate glucuronic acid (UDPGA) and is catalysed by UDP-glucuronosyltransferases (UGTs). The conjugation with glucuronic acid leads to inactivated products which are more hydrophilic and can thus be excreted easily via urine or bile [35]. An exception are acyl glucuronides, which are toxic metabolites of most carboxylic acid drugs [42]. In addition to the formation of toxic conjugation products, an API glucuronide may undergo the so-called enterohepatic circulation [43]. This could occur when the resulting β -glucuronides are excreted into bile or intestine. There they can be hydrolysed to the aglycon by the intestinal microbiome and finally reabsorbed. Formally, glucuronidation is an S_N2 reaction that generally occurs at electron-rich nucleophilic heteroatom such as oxygen, nitrogen, or sulfur [44] (Fig 4).

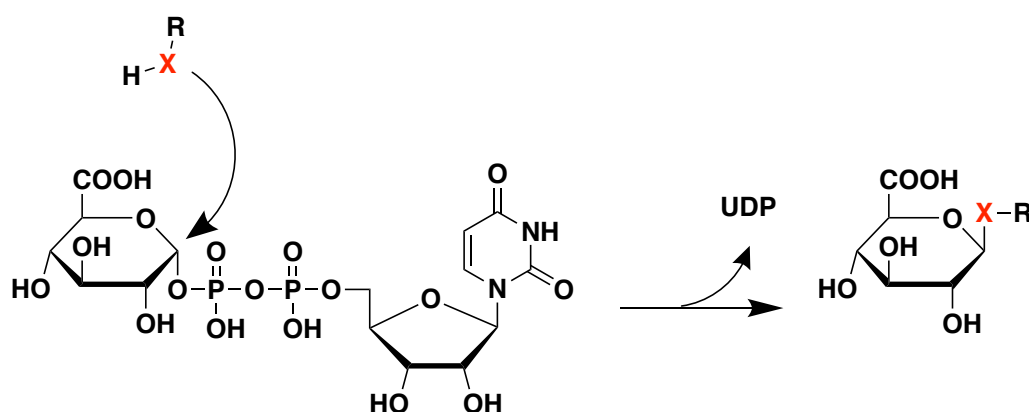


Fig. 4: Glucuronic acid transfer of UDPGA to the substrate resulting in the release of UDP and formation of the corresponding β -glucuronide [45].

UGT proteins are localized on the luminal side of the endoplasmic reticulum with a transmembrane domain [46]. Based on evolutionary divergence, mammalian UGTs are divided into two families UGT1 and UGT2. These are further divided into three

subfamilies UGT1A, UGT2A and UGT2B [47]. According to current knowledge, these include nine, three and seven types of functional isoforms, respectively. The substrate and inhibitor specificity of each form is distinct but partially overlapping and they metabolise a wide range of compounds [48]. Both the amount of cofactor and enzyme available control the functional conjugation activity of the UGTs. Some compounds, *e.g.*, phenobarbital and rifampin, are known to induce the expression levels of UGTs *in vivo*, thus decreasing drug exposure [35]. In addition, the presence of isoform-specific inhibitors as well as genetic polymorphisms or even certain diseases can lead to altered UGT activities [49].

1.2.6. Excretion

The final step in the ADME process is the removal of an administered drug from the body and is termed elimination. This process involves the metabolic conversion and the physical excretion [50]. Lipophilic compounds are transformed to more polar, water-soluble molecules to increase their excretion efficacy. There are two major routes for xenobiotic and metabolite removal from the body. The kidneys are the main organs for eliminating water-soluble compounds. Polar or charged substances with only little plasma protein binding are primarily excreted by glomerular filtration. Some drugs are removed from plasma via secretion by active transport mechanisms. The extent of renal excretion is not only dependent on the properties of the drug but also on the urine pH. Some compounds and their metabolites are extensively excreted into the bile which represents the second major route. As they are transported through the biliary epithelium against a concentration gradient, active secretory transport is needed. When drug concentrations in plasma are high, secretory transport may reach an upper limit and xenobiotics with similar physicochemical properties can compete for elimination. Drugs with a molecular weight of more than 300 g/mol and with both polar and lipophilic groups are more likely to be excreted into the bile [51]. The active transport mechanisms of the liver have an inverse relationship to the mechanisms of the kidneys since the substances excreted possess opposing properties. Thus, the renal and biliary excretory pathways seem to work complementary to achieve the elimination of as many xenobiotics as possible [27]. In addition to renal and biliary excretion, some drugs can also be excreted through the lungs, saliva, sweat, tears, semen, and breast milk [52]. Pharmacokinetically, elimination is expressed by Cl and

$t_{1/2}$. Systemic Cl describes the sum of the individual elimination processes, e.g., renal and hepatic excretion.

1.3. Enzyme Kinetics

Enzymes catalyse chemical reactions in organisms by lowering the activation energy. The reversible binding of the substrate to the active centre of the enzyme first forms an enzyme-substrate complex, which subsequently decomposes irreversibly into the enzyme and the product [53]. The rate of an enzymatic reaction also depends on the substrate concentration. Generally, the reaction velocity increases with increasing substrate concentration until a maximum saturation value V_{\max} is reached. At V_{\max} all enzyme molecules are saturated with substrate. A plot of the conversion rate over the substrate concentration usually results in a hyperbolic curve, which is described by the Michaelis-Menten equation (Eq. 1) [54]. The K_m value, which is referred to as Michaelis-Menten constant, indicates the substrate concentration at which the half-maximum conversion rate is achieved. The lower K_m , the higher the substrate-enzyme affinity. The conversion rate V results from the amount of metabolite produced per unit of time.

$$V = \frac{V_{\max} \cdot [S]}{K_m + [S]} \quad (\text{Eq. 1})$$

V	reaction velocity
V_{\max}	maximum reaction velocity
$[S]$	substrate concentration
K_m	Michaelis-Menten constant

The substrate saturation curve is obtained by determining the conversion rate at different substrate and constant enzyme concentrations. However, V_{\max} cannot be derived accurately from the Michaelis-Menten plot. Consequently, K_m cannot be determined exactly either. By linear regression, the kinetic parameters can be obtained from the intersections of the straight line with the coordinate axes or from their slope. Due to the modified coordinate axes, however, these values can be strongly subject to error [55]. The most widely used representation is the double reciprocal plot according to Lineweaver-Burk (Eq. 2) [56]. A disadvantage of this reciprocal plot is that

around the axis cross a compression of the data, and expansion in the opposite region exists.

$$\frac{1}{V} = \frac{K_m}{V_{\max}} \cdot \frac{1}{[S]} + \frac{1}{V_{\max}} \quad (\text{Eq. 2})$$

In addition to a hyperbolic shape of the substrate saturation curve, several deviating curve shapes can occur. This is referred to as atypical or non-Michaelis-Menten kinetics and may be because enzymes often have several catalytic centres. The binding of a substrate molecule can lead to a conformational change, which can result in a changed affinity of neighbouring catalytic subunits. Furthermore, the conversion rate can slow down in the presence of high substrate concentrations after an initial increase. This results from inhibition of the conversion by the substrate. In this case, the calculated maximum conversion rate is only a fictitious value. Substrate inhibition is a special case of non-competitive inhibition, since another substrate molecule, acting as an inhibitor, binds to the enzyme-substrate complex [55].

1.4. Drug Interactions

1.4.1. Enzyme Inhibition

Enzyme inhibition is the negative influence of an enzymatic reaction by an inhibitor. The reaction rate is decreased, resulting in reduced or completely blocked product formation. Depending on the binding of the inhibitor to the enzyme, the type of inhibition can be divided into reversible and irreversible. During reversible inhibition, the inhibitor binds to a specific binding site on the enzyme by forming non-covalent bonds. Reversible inhibition types include competitive (a), un-competitive (b) and mixed inhibition (c) as shown in figure 5. In competitive inhibition, the substrate and the inhibitor compete for the same binding site on the enzyme, usually the active site. In uncompetitive inhibition, the inhibitor binds to a different binding site than the substrate, but only to the enzyme-substrate complex. In the mixed inhibition type, the inhibitor also binds at a site other than the active site. However, the binding can be both at the free enzyme and the enzyme-substrate complex [57].

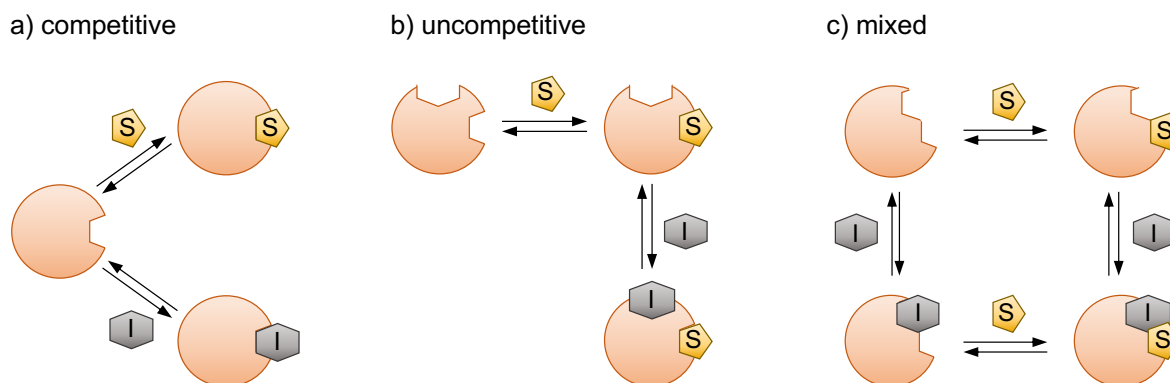


Fig. 5: Types of reversible enzyme inhibition. a) Competitive inhibitors bind to the active site. b) Uncompetitive inhibitors bind to a different site, but only to the enzyme-substrate complex. c) Mixed inhibitors also bind to a site other than the active site but can bind to both the free enzyme and the enzyme-substrate complex. Graphic adapted from [57]. S = substrate; I = inhibitor

In irreversible inhibition, there is a covalent bond between the inhibitor and the group of the enzyme that is essential for its function. This leads to permanent inactivation of the enzyme. Thus, to restore the activity, the enzyme must be re-synthesized [58]. The inhibitor concentration at which the half-maximal inhibitory effect is achieved (IC_{50}) serves as value for the potency of inhibition.

1.4.2. Allosteric Regulation

Allosteric regulation is a further mechanism for controlling enzymatic activity. The regulatory molecule binds outside the active site, at the so-called allosteric site, as described for uncompetitive or mixed inhibition. This binding leads to a conformational change of the active site, which can result in both reduced (allosteric inhibition) and increased (allosteric activation) enzyme activity [59]. Usually, allosteric enzymes consist of several subunits with active and regulatory binding sites. In some cases, the regulatory and active centres may even be present on different subunits. Since the allosteric modulator differs from the substrate, this is also referred to as a heterotropic effect. Allosteric centres are often located where the subunits are in contact with each other [55].

1.4.3. Drug-Drug Interactions

The impact of a drug on the pharmacological behaviour of a co-administered drug is referred to as drug-drug interaction (DDI). The investigation and knowledge about

potential DDIs are becoming increasingly important due to the increased use of polypharmacy or combined therapy, for example in cancer. They are a significant concern since substantial changes in blood and tissue concentration of the drug or metabolite could alter its safety and efficacy profile. Interactions with metabolising enzymes or drug transporters account for the majority of clinically relevant DDIs [60]. The biotransformation of a drug can be reduced by inhibition of the enzymes involved, which can lead to increased exposure and associated side effects. In contrast, induction of the metabolising enzymes results in increased degradation. This can lead to a loss of the therapeutic effect but also in the enhanced formation of toxic metabolites. Interactions related to plasma protein binding, food effects, pH effects and others may also occur.

1.5. Instrumental Analytic

1.5.1. Electrospray Ionisation Mass Spectrometry

As a new ionisation technique, electrospray ionisation (ESI) mass spectrometry (MS) was developed first by M. Dole [61] and established by J. Fenn [62], who received the Nobel Prize in Chemistry 2002. In contrast to the former electron impact ionisation, ESI is a much softer method. This means that significantly fewer or no fragment ions occur. Another characteristic is that the ESI process is performed under atmospheric pressure. The analysis of non-volatile or thermally labile substances such as proteins, peptides and drugs is the main field of application for ESI-MS [63, 64]. The ESI process allows coupling of a liquid chromatography (LC) system to a mass selective detector. This setup is referred to as LC-MS coupling.

The analyte solution is introduced into the electrospray chamber through a stainless-steel capillary and sprayed there using high-purity nitrogen. A voltage of several kV is applied between the heated capillary and the inlet of the MS, resulting in charge separation within the droplets. With the help of the continuous nitrogen flow, the droplet size is reduced by evaporation of the solvent. This increases the charge density on the drop surface until the stability limit, the so-called Rayleigh limit, is reached. If this is exceeded, Coulomb explosions cause spontaneous decay and the formation of many smaller charged droplets. This is repeated until charged droplets

are formed that contain only one analyte molecule. Collisions with nitrogen molecules and the resulting desolvation lead to the formation of gaseous ions.

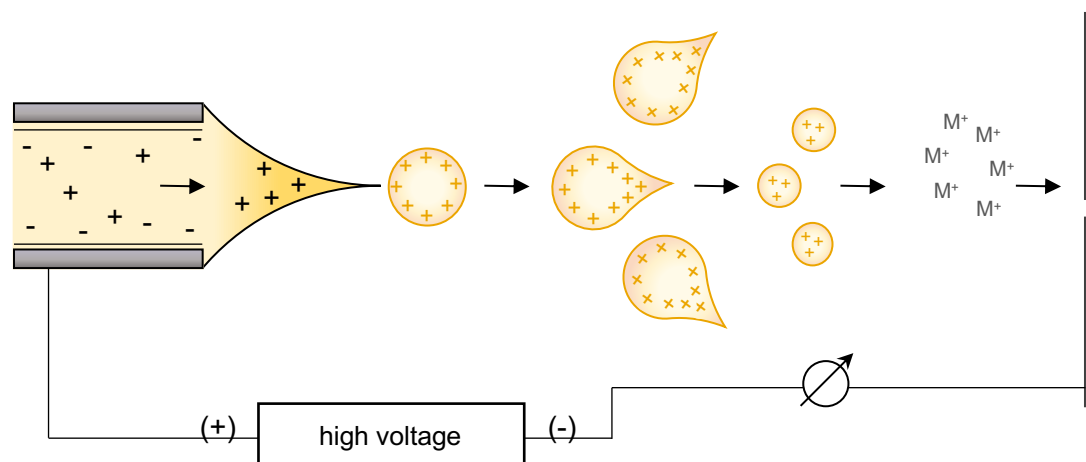


Fig. 6: Schematic representation of the ESI process in positive mode, modified according to [65, 66].

Figure 6 schematically shows the mechanism of the ESI process. Following ionisation, the generated ions are detected with a mass-selective analyser. Among the most common are the ion trap, the time-of-flight analyser as well as the single- and triple-quadrupole. The latter is described in more detail below.

1.5.2. Quadrupole Mass Analyser

The mass to charge ratio (m/z) of the introduced ions influences their trajectory through an electric field. This is the main principle of ion separation in MS. A quadrupole analyser is constructed from four parallel cylindrical rod electrodes. An alternating current potential (V) at a fixed frequency ω in the radio-frequency range is applied to the diagonally opposite metal rods. In addition, on one pair a positive direct current potential U is applied while a negative potential is applied on the other pair of rods. In this electric field composed by a constant field and a quadrupolar alternating field, the ions are excited to oscillating trajectories. These are stable for ions whose m/z corresponds to the specific ratio of ω and U/V . Ions whose trajectories are unstable are discharged by collision with the rods and thus do not reach the detector. To cover the entire mass range, the applied electric field is varied accordingly. This can either be done by varying ω at a constant U/V or by scanning U and V at a constant ω .

The further development of the single quadrupole is the tandem MS (MS/MS) which combines three single quadrupoles. The middle quadrupole can be filled with collision gas (argon or nitrogen) and used as collision cell. The other quadrupoles are used for selection and analysis of the m/z ratios (Fig. 7). This setup provides the possibility to obtain additional mass spectra information through various scan modes.

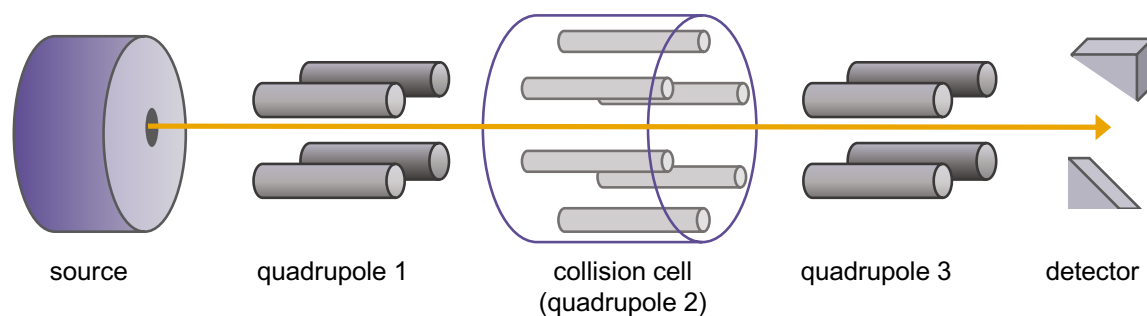


Fig. 7: Schematic diagram of a triple quadrupole system. Modified according to [65, 67].

The full scan is the simplest analysis mode. In this scanning mode, the use of the triple quadrupole corresponds to that of a single quadrupole. Quadrupole 1 is used for analysis, while quadrupole 3 does not select any ions. In the product or daughter scan mode, a fixed m/z ratio (precursor ion) is filtered in the first mass analyser. Following fragmentation in the second quadrupole by collision-induced disassociation, the resulting fragment ions (product ions) are analysed by the third quadrupole. The precursor or parent scan can be seen as a reversal of this mode. The first quadrupole operates in scan mode while the third quadrupole analyses product ions with a specific m/z ratio. This provides information on which analyte yields a specific fragment. The most selective and sensitive of the measuring modes mentioned is the selective or multiple reaction monitoring (MRM) mode. The first analyser filters a specific mass, which is fragmented in the collision cell. The third quadrupole selects one or more defined fragments associated with the analyte. However, the substance to be analysed and its fragments must be known. Therefore, the MRM mode is mainly suitable for quantification.

1.6. Hepatocellular Carcinoma

In 2020, primary liver cancer was one of the most frequently diagnosed cancer globally and a major cause of cancer-related deaths. The disease and mortality rates are two to three times higher in men than in women, but the relative 5-year survival rate is

about 15 % in both genders [68]. Hepatocellular carcinoma (HCC) is the most common form of primary liver cancer and accounts for about 90 % of all cases [69]. The main risk factors for developing HCC include existing cirrhosis, chronic hepatitis B and hepatitis C infection, aflatoxin-contaminated foods, type 2 diabetes, excess body weight, profuse alcohol intake and smoking [70]. Thus, 1st world health problems, mainly due to lifestyle in the western world, play a role in the development and increasing importance of HCC. To date, the most effective and in general curative treatment for early-stage HCC patients is surgery such as resection or transplantation. However, this can only be performed in 20 % of all patients, as the majority already have advanced tumour development, usually with additional liver disease [71]. At an advanced stage, when diagnosis usually first occurs, there are few treatment options available with very low and variable survival rates [72]. For years, the only first-line systemic therapy approved for unresectable HCC was the multikinase inhibitor sorafenib (SRF). Its mechanism of action includes the inhibition of B-Raf and the vascular endothelial growth factor receptor (VEGFR) which are involved in tumour angiogenesis and proliferation [73],[74]. After treatment failure with SRF, two other agents are available in Germany as second-line therapy: regorafenib (RGF) and cabozantinib. However, the overall survival rate of 10.7 months and 30.9 weeks after SRF therapy and subsequent RGF treatment, respectively, is very low [75] and accompanied by severe side effects [76]. Only recently lenvatinib has been approved for the first-line treatment of HCC, and trials of combination therapies of atezolizumab plus bevacizumab are still being performed [77]. The latter showed an overall survival at 12 months of 67.2 % compared to 54.6 % with SRF [78]. This illustrates the extremely limited survival benefits of these approaches. Thus, HCC remains a severe disease with high level of suffering and limited treatment options, highlighting the urgency of new therapeutic approaches.

1.7. Protein Kinase Inhibitors

So far, 535 human protein kinases have been discovered [79] and over 85 % of the kinome is linked to human diseases or developmental disorders [80]. Thus, the protein kinase enzyme family has become one of the most important drug targets over the past 25 years and concerns about potential toxicity or lack of selectivity of kinase inhibitors have not been confirmed so far [81]. Currently (March 2021) there are 62

FDA-approved protein kinase inhibitors. 52 of these drugs are prescribed for the treatment of solid tumours including breast, lung, and colon [82]. In addition to the treatment of cancer, there are numerous other therapeutic indications for the application of kinase inhibitors, such as inflammation, neurodegenerative diseases, tropical diseases, or antiviral, including SARS-CoV2 [81].

1.7.1. Sorafenib

The oral multikinase inhibitor SRF targets, as given in figure 8, RAF serine/threonine kinases which suppresses endothelial and tumoral cell proliferation [83]. SRF prevents tumour angiogenesis by inhibition of platelet-derived growth factor receptor (PDGFR), VEGFR, hepatocyte factor receptor and other proteins [84].

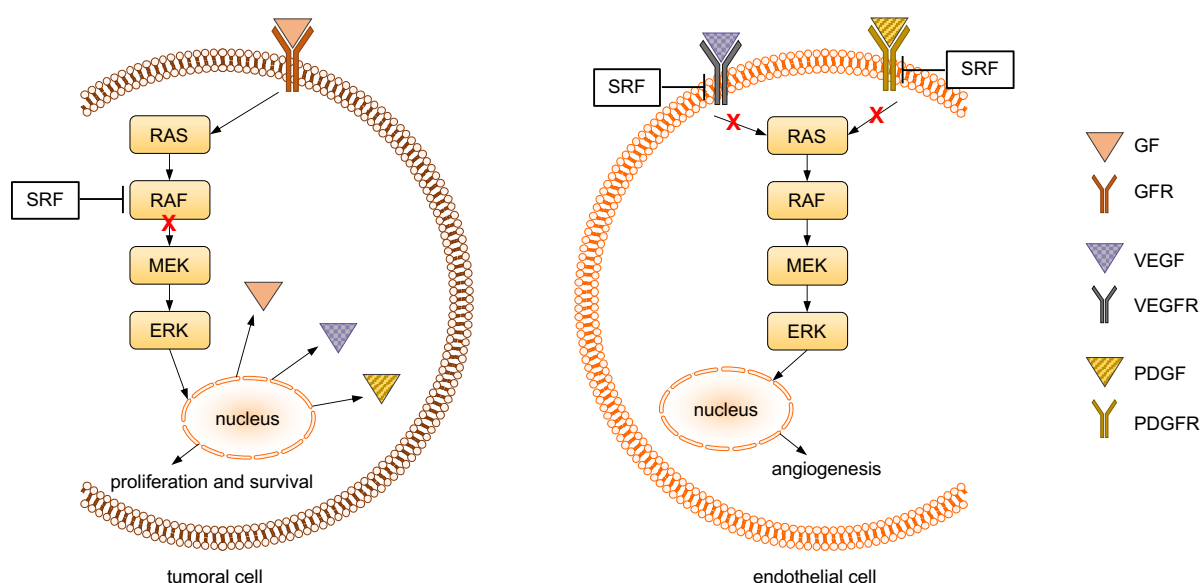


Fig. 8: Schematic representation of SRF's cellular targets and mechanism of action in tumour cells and endothelial cells. Blockage of tyrosine receptor signalling (e.g. VEGFR and PDGFR) and inhibition of downstream RAF serine/threonine kinase activity by SRF leads, *inter alia*, to suppressed tumoral cell proliferation and angiogenesis. Graphic modified from [83, 85]. GF = growth factor; GFR = GF receptor

In addition to the treatment of unresectable HCC, SRF is also approved for the therapy of advanced renal cell carcinoma and differentiated thyroid carcinoma [86]. However, strong severe side effects occur during treatment, which is why therapy with SRF must be discontinued in 20 % of patients within one month [87]. In addition, therapy resistance usually develops within six months of treatment [88].

During clinical studies the pharmacokinetic parameters of SRF exhibited large interindividual variability. SRF is highly bound (99 %) to plasma proteins [89] and its

$t_{1/2}$ ranges from 25 to 38 h [90]. SRF undergoes enterohepatic circulation, and the majority is eliminated in the faeces [91]. In human, SRF is subject to two important biotransformation pathways which occur mainly in the liver. As shown in figure 9, the conversion to its major oxidative metabolites SRF-N-oxide (NOX), N-hydroxymethyl-SRF (HOM) and N-desmethyl-SRF (DES) is mediated by CYP3A4 [92]. Glucuronidation reaction is catalysed by UGT1A9 and results mainly in SRF-N-glucuronide (SRF-N-Glc). The main circulating metabolite in plasma is NOX, which is known to be pharmaceutically active [93]. It is further minor metabolised to HOM-NOX, DES-NOX and glucuronidated to NOX-Glc [94]. Another secondary biotransformation pathway is the reduction of NOX to SRF, in which CYP2B6 and CYP1A1 are involved [93]. Although not a substrate, SRF inhibits the activities of CYP2B6, CYP2C8, CYP2C9 and UGT1A1 *in vitro* [94].

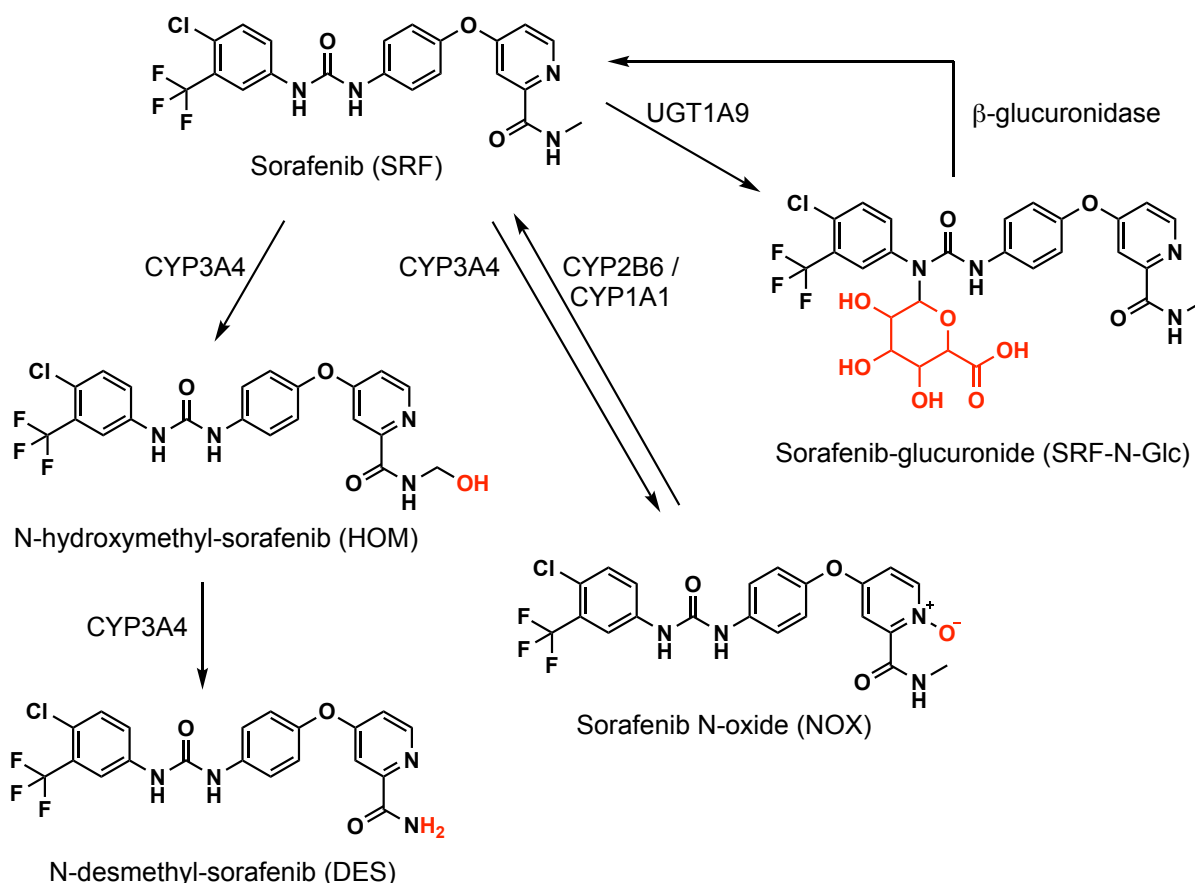


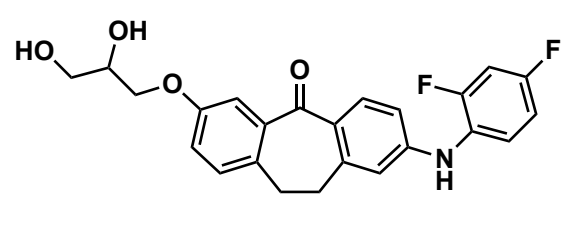
Fig. 9: Biotransformation pathway of SRF and its major metabolites NOX, HOM, DES and SRF-N-Glc. Scheme modified according to [93, 95].

Some SRF metabolites seem to contribute to the SRF-related adverse effects. For instance, the major circulating NOX has less kinase inhibition selectivity than SRF [96] and is associated with the SRF-induced skin toxicity [97]. In addition, reduction of NOX

back to SRF may result in increased SRF exposure which could in turn enable adverse effects [93]. Since SRF-N-Glc is subject to enterohepatic circulation [98], its cleavage to the parent compound and reuptake may also lead to higher and longer SRF-exposure. The hypothetic cause of SRF-induced diarrhea is the glucuronidation of the SRF-carboxylic acid [99]. This is the major metabolite of SRF found in feces but hardly circulates in plasma [100]. In addition to biotransformation, gender also appears to be a risk factor for the development of severe side effects. Women are generally overexposed to SRF due to their lower average body weight and thus reduced SRF-clearance [99].

1.7.2. Skepinone-L

Skepinone-L (SKL) is a small molecule (Fig. 10) inhibitor of p38 α mitogen-activated protein kinase (MAPK). This kinase is one of the four members of the p38 MAPK family, also known as stress-activated serine/threonine-specific kinases. They are involved in signalling cascades and are activated by inflammatory cytokines and environmental stresses such as oxidative stress, UV radiation, mechanical wear, heat shock or osmotic shock [101]. Their activation results in multiple biological effects like the synthesis of proinflammatory cytokines which could cause severe diseases [102]. These cytokines include interleukin 1 β , tumour necrosis factor α , and the oncogenic activating transcription factor 2 [103]. Further, p38 α MAPK is involved in cell cycle regulation and impacts in normal cells, *inter alia*, senescence and apoptosis but increases cell proliferation in cancer cells [104]. This explains the high interest in p38 α MAPK as a therapeutic target [105]. A specific inhibition with sufficiently high potency is required to investigate the p38 α MAPK signalling pathways and to silence them in the event of dysfunction or misregulation [106].

	probe criteria	goal	SKL
	inhibitor potency IC ₅₀	<100 nM	5 nM

	selectivity within target family	> 30 fold	> 1,000 fold

Fig. 10: Structure and overview of probe criteria and achievements by SKL. Adapted and modified from [107].

SKL more than meets these requirements, which is why it is widely used as a valuable probe for chemical biology research. For example, the precise role of p38 MAPK in platelet activation and thrombus formation was elucidated using SKL [108]. Moreover, targeted inhibition of p38 α MAPK represents a promising therapeutic approach regarding treatments for Alzheimer's disease [109] and rheumatoid arthritis [110]. Thus, the therapeutic possibilities with the help of SKL appear to be manifold on the one hand and far from limited on the other.

1.8. Combinatorial Treatment with Skepinone-L and Sorafenib

The options for the treatment of HCC are currently almost exclusively limited to SRF. Although this therapy significantly increases the median overall survival, the advantage averages only 2.8 months [76]. Furthermore, its efficacy is short-lived due to acquired resistance to therapy. Rudalska, et al. [104] were able to identify a mechanism of SRF resistance in HCC by performing an *in vivo* RNA interference screening. Hence an alternative pathway through p38 α MAPK-dependent activation (Fig. 11) of further signalling proteins was detected. This escape mechanism seems to play a key role in SRF resistance in both mouse and human liver cancer.

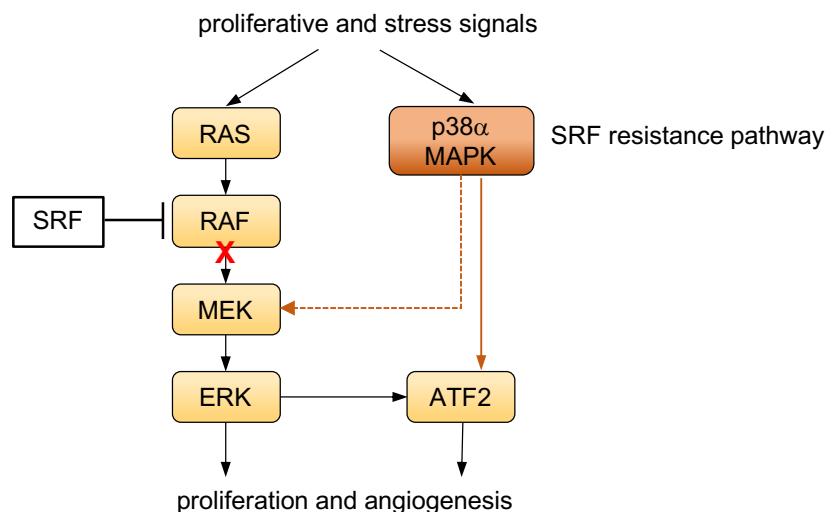


Fig. 11: Scheme representing the involvement of p38aMAPK in the RAF-MEK-ERK signalling pathway in SRF sensitivity and resistance in HCC. Adapted and modified from [104].

Due to its highly selective and potent inhibitory activity against p38 α MAPK, SKL was combined with SRF. Through this combinatory therapy, Rudalska et al. were able to demonstrate reduced proliferation of HCC *in vivo* and significantly prolonged survival

of tumour-bearing mice. In addition, inhibition of p38 α MAPK in combination with SRF led to restoration of SRF sensitivity in SRF-resistant tumours and thus overcoming therapy resistance. As part of the publication by Rudalska et al., the weight development of the mice treated with SRF plus SKL was also examined. Weight reduction as an indicator of potential adverse drug effects was not observed. Thus, a combination therapy of SRF with SKL-mediated inhibition of p38 α MAPK represents a promising approach for the treatment of late-stage HCC, even in the presence of existing SRF resistance. However, SKL was still in preclinical testing and its pharmacokinetic properties need to be fully investigated before clinical trials can be initiated.

2. AIM OF THE WORK

The prognosis of late-stage HCC is currently very poor, especially if no surgical treatment of the carcinoma is possible. Current drug treatment options are almost exclusively limited to the multikinase inhibitor SRF. Although this significantly increases the median overall survival, its efficacy is only short-lived due to acquired resistance to therapy. Rudalska et al. [104] were able to show that a combination of SRF with the inhibition of p38 α MAPK represents a promising approach to overcome acquired drug resistance. As SKL is a highly potent inhibitor of p38 α MAPK with outstanding selectivity [111], combination therapy of SKL with SRF is being pursued for the treatment of HCC in humans.

However, little is known about the pharmacokinetic behaviour of SKL both *in vitro* and *in vivo*. In addition, there is a lack of information about possible interactions of SRF and SKL. As described in the introduction, the approval of an NCE fails predominantly due to insufficient pharmacokinetic properties [8]. Aim of the present thesis is therefore to determine the ADME profile of SKL and to investigate potential DDIs with SRF. This serves to exclude that the desired combination therapy with SKL and SRF might fail in humans due to an unfavourable pharmacokinetic profile of SKL or severe DDIs with SRF. For this purpose, pharmacokinetic studies of SKL and SRF were performed externally in different pre-clinical animal species. These shall be analysed with an LC-MS method to be developed and validated to quantify SKL and SRF in plasma of

those species. The accurate determination of SKL and SRF must be possible both individually and simultaneously over a wide range of concentrations. The developed method will enable to analyse the plasma samples and subsequently calculate the pharmacokinetic parameters of SKL and SRF. Besides, possible factors that could influence the pharmacokinetic behaviour of SKL *in vivo* are to be examined more closely and for mutual influence with SRF.

Furthermore, the metabolic transformation of SKL mediated by different microsomal enzyme families of different species needs to be elucidated and any metabolites formed shall be identified. Moreover, the influence of SRF on the biotransformation of SKL *in vitro*, and vice versa, will be investigated, including the identification of the involved enzymes. Lastly, the pathway by which SKL and its possible metabolites are finally removed from the organism should be determined.

Schematic representation of the aim of the thesis:

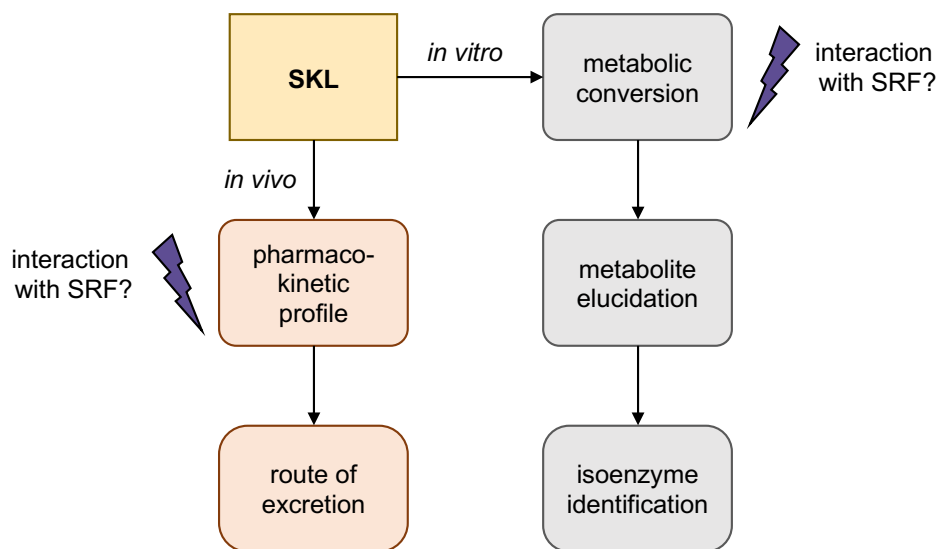


Fig. 12: Comprehensive presentation of the objectives of the thesis.

3. RESULTS AND DISCUSSION

3.1. Development of the Analytical Method

An analytical method was needed to investigate the pharmacokinetic behaviour of SKL in different animal species. Therefore, a reliable and robust method which is simple and fast to implement had to be developed. In addition, it should exhibit reproducibility, high selectivity and sensitivity. A fast sample preparation should enable the simultaneous qualification as well as quantification of compounds.

High selectivity and sensitivity of the developed method was achieved by using an LC-device as separation module coupled to an MS as detection unit. Thus, it is possible to adapt the developed method to new compounds by small changes of the LC- and MS-parameters, like gradient modifications or ion selection. A triple quadrupole MS as a detection unit is suitable for wide range quantification. By selecting substance specific product- and fragment-ions it is possible to gain a maximum of selectivity and sensitivity. Reproducibility of a new analytical method also depends on the selected separation column. Since the substances to be analysed are lipophilic small molecules, a hydrophobic stationary phase is particularly suitable for their chromatographic separation. The phase particles of the selected separation column consist of n-octadecylsilyl moieties covalently bonded to silica gel.

The requirements for a fast and simple sample preparation that is also applicable for small sample volumes were realised by performing a protein precipitation with an organic solvent. Since all analytes are soluble in acetonitrile (ACN) [112] in the required concentrations, ACN was chosen as precipitation solvent. ACN has additional advantages regarding the chromatographic separation such as shorter analyte retention due to higher elution strength compared to methanol [113, 114]. In addition, acetonitrile/water mixes have a low viscosity, resulting in lower back pressure, which puts less stress on the LC system, including the column.

3.1.1. Description of the Developed Method

With the developed analytical method, which is described in detail below, it was possible to qualify and quantify simultaneously SKL and SRF in plasma of various animal species as well as in human plasma. Furthermore, three Ph1 metabolites of SRF (NOX, HOM and DES) can be determined, although their analysis and quantification were not included in the validation of the method. Nevertheless, none of them are essential to examine the pharmacokinetic profile of SKL.

The triple quadrupole was used in the multiple reaction monitoring (MRM) scan mode for increased sensitivity and selectivity. This specific scan mode generates product ions from defined precursor ions by collision induced dissociation. The corresponding peak-area-ratios (PAR) of the analyte and the internal standard (ISTD) were used for quantification. The substance used as ISTD should be structurally similar to the analyte. Unless it is not isotopically labelled, it should not coelute to prevent mass spectrometric interferences, e.g., an isobaric overlap. Compound FS112, which is a structural analogue of SKL (Fig. 13), fulfils these requirements and was therefore selected as ISTD. Chromatographic separation was performed on a reversed phase C18 column (Symmetry®, 5 µm, 4.6 x 150 mm) using a constant eluent composition. The isocratic elution enabled a quick analysis time of total 7.5 min, therefore the first two minutes of each run were directly transferred to the waste. This step was necessary to ensure that any remaining but unwanted plasma or sample components do not contaminate the MS ion source, thus avoiding any ion suppression. Further

chromatographic conditions are given in detail in section 2.2 of chapter 5 (Material and Methods).

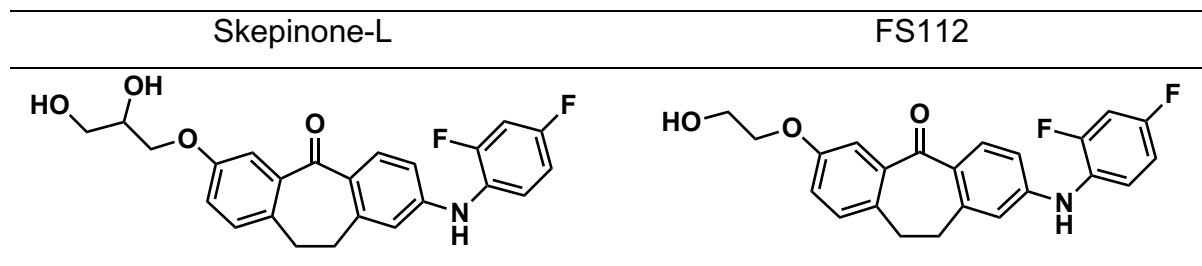


Fig. 13: Structures of analyte SKL and internal standard FS112.

The mass spectrometric detection was optimized by direct injection of each analyte separately and all combined with a syringe pump, taking the method specific eluent composition into account. This experimental setup enabled the determination of the optimal settings for the MS-parameter such as capillary and cone voltage, source and desolvation temperature as well as cone and desolvation gas flow.

Further instrumental adjustments for cone voltage, collision energy and dwell-time were performed. These are compound specific and contribute to gain the highest signal intensity and resolution. For each analyte the monitored pair of m/z values in the MRM mode consisted of the precursor ion $[M+H]^+$ and the corresponding most intense daughter ion. These pairs and adjusted instrumental parameters are displayed in table 75 (Ch. 5.2.2). Illustrative mass spectra, acquired in ESI(+) full scan as well as in daughter scan mode of SKL, SRF and ISTD are presented in the following figures 14 to 19.

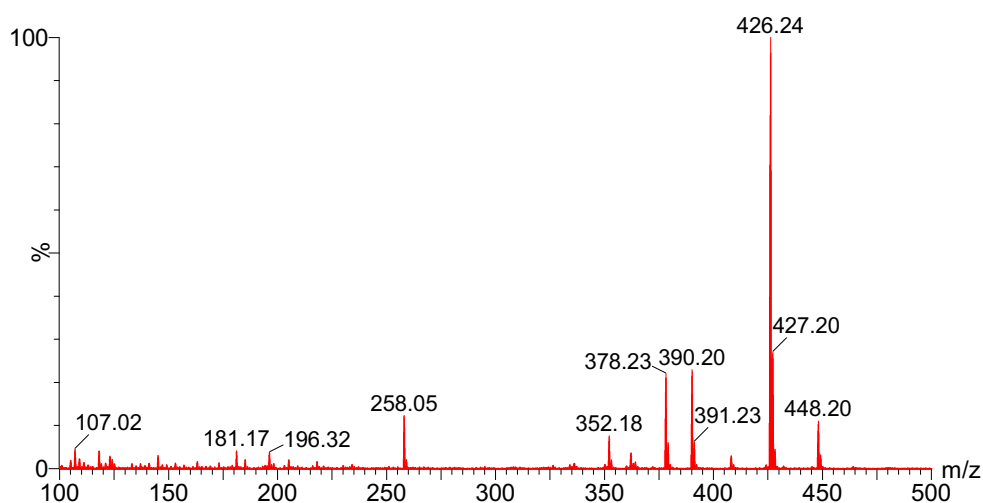


Fig. 14: ESI(+) mass spectrum of SKL (425.43 g/mol), with base peak at m/z 426.2 for $[M+H]^+$. Acquired during method development by application of the full scan mode.

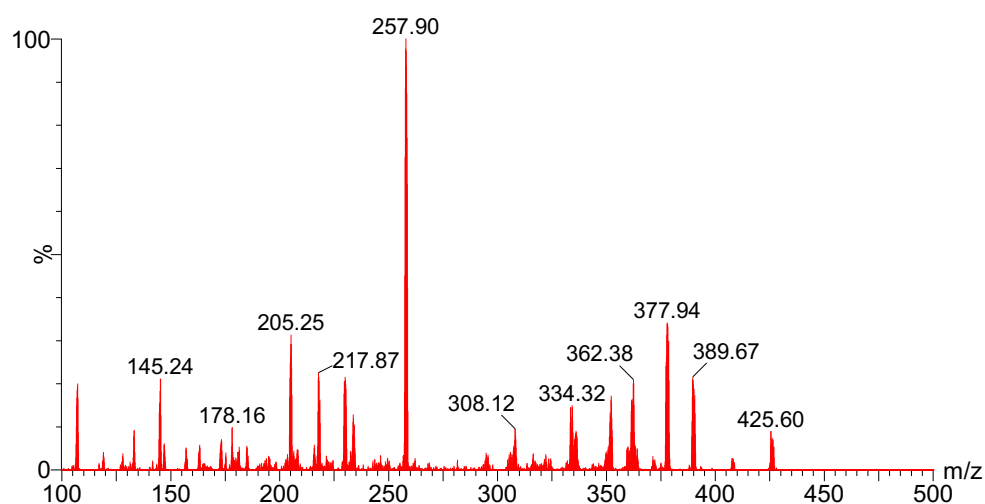


Fig. 15: Daughter ion mass spectrum of SKL, showing a prominent fragment ion at m/z 257.9. Acquired during method development by application of collision induced dissociation.

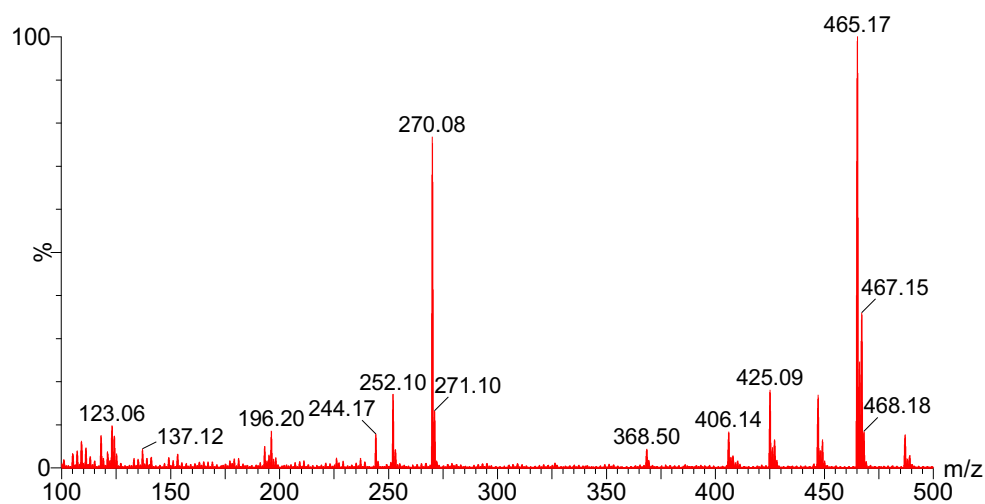


Fig. 16: ESI(+) mass spectrum of SRF (464.83 g/mol), with base peak at m/z 465.2 for $[M+H]^+$. Acquired during method development by application of the full scan mode.

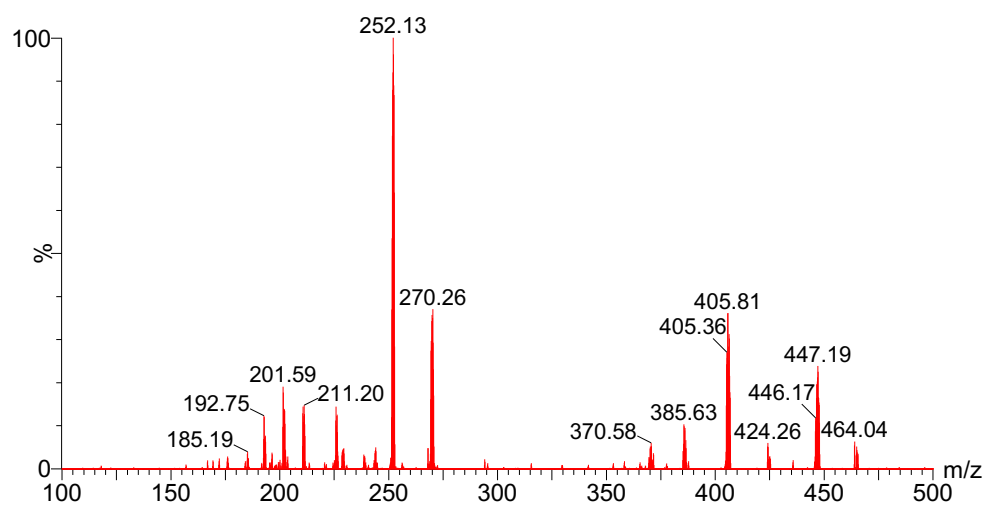


Fig. 17: Daughter ion mass spectrum of SRF, showing a prominent fragment ion at m/z 252.1. Acquired during method development by application of collision induced dissociation.

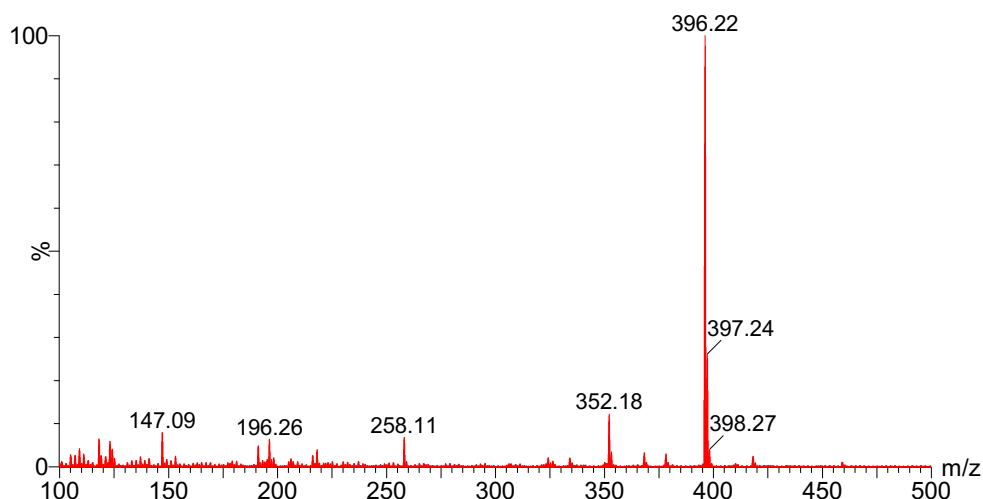


Fig. 18: ESI(+)-mass spectrum of ISTD FS112 (395.41 g/mol), with base peak at m/z 396.2 for $[M+H]^+$. Acquired during method development by application of the full scan mode.

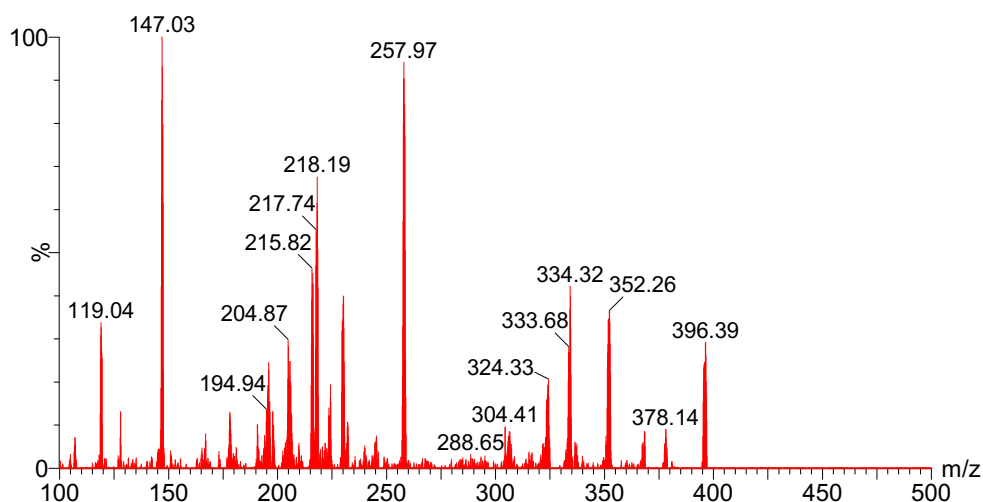


Fig. 19: Daughter ion mass spectrum of ISTD FS112, showing a prominent fragment ion at m/z 258.0. Acquired during method development by application of collision induced dissociation.

Unfortunately, the structures of the resulting fragments of SKL and the ISTD could not be clearly elucidated. The chemical formula of the daughter ion m/z 257.9 used for qualitative and quantitative analysis is possibly $C_{15}H_9F_2NO$. Further fragment analyses of dibenzosuberones suggest that the structure of this formed fragment ion contains the 2,4-difluoro-N-phenylaniline moiety. The m/z of the generated SRF fragments are consistent with descriptions from the literature. Yu and Liang [115] were able to elucidate both the structures and the fragmentation pathway of SRF.

3.2. Validation of the Analytical Method

The developed method to study the pharmacokinetic behaviour of SKL in different animal species was validated according to the FDA Guidance for Industry, Bioanalytical Method Validation [116]. The validation was performed in plasma of rats (Sprague Dawley), dogs (beagle) and monkeys (Cynomolgus). Although due to poor availability of monkey plasma, most of the validation was performed in human plasma, which was prepared freshly from various human blood samples. The quantification of SRF in the presence or absence of SKL was also performed in rat, monkey and human plasma. Therefore, the method validation included the determination of specificity, sensitivity, reproducibility and stability of SKL single or simultaneous with SRF in plasma of each species. In addition, the quality assurance of the analytical method was validated containing linearity, accuracy, within- and between-day precision of the determination of SKL and SRF in plasma. For each validated compound and the ISTD in each matrix, two separate stock solutions (SS1 and SS2) were prepared. SS1 was used to generate the calibration standards, quality control samples were diluted from SS2. The detailed preparation of SKL, SRF and FS112 stock solutions, calibration standards and quality control samples in rat, dog, monkey and human plasma is described in section 5.2.2.3 (Stock Solutions).

3.2.1. Selectivity of the Analytical Method

The ability of an analytical method to differentiate and quantify the analyte in the presence of other sample components, is defined as selectivity [116]. During the validation process method selectivity was confirmed by analysis of blank plasma, ISTD-spiked plasma and the lowest concentrated calibration standard. Respective MRM chromatograms in rat, dog, monkey and human plasma are displayed in figures 20 to 23.

Selectivity in rat plasma:

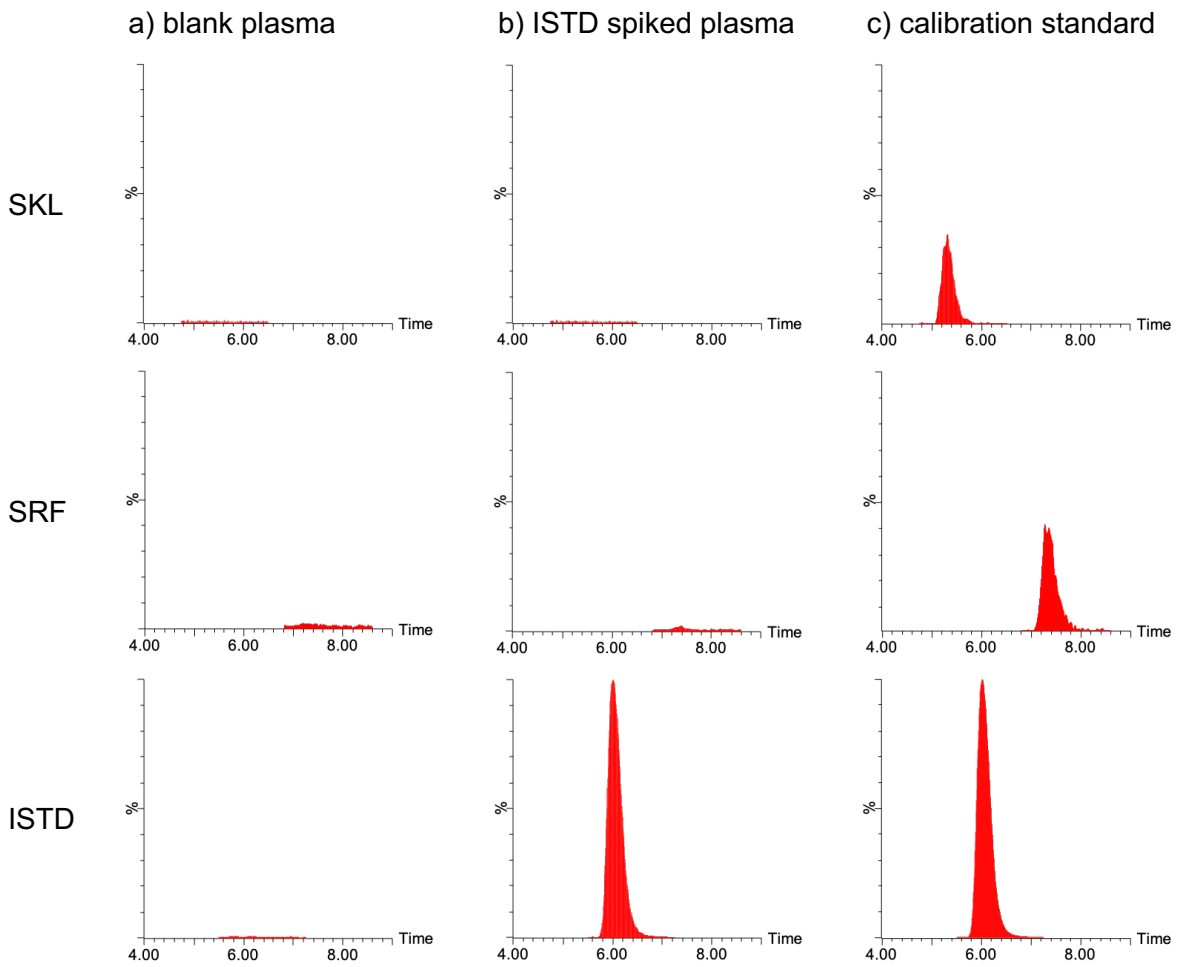


Fig. 20: MRM chromatograms of SKL, SRF and ISTD in rat plasma to demonstrate method selectivity; a) blank plasma; b) plasma spiked with ISTD; c) chromatogram of lowest concentrated calibration standard (7.81 ng/mL SKL, 7.81 ng/mL SRF).

Selectivity in dog plasma:

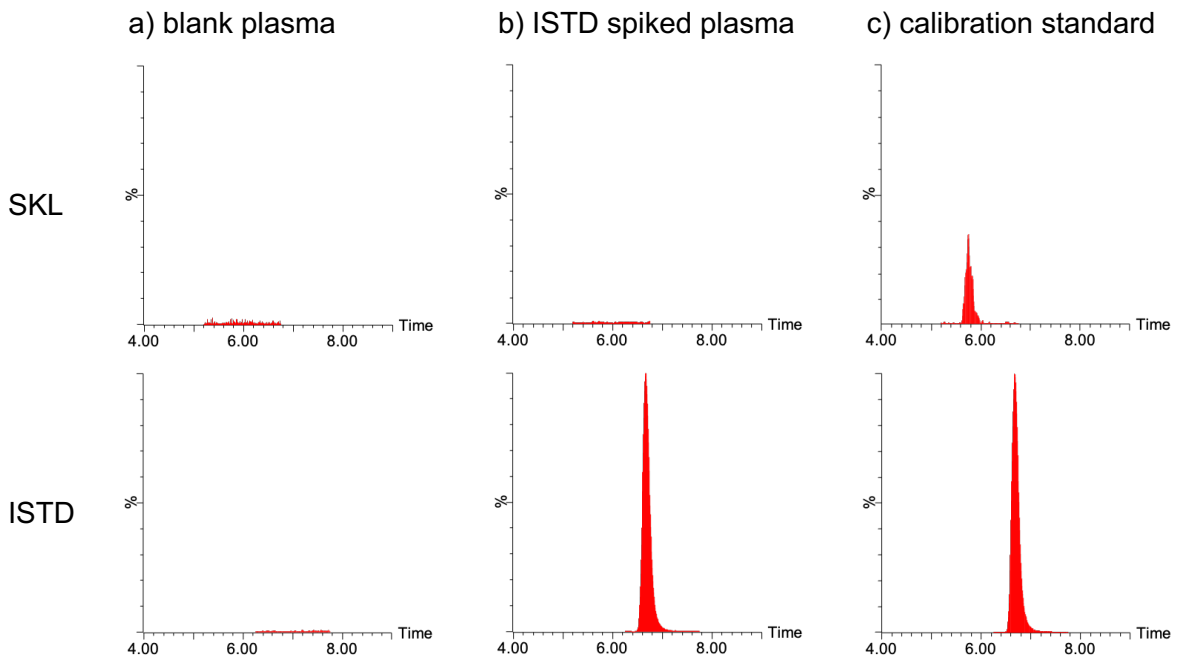


Fig. 21: MRM chromatograms of SKL and ISTD in dog plasma to demonstrate method selectivity; a) blank plasma; b) plasma spiked with ISTD; c) chromatogram of lowest concentrated calibration standard (10.00 ng/mL SKL).

Selectivity in monkey plasma

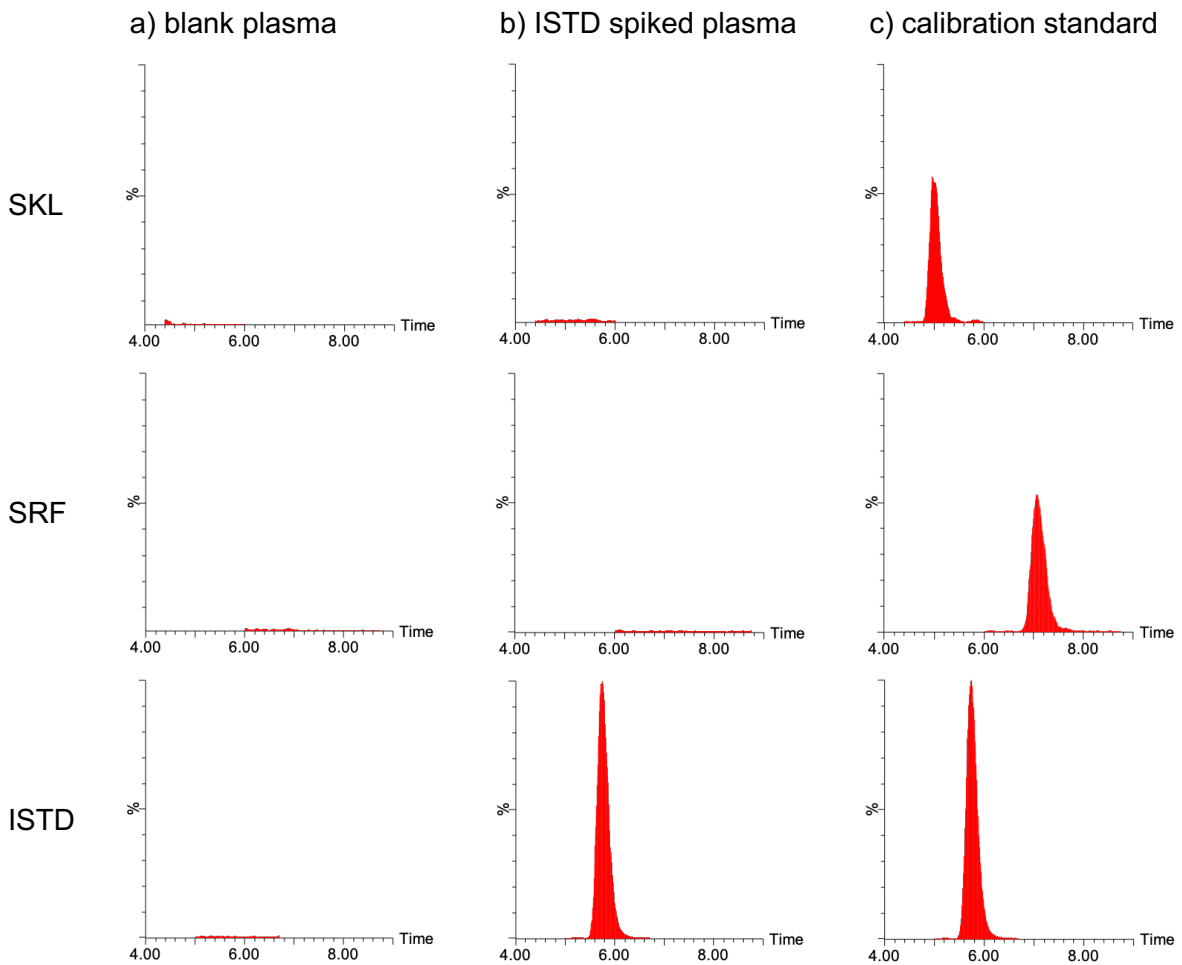


Fig. 22: MRM chromatograms of SKL, SRF and ISTD in monkey plasma to demonstrate method selectivity; a) blank plasma; b) plasma spiked with ISTD; c) chromatogram of lowest concentrated calibration standard (15.63 ng/mL SKL, 15.63 ng/mL SRF).

Selectivity in human plasma

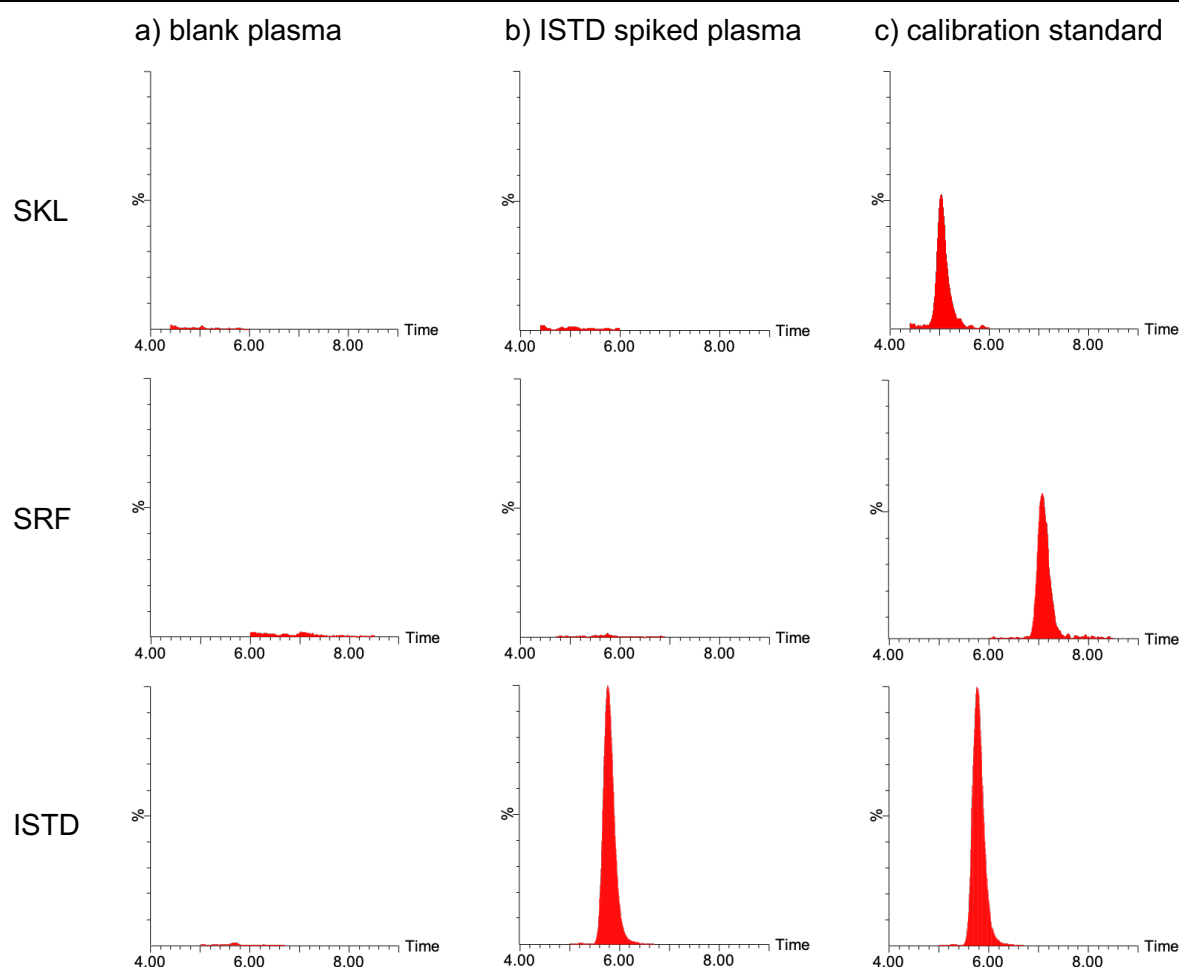


Fig. 23: MRM chromatograms of SKL, SRF and ISTD in human plasma to demonstrate method selectivity; a) blank plasma; b) plasma spiked with ISTD; c) chromatogram of lowest concentrated calibration standard (15.63 ng/mL SKL, 15.63 ng/mL SRF).

These chromatograms display the achieved specificity of the developed analytical method. In the absence of the respective analyte, only background noise is recognisable, whereas the lowest analyte concentration shows a distinct peak. In addition, the chosen ISTD does not interfere with the analyte detection. This confirms the selective determination of SKL and SRF in plasma of all analysed species.

3.2.2. Sensitivity of the Analytical Method

To describe the sensitivity of the analytical method, the limit of detection (LOD) and quantification (LOQ) was determined as recommended by the International Council for Harmonisation of Technical Requirements for Pharmaceuticals for Human Use (ICH) [117]. The standard deviation σ of the response and the slope S of the

calibration curve were used to calculate LOD and LOQ according to the following equations 3 and 4.

$$\text{LOD} = \frac{3.3\sigma}{s} \quad (\text{Eq. 3})$$

$$\text{LOQ} = \frac{10\sigma}{s} \quad (\text{Eq. 4})$$

Table 1 shows the LOD and LOQ calculated using the three lowest calibration standards for the determination of SKL and SRF in plasma from rat, dog, monkey and human. The LOQ applied in each case is also given. The determined LOD and calculated LOQ of SKL and SRF differ only slightly between the species.

	SKL			SRF		
	LOD	LOQ calc.	applied	LOD	LOQ calc.	applied
rat	1.79	5.43	7.81	0.51	1.56	7.81
dog	2.17	6.59	10.00	-/-	-/-	-/-
human	2.67	8.08	15.63	1.81	5.47	15.63

Tab. 1: Calculated (calc.) limits of detection (LOD) and quantification (LOQ) in ng/mL for the determination of SKL and SRF in rat, dog, monkey and human plasma. In addition, the LOQ applied in the validated method is given.

According to the ICH definition of LOQ, the "lowest amount of analyte in a sample, which can be quantitatively determined with suitable precision and accuracy" of SKL is 5.43 ng/mL in rat, 6.59 ng/mL in dog and 8.08 ng/mL in human and monkey plasma. The LOQ of SRF in rat plasma is 1.56 ng/mL and 5.47 ng/mL in plasma from humans and monkeys. The applied LOQs of both analytes are thus somewhat higher in all species and also clearly exceed the determined LODs. This contributes to the reliability of the results and confirms the sensitivity of the method.

3.2.3. Linearity of Skepinone-L and Sorafenib Determination

The linearity of an analytical method is the ability to deliver signals which are directly proportional to the analyte concentration in a defined range. Confirmation of linearity can be verified either visually or, in accordance with the ICH-guidelines, by the coefficient of correlation R^2 . The respective R^2 for the calibration of SKL and SRF in different species was obtained via 1/x-weighting and linear regression where x represents the concentration (Tab. 2). The primary calibration lines established during

method validation are given in figures 103-105 in chapter 7.1 (Appendix, Primary Calibration Lines).

	SKL			SRF		
	calibration range [ng/mL]	R ²	n	calibration range [ng/mL]	R ²	n
rat	7.81 – 4,000.00	0.9999	30	7.81 – 4,000.00	0.9999	30
dog	10.00 – 4,000.00	1.0000	30	-/-	-/-	-/-
human	15.63 – 4,000.00	0.9999	27	15.63 – 4,000.00	0.9999	27

Tab. 2: Summarized results of the linearity of SKL and SRF determined in rat, dog and human plasma. R² = coefficient of correlation; n = number of analyses, threefold determination of 10 (rat and dog) and 9 (human) calibration standards

The resulting R² during the method validation expresses the excellent linear relationships of analyte concentration and signal intensity, given as PAR (analyte/ISTD). This illustrates the excellent linearity of the analytical method for SKL and SRF within the specified concentration range. Furthermore, the species investigated does not seem to have any influence on the linearity.

3.2.4. Accuracy and Precision of the Analytical Method

Five different concentrations of quality control (QC) samples were analysed fivefold on one single day and on a total of three consecutive days. Based on the results obtained, the accuracy, intra-day and inter-day precisions were determined. At least 50 % of each concentration level should be within 15.0 % of their nominal value. In addition, a minimum of 67 % of all replicate analyses should not exceed deviations of 15.0 % from their nominal value or 20.0 % at LOQ.

Accuracy describes in percent the level of conformity between the values obtained by the method and the nominal concentrations of analyte. It is calculated using equation (Eq. 55), where X_m describes the measured and X_n the nominal value.

$$\text{accuracy [\%]} = 100 \cdot \frac{X_m}{X_n} \quad (\text{Eq. 5})$$

Precision is a measure of statistical variability. It describes the variance of the individual analysis results about the average value due to random errors. The precision is represented by the coefficient of variation (CV) in percent and is calculated using descriptive statistics as described in chapter 5.2.1 (Descriptive Statistics). The

resulted CV of multiple sampling should not exceed 15.0 %, or near LOQ 20.0 %. The mean values of the measured SKL and SRF concentrations in QC samples in rat, dog and human plasma are presented in tables 3 to 5. In addition, the accuracy as well as intra- and inter-day precisions determined are given.

rat plasma		intra-day			inter-day		
	QC sample concentration [ng/mL]	mean back calculated concentration [ng/mL]	accuracy [%]	CV [%]	mean back calculated concentration [ng/mL]	accuracy [%]	CV [%]
SKL	19.80	16.95	85.6	4.6	18.07	91.3	5.5
	198.00	191.58	96.8	6.2	195.84	98.9	5.0
	990.00	988.30	99.8	3.1	976.21	98.6	3.0
	1,980.00	1,784.28	90.1	9.6	1,883.06	95.1	5.3
	3,960.00	4,012.13	101.3	1.7	3,934.60	99.4	1.9
SRF	19.80	19.39	97.9	7.3	18.94	95.7	7.8
	198.00	187.77	94.8	4.6	198.26	100.1	6.2
	990.00	998.96	100.9	3.6	1,004.85	101.5	1.5
	1,980.00	2,015.45	101.8	2.7	1,997.36	100.9	0.9
	3,960.00	3,940.93	99.5	3.5	3,943.07	99.6	0.3

Tab. 3: Intra-day and inter-day accuracy and precision of SKL and SRF in rat plasma. Obtained during method validation by fivefold analysis of five QC samples on one day (intra-day, n = 5) and on two further days (inter-day, n = 15).

dog plasma		intra-day			inter-day		
	QC sample concentration [ng/mL]	mean back calculated concentration [ng/mL]	accuracy [%]	CV [%]	mean back calculated concentration [ng/mL]	accuracy [%]	CV [%]
SKL	19.61	19.61	100.0	3.7	19.27	98.3	1.9
	196.08	190.01	96.9	3.3	191.10	97.5	0.5
	980.39	977.67	99.7	2.4	973.70	99.3	0.6
	1,960.78	1,954.61	99.7	0.7	1,945.85	99.2	0.8
	3,921.57	3,912.37	99.8	0.8	3,914.61	99.8	0.1

Tab. 4: Intra-day and inter-day accuracy and precision of SKL and SRF in dog plasma. Obtained during method validation by fivefold analysis of five QC samples on one day (intra-day, n = 5) and on two further days (inter-day, n = 15).

human plasma		intra-day			inter-day		
	QC sample concentration [ng/mL]	mean back calculated concentration [ng/mL]	accuracy [%]	CV [%]	mean back calculated concentration [ng/mL]	accuracy [%]	CV [%]
SKL	22.00	19.94	90.6	5.8	21.49	97.7	6.8
	220.00	219.96	100.0	2.8	218.07	99.1	3.6
	660.00	647.39	98.1	2.9	659.59	99.9	2.8
	1,980.00	1,949.34	98.5	2.5	1,970.06	99.5	1.8
	3,960.00	3,842.96	97.0	3.8	3,794.73	100.4	2.9
SRF	22.00	20.18	91.7	1.4	23.98	109.0	13.7
	220.00	220.69	100.3	3.6	218.29	99.2	1.0
	660.00	653.88	99.1	3.1	657.25	99.6	0.6
	1,980.00	1,960.00	99.0	1.1	1,969.33	99.5	0.5
	3,960.00	3,929.04	99.2	1.0	3,987.48	100.7	1.3

Tab. 5: Intra-day and inter-day accuracy and precision of SKL and SRF in human plasma. Obtained during method validation by fivefold analysis of five QC samples on one day (intra-day, n = 5) and on two further days (inter-day, n = 15).

Tables 3 to 5 show that the results obtained for accuracy and precision of SKL and SRF comply with the respective acceptance criteria. The minimum requirement that 67 % of all replicate analysis should not exceed deviations of 15.0 or 20.0 % was more than fulfilled, as almost all values were well below these specified limits. The accuracy in rat plasma was 85.6 to 101.8 % for SKL and 94.8 to 101.8 % for SRF. The maximum CV and thus the lowest precision was 9.6 % for SKL and 7.8 % for SRF. In dog plasma, SKL had an excellent accuracy of 96.9 to 100.0 % with a maximum deviation of 3.7 %. In human plasma, SKL achieved an accuracy of 90.6 to 100.4 % and a CV of no more than 6.8 %. SRF was determined with an accuracy of 91.7 to 109.0 %, with the largest deviation being 13.7 %. These values, which are well within the defined limits, confirm the accuracy and precision, *i.e.* the reliability of the established LC-MS/MS method.

3.2.5. Reproducibility and Carry-Over

The reproducibility of an analytical method expresses the accuracy and precision of replicate determinations. Reanalysis of an analytical run must be ensured, in the event of instrument failure. The reproducibility of reinjection was evaluated by analysing each calibration standard three times. Through the obtained PARs, the concentrations of the analysed standards were back-calculated. From their arithmetic mean values, the standard deviations and the CVs (Tab. 6-8) were determined using descriptive statistics as given in chapter 5.2.1. The CV expresses in percent the precision of the SKL and SRF determination for each calibration concentration and is considered here

as a measure of their reproducibility. The acceptance range was a maximum of 15.0 % deviation from the respective nominal value, or 20.0 % for concentrations close to the LOQ.

rat plasma nominal concentration [ng/mL]	SKL			SRF		
	mean back calculated concentration [ng/mL]	± s.d.	CV [%]	mean back calculated concentration [ng/mL]	± s.d.	CV [%]
7.81	8.29	0.95	11.5	8.46	0.62	7.3
15.63	16.75	0.55	3.3	15.78	0.52	3.3
31.25	31.05	0.42	1.4	31.08	1.16	3.7
62.50	63.06	1.86	2.9	59.95	0.22	0.4
125.00	125.45	4.80	3.8	122.94	3.28	2.7
250.00	249.51	12.46	5.0	225.02	22.70	10.1
500.00	490.25	10.83	2.2	493.23	10.95	2.2
1,000.00	1,016.74	48.24	4.7	974.66	14.67	1.5
2,000.00	1,991.44	87.35	4.4	1,977.98	35.82	1.8
4,000.00	4,005.11	144.55	3.6	3,892.57	93.11	2.4

Tab. 6: Evaluation of SKL and SRF reproducibility in rat plasma. Expressed by coefficient of variation (CV) in percent. Determined by threefold analysis of each calibration standard and the resulting standard deviations of mean back-calculated concentrations.

dog plasma nominal concentration [ng/mL]	SKL		
	mean back calculated concentration [ng/mL]	± s.d.	CV [%]
10.00	11.50	1.69	14.7
25.00	25.19	3.17	12.6
50.00	50.92	3.11	6.1
100.00	98.30	4.35	4.4
250.00	244.83	5.18	2.1
500.00	500.14	21.87	4.4
1,000.00	1,018.5	27.90	2.7
2,000.00	2,041.54	81.53	4.0
3,000.00	3,062.74	113.64	3.7
4,000.00	4,071.72	156.13	3.8

Tab. 7: Evaluation of SKL reproducibility in dog plasma. Expressed by coefficient of variation (CV) in percent. Determined by threefold analysis of each calibration standard and the resulting standard deviations of mean back-calculated concentrations.

human plasma nominal concentration [ng/mL]	SKL			SRF		
	mean back calculated concentration [ng/mL]	± s.d.	CV [%]	mean back calculated concentration [ng/mL]	± s.d.	CV [%]
15.63	13.19	2.26	17.1	14.46	1.08	7.5
31.25	28.96	3.08	10.6	32.04	1.01	3.1
62.50	62.27	0.69	1.1	65.39	0.49	0.8
125.00	127.50	3.87	3.0	131.15	1.23	0.9
250.00	255.18	3.24	1.3	254.14	4.61	1.8
500.00	506.36	5.88	1.2	519.65	14.47	2.8
1,000.00	989.82	43.95	4.4	1,001.94	14.38	1.4
2,000.00	1,980.15	45.12	2.3	2,009.91	17.07	0.9
4,000.00	3,991.86	84.16	2.1	4,051.09	25.40	0.6

Tab. 8: Evaluation of SKL and SRF reproducibility in human plasma. Expressed by coefficient of variation (CV) in percent. Determined by threefold analysis of each calibration standard and the resulting standard deviations of mean back-calculated concentrations.

Tables 6 to 8 show that the results obtained for reproducibility of SKL and SRF expressed as CV comply with the respective acceptance criteria. The highest deviation in rat plasma was 11.5 % for SKL and 10.1 % for SRF. In dog plasma the maximum deviation from the nominal value for SKL was 14.7 % and 17.1 % in human plasma. The reproducibility achieved for SRF in human plasma was excellent, deviating at most 7.5 % from the nominal value. These values, which are well within the acceptable range, confirm that reanalysis is possible with the developed method. Moreover, no large deviations between the measured values of the same sample are to be expected.

Blank plasma samples of all applied species were injected directly after a calibration standard spiked with the highest SKL and SRF concentration. In each of these analyses no signal of either SKL or SRF greater than 20 % of the lower LOQ was detected. Further, no ISTD-peak area exceeding 5 % was observed. Therefore, in accordance with the European Medicines Agency (EMA) [118] no carry-over effect affects the accuracy and precision of the validated method. Thus, no additional injections of blank samples after analytical samples with an expected high concentration are required, which in turn positively influences the overall analysis time.

3.2.6. Stability of Skepinone-L and Sorafenib in Plasma

In addition to their physicochemical properties, the stability of SKL and SRF in plasma can also be influenced by storage conditions and storage systems. Therefore,

experiments were performed to determine if and to what extent sample handling and analysis affects the stability of SKL and SRF. For this purpose, plasma from rat, dog and monkey was spiked with known concentrations of SKL. Since *in vivo* administration of SRF was also planned, the stability samples from rats and monkeys were additionally spiked with SRF.

One experimental condition included sealed storage of the spiked plasma samples at 4°C for several days. Since plasma samples from pharmacokinetic studies should be stored on ice or in the refrigerator for max. 30 min after thawing until processing. The pharmacokinetic plasma samples would be stored at -80°C and reanalyses should be possible. Therefore, the stability of SKL and SRF in plasma was determined after several freeze and thaw cycles from -80 to 25°C. Due to the expected sample quantity, a longer storage period of the sample extracts in the autosampler could not be avoided. Hence, the stability of SKL and SRF in the extract of the spiked plasma sample was also determined through several days of storage in a vial in the temperature-controlled autosampler.

All stability experiments were performed as duplicates. Respective deviations between measured (X_m) and nominal (X_n) values were calculated using equation 6.

$$\text{deviation [\%]} = 100 \cdot \frac{X_n - X_m}{X_n} \quad (\text{Eq. 6})$$

The results of the determined stabilities of SKL and SRF at the above-mentioned experimental conditions are shown in tables 9 to 11.

rat plasma:		SKL		SRF	
stability experiment	storage day / cycle	determined concentration [ng/mL]	deviation [%]	determined concentration [ng/mL]	deviation [%]
plasma, 4°C	0	3,428.89	-2.0	1,464.02	-2.4
	1	3,482.10	-0.5	1,510.42	0.7
	3	3,510.69	0.3	1,493.46	-0.4
	5	3,439.74	-1.7	1,475.69	-1.6
extract in AS, 4°C	0	3,428.89	-2.0	1,464.02	-2.4
	1	3,597.59	2.8	1,481.40	-1.2
	3	3,529.88	0.9	1,479.78	-1.4
	5	3,581.15	2.3	1,570.74	4.7
plasma, -80/+25°C	0	3,428.89	-2.0	1,464.02	-2.4
	1	3,502.22	0.1	1,460.56	-2.6
	2	3,556.45	1.6	1,393.22	-7.1
	3	3,496.54	-0.1	1,469.04	-2.1
	4	3,464.56	-1.0	1,437.17	-4.2

Tab. 9: Stability analysis of SKL and SRF in rat plasma, determined concentrations and deviations of nominal values. Stability was determined in plasma and extract, both stored at 4°C, and in plasma after freeze-thaw cycles. The nominal concentration of SKL was 3,500.00 ng/mL, of SRF 1,500.00 ng/mL. AS = autosampler

dog plasma:		SKL	
stability experiment	storage day / cycle	determined concentration [ng/mL]	deviation [%]
plasma, 4°C	0	1,801.64	0.1
	1	1,798.12	-0.1
	2	1,779.26	-1.2
	3	1,769.83	-1.7
	4	1,748.71	-2.9
extract in AS, 4°C	0	1,801.64	0.1
	1	1,834.05	1.9
	2	1,782.81	-1.0
	3	1,736.56	-3.5
plasma, -80/+25°C	0	1,801.64	0.1
	1	1,808.29	0.5
	2	1,770.47	-1.6
	3	1,783.10	-0.9
	4	1,770.63	-1.6

Tab. 10: Stability analysis of SKL in dog plasma, determined concentrations and deviations of nominal values. Stability was determined in plasma and extract, both stored at 4°C, and in plasma after freeze-thaw cycles. The nominal concentration of SKL was 1,800.00 ng/mL. AS = autosampler

human plasma:		SKL		SRF	
stability experiment	storage day / cycle	determined concentration [ng/mL]	deviation [%]	determined concentration [ng/mL]	deviation [%]
plasma, 4°C	0	806.94	0.9	794.11	-0.7
	1	800.16	0.0	796.39	-0.5
	3	797.43	-0.3	799.65	-0.0
extract in AS, 4°C	0	4,002.22	0.1	4,062.17	1.55
	1	-/-	-/-	4,042.56	1.1
	2	3,997.31	-0.1	-/-	-/-
	3	-/-	-/-	3,999.51	0.0
plasma, -80/+25°C	0	806.94	0.9	794.11	-0.7
	1	800.06	0.0	795.79	-0.5
	2	799.93	0.0	796.29	-0.5

Tab. 11: Stability analysis of SKL and SRF in human plasma, determined concentrations and deviations of nominal values. Stability was determined in plasma and extract, both stored at 4°C, and in plasma after freeze-thaw cycles. The extract in the autosampler contained 4,000.00 ng/mL SKL and SRF. Nominal concentrations in both plasma samples were 800.00 ng/mL of SKL and SRF. AS = autosampler; -/- = not analysed

The experimental conditions applied represented a clear exaggeration of the actually expected sample handling with regard to storage time and free-thaw cycles. Even so, the concentrations of SKL and SRF show almost no changes throughout the duration of the experiments. Thus, it can be said that both substances are stable in plasma as well as in the extract of all tested species for at least two days and cycles each.

3.2.7. Analytical Quality Assurance

Before and after each sequence a standard series of all calibration standards (9-10, depending on analysed species) was measured. If they complied with the requirements of the validation, they were used for sample quantification. When measuring the pharmacokinetic samples, a set of five QC samples was analysed latest after 18 sample runs, all calibration standards after 36 sample runs. The measurements were classified as valid if the results for the accuracy were within 15 % of the nominal value, or within 20 % at LOQ.

3.3. Pharmacokinetic Studies of Skepinone-L *in vivo*

Preclinical pharmacokinetic studies of SKL were performed in rodent, canine and non-human primate species. A preliminary study in C57BL/6 mice was performed to evaluate the optimal dose levels for upcoming studies. Pharmacokinetic studies in the Sprague Dawley rat, the second rodent species, were carried out to investigate the potential interaction of SKL and SRF. The determination of SKL bioavailability was performed via pharmacokinetic studies in beagle dogs. Due to their strong similarities to humans, *inter alia*, in physiology [119] and drug-metabolizing enzymes [120], the cynomolgus monkey was used to study the pharmacokinetic profile of SKL in a non-human primate species. A summary of all selected species and the respective route of administration of SKL is given in table 12. Further, it is listed whether SKL and SRF were administered as monotherapy or in combination with each other.

	test item			route of administration*	
	SKL	SRF	SKL+SRF	intravenous	per oral
C57BL/6 mouse	X	-/-	-/-	X	X
beagle dog	X	-/-	-/-	X	X
Sprague Dawley rat	X	X	X	X	X
cynomolgus monkey	X	X	-/-	-/-	X

Tab. 12: Overview of selected species, test items and route of administration to investigate the PK profile of SKL *in vivo*; X denotes the tests performed. *relates to SKL only

The tables 85 to 89 given in chapter 5.2.3.1 (Animal Treatment Conditions) provide a more detailed overview of treatment for each tested species. They contain the routes and the corresponding doses of administered compounds as well as the gender and number of all tested animals.

The concentration profiles of SKL in plasma of all applied species obtained after intravenous and oral administration were used to determine pharmacokinetic parameters. These include the extrapolated initial plasma concentration at time zero (C_0), the volume of distribution at steady state (V_{ss}) and the total body clearance (Cl) after i.v. administration. For p.o. application, they contain the observed maximum concentration in plasma (C_{max}) and the time of their occurrence (t_{max}) as well as the calculated bioavailability (F). Furthermore, the terminal plasma half-life ($t_{1/2}$) of SKL, the area under the plasma concentration-time curve from zero to the last sampling

point (AUC_{0-t}) and from zero to infinity ($AUC_{0-\infty}$) were calculated as described in chapter 5.2.5.1 (Non-Compartmental Analysis).

3.3.1. Preliminary Pharmacokinetic Study of Skepinone-L in Mice

The preliminary pharmacokinetic study of SKL in mice was first performed and analysed by Synovo GmbH in Tübingen. Male C57BL/6 mice received in composite design two cassettes, C#1 and C#2, containing doses of 0.4 mg/kg SKL through intravenous application and 1.2 mg/kg through oral administration. Chapter 5.2.3.2 (Preliminary Study of Skepinone L in Mice) further describes the procedure for this study part, *inter alia* regarding vehicle formulation, number of animals tested and time of sampling. The second part of this study included the oral administration of 10 mg/kg SKL to three female C57BL/6 mice. Animal treatment was conducted at the Department of Physiology of the University Hospital in Tübingen. Experimental implementation and the analytical method to quantify SKL in mouse plasma is depicted in chapter 5.2.3.2.

3.3.1.1. Pharmacokinetic Data Analysis and Parameter Calculation

Non-Compartmental Analysis

The pharmacokinetic parameters of SKL were first determined by non-compartmental analysis (NCA), based on the obtained plasma concentration profiles (Fig. 24) using the add-in program PKSolver2.0. Regarding study part one, the arithmetic mean values of all individual plasma concentrations at the appropriate sampling times were calculated for each cassette and corresponding route of administration. This proceeding is due to the study design, where blood samples were taken from a varying number of mice on each sampling time point. The calculation of pharmacokinetic parameter via NCA in female mice was performed by using the individual plasma concentration versus time profiles.

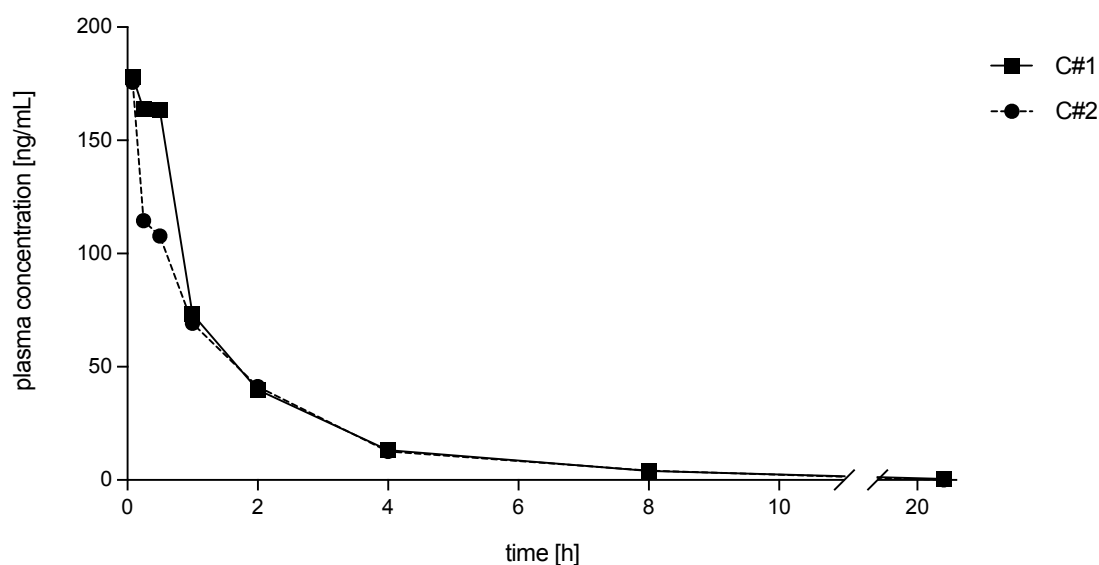


Fig. 24: Plasma concentration vs. time profile of SKL following cassette dosing in male mice after single intravenous bolus injection of 0.4 mg/kg SKL.

The values obtained by NCA following intravenous injection in male mice are given in table 13. These show that there is hardly any difference between the two administered cassettes regarding the pharmacokinetic profile and parameters of SKL. The initial and therefore highest plasma concentrations of SKL are 186 ng/mL for C#1 and 218 ng/mL for C#2. These values of C_0 were obtained though extrapolation to time zero, based on the first experimentally determined plasma concentrations after injection.

single bolus injection of 0.4 mg/kg SKL in male mice							
	C_0 [ng/mL]	AUC_{0-t} [ng·h/mL]	λ_z [1/h]	$t_{1/2}$ [h]	$AUC_{0-\infty}$ [ng·h/mL]	V_{ss} [L/kg]	Cl [L/h/kg]
C#1	186	324	0.2	4.3	327	3.3	1.2
C#2	218	290	0.2	3.1	291	3.5	1.4

Tab. 13: Pharmacokinetic parameters for SKL derived from NCA of mean plasma concentration vs. time profiles in male mice after intravenous bolus injection of 0.4 mg/kg SKL via cassette dosing (C#1, C#2).

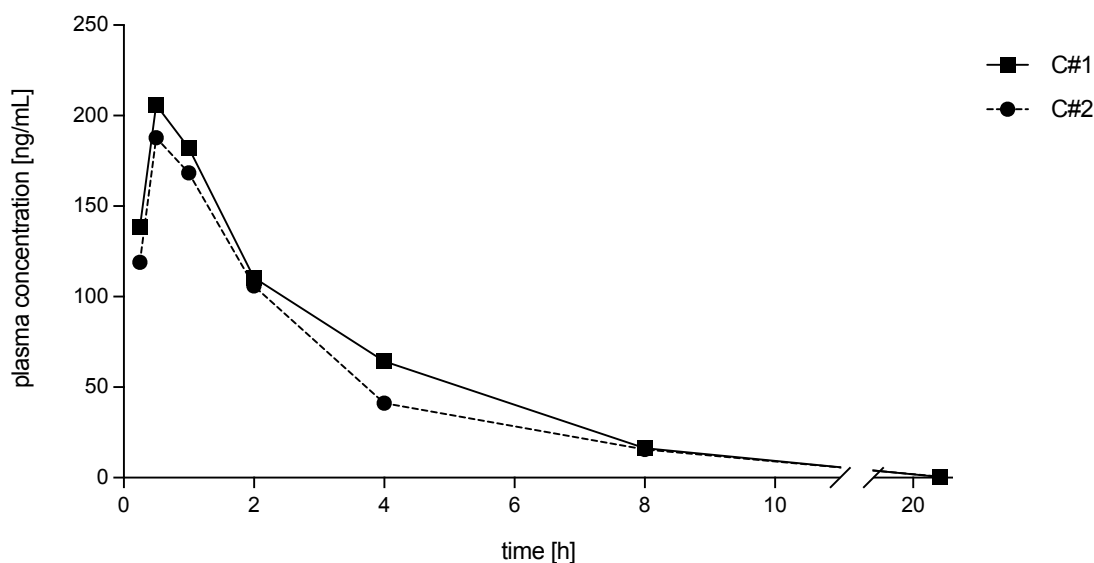


Fig. 25: Plasma concentration vs. time profile of SKL following cassette dosing in male mice after single oral administration of 1.2 mg/kg SKL.

single oral administration of 1.2 mg/kg SKL in male mice							
	C_{max} [ng/mL]	t_{max} [h]	AUC_{0-t} [ng·h/mL]	λ_z [1/h]	$t_{1/2}$ [h]	$AUC_{0-\infty}$ [ng·h/mL]	F [%]
C#1	206	0.5	773	0.2	2.8	775	79.0
C#2	188	0.5	670	0.2	3.3	673	77.2

Tab. 14: Pharmacokinetic parameters for SKL derived from NCA of mean plasma concentration vs. time profiles in male mice after oral administration of 1.2 mg/kg SKL via cassette dosing (C#1, C#2).

Considering the via NCA determined parameters following oral administration in male mice (Tab. 14), it is noticeable that both cassettes show again similar and therefore comparable values. Rapid absorption is observed and C_{max} with 206 and 188 ng/mL is reached already after 0.5 h. Plasma half-life seems to be slightly lower compared to i.v. administration. The bioavailability F of SKL is determined with 77 - 79 % in male mice after oral dosing.

Figure 26 illustrates the individual plasma concentration time-curves of SKL in female mice following oral administration and the pharmacokinetic parameters derived from them are given in table 15. It is noticeable that there are both strong similarities and differences between the individual animals. For example, the maximum concentrations differ by up to almost 500 ng/mL, which also results in significant variations of AUC_{0-t} and $AUC_{0-\infty}$. With 1,104 ng/mL mouse 3 shows the lowest C_{max} , which is also reached earlier than in the other animals (0.5 h compared to 1.0 h). This indicates that the actual time at which C_{max} appears in mouse 3 was not recorded due

to the experimental setup. Despite this unfortunate circumstance and the strong differences in plasma concentrations, the plasma half-lives of the individuals are nearly the same.

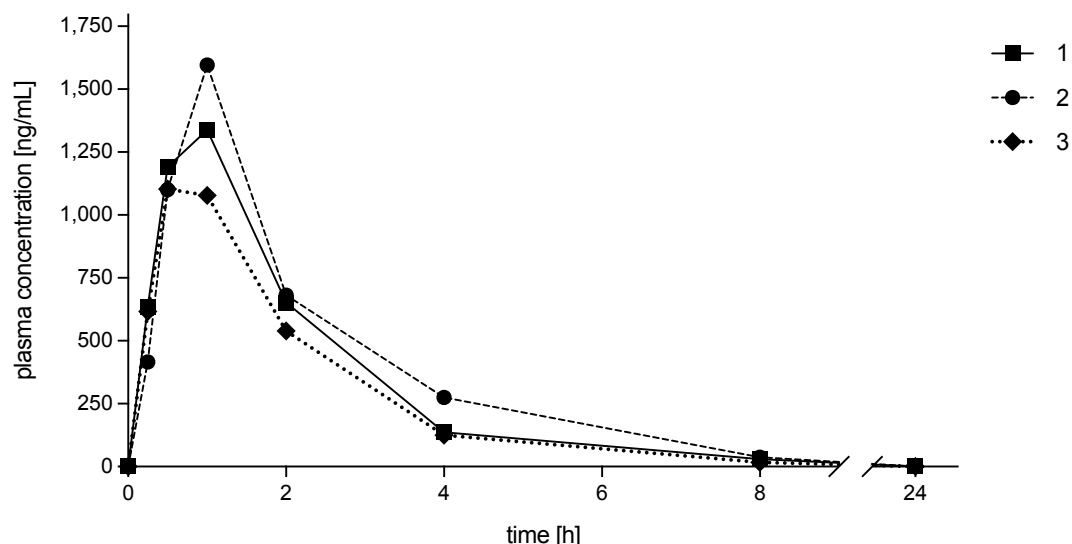


Fig. 26: Individual plasma concentration vs. time curves of SKL in female mice 1, 2 and 3 following single oral administration of 10 mg/kg SKL.

single oral administration of 10 mg/kg SKL in female mice							
animal	C_{max} [ng/mL]	t_{max} [h]	AUC_{0-t} [ng·h/mL]	λ_z [1/h]	$t_{1/2}$ [h]	$AUC_{0-\infty}$ [ng·h/mL]	F [%]
1	1,338	1.0	3,055	0.5	1.3	3,109	40.3
2	1,596	1.0	3,635	0.5	1.4	3,713	48.1
3	1,104	0.5	2,594	0.6	1.2	2,624	34.0
mean	1,346	0.8	3,095	0.5	1.3	3,149	41
\pm s.d.	201	0.2	426	0.0	0.1	445	6
C.V.	15%	28%	14%	9%	6%	14%	14%

Tab. 15: Pharmacokinetic parameters for SKL derived from NCA of individual plasma concentration vs. time curves in female mice after administration of 10 mg/kg SKL via oral gavage.

Since SKL was not administered intravenously, the bioavailability in female mice was calculated using the $AUC_{0-\infty}$ derived from male mice after i.v. application of 0.4 mg/kg SKL (Tab. 13). With an average of 41 % in females, F is significantly lower as for male mice (77 - 79 %, Tab. 14). This decreased bioavailability is also reflected in other pharmacokinetic parameters. Although the orally administered dose was higher by a factor of 8.3 in female mice, the average C_{max} is only 6.8 times and the AUC_{0-t} even only 4.3 times higher compared to the results from study part one. In addition to these findings, the plasma concentration seems to halve faster, which is reflected by a mean plasma half-life of 1.3 in female and individual $t_{1/2}$ of 2.8 and 3.3 h in male mice.

Furthermore, in contrast to the males, the plasma of female mice seemed to be completely cleared of SKL within 24 h. This could be due to the fact that females actually excrete it faster, or the detection limit of the method has been reached. Unfortunately, the limit of detection was not determined for this preliminary study, due to the lack of method validation both in the external and internal laboratory.

Overall, the low CI of 1.2 and 1.4 L/h/kg, the moderate V_{ss} with 3.3 and 3.5 L/kg [22] after i.v. application and also the high plasma concentrations achieved, regardless of the route of administration and gender, indicate that SKL has a favourable pharmacokinetic profile in mice.

Compartmental Analysis and Model Assessment

The plasma concentration versus time profiles of SKL show after both i.v. and p.o. administration a nonlinear pharmacokinetic behaviour. This becomes apparent during the elimination process, which can be described as biphasic, due to the initially rapid decline of concentration followed by a significantly slower decrease. Therefore, the two-compartment model was used to further calculate the pharmacokinetic parameter also via PKSolver2.0. In order to perform compartmental analysis (CA), the arithmetic mean of the observed plasma concentrations was calculated utilizing descriptive statistics as described in chapter 5.2.1. The coefficient of correlation R^2 , Akaike's information criterion (AIC) and the Schwarz criterion (SC) were used to assess the precision of the selected pharmacokinetic model and its estimated parameter.

compartmental analysis following i.v. administration in mice							model diagnostics		
		C_0 [ng/mL]	AUC_{0-t} [ng·h/mL]	$AUC_{0-\infty}$ [ng·h/mL]	V_{ss} [L/kg]	CI [L/h/kg]	R^2	AIC	SC
		187	274	275	3.6	1.5	0.9944	56.4	56.7
Δ to	C#1	1	-50	-52	0.3	0.3			
NCA	C#2	-31	-16	-16	0.1	0.1			

Tab. 16: Pharmacokinetic parameters for SKL determined by compartmental analysis of mean plasma concentration vs. time profiles ($n=2$) compared to values obtained via NCA in male mice after intravenous bolus injection of 0.4 mg/kg.

Comparing the values of NCA with those generated by CA (Tab. 16) after i.v. administration, the predicted C_0 as well as the AUC_{0-t} and $AUC_{0-\infty}$ are lower. In contrast, the V_{ss} and CI are estimated to be slightly higher than observed. However, especially regarding the average of both cassettes, these differences are not very

pronounced and could be due to the fact that only two sets of data were available to create this two-compartment model.

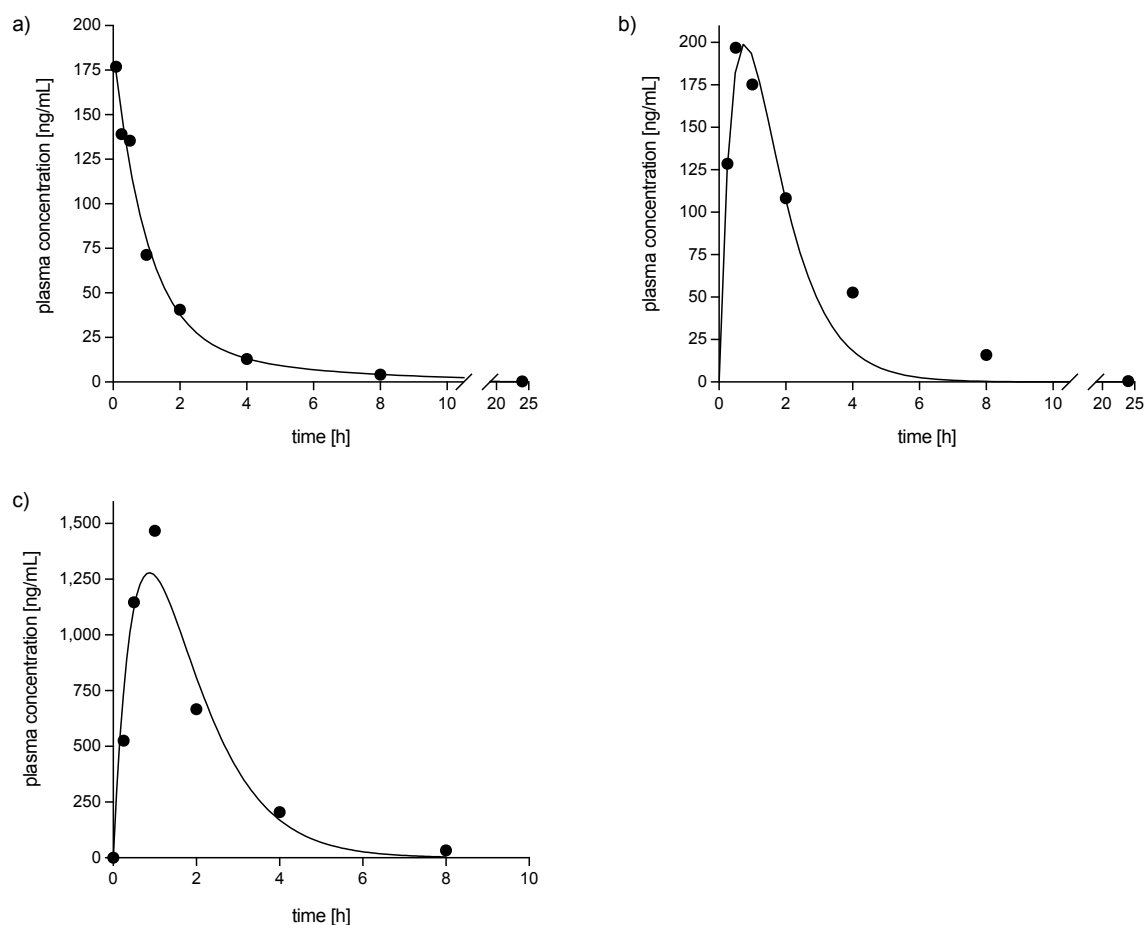


Fig. 27: Two-compartment model plots of SKL in male mice following i.v. administration of 0.4 mg/kg SKL (a) and p.o. dosage (b) of 1.2 mg/kg SKL; c) after p.o. administration of 10 mg/kg in female mice. The mean values of the observed concentrations are displayed by circles and the solid line represents the calculated curve.

Compartmental analysis after p.o. administration compared to NCA shows in male mice a partly high discrepancy (Tab 17). Especially the values for AUC_{0-t} and $AUC_{0-\infty}$ predicted by CA are significantly lower than those observed. In contrast, the model was able to estimate the values for C_{max} and t_{max} relatively accurately. Interestingly, the precision of the estimated pharmacokinetic parameters is assessed by AIC and SC as relatively good.

compartmental analysis following p.o. administration in mice								
		C _{max} [ng/mL]	t _{max} [h]	AUC _{0-t} [ng·h/mL]	AUC _{0-∞} [ng·h/mL]	model diagnostics		
						R ²	AIC	SC
♂		199	0.8	430	430	0.9815	62.7	62.4
Δ to NCA	C#1	-7	0.3	-343	-343			
	C#2	11	0.3	-240	-243			
♀		1,279	0.9	3,061	3,065	0.9733	91.5	91.2
Δ to NCA		-67	0.1	-34	-84			

Tab. 17: Calculated pharmacokinetic parameters for SKL via compartmental analysis of mean plasma concentration vs. time profiles compared to values obtained via NCA in male (n=2) and female (n=3) mice following extravascular administration of 1.2 and 10 mg/kg respectively.

Table 17 also shows that the selected pharmacokinetic model aptly predicted the parameters for SKL in female mice following oral dosing. Although the values obtained by CA reveal only slight differences compared to NCA, their precision is rated not so well regarding the diagnosis criteria compared to male mice. Despite the deviations mentioned, the selected pharmacokinetic model seems to be suitable to estimate the parameters for SKL in mice accurately. In addition, the pharmacokinetic parameters of SKL determined in the present study, correlate very well with those already described in literature [121].

3.3.2. Bioavailability Study of Skepinone-L in Dogs

The pharmacokinetic study of SKL in dogs was performed at the Research Toxicology Centre in Baugy (France) and sponsored by c-a-i-r biosciences GmbH in Ulm, Germany. Dogs are widely used as animal models in drug research and development [122]. This is due to their anatomical and physiological similarity to other mammals [123] and the resulting comparable metabolic and pharmacokinetic profiles [124],[125]. The objective of this study was to examine the bioavailability of SKL following oral administration with a dosage of 50 mg/kg compared to intravenous bolus injection of 5 mg/kg SKL. For this purpose, the study was conducted on a group of two male and two female beagle dogs. The determination of the oral bioavailability of SKL is important because oral dosing has been selected as route of administration in humans. Further experimental setup and the analytical method used to quantify SKL in dog plasma is described in chapter 5.2.3.3 (Bioavailability Study of Skepinone-L in Dogs).

3.3.2.1. Pharmacokinetic Data Analysis and Parameter Calculation

Non-Compartmental Analysis

The determination of the pharmacokinetic parameter for SKL in beagle dogs following intravenous and oral dosing was carried out via NCA as described for female mice in chapter 3.3.1.1.

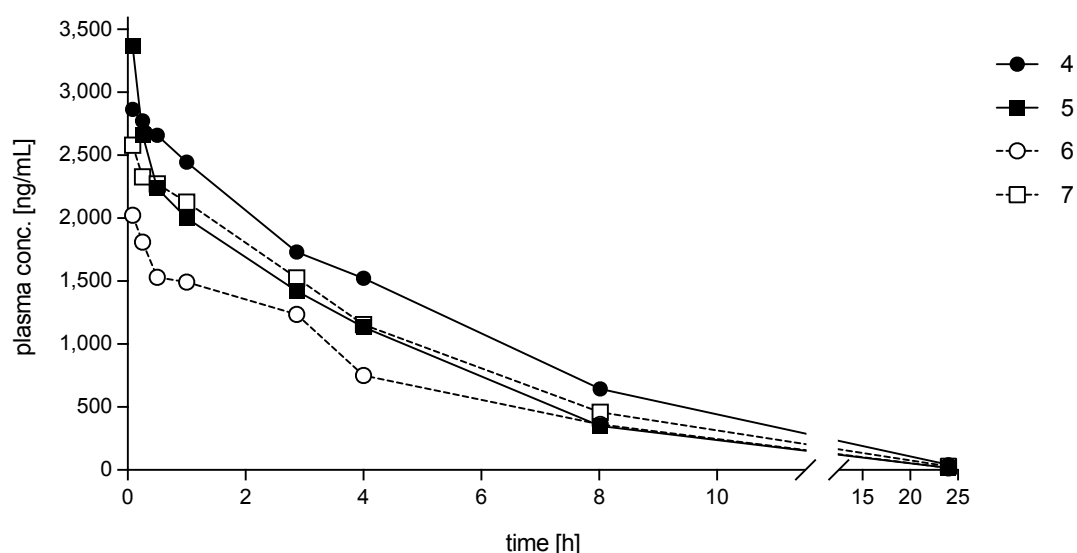


Fig. 28: Individual plasma concentration vs. time curves of SKL in male (4, 5) and female (6, 7) beagle dogs after single i.v. administration of 5 mg/kg SKL.

single bolus injection of 5 mg/kg SKL in dogs								
animal		C_0 [ng/mL]	AUC_{0-t} [ng·h/mL]	λ_z [1/h]	$t_{1/2}$ [h]	$AUC_{0-\infty}$ [ng·h/mL]	V_{ss} [L/kg]	CI [L/h/kg]
4	♂	2,912	18,254	0.2	3.9	18,496	1.4	0.3
5	♂	3,782	12,948	0.2	3.3	13,021	1.6	0.4
6	♀	2,137	10,600	0.2	3.7	10,691	2.2	0.5
7	♀	2,715	14,306	0.2	3.7	14,466	1.6	0.4

Tab. 18: Pharmacokinetic parameters for SKL derived from NCA of individual plasma concentration vs. time curves in male and female beagle dogs after single i.v. administration of 5 mg/kg SKL.

The via NCA calculated parameters for SKL after i.v. administration (Fig. 28) are given in table 18. Considering these values, the wide range in the resulted C_0 , the AUC_{0-t} and the $AUC_{0-\infty}$ is immediately noticeable. The respective maximum difference between the individual animals is 1,645 ng/mL, 7,654 and 7,805 ng·h/mL. The highest concentrations and areas were observed in male dogs. In contrast, there seems to be no gender-related difference in $t_{1/2}$ with 3.3 - 3.9 h. As already observed in male mice, SKL also shows a low CI with 0.3 - 0.5 L/h/kg and a moderate V_{ss} with 1.4 - 2.2 L/kg in this study.

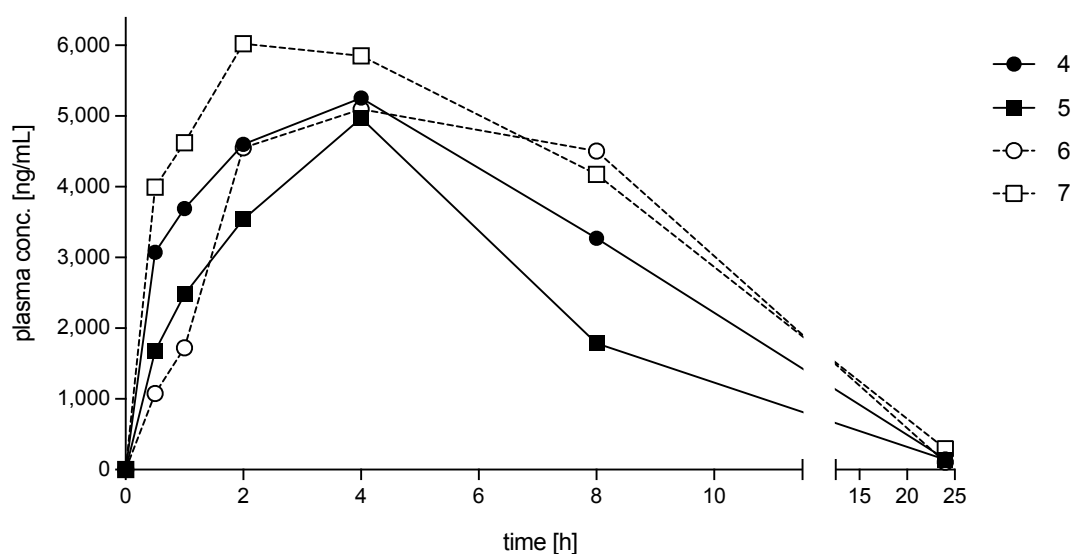


Fig. 29: Individual plasma concentration vs. time curves of SKL in male (4, 5) and female (6, 7) beagle dogs after single oral administration of 50 mg/kg SKL.

single oral administration of 50 mg/kg SKL in dogs								
animal		C_{max} [ng/mL]	t_{max} [h]	AUC_{0-t} [ng·h/mL]	λ_z [1/h]	$t_{1/2}$ [h]	$AUC_{0-\infty}$ [ng·h/mL]	F [%]
4	♂	5,257	4.0	61,249	0.2	3.9	62,093	33.6
5	♂	4,969	4.0	41,976	0.2	4.1	42,813	32.9
6	♀	5,099	4.0	69,832	0.2	3.4	70,338	65.8
7	♀	6,025	2.0	76,021	0.2	4.5	77,953	53.9

Tab. 19: Pharmacokinetic parameters for SKL derived from NCA of individual plasma concentration vs. time curves in male and female beagle dogs after single oral administration of 50 mg/kg SKL.

The plasma concentration-time profile of SKL after oral administration (Fig. 29) to beagle dogs show a fast absorption at first. But reaching the maximal plasma concentrations C_{max} requires some time and is followed by slow and flat elimination phases, especially in females. These profiles are reflected in the via NCA determined pharmacokinetic parameters, such as high t_{max} with 2.0 till 4.0 h and long plasma half-life $t_{1/2}$ of 3.4 till 4.5 h, given in table 19. As before in the i.v. administration, there are differences between male and female animals in terms of C_{max} , AUC_{0-t} and $AUC_{0-\infty}$. However, here the highest areas were observed in females. But the most significant gender-related difference can be seen in the bioavailability. While in males only 33 - 34 % of the administered amount of SKL seems to be bioavailable, females were able to absorb 54 - 66 % of the applied dose. These results show that in the present study the oral bioavailability of SKL can be considered as low in male dogs and as high in female dogs [126].

Unfortunately, RTC observed and reported indications of adverse effects like vomiting and liquid faeces after oral administration. These symptoms were not linked to SKL but to the vehicle of the oral formulation since they did not occur after intravenous administration. As consequence the dosage form was changed from liquid, i.e. pre-dissolved to solid dosage form. Thus, 50 mg/kg SKL were administered orally by capsule dosing. Except for this modification, the further study design remained unchanged.

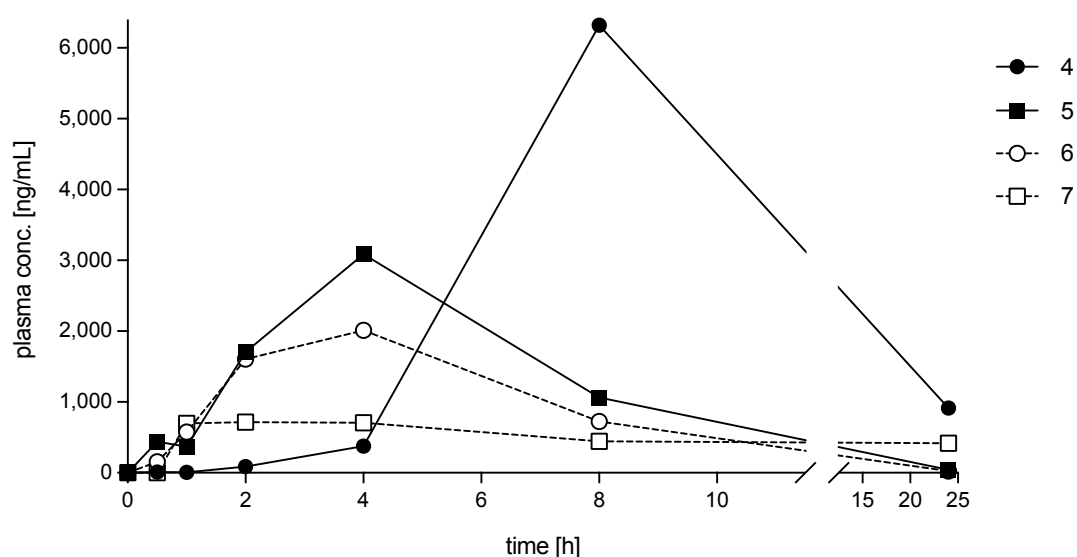


Fig. 30: Individual plasma concentration vs. time curves of SKL in male (4, 5) and female (6, 7) beagle dogs after single oral administration of 50 mg/kg SKL via capsule dosing.

oral administration of 50 mg/kg SKL as capsule								
animal		C_{max} [ng/mL]	t_{max} [h]	AUC_{0-t} [ng·h/mL]	λ_z [1/h]	$t_{1/2}$ [h]	$AUC_{0-\infty}$ [ng·h/mL]	F [%]
4	♂	6,323	8.0	71,873	N/A	N/A	N/A	N/A
5	♂	3,087	4.0	23,287	0.2	3.3	23,503	18.1
6	♀	2,012	4.0	16,397	0.2	3.2	16,507	15.4
7	♀	714	2.0	11,675	0.0	29.6	29,574	20.4

Tab. 20: Pharmacokinetic parameters for SKL from individual plasma concentration vs. time curves in male and female beagle dogs after single oral administration of 50 mg/kg SKL as capsule. N/A = not available

The concentration-time profiles obtained after capsule dosing are illustrated in figure 30 and shows a completely different pharmacokinetic behaviour of SKL in each tested animal. In addition, the values derived from NCA (Tab. 20) indicate clearly that the results are neither comparable nor interpretable. The maximal plasma concentration ranges from 714 till 6,323 ng/mL and the corresponding time of their occurrence from 2.0 till 8.0 h. The variations between the AUC_{0-t} , $t_{1/2}$, and $AUC_{0-\infty}$ of

all animals are even more pronounced. Animal 4 shows a strongly delayed absorption and elimination phase which results in the lack of at least three terminal data points. This is why λ_z , $t_{1/2}$, $AUC_{0-\infty}$ and F could not have been calculated and are therefore not available.

Obviously, this part of the study did not proceed best. Maybe the dogs did not swallow the test item capsule immediately or entirely at once. It is also possible that the capsule did not dissolve and release SKL completely and in a homogenous manner. Besides these presumptions, the actual reason for these inconclusive results could not be clearly identified. However, both the pharmacokinetic profiles and the parameters derived from NCA show that the dosage form capsule is unsuitable in the present study.

Compartmental Analysis and Model Assessment

As observed in mice, SKL shows likewise in dogs a nonlinear pharmacokinetic behaviour in both routes of administration. Therefore, the two-compartment model was also applied to calculate the pharmacokinetic parameter following i.v. and oral dosing. The analysis and model diagnosis were performed as described in chapter 3.3.1.1.

compartmental analysis following i.v. administration in dogs									
		C_0	AUC_{0-t}	$AUC_{0-\infty}$	V_{SS}	Cl	model diagnostics		
animal		[ng/mL]	[ng·h/mL]	[ng·h/mL]	[L/kg]	[L/h/kg]	R^2	AIC	SC
♂		3,558	14,067	14,207	1.8	0.4	0.9996	84.2	84.5
Δ to NCA	4	646	-4,187	-4,289	0.4	0.1			
	5	-224	1,119	1,186	0.5	0.0			
♀		2,991	11,215	11,328	2.3	0.4	0.9987	89.0	89.3
Δ to NCA	6	854	615	637	0.1	-0.1			
	7	276	-3,091	-3,138	0.7	0.0			

Tab. 21: Pharmacokinetic parameters for SKL determined by compartmental analysis of mean plasma concentration vs. time profiles (n=2) compared to values obtained via NCA in male and female beagle dogs after intravenous bolus injection of 5 mg/kg SKL.

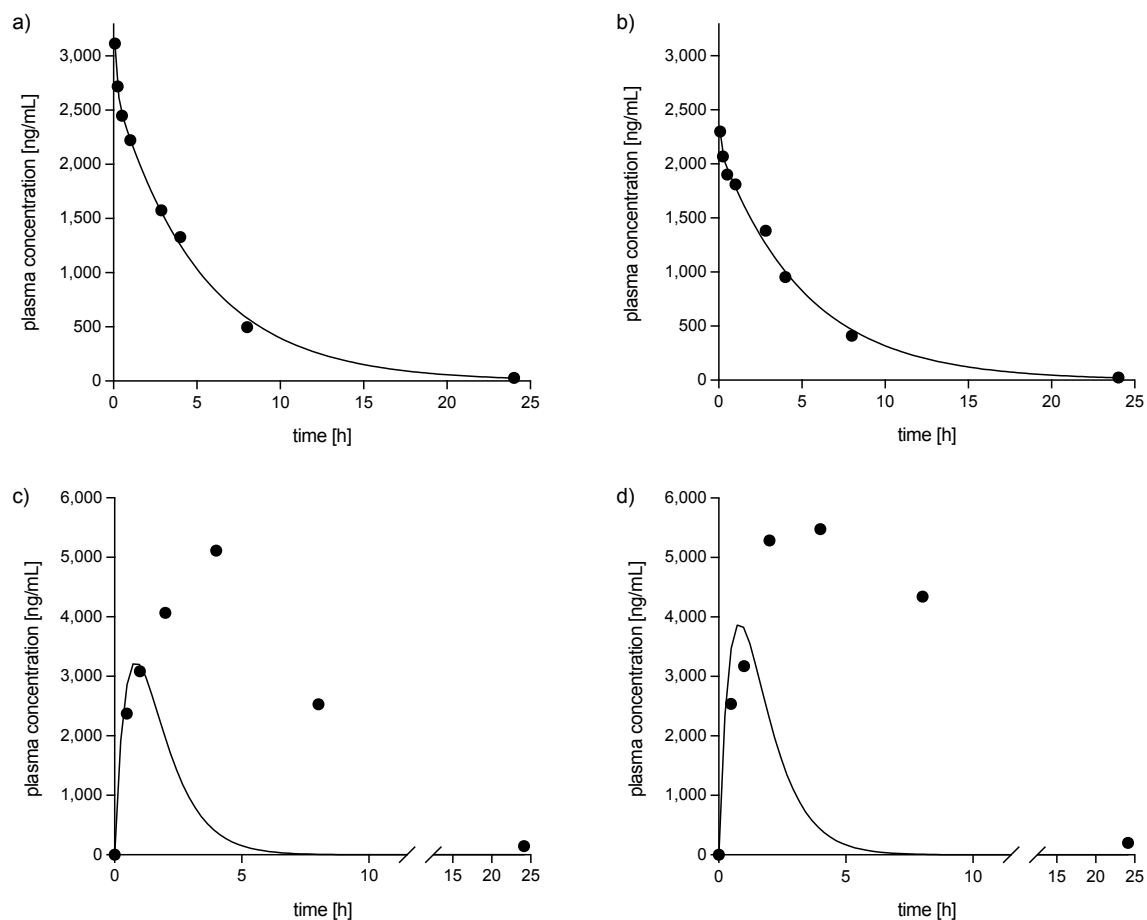


Fig. 31: Two-compartment model plots of SKL following i.v. administration of 5 mg/kg in male (a) and female (b) dogs and 50 mg/kg SKL per oral dose in male (c) and female (d) dogs. The mean values of the observed concentrations are displayed by circles and the solid line represents the calculated curve.

The parameters obtained by CA following i.v. dosing show relatively strong deviations to the values derived by NCA when the animals are considered individually (Tab. 21). If, however, the values are not compared separately but rather the mean value of the respective gender, the estimated parameters correspond quite well with the actual parameters. This is also reflected in the graphical representation (Fig. 31a,b), which compares the plasma concentration profile predicted by the two-compartment model with the actual one, derived from the mean values. The assessment of the precision of model's prediction is accordingly good. Especially noteworthy is the coefficient of correlation R^2 , which is very close to 1.

However, the quality of the selected pharmacokinetic model after oral administration is completely different. The large deviations of the estimated values from the calculated ones (Fig. 31c,d) lead to the conclusion that this model is not suitable to

describe the pharmacokinetic profile of SKL in dogs after p.o. administration. The reason for the inadequate curve fitting may be the unusual absorption and elimination profile of SKL in dogs observed after oral dosing. Unfortunately, the possibilities for model modifications in the add-in program PKSolver2.0 are limited.

As expected from the NCA-results, compartmental analysis to determine the pharmacokinetic parameters of SKL following capsule dosing could not be performed. This is due to the completely obscure plasma concentration-time profiles that resulted from this route of administration. Thus, on the basis of the available data, no compartmental model could be created to describe the pharmacokinetic profile of SKL after extravascular administration. Nevertheless, it was possible to establish a two-compartment model to estimate the parameters of SKL following i.v. administration in dogs.

3.3.3. Pharmacokinetic Studies of Skepinone-L and Sorafenib in Rats

The rat was the second rodent species used and the strain of choice was the Sprague Dawley rat. The *in vivo* section was performed at the Research Toxicology Centre in Pomezia (Italy) and sponsored by c-a-i-r biosciences GmbH in Ulm, Germany. The study consisted of two parts (I and II) and its purpose was to examine the potential interaction in the disposition of SKL and SRF. The experimental setup for each part is further described in the following sections 3.3.3.1 and 3.3.3.3. Study design in detail and the analytical method used to quantify SKL and SRF simultaneously in rat plasma are described in chapter 5.2.3.4 (Pharmacokinetic Study of Skepinone-L and Sorafenib in Rats).

3.3.3.1. Part I: Skepinone-L in Rats via Single Dosing

The objective of study part I was to investigate the pharmacokinetic profile of SKL after single oral administration. Low, mediate and high dosing was applied in order to select dose levels and frequency of dosing for the following study part II. Single intravenous application served to compare the data obtained. As given in table 22, five groups of three male rats each, were treated once with 5, 15 or 50 mg/kg per oral dose and with 3 or 10 mg/kg via single bolus injection.

group number	route of administration	dose [mg/kg]
1	oral	5
2	oral	15
3	oral	50
4	intravenous	3
5	intravenous	10
6*	intravenous	5

Tab. 22: Overview of the treatment groups during pharmacokinetic studies of SKL in rats part I. Each treatment group consisted of three animals. *group was included after end of treatment of group 1-5

Since unfortunately some animals of group 5 died during the testing phase, group number 6 was included after experimental completion of the treatment of group 1 till 5. The concentration-time profiles of all treated groups are shown in figure 32a-c and 33a-c.

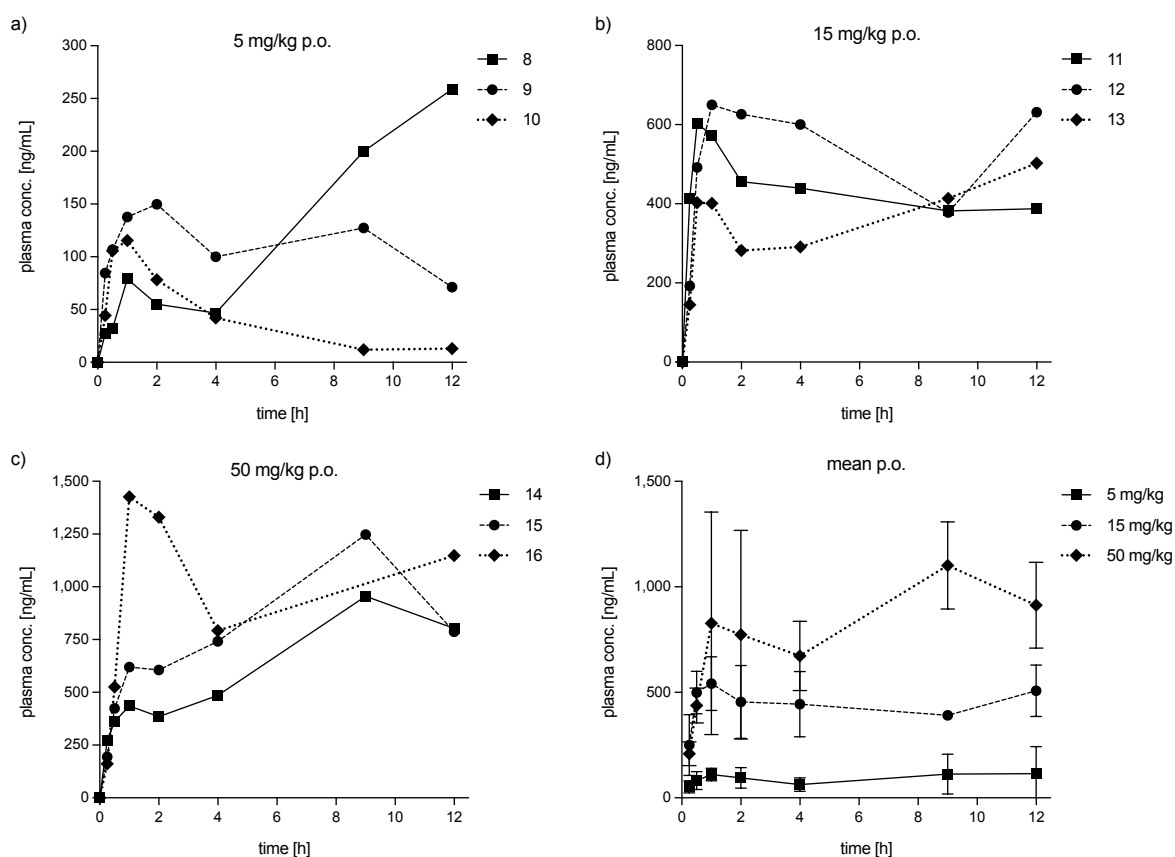


Fig. 32: Individual plasma concentration vs. time curves of SKL in rats from treatment group 1 (a), 2 (b) and 3 (c) as well as their mean plasma concentration vs. time profiles (d) including the standard deviation represented by error bars.

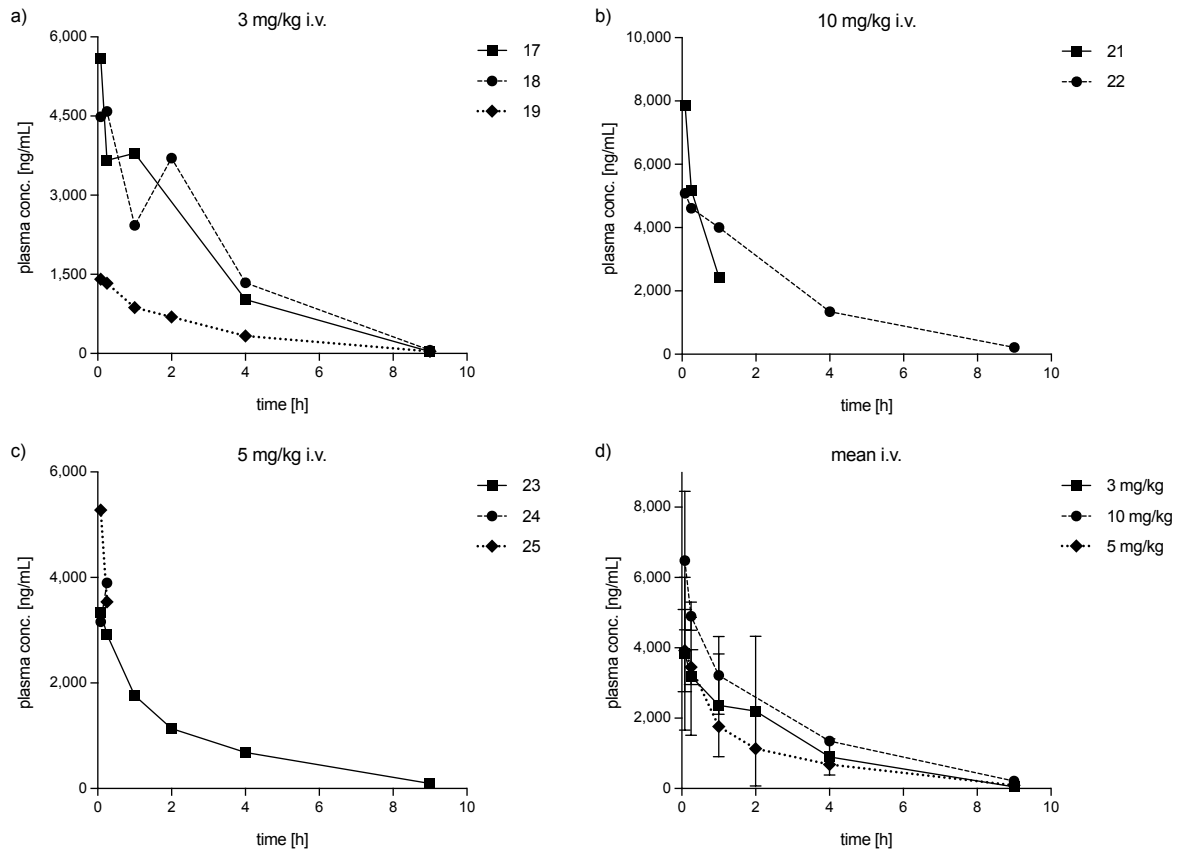


Fig. 33: Individual plasma concentration vs. time curves of SKL in rats from treatment group 4 (a), 5 (b) and 6 (c) as well as their mean plasma concentration vs. time profiles (d) including the standard deviation represented by error bars.

3.3.3.2. Part I: Pharmacokinetic Data Analysis and Parameter Calculation

Non-Compartmental Analysis

The calculated parameters (Tab. 23-25) as well as the plasma concentration curves (Fig. 33a-d) of groups 1 till 3 show non-expected pharmacokinetic profiles of SKL in rats after extravascular administration. Within the first two hours post-dosing, the absorption of SKL occurs with minor differences and deviations. In most animals C_{max} has been reached and the decrease of plasma concentration has already started. Surprisingly, after these first two hours, further degradation flattens sharply and, contrary to expectations, the concentration in the plasma rises to partially higher concentrations than the first observed maximum. The higher the oral dose of SKL, the flatter the subsequent elimination phase, and the more pronounced the effect of the increase in concentration. Regardless of the dose applied, at least one rat in each treatment group shows no clearly discernible terminal elimination phase, which is

reflected by the missing values for λ_z , $t_{1/2}$ and $AUC_{0-\infty}$. Even some animals, for which all parameters could be calculated, showed no valuable elimination slope in plasma concentration within the observed time. Animal number 10 from treatment group 1 (*, Tab 23) is the only tested rat which displays an expected pharmacokinetic profile following single oral administration of SKL. But higher AUC and $t_{1/2}$ than expected are not necessarily disadvantageous. They could indicate that a lower dosage would be sufficient.

treatment group 1						
animal	C_{max} [ng/mL]	t_{max} [h]	AUC_{0-t} [ng·h/mL]	λ_z [1/h]	$t_{1/2}$ [h]	$AUC_{0-\infty}$ [ng·h/mL]
8	259	12.0	1,512	N/A	N/A	N/A
9	150	2.0	1,356	0.1	13.8	2,772
10*	115	1.0	469	0.2	3.3	532
mean	175	5.0	1,112	0.1	8.6	1,652
± s.d.	61	5.0	459	0.1	5.2	1,120
C.V.	35 %	99 %	41 %	61 %	61 %	68 %

Tab. 23: Pharmacokinetic parameters for SKL determined by NCA from individual plasma concentration vs. time curves in male rats after single oral administration of 5 mg/kg SKL. N/A = not available; mean, s.d. and CV values for λ_z , $t_{1/2}$ and $AUC_{0-\infty}$ are calculated from animal 9 and 10. *only animal of this group with relatively expected pharmacokinetic profile

Peak concentrations in the first group range from 115 - 259 ng/mL, with the highest concentration observed in animal 8 occurring at the last sampling period of 12 h. A t_{max} of 12 h was also observed in treatment group 2, but here it corresponds to the lowest determined concentration from a range of 503 to 650 ng/mL (Tab. 24). The maximum observed concentrations of 955 - 1,427 ng/mL in group 3 occurred after 1.0 and 9.0 h post-dosing. However, since the sample at 9 h from animal 16 is not available and its plasma concentration shows a significant increase after 12 h, it could not be excluded that all three animals show the same t_{max} of 9 h (Tab. 25).

treatment group 2						
animal	C_{max} [ng/mL]	t_{max} [h]	AUC_{0-t} [ng·h/mL]	λ_z [1/h]	$t_{1/2}$ [h]	$AUC_{0-\infty}$ [ng·h/mL]
11	603	0.5	5,091	0.0	37.7	26,183
12	650	1.0	6,221	0.0	35.0	38,121
13	503	12.0	4,339	N/A	N/A	N/A
mean	586	4.5	5,217	0.0	36.4	32,152
± s.d.	62	5.3	773	0.0	1.4	5,969
C.V.	11 %	118 %	15 %	4 %	4 %	19 %

Tab. 24: Pharmacokinetic parameters for SKL calculated by NCA from individual plasma concentration vs. time curves in male rats after single oral administration of 15 mg/kg SKL. N/A = not available; mean, s.d. and CV values for λ_z , $t_{1/2}$ and $AUC_{0-\infty}$ are calculated from animal 11 and 12.

treatment group 3						
animal	C _{max} [ng/mL]	t _{max} [h]	AUC _{0-t} [ng·h/mL]	λ _z [1/h]	t _{1/2} [h]	AUC _{0-∞} [ng·h/mL]
14	955	9.0	7,830	N/A	N/A	N/A
15	1,248	9.0	10,349	N/A	N/A	N/A
16	1,427	1.0	11,853	0.0	54.9	102,664
mean	1,210	6.3	10,011	-/-	-/-	-/-
± s.d.	195	3.8	1,660	-/-	-/-	-/-
C.V.	16 %	60 %	17 %	-/-	-/-	-/-

Tab. 25: Pharmacokinetic parameters for SKL derived by NCA from individual plasma concentration vs. time curves in male rats after single oral administration of 50 mg/kg SKL. N/A = not available

Because almost every plasma concentration profile of SKL obtained is different for each tested animal, independent of its group, no direct correlation between the level of oral doses and the determined parameters can be observed. The only thing that really stands out is that the higher the administered dose, the more unexpected the concentration profiles are. Usually, after reaching C_{max}, the elimination rate exceeds the absorption rate until only elimination processes are present. Here, however, it seems that SKL is absorbed over almost the entire experimental duration and is being eliminated only relatively slowly. The extent of this effect seems to correlate with the dose applied. Therefore, it can be assumed that the absorption and/or elimination processes are influenced in an unknown way.

Possibly, due to the rats' anatomy and the poor aqueous solubility of SKL, precipitation processes in the gastrointestinal tract may occur. The solubility and thus absorption of SKL may also have been influenced by interactions with dietary components [127], since the animals had *ad libitum* access to the high fat diet. Plasma-protein binding and the associated prevention of renal elimination can also not be excluded. Enterohepatic circulation should also be considered, as the secondary absorption phases and the resulting multiple peaks in pharmacokinetic profiles in combination with the relatively long t_{1/2} are among its characteristics [128]. Based on the data obtained and generated so far, unfortunately none of these assumptions can be confirmed or even disproved.

In contrast, the pharmacokinetic profiles of SKL after i.v. injection (Fig. 33) initially show expected and comprehensible curves. However, during the *in vivo* phase some animals died shortly post-dosing. Therefore, only few complete plasma concentration curves were available to determine the pharmacokinetic parameters.

treatment group 4							
animal	C_0 [ng/mL]	AUC_{0-t} [ng·h/mL]	λ_z [1/h]	$t_{1/2}$ [h]	$AUC_{0-\infty}$ [ng·h/mL]	V_{ss} [L/kg]	CI [L/h/kg]
17	6,928	13,961	0.6	1.2	14,021	0.4	0.2
18	4,486	15,372	0.6	1.2	15,473	0.4	0.2
19	1,449	3,921	0.4	1.7	4,022	1.8	0.7
mean	4,288	11,085	0.5	1.4	11,172	0.9	0.4
± s.d.	2241	5,098	0.1	0.3	5,090	0.7	0.3
C.V.	52 %	46 %	17 %	19 %	56 %	75 %	67 %

Tab. 26: Pharmacokinetic parameters for SKL derived by NCA from individual plasma concentration vs. time curves in male rats after single intravenous administration of 3 mg/kg SKL.

While considering the results of treatment group 4, it should be mentioned that almost all pharmacokinetic data sets are complete here, only the sample at 2 h from animal 17 is not available. The obtained profiles and the determined pharmacokinetic parameters following 3 mg/kg SKL per intravenous route are displayed in figure 33a and table 26, respectively. Both the graphical and tabular representation show that rats 17 and 18 have very similar pharmacokinetic behaviours. Roughly analysed, they have a comparable maximum concentration and a similar trend in the elimination phase. However, within the first two hours post-dosing pharmacokinetic profiles of both rats also show unexpected increases in concentration. The plasma level of SKL after 15 minutes in animal 18 is even higher than the concentration at 5 minutes, which should actually be the measured C_{max} . These variations are also embodied by the associated areas under the curves. Although rat 17 has the highest extrapolated C_0 with 6,928 ng/mL, its AUC_{0-t} and $AUC_{0-\infty}$ with values of 13,961 and 14,021 ng·h/mL are slightly below those of animal 18. Another conspicuous feature of both profiles is the determined V_{ss} with 0.4 L/kg, which is < 0.6 L/kg and can thus be classified as low [22].

Animal 19, the third rat from this treatment group, has a plasma concentration profile which meets the expectations following intravenous administration. On the one hand, the maximum concentration occurred at the first sampling time. On the other hand, it decreased steadily without unexpected further concentration peaks. However, this shows strong deviations from the previous profiles of this group. The calculated maximum concentration C_0 of 1,449 ng/mL, the AUC_{0-t} of 3,921 ng·h/mL and the $AUC_{0-\infty}$ of 4,022 ng·h/mL are about 68-79% below the scores of the other two animals. This explains the relatively high standard deviations and coefficients of variation. Despite this significantly lower plasma concentrations, SKL could also be detected in the plasma of this rat over the entire test period.

Treatment group 5 received a high dose of 10 mg/kg SKL administered by intravenous injection. Unfortunately, one rat died immediately after dosing and a second rat, number 21, passed away before the sample at 2 h could be taken. This means, only one complete profile was available to determine the pharmacokinetic parameters (Tab. 27). Thus, no averages have been calculated, as the values of rat 21 are not taken into account due to the limited data available, and therefore incomplete pharmacokinetic profile.

treatment group 5							
animal	C ₀ [ng/mL]	AUC _{0-t} [ng·h/mL]	λ _z [1/h]	t _{1/2} [h]	AUC _{0-∞} [ng·h/mL]	V _{ss} [L/kg]	Cl [L/h/kg]
21	9,710	4,677	1.2	0.6	6,711	1.2	1.5
22	5,341	16,405	0.4	1.9	16,996	1.4	0.6

Tab. 27: Pharmacokinetic parameters for SKL derived by NCA from individual plasma concentration vs. time curves in male rats after single intravenous administration of 10 mg/kg SKL.

Regarding the values obtained, the unexpectedly low plasma concentration is immediately noticeable. As group 5 received 3.3-times more SKL than group 4, the low C₀ of 5,341 ng/mL stands out, which is only 1.2-times the average of group 4. Also, none of the other pharmacokinetic parameters determined show significant dose-dependent differences compared to the low-dose group. As only few data are available, these results should be viewed critically.

Treatment group 6 was added after the experimental trial of the previous groups was completed. Reason for including more animals in this part of the study was that two of three animals died shortly after receiving 10 mg/kg SKL per i.v. injection. The cause of this high mortality rate could not be clearly identified, but as in the bioavailability study in dogs, the focus of suspicion is on the formulation rather than the test substance. Based on this hypothesis, the volume of the administered dose was halved from 5 mL/kg to 2.5 mL/kg. Apart from this amendment, the rest of the study design remained unchanged, so that the intravenous dose of group 6 was 5 mg/kg.

Unfortunately, the concentration-time profiles obtained (Fig.33c) and the values derived from NCA (Tab. 28) show almost the same outcome as after treatment of group 5. Again, only one animal survived the study and provided a complete pharmacokinetic profile. The remaining rats died within one hour after administration. It is possible that despite the halved amount, the administered dose exceeded the

tolerable range of substance/vehicle. Therefore, as described above, no mean values were calculated due to incomplete data sets.

Fortunately, expected behaviour and usable data are shown from the only available complete pharmacokinetic profile and resulting parameters of animal 23. It is remarkable that the values of AUC_{0-t} and $AUC_{0-\infty}$ of 7,776 and 8,036 ng·h/mL, respectively, correspond to about half of the values when compared with the data derived from animal 22 which was treated with the doubled dose. The maximum concentration C_0 of 3,573 ng/mL determined here is about 67 % of the concentration observed after the i.v. administration of 10 mg/kg SKL. The other pharmacokinetic parameters as $t_{1/2}$, V_{ss} and Cl show similar or even identical values between the medium and high dose.

treatment group 6							
animal	C_0 [ng/mL]	AUC_{0-t} [ng·h/mL]	λ_z [1/h]	$t_{1/2}$ [h]	$AUC_{0-\infty}$ [ng·h/mL]	V_{ss} [L/kg]	Cl [L/h/kg]
23	3,573	7,776	0.4	1.9	8,036	1.6	0.6
24	3,159	851	N/A	N/A	N/A	N/A	N/A
25	6,443	1,223	N/A	N/A	N/A	N/A	N/A

Tab. 28: Pharmacokinetic parameters for SKL derived by NCA from individual plasma concentration vs. time curves in male rats after single intravenous administration of 5 mg/kg SKL.

However, if all three concentration levels of the i.v. dosage are considered, these correlations change. Surprisingly, the lowest dose of 3 mg/kg does not result in the lowest values for C_0 , AUC_{0-t} and $AUC_{0-\infty}$, but instead relatively minor values for $t_{1/2}$, V_{ss} and Cl with more or less pronounced differences. However, these observations refer to the mean values of treatment group 4, without taking into account the partly high standard deviations and coefficients of variation. Although this is the only group where all pharmacokinetic profiles are almost completely available, it was also the only group where two out of three curves showed unexpected and inexplicable behaviour. Interestingly, the correlations between dose level and observed pharmacokinetic parameters gain plausibility when only the values of animal 19 were considered instead of the mean values of the low-dose group. However, this approach cannot be verified as there is too little data available, especially from group 5 and 6.

With regard to intravenous injection, the resulted and necessary values of $AUC_{0-\infty}$ are suitable for calculating bioavailability, although some profiles are not available, and

some have an atypical course. Unfortunately, none of the $AUC_{0-\infty}$ -values obtained from p.o. administration is usable, regardless of the dose level. Therefore, it was not possible to determine the oral bioavailability of SKL in rats with this study. In addition, no compartmental analysis could be performed to calculate the pharmacokinetic parameters of SKL. On the one hand, the plasma concentration-time profiles resulted from oral administration are not evaluable due to their completely atypical curves. On the other hand, too few data sets are available after i.v. administration to be able to perform a useful calculation.

Despite the unexpected plasma profiles and relatively high mortality of the rats, both dose and frequency of dosing for part II of the study could be selected based on the data obtained here in part I.

3.3.3.3. Part II: Skepinone-L in Rats via Repetitive Dosing

The purpose of study part II was to examine the pharmacokinetic profile of SKL after repeated oral administration in male and female rats. In addition, SRF was also dosed to both sexes on consecutive days and served as reference. The treatment period in part II lasted 14 days and was divided into phase A and B (Tab. 29). At the beginning of this study part, the three treatment groups consisted of six male and six female rats each. Another group served as control group and included three rats per gender. During phase A, group 7 received the test vehicle while the treated group 8 was dosed with 15 mg/kg SKL and group 9 with 50 mg/kg SKL. The last treatment group no. 10 received 25 mg/kg SRF, as the other groups per oral dose once daily for seven consecutive days. After the completion of phase A on day 8, the first three animals per gender of group 8, 9 and 10 were sacrificed and phase B was started. During this phase, the remaining animals were treated with 25 mg/kg SRF or a combination of 15 or 50 mg/kg SKL with 25 mg/kg SRF for a further seven days.

group number	phase A		phase B		number of animals	
	treatment day 1 - 7	dose day 1 – 7 [mg/kg/day]	treatment day 8 - 14	dose day 8 - 14 [mg/kg/day]	♂	♀
7	-/-*	-/-*	SRF	25	3	3
8	SKL	15	SKL+SRF	15+25	6	6
9	SKL	50	SKL+SRF	50+25	6	6
10	SRF	25	SKL+SRF	50+25	6	6

Tab. 29: Overview of treatment groups during the PK studies of SKL in rats part II. *group 7 served as control group and received blank vehicle

This made it possible to investigate the potential interaction between SKL and SRF and to determine whether there are any gender-related differences. In addition, the extensive set-up enabled to examine whether these possible correlations were influenced by dose levels of SKL or the order of the two compounds administered.

3.3.3.4. Part II: Pharmacokinetic Data Analysis and Parameter Calculation for Skepinone-L

The pharmacokinetic profiles (Fig. 34) of treatment group 8 after completion of phase A show a similar behaviour to that observed in part I after single oral administration. Almost all profiles of both genders show, to varying extent, a peak in concentration shortly after dosage, followed by a brief decrease before increasing again. Thus, no clear absorption and elimination phases can be identified. Despite the repeated unexpected plasma concentration profiles all parameters could be determined this time (Tab. 30). However, they reflect the visually observed inconsistency by showing high coefficients of variation for t_{max} , $t_{1/2}$ and $AUC_{0-\infty}$ of up to 97 %. In contrast, the resulting AUC_{0-t} appears to be comparable with C.V. of 14 % for male and 4 % for female rats.

The maximum concentration in plasma to occurs 2.9 h later in male rats, so that a slight difference between both gender groups can be observed with regard to t_{max} . However, the individual values are quite scattered, especially among the three female rats. Therefore, it cannot be clearly concluded that this difference is gender-specific.

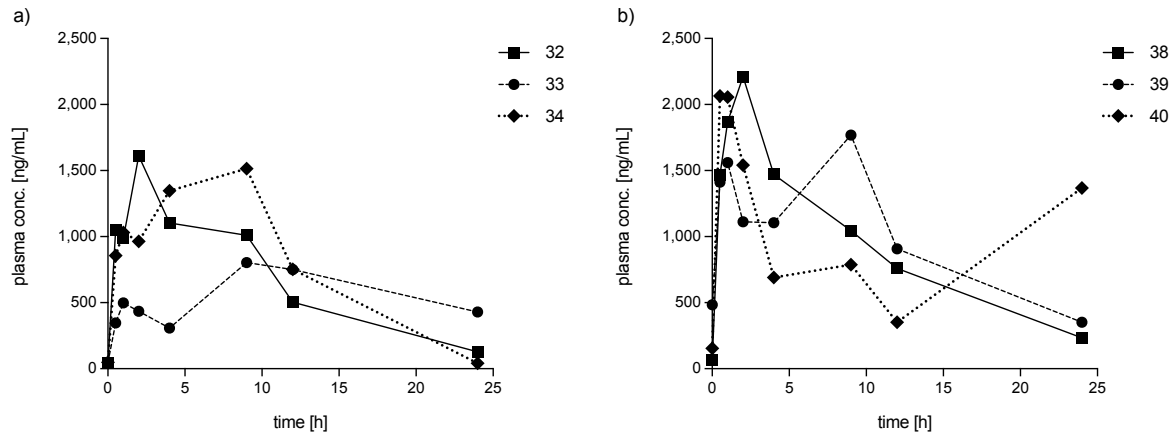


Fig. 34: Individual plasma concentration vs. time curves of SKL in male (a) and female (b) rats from treatment group 8, phase A (oral administration of 15 mg/kg/day SKL on seven consecutive days).

Interestingly, the concentrations within the same gender have relatively similar values, but their mean C_{max} with 1,310 ng/mL in male and 2,015 ng/mL in female rats are clearly different. Despite this relatively low C_{max} in male compared to female rats, the concentration here is almost twice as high as that obtained after single oral administration in study part I. While this result suggests a stationary state of SKL in rats obtained via repetitive dosing on seven consecutive days, it should be noted that interestingly, plasma concentrations at 0 h were mostly below those observed 24 h post-dosing.

treatment group 8, phase A							
animal		C_{max} [ng/mL]	t_{max} [h]	AUC_{0-t} [ng·h/mL]	λ_z [1/h]	$t_{1/2}$ [h]	$AUC_{0-\infty}$ [ng·h/mL]
32	♂	1,611	2.0	16,158	0.1	6.1	17,293
33	♂	805	9.0	13,712	0.0	16.1	23,695
34	♂	1,515	9.0	19,325	0.2	2.9	19,497
38	♀	2,212	2.0	21,894	0.1	7.0	24,244
39	♀	1,768	9.0	23,521	0.1	7.0	27,060
40	♀	2,066	0.5	21,341	0.0	27.7	75,978
mean		1,310	6.7	16,398	0.1	8.4	20,162
± s.d.	♂	360	3.3	2,298	0.1	5.6	2,656
C.V.		27 %	49 %	14 %	62 %	67 %	13 %
mean		2,015	3.8	22,252	0.1	13.9	42,428
± s.d.	♀	185	3.7	925	0.0	9.8	23,752
C.V.		9 %	97 %	4 %	47 %	70 %	56 %

Tab. 30: Pharmacokinetic parameters for SKL derived by NCA from individual plasma concentration vs. time curves in male and female rats of treatment group 8 during phase A after oral administration of 15 mg/kg/day SKL on seven consecutive days.

Treatment group 8 received a combination of 15 mg/kg/day SKL and 25 mg/kg/day SRF for another seven consecutive days during phase B. Both the resulting

pharmacokinetic profiles and the parameters derived from NCA, which are illustrated in figure 35 and given in table 31 show relatively expected curves and quite useable data. With the exception of the half-life in plasma observed in female rats, almost all values obtained show relatively acceptable variations.

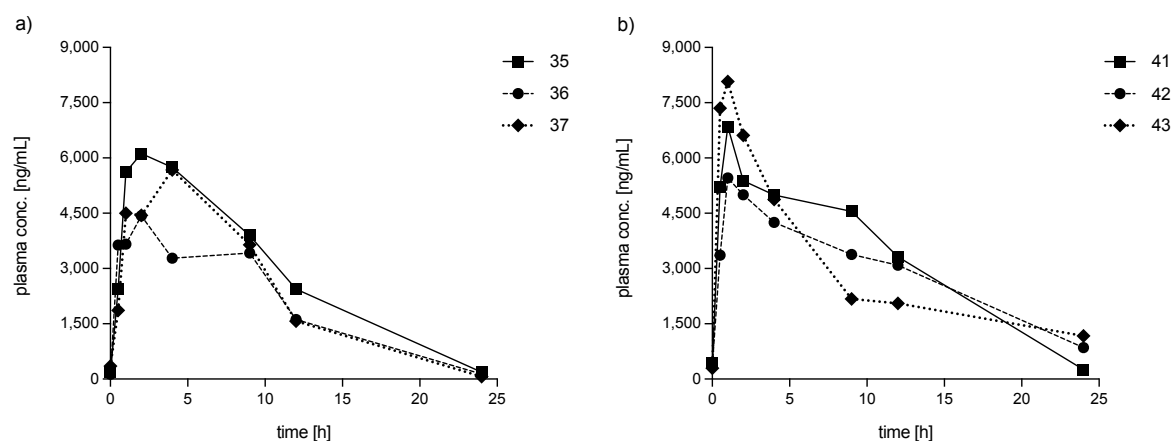


Fig. 35: Individual plasma concentration vs. time curves of SKL in male (a) and female (b) rats from treatment group 8, phase B (oral administration of 15 mg/kg/day SKL combined with 25 mg/kg/day SRF on seven consecutive days).

Remarkably high peak concentrations of 4,432 to 8,073 ng/mL were reached, and the time of their occurrence is quite similar in the whole treatment group. In addition, compared to the previous studies in rat, it occurs relatively shortly after the dose is administered.

treatment group 8, phase B							
animal		C_{max} [ng/mL]	t_{max} [h]	AUC_{0-t} [ng·h/mL]	λ_z [1/h]	$t_{1/2}$ [h]	$AUC_{0-\infty}$ [ng·h/mL]
35	♂	6,121	2.0	69,784	0.2	3.4	70,692
36	♂	4,432	2.0	49,323	0.2	3.3	49,955
37	♂	5,676	4.0	57,677	0.3	2.6	57,929
41	♀	6,848	1.0	78,014	0.2	3.5	79,316
42	♀	5,456	1.0	70,084	0.1	7.2	78,957
43	♀	8,073	1.0	67,904	0.0	16.1	95,141
mean		5,410	2.7	58,928	0.2	3.1	59,525
± s.d.	♂	715	0.9	8,400	0.0	0.3	8,541
C.V.		13 %	35 %	14 %	12 %	11 %	14 %
mean		6,792	1.0	72,001	0.1	9.0	84,471
± s.d.	♀	1,069	0.0	4,344	0.1	5.3	7,546
C.V.		16 %	0 %	6 %	57 %	59 %	9 %

Tab. 31: Pharmacokinetic parameters for SKL derived by NCA from individual plasma concentration vs. time curves in male and female rats of treatment group 8 during phase B after oral administration of 15 mg/kg/day SKL combined with 25 mg/kg/day SRF on seven consecutive days.

Particularly strong differences are observed in the values for AUC_{0-t} and $AUC_{0-\infty}$ with 72,001 and 84,471 ng·h/mL in female animals. These are thus significantly higher than

the values of 58,928 and 59,525 ng·h/mL observed in male rats. Interestingly, the differences between both genders in terms of C_{max} and t_{max} are no longer as pronounced as before.

Figure 36 illustrates the mean plasma-concentration versus time profiles of SKL obtained from treatment group 8 during phase A and B in male and female rats.

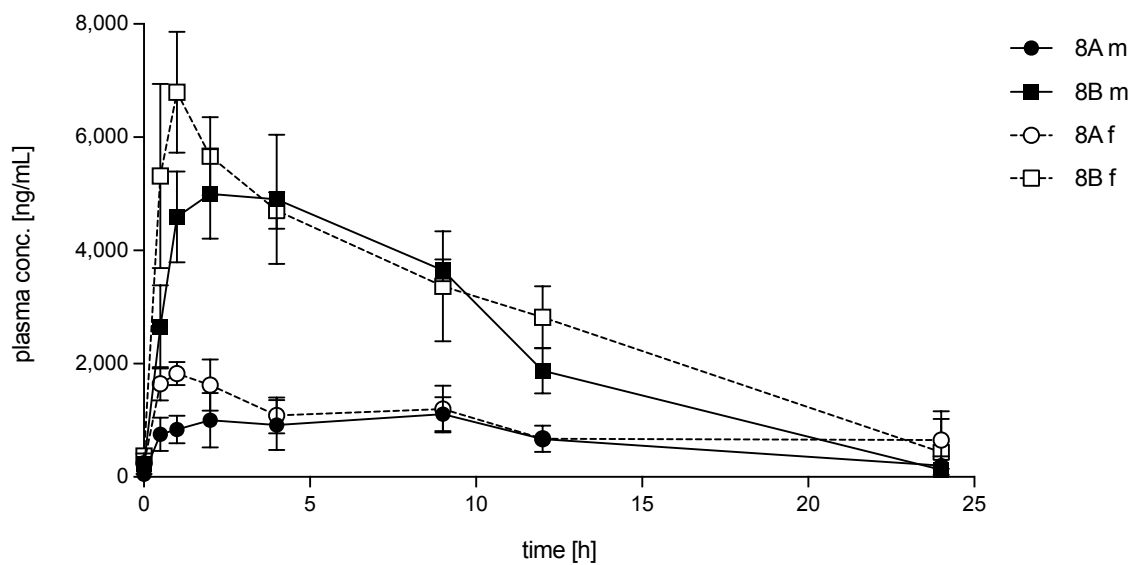


Fig. 36: Mean plasma concentration vs. time curves of SKL in male (solid line) and female (dashed line) rats from treatment group 8, phase A (circles) and phase B (squares). Phase A included oral administration of 15 mg/kg/day SKL for seven days. During phase B treatment consisted of a combination of 15 mg/kg/day SKL with 25 mg/kg/day SRF for seven consecutive days. $n = 3$; standard deviation (\pm) is represented by error bars

When comparing the plasma profiles of male and female rats, notwithstanding the study phase, it is clearly noticeable, that the concentration levels in females are almost consistently higher. This difference is particularly marked in the first 4 hours after administration. Interestingly, female rats show rather expected pharmacokinetic profiles with relatively clear phases of absorption and elimination, while plasma concentration of SKL in male rats seem to remain on a kind of plateau for several hours.

The differences between concentrations of SKL in rat plasma obtained after study phase A and B are more than obvious. Following phase B, a significant increase in the plasma concentration can be seen. This can be observed in male and female rats to nearly the same extent. After seven days of treatment, SRF appears to affect plasma levels of SKL in rats by increasing them in a hitherto unexplained way. However, this

is the first study in which SKL was administered daily to rats over a prolonged period. Therefore, apart from theoretical calculations, there is no experimental data on the time it takes for SKL to reach steady state. Possibly, after completion of phase A, which took seven days, steady state of SKL was not yet achieved. Moreover, almost nothing is known about possible saturable first-pass metabolism so far. Thus, the observed effect can be induced by the presence of SRF or is merely due to the prolonged treatment with SKL.

treatment group 9, phase A							
animal		C_{max} [ng/mL]	t_{max} [h]	AUC_{0-t} [ng·h/mL]	λ_z [1/h]	$t_{1/2}$ [h]	$AUC_{0-\infty}$ [ng·h/mL]
44	♂	2,118	9.0	35,457	0.2	4.6	37,131
45	♂	1,732	9.0	32,246	0.0	18.6	57,420
46	♂	1,949	9.0	29,175	0.1	10.1	37,703
50	♀	5,959	1.0	83,784	0.1	12.6	117,995
51	♀	5,775	9.0	91,412	0.1	10.7	125,728
52	♀	4,096	2.0	70,629	0.0	31.8	177,047
mean		1,933	9.0	32,293	0.1	11.1	44,084
± s.d.	♂	158	0.0	2,565	0.0	75.7	9,432
C.V.		8 %	0 %	8 %	56 %	52 %	21 %
mean		5,277	4.0	81,942	0.1	18.4	140,257
± s.d.	♀	839	3.6	8,584	0.0	9.5	26,206
C.V.		16 %	89 %	10 %	39 %	52 %	19 %

Tab. 32: Pharmacokinetic parameters for SKL derived by NCA from individual plasma concentration vs. time curves in male and female rats of treatment group 9 during phase A after oral administration of 50 mg/kg/day SKL on seven consecutive days.

The pharmacokinetic parameters determined by NCA for treatment group 9 after completing phase A of study part II (Tab. 32) show within the group, similar results with relatively low variance, except for the values for $t_{1/2}$ of both genders and for t_{max} in female rats. Although this group received 3.3-times the dose compared to treatment group 8, the mean values of the obtained C_{max} of 1,933 in male and 5,277 ng/mL in female rats were only 1.5- and 2.6-times respectively. However, they occur later after administration, and the respective AUC_{0-t} and $AUC_{0-\infty}$ are also significantly higher. The underlying plasma concentration-time curves used to determine the data are shown in figure 37 and explain these results.

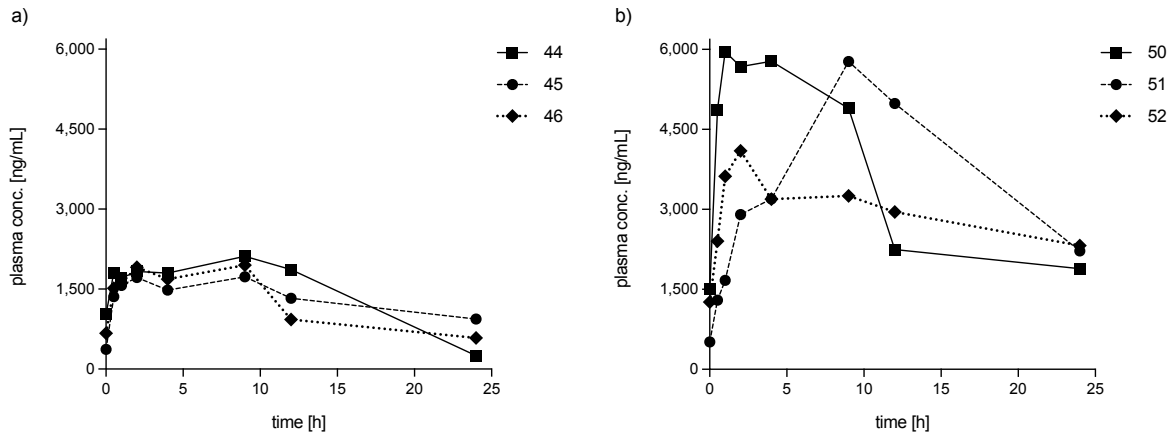


Fig. 37: Individual plasma concentration vs. time curves of SKL in male (a) and female (b) rats from treatment group 9, phase A (oral administration of 50 mg/kg/day SKL on seven consecutive days).

These profiles show similar behaviour to that observed in study part I after a single oral administration of 50 mg/kg SKL. But the plasma concentrations within the first two hours post-dosing are clearly higher and therefore the plasma levels seem to remain on a kind of plateau instead of rising further, which explains the mean values of C_{max} , AUC_{0-t} and $AUC_{0-\infty}$. Gender-specific differences in terms of maximum plasma concentration and time of their appearance as well as the observed half-life in plasma are more pronounced than at lower doses.

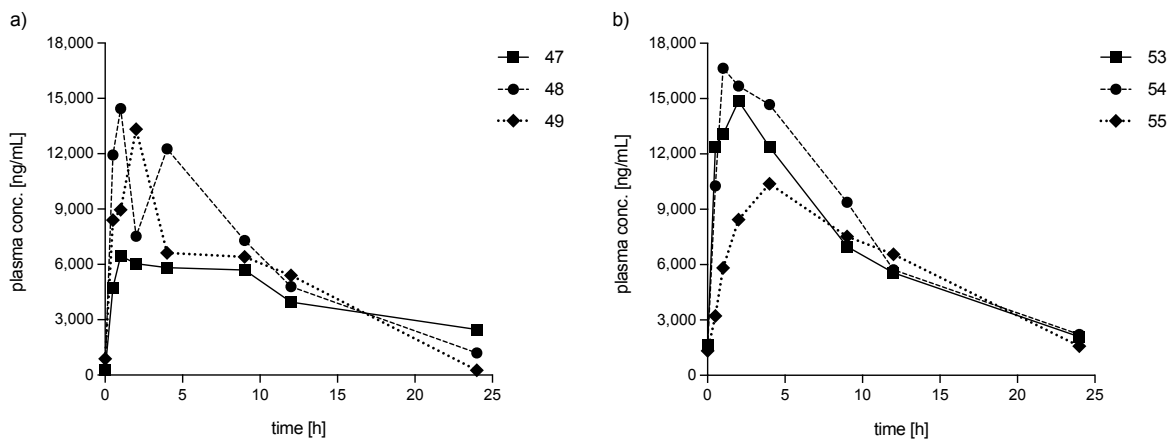


Fig. 38: Individual plasma concentration vs. time curves of SKL in male (a) and female (b) rats from treatment group 9, phase B (oral administration of 50 mg/kg/day SKL combined with 25 mg/kg/day SRF on seven consecutive days).

Subsequently to treatment with 50 mg/kg/day SKL, group 9 was given additional 25 mg/kg/day SRF for further seven days. The obtained individual plasma concentration profiles of SKL in male rats after phase B (Fig. 38) show clearly unlike characteristics compared to phase A. In contrast to the similarities observed before,

all three concentration curves show different courses. The plasma concentration of animal number 47 seems to remain stable at a low level for several hours. Whereas the profile of 48 exhibits after a fast and strong increase a significant drop in concentration two hours after administration, which surprisingly increased again at the next sampling time and is even close to C_{max} . After a significant peak the concentration in animal 49 remains almost unchanged for several hours before it slowly decreases nearly completely.

As given in table 33, the observed C_{max} range from 6,458 to 14,451 ng/mL and the $t_{1/2}$ values of 3.1, 5.9 and 16.6 h differ strongly from each other. These wide ranges, especially in terms of C_{max} , are also present in female rats, but not as pronounced. Overall, their profiles show an absorption and elimination behaviour which can be expected following oral administration. Despite these observations, it should be emphasised that compared to phase A the mean values for C_{max} , AUC_{0-t} and $AUC_{0-\infty}$ are again significantly higher, while t_{max} and $t_{1/2}$ are clearly shorter. This effect appears to the same extent in male and female rats. Consequently, the combined treatment of SKL with SRF show the same tendencies as already observed in group 8 after phase B.

treatment group 9, phase B							
animal		C_{max} [ng/mL]	t_{max} [h]	AUC_{0-t} [ng·h/mL]	λ_z [1/h]	$t_{1/2}$ [h]	$AUC_{0-\infty}$ [ng·h/mL]
47	♂	6,458	1.0	104,071	0.0	16.6	163,309
48	♂	14,451	1.0	143,474	0.1	5.9	153,684
49	♂	13,336	2.0	122,043	0.2	3.1	123,230
53	♀	14,781	2.0	164,215	0.1	8.6	190,238
54	♀	16,647	1.0	186,625	0.1	7.6	211,037
55	♀	10,391	4.0	144,149	0.1	6.4	158,817
mean		11,415	1.3	123,196	0.1	8.5	146,741
± s.d.	♂	3,534	0.5	16,107	0.1	5.8	17,083
C.V.		31 %	35 %	13 %	58 %	68 %	12 %
mean		13,970	2.3	164,996	0.1	7.6	186,697
± s.d.	♀	2,632	1.2	17,350	0.0	0.9	21,465
C.V.		19 %	53 %	11 %	12 %	12 %	11 %

Tab. 33: Pharmacokinetic parameters for SKL derived by NCA from individual plasma concentration vs. time curves in male and female rats of treatment group 9 during phase B after oral administration of 50 mg/kg/day SKL combined with 25 mg/kg/day SRF on seven consecutive days.

The mean concentration curves of SKL in the plasma of male and female rats of treatment group 9 after completion of phase A and phase B are shown in figure 39. As already observed with the lower SKL dose, significant differences are also apparent

after administration of the higher dose, both between study phases A, B as well as between genders.

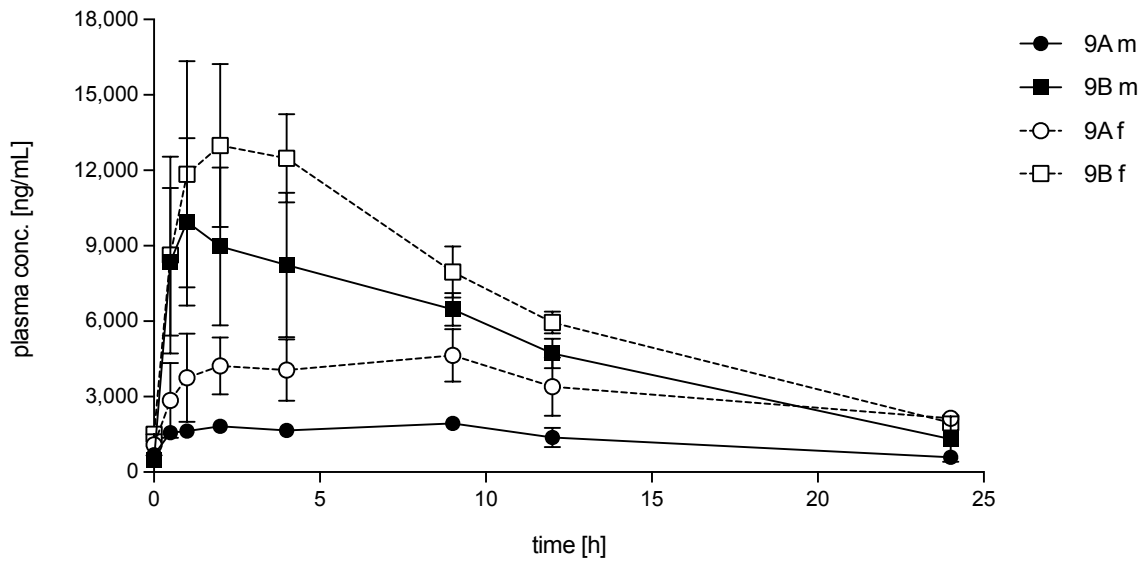


Fig. 39: Mean plasma concentration vs. time curves of SKL in male (solid line) and female (dashed line) rats of treatment group 9, phase A (circles) and phase B (squares). Phase A included oral administration of 50 mg/kg/day SKL on seven days. During phase B treatment consisted of a combination of 50 mg/kg/day SKL with 25 mg/kg/day SRF on seven consecutive days. $n = 3$; standard deviation (\pm) is represented by error bars

The question now arises explicitly whether this observed effect on the concentration of SKL in plasma is related to the presence of SRF or may be explained by the longer treatment duration. The results of the following group 10 could provide some answers in this respect.

Although groups 9 and 10 each received the same dose levels of SKL and SRF, their dosage regimens have an important difference that could provide the appropriate information. Both substances were administered in reverse order. This means that group 10 was first treated with 25 mg/kg/day SRF in phase A, before the animals were given an additional 50 mg/kg/day SKL in phase B. Thus, the rats of treatment group 10 were treated with SRF for a total of 14 days and consequently with SKL for only 7 days. The results from treatment group 10 obtained after study phase B are given in figure 40 and table 34.

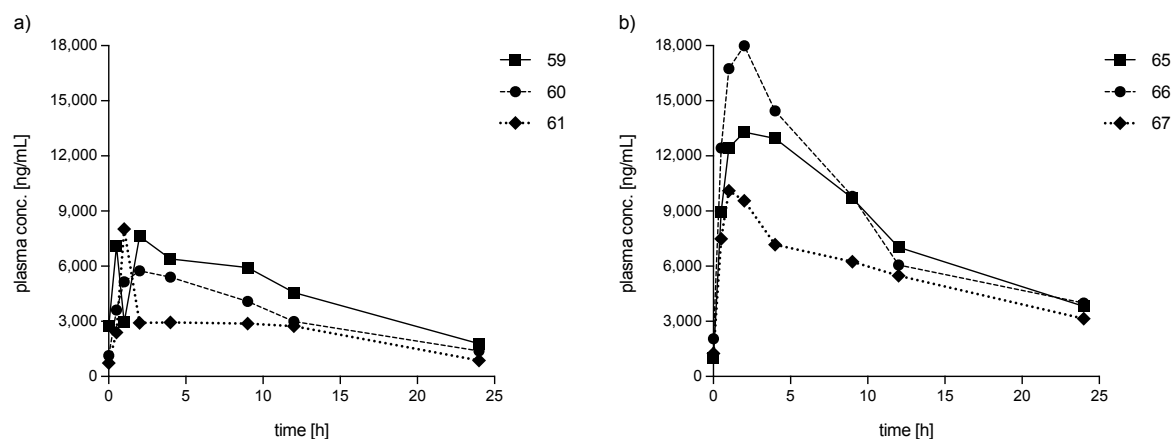


Fig. 40: Individual plasma concentration vs. time curves of SKL in male (a) and female (b) rats of treatment group 10, phase B (oral administration of 25 mg/kg/day SRF combined with 50 mg/kg/day SKL on seven consecutive days).

The resulting individual plasma curves of both male and female rats show rather similar courses compared to group 9 after phase B. Again, the male animals show unexplainable variations in their profiles. Two out of three exhibit both unexpected decreases and surprising increases in plasma concentration of SKL within the first two hours after administration.

treatment group 9, phase B							
animal		C_{max} [ng/mL]	t_{max} [h]	AUC_{0-t} [ng·h/mL]	λ_z [1/h]	$t_{1/2}$ [h]	$AUC_{0-\infty}$ [ng·h/mL]
59	♂	7,622	2.0	108,918	0.1	8.7	131,449
60	♂	5,748	2.0	80,714	0.1	10.1	101,099
61	♂	8,028	1.0	59,351	0.1	8.2	69,654
65	♀	13,292	2.0	193,750	0.1	11.7	258,257
66	♀	17,996	2.0	205,542	0.1	10.1	263,751
67	♀	10,105	1.0	136,065	0.0	15.1	204,718
mean		7,133	1.7	82,994	0.1	9.0	100,734
± s.d.	♂	993	0.5	20,300	0.0	0.8	25,229
C.V.		14 %	28 %	24 %	9 %	9 %	25 %
mean		13,798	1.7	178,453	0.1	12.3	242,242
± s.d.	♀	3,241	0.5	30,356	0.0	2.1	26,628
C.V.		23%	28 %	17 %	16 %	17 %	11 %

Tab. 34: Pharmacokinetic parameters for SKL derived by NCA from individual plasma concentration vs. time curves in male and female rats of treatment group 10 during phase B after oral administration of 25 mg/kg/day SRF combined with 50 mg/kg/day SKL on seven consecutive days.

In contrast, although the female rats differ significantly in the C_{max} achieved, their profiles show clear similarities. Furthermore, its average of 13,798 ng/mL is almost twice the C_{max} observed in male plasma. Despite the differences between all individual plasma profiles, especially within the first 10 h after administration, their standard

deviations and coefficients of variation in males and females are within an acceptable range.

As mentioned above, the results of treatment group 10 may help explain the reasons for the outcomes from previous groups after repeated administration of SKL in combination with SRF. This is because groups 8 and 9 were treated with SKL for 14 days, while group 10 received SKL for a total of seven days throughout part II of the study. Therefore, if the effect of elevated plasma concentrations of SKL is due to prolonged treatment duration, the mean values of SKL in plasma of group 10 should be similar to those after phase A of group 9. However, if the presence of SRF induces the effect, the results here should be comparable to phase B of group 9.

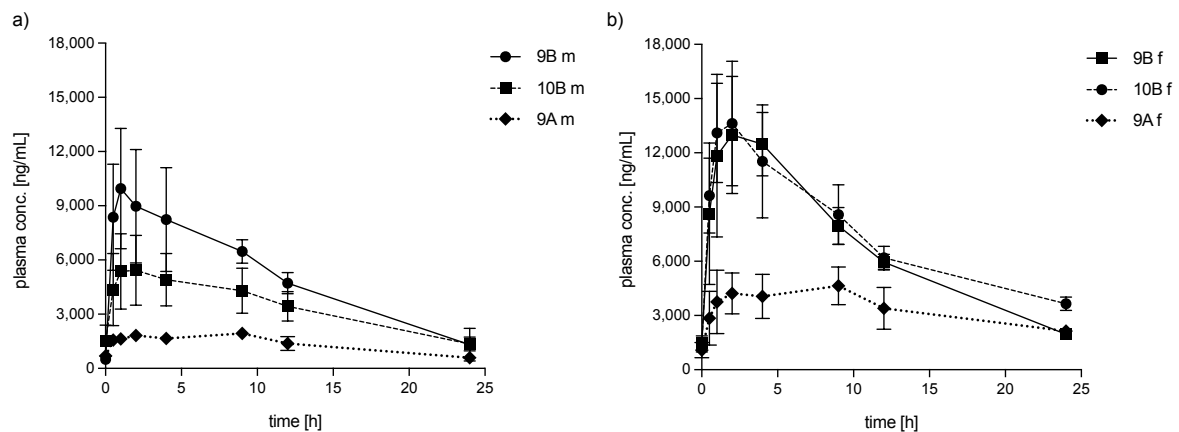


Fig. 41: Mean plasma concentration vs. time curves of SKL in male (a) and female (b) rats from treatment group 9, phase A (rhombus), phase B (circles) and group 10 phase B (squares). Treatment consisted of a combination of 50 mg/kg/day SKL with 25 mg/kg/day SRF on seven consecutive days, whereby both groups differ in the order in which the substances were administered. $n = 3$; standard deviation (\pm) is represented by error bars

Therefore, a direct comparison of the mean plasma concentration profiles of group 9 and 10 each after completion of phase B could help to clarify the question. The profiles mentioned above are shown in figure 41 in comparative representation for male (a) and female (b) rats. Including the concentration curves of group 9 obtained after phase A served to highlight possible differences or similarities more clearly.

This graph clearly shows the previously observed differences between male and female rats in the plasma concentrations of SKL achieved. Interestingly, the mean plasma concentration curve for male rats, which resulted from group 10 after phase B, lies almost exactly between the two phases from group 9. In addition, the values

obtained during phase B for both group 9 and group 10 show relatively high standard deviations, although they partly overlap. Thus, despite those deviations, a similar course can be observed between the plasma curves of group 9 and 10 after phase B. Although SKL was administered at the same dose level and the same period of treatment to group 9 during phase A and group 10 during phase B, both profiles show relatively clear differences.

Those observed differences between group 9, phase A and 10, phase B are even more pronounced in female rats. In addition, the mean plasma curves of phases B of both groups show almost similar courses of the SKL concentration. Furthermore, the standard deviations of these values are within an acceptable and comparable range. Although the results in male rat plasma do not seem to be as clear-cut as in females, the profiles obtained here suggest that there appears to be a connection between the presence of SRF and the enhanced level of SKL in rat plasma of both genders.

Recently Karbownik et. al [129] assessed the pharmacokinetic interaction between SRF and atovarstatin in rats. Several protein transporters are involved in the response to treatment of both drugs. They observed that combined treatment with SRF significantly increases the AUC of atovarstatin and its metabolites. As a suspected cause, they describe SRF-induced changes in the activity of the protein transporters involved. Since the mechanisms underlying the absorption of SKL have not yet been clarified in detail, it cannot be excluded that SRF influences these mechanisms in a similar way as described by Karbownik et. al for atovarstatin. Therefore, the elucidation of whether and via which transporters SKL is absorbed into the liver could provide information about the interactions of SKL and SRF observed in rats.

3.3.3.5. Part II: Sorafenib in Rats via Repetitive Dosing

SRF in rats served as reference compound in the present study, as mentioned in chapter 3.3.3.3. Group 10 was the only group treated with SRF during phase A of part II. The dose administered was 25 mg/kg/day for seven consecutive days. Treatment group 7 served as control group and therefore received during phase A the blank vehicle. During phase B, all groups received SRF at the concentration mentioned above on treatment days 8 till 14. Group 7 was thus the sole group to

received SRF only, while groups 8, 9 and 10 were treated simultaneously with SKL at different dose levels.

3.3.3.6. Part II: Pharmacokinetic Data Analysis and Parameter Calculation for Sorafenib

The individual plasma concentration profiles in male and female rat and the calculated parameters for treatment group 7 after completion of phase B are given in figure 42 and table 35. The profiles obtained in male rats show partly clear secondary and even tertiary peaks. The female rats also show multiple concentration peaks, but these are not as pronounced as in the males, and their SRF plasma levels after 24 h are similar to those after administration. The achieved mean C_{max} of 28,625 ng/mL in females after 3.3 h is clearly higher and occurs slightly earlier than in males with 16,578 ng/mL after 5.0 h. In contrast, the half-life in plasma of 34.7 h is almost twice as long as that observed in male rats, which is 16.4 h. The calculated values for AUC_{0-t} and $AUC_{0-\infty}$ with 489,594 and 1,259,225 ng·h/mL in females are also significantly higher than those observed in male rats with values of 250,141 and 412,481 ng·h/mL, respectively.

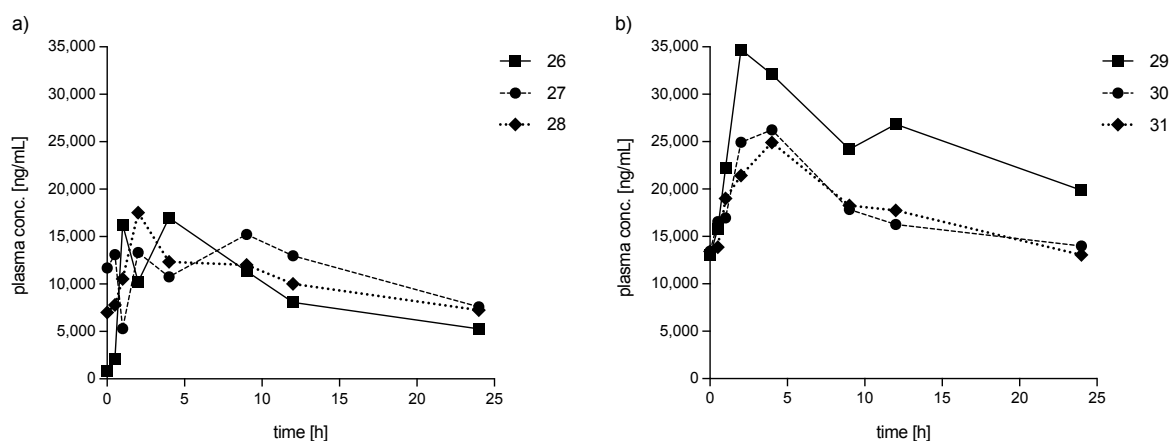


Fig. 42: Individual plasma concentration vs. time curves of SRF in male (a) and female (b) rats of treatment group 7, phase B (oral administration of 25 mg/kg/day SRF on seven consecutive days).

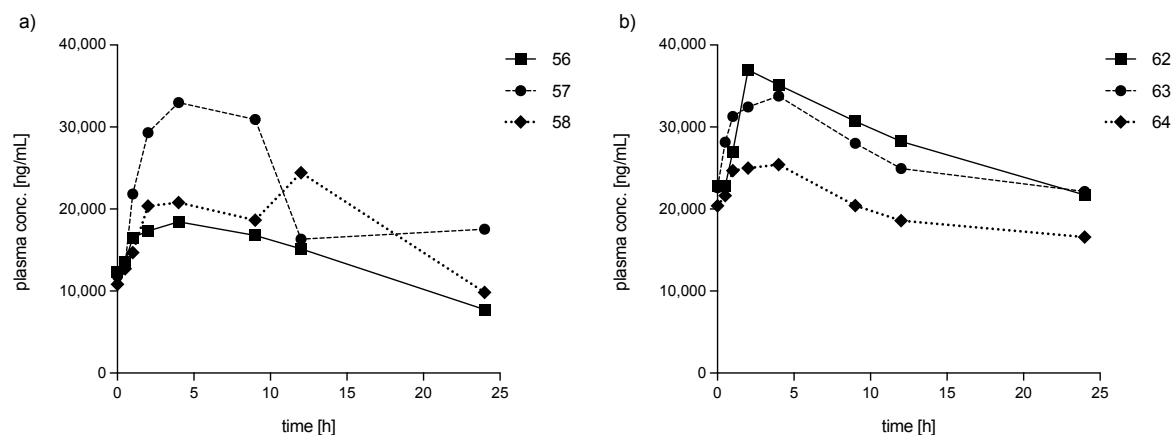


Fig. 43: Individual plasma concentration vs. time curves of SRF in male (a) and female (b) rats of treatment group 10, phase A (oral administration of 25 mg/kg/day SRF on seven consecutive days).

treatment group 7, phase B							
animal		C_{max} [ng/mL]	t_{max} [h]	AUC_{0-t} [ng·h/mL]	λ_z [1/h]	$t_{1/2}$ [h]	$AUC_{0-\infty}$ [ng·h/mL]
26	♂	16,983	4.0	225,670	0.1	12.2	318,612
27	♂	15,239	9.0	274,938	0.1	15.1	440,303
28	♂	17,514	2.0	249,816	0.0	21.8	478,529
29	♀	34,715	2.0	609,533	0.0	28.8	1,436,211
30	♀	26,252	4.0	430,887	0.0	45.7	1,352,840
31	♀	24,908	4.0	428,360	0.0	30.0	988,624
mean		16,578	5.0	250,141	0.1	16.4	412,481
± s.d.	♂	1,190	3.6	24,636	0.0	4.9	83,510
C.V.		7 %	72 %	10 %	28 %	30 %	20 %
mean		28,625	3.3	489,594	0.0	34.7	1,259,225
± s.d.	♀	5,317	1.2	103,878	0.0	9.5	238,026
C.V.		19 %	35 %	21 %	24 %	27 %	19 %

Tab. 35: Pharmacokinetic parameters for SRF derived by NCA from individual plasma concentration vs. time curves in male and female rats of treatment group 7 during phase B after oral administration of 25 mg/kg/day SRF for seven consecutive days.

Group 10 was treated with 25 mg/kg/day of SRF for seven consecutive days during study phase A (Fig.43). This corresponds to the dose and treatment duration of group 7 in phase B. Thus, both groups received the same treatment at that time with the only difference that group 7 obtained the blank formulation vehicle before the administration of SRF. Therefore, the results of group 7, phase B and group 10, phase A are expected to be similar. Table 36 shows that this assumed similarity is at least partially fulfilled, but there are more significant differences.

treatment group 10, phase A							
animal		C _{max} [ng/mL]	t _{max} [h]	AUC _{0-t} [ng·h/mL]	λ _z [1/h]	t _{1/2} [h]	AUC _{0-∞} [ng·h/mL]
56	♂	18,440	4.0	339,906	0.1	13.1	486,538
57	♂	32,999	4.0	536,752	0.0	21.4	1,077,688
58	♂	24,429	12.0	440,349	N/A	N/A	N/A
62	♀	36,960	2.0	680,845	0.0	30.6	1,638,876
63	♀	33,768	4.0	642,020	0.0	35.2	1,767,064
64	♀	25,419	4.0	481,638	0.0	55.0	1,799,637
mean		25,289	6.7	439,002	0.0	17.2	782,113
± s.d.	♂	5,974	3.8	80,368	0.0	4.1	295,575
C.V.		24 %	57 %	18 %	24 %	24 %	38 %
mean		32,049	3.3	601,501	0.0	40.3	1,735,193
± s.d.	♀	4,866	0.9	86,225	0.0	10.6	69,392
C.V.		15 %	28 %	14 %	23 %	26 %	4 %

Tab. 36: Pharmacokinetic parameters for SRF derived by NCA from individual plasma concentration vs. time curves in male and female rats of treatment group 10 during phase A after oral administration of 25 mg/kg/day SRF on seven consecutive days. N/A = not available; mean, s.d. and CV values for λ_z, t_{1/2} and AUC_{0-∞}, in male rat are calculated from animals 56 and 57.

The similarities include the t_{1/2} in male and the t_{max} in female rats. All further pharmacokinetic parameters of group 10, phase A are significantly increased compared to group 7, B. This applies in particular to the values of male animals. The achieved mean C_{max} of 25,289 ng/mL is clearly higher and occurs somewhat later, after 6.7 h. Consequently, the determined AUC_{0-t} and AUC_{0-∞} with 439,002 and 782,113 ng·h/mL also have significantly higher values. The differences between the two groups are not as pronounced in female rats. Nevertheless, the female animals of group 10, phase A, have higher values for most of their pharmacokinetic parameters than those of group 7, phase B. The gender-specific differences between the plasma concentration profiles in group 10, phase A, are not as pronounced, especially with regard to the mean C_{max} and AUC_{0-t}, but still significant.

Overall, the obtained pharmacokinetic parameters for SRF in rats are generally in line with the data described in literature [129]. In addition, it has already been described that the profiles of SRF in plasma can have multiple peaks due to enterohepatic circulation [130] and that females respond more to treatment in the form of higher plasma concentrations at the same dose [131]. If a different behaviour of SRF can be observed in the following pharmacokinetic profiles, it can be assumed that this is due to the presence of SKL.

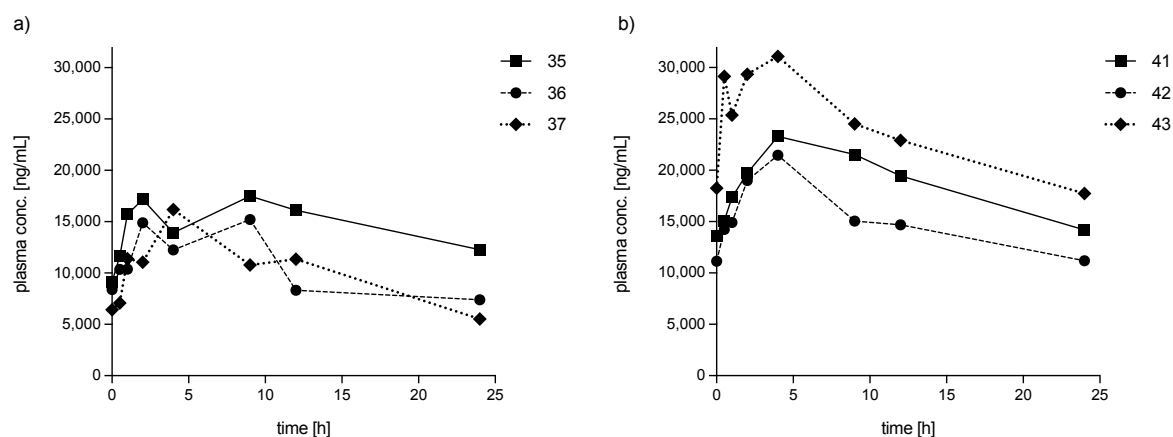


Fig. 44: Individual plasma concentration vs. time curves of SRF in male (a) and female (b) rats from treatment group 8, phase B (oral administration of 15 mg/kg/day SKL combined with 25 mg/kg/day SRF on seven consecutive days).

treatment group 8, phase B							
animal		C_{max} [ng/mL]	t_{max} [h]	AUC_{0-t} [ng·h/mL]	λ_z [1/h]	$t_{1/2}$ [h]	$AUC_{0-\infty}$ [ng·h/mL]
35	♂	17,479	9.0	358,835	0.0	29.7	885,316
36	♂	15,199	9.0	247,921	0.0	18.7	448,031
37	♂	16,171	4.0	248,271	0.1	13.4	354,489
mean		16,283	7.3	285,009	0.0	20.6	562,612
± s.d.	♂	934	2.4	52,203	0.0	6.8	231,360
C.V.		6 %	32 %	18 %	31 %	33 %	41 %
mean		25,284	4.0	460,585	0.0	30.4	1,089,803
± s.d.	♀	4,177	0.0	83,942	0.0	3.7	214,697
C.V.		17 %	0 %	18 %	13 %	12 %	20 %

Tab. 37: Pharmacokinetic parameters for SRF derived by NCA from individual plasma concentration vs. time curves in male and female rats of treatment group 8 during phase B after oral administration of 15 mg/kg/day SKL combined with 25 mg/kg/day SRF on seven consecutive days.

The animals of group 8 were initially treated with 15 mg/kg/day SKL for seven days, immediately followed by the simultaneous administration of 25 mg/kg/day SRF for further seven days. The individual plasma profiles and thereof determined parameters for SRF are illustrated in figure 44 and table 37. These show that the results obtained are quite similar to those of group 7, Phase B, apart from some minor deviations. So far, no significant differences in the plasma profiles of SRF alone could be observed compared to the combination with SKL.

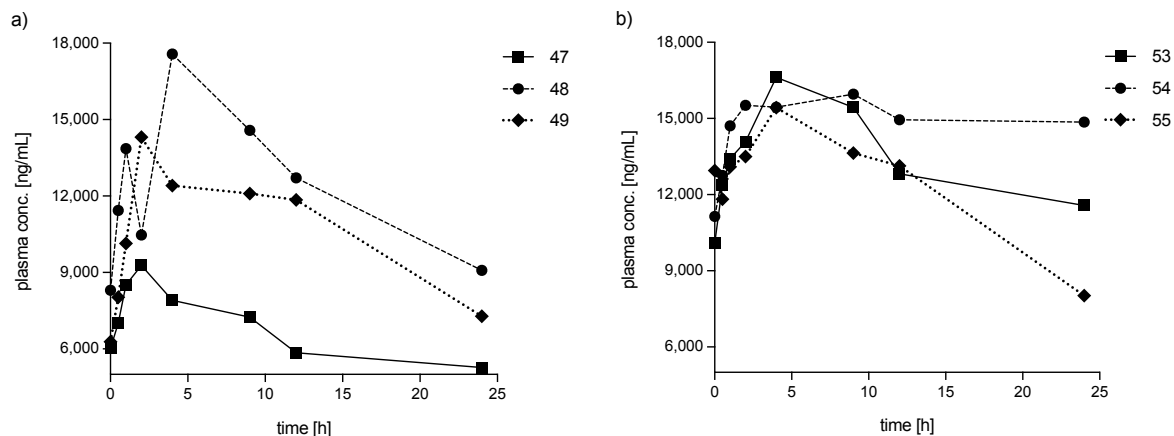


Fig. 45: Individual plasma concentration vs. time curves of SRF in male (a) and female (b) rats from treatment group 9, phase B (oral administration of 50 mg/kg/day SKL combined with 25 mg/kg/day SRF on seven consecutive days).

Treatment group 9 received SKL at a high dose of 50 mg/kg/day for a total of 14 days. After completion of phase A, SRF was administered at a dose of 25 mg/kg/day in addition to SKL from day 8 to 14 of treatment. The pharmacokinetic parameter for SRF derived by NCA from the pharmacokinetic profiles (Fig. 45) are given in table 38. It shows that the concentration of SRF in plasma ranges from 9,276 to 17,571 ng/mL in male rats and from 15,427 to 16,616 ng/mL in female rats. The mean time of their occurrence is 2.7 and 5.7 h respectively. Thus, the mean C_{max} occurs earlier in both genders compared to group 8, phase B. Furthermore, the concentrations achieved are lower, in particular their value of 16,000 ng/mL in female rats shows a decrease of nearly 10,000 ng/mL compared to the previous treatment group. Although slightly smaller in male rats of group 9, phase B, the AUC_{0-t} and $AUC_{0-\infty}$ show a relatively large CV from 18 to 50 %, so the differences between group 8 and 9 cannot be considered significant.

In female rats AUC_{0-t} shows the same behaviour, it is slightly decreased but with acceptable deviations. In contrast, the mean value of $AUC_{0-\infty}$ for group 9, phase B, is nearly twice the value obtained of group 8, but due to the completely different values between the animals it has a large CV of 90 %. For both genders, the calculated half-lives in plasma are very long and show partly strong deviations, especially in female rats. Since the administration of SRF was repetitive here, the high values for $AUC_{0-\infty}$ and $t_{1/2}$ with their corresponding differences can be caused by the achieved steady state and the well described enterohepatic recycling of SRF [130].

treatment group 9, phase B							
animal		C_{max} [ng/mL]	t_{max} [h]	AUC_{0-t} [ng·h/mL]	λ_z [1/h]	$t_{1/2}$ [h]	$AUC_{0-\infty}$ [ng·h/mL]
47	♂	9,276	2.0	157,481	0.0	28.4	373,691
48	♂	17,571	4.0	303,595	0.0	21.3	582,348
49	♂	14,308	2.0	259,043	0.0	19.4	462,751
53	♀	16,616	4.0	325,391	0.0	38.1	960,990
54	♀	15,957	9.0	362,666	0.0	195.8	4,560,396
55	♀	15,427	4.0	294,361	0.0	18.7	511,355
mean		13,718	2.7	240,040	0.0	23.0	472,930
± s.d.	♂	3,412	0.9	61,146	0.0	3.9	85,487
C.V.		25 %	35 %	25 %	15 %	17 %	18 %
mean		16,000	5.7	327,473	0.0	84.2	2,010,913
± s.d.	♀	486	2.4	27,924	0.0	79.3	1,812,077
C.V.		3 %	42 %	9 %	70 %	94 %	90 %

Tab. 38: Pharmacokinetic parameters for SRF derived by NCA from individual plasma concentration vs. time curves in male and female rats of treatment group 9 during phase B after oral administration of 50 mg/kg/day SKL combined with 25 mg/kg/day SRF on seven consecutive days.

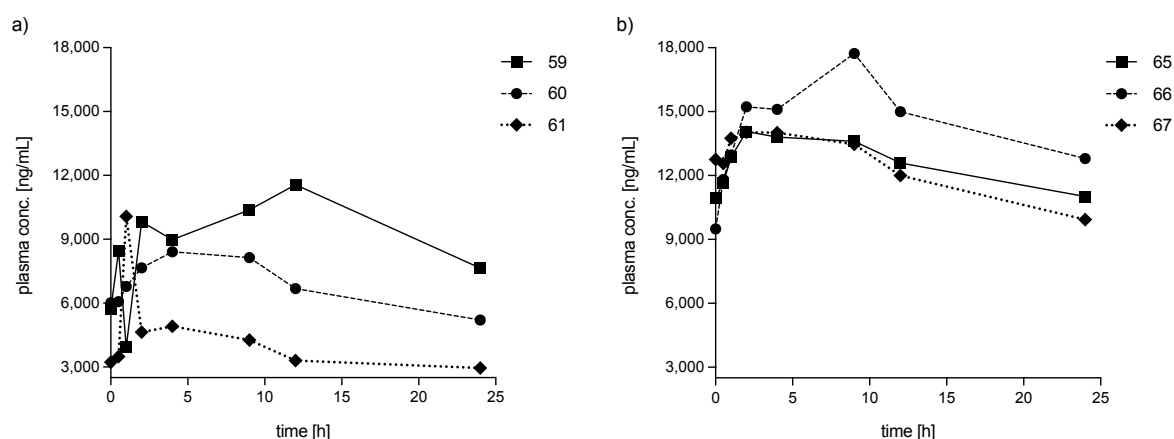


Fig. 46: Individual plasma concentration vs. time curves of SRF in male (a) and female (b) rats of treatment group 10, phase B (oral administration of 25 mg/kg/day SRF combined with 50 mg/kg/day SKL on seven consecutive days).

The last treatment group in this trial was the only one to receive 25 mg/kg/day of SRF in phase A, followed by combined treatment with SKL at a high dose of 50 mg/kg/day in phase B. Thus, group 10 was treated with SRF for 14 days to answer the question whether SKL affects the pharmacokinetic behaviour of SRF. The pharmacokinetic profiles and calculated parameters for SRF obtained from group 10 after phase A, have already been discussed (Fig. 43, Tab. 36).

treatment group 10, phase B							
animal		C _{max} [ng/mL]	t _{max} [h]	AUC _{0-t} [ng·h/mL]	λ _z [1/h]	t _{1/2} [h]	AUC _{0-∞} [ng·h/mL]
59	♂	11,560	12.0	228,933	N/A	N/A	N/A
60	♂	8,409	4.0	164,485	0.0	27.5	371,301
61	♂	10,075	1.0	93,824	0.0	29.3	218,628
65	♀	14,073	2.0	302,634	0.0	60.9	1,269,418
66	♀	17,737	9.0	353,943	0.0	35.9	1,016,367
67	♀	14,038	2.0	293,433	0.0	38.8	849,475
mean		10,014	5.7	162,414	0.0	28.4	294,964
± s.d.	♂	1,287	4.6	55,177	0.0	0.9	76,336
C.V.		13 %	82 %	34 %	3 %	3 %	26 %
mean		15,282	4.3	316,670	0.0	45.2	1,045,086
± s.d.	♀	1,735	3.3	26,623	0.0	11.1	172,640
C.V.		11 %	76 %	8 %	21 %	25 %	17 %

Tab. 39: Pharmacokinetic parameter for SRF derived by NCA from individual plasma concentration vs. time curves in male and female rat of treatment group 10 during phase B after oral administration of 25 mg/kg/day SRF combined with 50 mg/kg/day SKL on seven consecutive days. N/A = not available; mean, s.d. and CV values for λ_z, t_{1/2} and AUC_{0-∞} in male rats are calculated without taking animal 59 into account.

The individual profiles of SRF (Fig. 46a) in male rats show similar curves but differ significantly in the level of plasma concentrations. In contrast, both the individual profiles (Fig. 46b) and the concentration levels observed among female rats in group 10 show strong similarities, which is reflected in the mostly low CV (Tab. 39).

During phase B, groups 9 and 10 received the same treatment, consisting of the simultaneous administration of 50 mg/kg/day SKL and 25 mg/kg/day SRF. The difference between both groups is the varying duration of treatment with either SKL or SRF, which was 7 or 14 days respectively. Therefore, the comparison of the results obtained by both groups at the end of phase B could provide information on whether and to what extent the potential interaction in the disposition of SKL and SRF is influenced by the dose regimen and/or the respective treatment period.

When comparing the mean values of both groups, it is striking that there are almost no differences in the pharmacokinetic parameters of SRF in female rats. In the male rats, however, despite the partly high standard deviations, clear differences in the values determined can be observed. Thus, the achieved C_{max} of 10,014 ng/mL from group 10 is noticeably lower than the observed 13,718 ng/mL in group 9. This results in the also lower values for AUC_{0-t} of 162,414 compared to 240,040 ng·h/mL and AUC_{0-∞} with 294,964 against 472,930 ng·h/mL. As the individual values for t_{max} within group 10 vary considerably, the differences between the mean values of group 9 and

10 are not representative. The plasma half-life of 28.4 h of group 10 is comparable with the observed 23.0 h from group 9 considering the deviation of 4.8 h.

Thus, in female rats, treatment duration and sequence of SKL and SRF does not appear to have any effect on the pharmacokinetic behaviour of SRF in the presence of SKL. In contrast, these factors seem to play a role in male rats. However, due to the relatively different individual profiles within each group, the extent of this influence cannot be clearly determined.

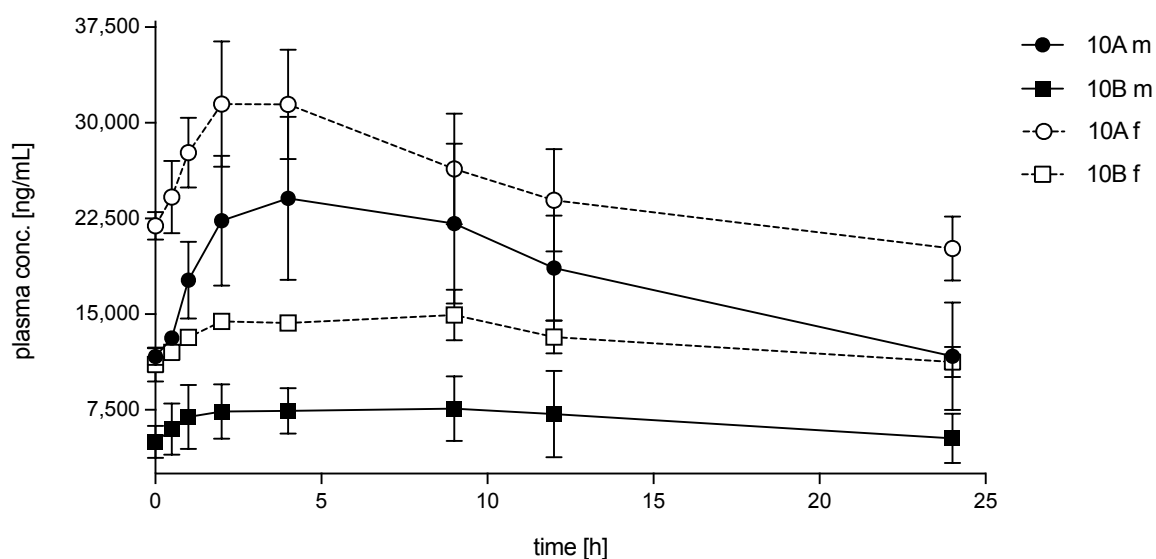


Fig. 47: Mean plasma concentration vs. time curves of SRF in male (solid line) and female (dashed line) rats from treatment group 10, phase A (circles) and phase B (squares). Phase A included oral administration of 25 mg/kg/day SRF for seven days. During phase B treatment consisted of a combination of 25 mg/kg/day SRF with 50 mg/kg/day SKL for seven consecutive days. $n = 3$; standard deviation (\pm) is represented by error bars

The direct comparison of the plasma concentration profiles of SRF after phase A and B of group 10 shows what can already be assumed from the previous results. The curves are illustrated in figure 47 and clearly show that the SRF concentration in the plasma is significantly lower after phase B, *i.e.*, in the presence of SKL. The difference between both phases is clearly visible in both genders. In males, the decrease in concentration that can be observed in correlation with SKL seems to be somewhat more pronounced.

In addition to the analysis of SKL and SRF, three of six Ph1 metabolites of SRF [94] could be determined in rat plasma. Unfortunately, NOX, HOM and DES were not available as reference compounds at the time of the analysis. Thus, although no

quantification was possible, the PAR could be used to investigate whether, in addition to SRF, the concentrations of NOX, HOM and DES are also influenced by the presence of SKL.

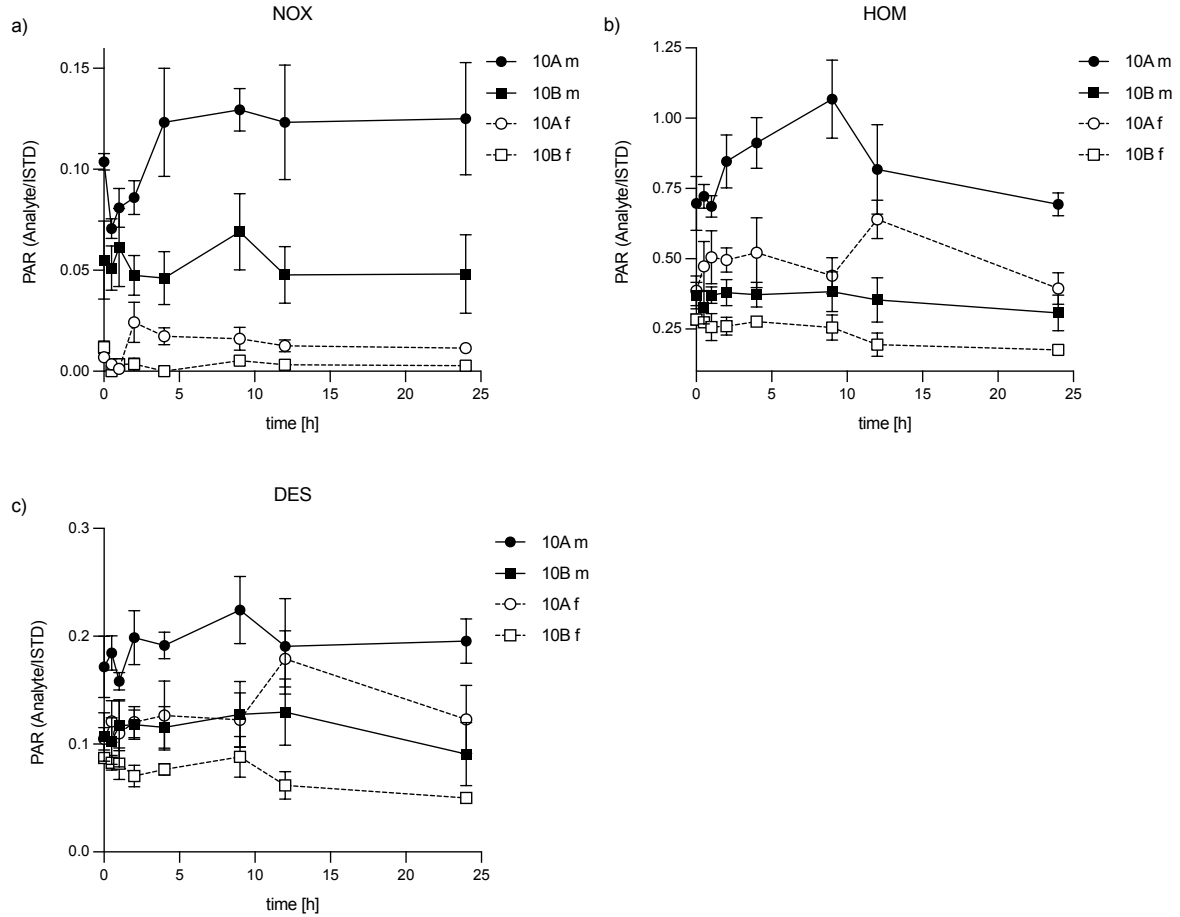


Fig. 48: Mean PAR vs. time profiles of SRF phase 1 metabolites NOX (a), HOM (b) and DES (c) in male (solid line) and female (dashed line) rats from treatment group 10, phase A (circles) and phase B (squares). $n = 3$; standard deviation (\pm) is represented by error bars

The obtained plasma levels of NOX, HOM and DES of treatment group 10 after completing phase A and B are given in figure 48a-c. As previously observed for SRF, co-administration of SKL appears to affect SRF-Ph1 metabolites by decreasing their PAR and thus their concentration in rat plasma. The degree of the reduction in concentration seems to be equally pronounced in both genders. The graph implies that the concentration of HOM changes most in the presence of SKL. But it should be noted that differences in PAR do not correlate with actual changes in concentration, as the specific ion yield of each analyte can be significantly different. Therefore, no statement can be made as to whether this concentration-reducing effect is equally or differently pronounced for the metabolites analysed.

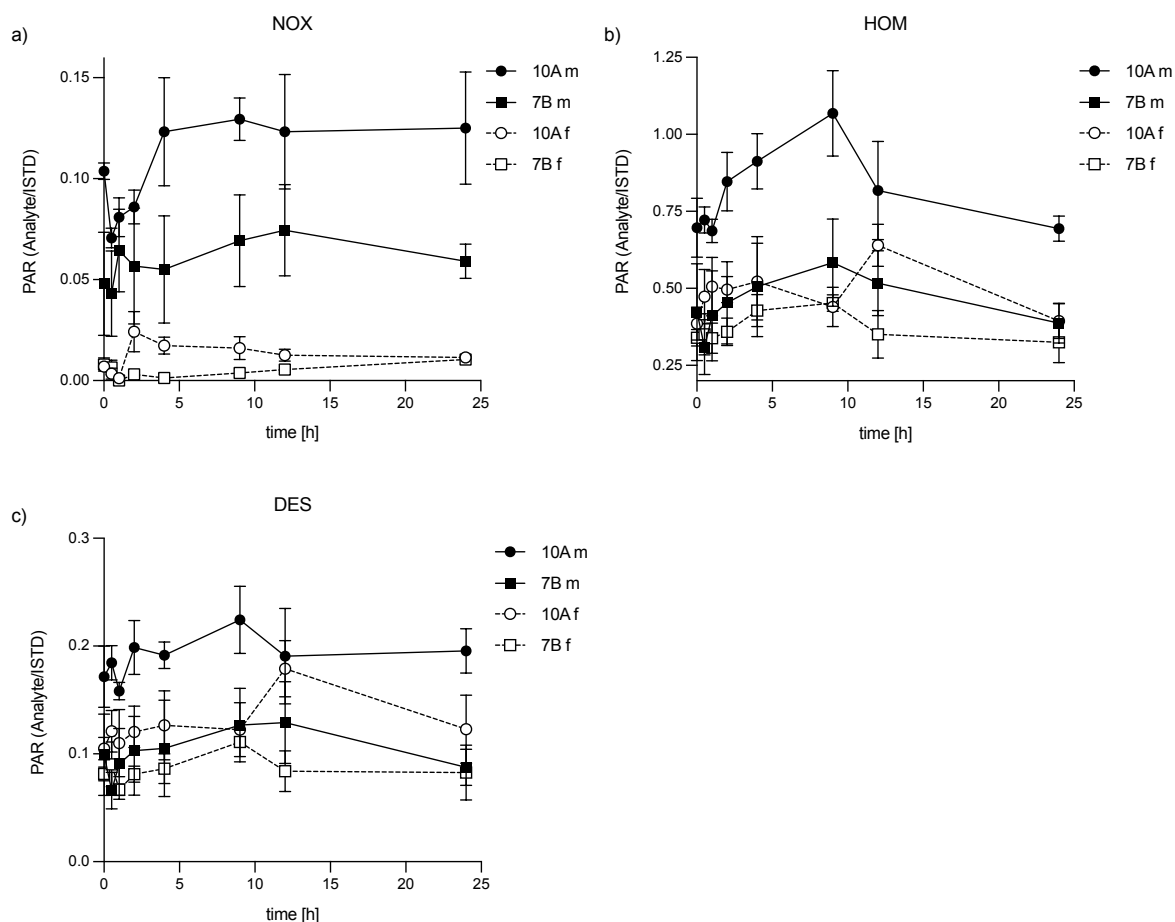


Fig. 49: Mean PAR vs. time profiles of SRF phase 1 metabolites NOX (a), HOM (b) and DES (c) in male (solid line) and female (dashed line) rats from treatment group 10, phase A (circles) and group 7, phase B (squares). n = 3; standard deviation (\pm) is represented by error bars

However, there is also a clear difference between the plasma concentrations of group 10 after phase A with phase B of group 7 (Fig. 49), although both groups received the same treatment in the respective phase. Thus, it is questionable whether the decrease in plasma concentrations of NOX, HOM and DES observed in group 10 is actually due to the simultaneous administration of SKL. In addition, it is noticeable that the metabolite concentrations in the plasma of the male rats are higher than in the females in both phases of both groups. Hence, SRF seems to be metabolised more extensively and more rapidly in male rats. This could be an explanation for the distinctly lower C_{max} and shorter $t_{1/2}$ in male rats compared to those obtained in females after SRF administration.

These male-female differences may be caused by the species-specific CYP isoforms involved. Most likely, these are expressed differently in the two sexes. This is known, for example, for CYP3A2, which is mainly present in male rats [132], whereas CYP3A9

is more present in females [133]. It is not known which rat-specific CYP isoforms catalyse the metabolic degradation of SRF. But in humans, the Ph1 oxidation of SRF to NOX, HOM and DES is mediated by CYP3A4 [94]. It is known that this human isoform is more active in females than in males [134]. This contrast complicates the interpretation and translation of the mutual influence of SKL and SRF observed in rats to humans.

3.3.3.7. Part I and II: Summary and Discussion of the Results Obtained

In both parts of the pharmacokinetic study of SKL in rats, high plasma levels were achieved. Maximum concentrations of 175, 586 and 1,210 ng/mL after single oral administration of 5, 15 and 50 mg/kg SKL respectively could be observed. However, the resulting plasma concentration-time profiles showed several concentration peaks and almost no distinct elimination phases. The higher the dose administered, the more pronounced this unexpected behaviour is. In contrast, intravenous administration resulted in relatively favourable and expected concentration-time curves. However, some animals did not survive the test duration which is why only few i.v. data were available.

The results obtained during part I of the study, *e.g.*, C_{max} , were also observed in part II. However, this refers only to the administration of SKL to male rats. This is because female rats responded more to the treatment, resulting in higher plasma levels than those observed in males at the same SKL dose. However, the difference between the gender-specific treatment response was more pronounced the higher the dose administered. The multiple peak phenomena of SKL, which was observed in part I, is also present in part II in both genders. Again, the higher the dose, the more pronounced this behaviour seems to be.

The reasons for these findings can be manifold, as numerous factors can lead to the occurrence of secondary peaks in plasma concentration profiles. Among others, it could be due to the ingredients of the formulation or even induced by SKL itself. The profiles of the preliminary study in mice after both i.v. and p.o. administration show no similarity to those in rats after p.o. administration, so SKL can be excluded as the sole causative factor. Considering the formulation components, it is known that PEG400

for example increases the solubility of lipophilic compounds and thus leads to an increased systemic exposure [135]. NMP has antimyeloma and immunomodulatory activities and is therefore not as biological inert as assumed [136]. But these properties will most likely not lead to secondary peaks in the plasma concentrations profiles. In addition, the amount of NMP administered was relatively low as its share was only 5 % of the vehicle. For the third excipient PG, no effect on the expression of drug-metabolizing enzymes could be demonstrated, at least in humans [137]. Thus, the vehicle components are not known to influence or induce other mechanism which would lead to secondary peaks.

The physiology and the associated specific properties of the gastrointestinal tract, like pH values, transit time and gastric emptying may also contribute [138]. One prominent cause of the multiple peak phenomena is known to be enterohepatic recycling, which consists of the secretion of bile and subsequent reabsorption [139] and is also characterized by prolonged terminal plasma half-lives [140]. The presence of multiple peaks in the plasma concentration profile following intravenous administration strongly indicate that enterohepatic recycling is involved [138]. However, secondary peaks were observed only after oral administration, which indicates that they were caused by complex absorption kinetics [140], leading to the conclusion that enterohepatic recycling can be excluded at least in rats. Another possible cause would be a strong binding of SKL to the plasma proteins. The observed low V_{ss} is a clear indication of its presence and bound substance is not available for both renal elimination and metabolism [141]. However, this can also be ruled out as a reason for the occurrence of multiple peaks due to the different profiles obtained after i.v. and p.o. administration.

The outcome of part II clearly shows that plasma levels of SKL are increased when SRF is administered simultaneously. In return, the combined therapy with SKL leads to a reduction in SRF plasma levels. A simple factor (f), consisting of the ratio of the resulted mean C_{max} of phase B to mean C_{max} of phase A, is intended to illustrate the extent of the influence of SKL or SRF on the respective C_{max} when simultaneously present. In table 40 the mean C_{max} of SKL and SRF in male and female rats of treatment groups 8, 9 and 10, phase A and B and the resulting factors are given. The C_{max} obtained from SRF in treatment group 7, phase B was used to determine the factors for SRF in groups 8 and 9 because they were not given SRF in phase A. These

values were chosen because the achieved C_{max} of SRF was the highest in this group for both genders. Since the dose administered of SKL was the same for groups 9 and 10, the C_{max} values of group 9 were used to calculate the factor for 10. This was because group 10 did not receive SKL during phase A.

treatment group	compound	male			female		
		C_{max} [ng/mL]			C_{max} [ng/mL]		
		phase A	phase B	f	phase A	phase B	f
8	SKL	1,310	5,410	4.1	2,015	6,792	3.4
	SRF	#	16,283	1.0	#	25,284	0.9
9	SKL	11,415	1,933	5.9	5,277	13,970	2.6
	SRF	#	13,718	0.8	#	16,000	0.6
10	SKL	*	7,133	3.7	*	13,798	2.6
	SRF	25,289	10,014	0.4	32,049	15,282	0.5

Tab. 40: Overview of mean C_{max} of SKL and SRF in male and female rats of treatment groups 8, 9 and 10 and the resulting factors (f), which are the ratio of C_{max} phase B to phase A. #values used from group 7, phase B, C_{max} , male: 16,578 ng/mL, female: 28,625 ng/mL; *values used from group 9

A direct correlation between the dose of SKL applied and the increase in concentration caused by the simultaneous administration of SRF, expressed as factor, cannot be observed in either gender. The calculated factor clearly illustrates that the concentration-increasing effect of SRF on SKL is particularly pronounced in male rats. Nevertheless, the highest plasma concentration in each treatment group and each phase is observed in female rats. In contrast, the influence on SRF plasma concentration seems to depend on the applied SKL amount and is the more pronounced the higher this dose is. However, this effect of SKL in relation to SRF seems to be equally pronounced in both genders.

So far, only conjectures can be made about the underlying processes or mechanisms regarding the influence of SRF on the concentration of SKL in plasma. As already mentioned, the low V_{ss} indicates that SKL is strongly bound to plasma proteins. This in turn leads to the opportunity for SKL to be released from the protein complex through the presence of SRF. This supposition is confirmed by the marked increases in C_{max} and shorter t_{max} after simultaneous administration of SKL and SRF compared to SKL solely. However, this leaves unexplained the changes in plasma SRF concentration induced by the presence of SKL. Since it is known that SRF is highly bound to plasma proteins at levels greater than 99.5 % in humans [142], it is almost not possible to increase the amount of fraction bound. Due to the almost halved C_{max} of SRF and the decreased amount of its metabolites in plasma, it is more likely that the interference of SKL already occurs at the level of absorption.

Despite initial problems, such as the unexpected death of the animals after intravenous administration and the unforeseen pharmacokinetic profiles following oral dosing, various information and results could be obtained from this study. On the basis of part I, it was possible to determine the dosage and frequency of administration for upcoming studies. Unfortunately, due to the limited data available and the constraints of the software used, it was not possible to establish a suitable model to reliably predict the pharmacokinetic parameters of SKL in the rat, either after oral or intravenous administration. However, the difference in the concentration of SKL in plasma between male and female rats, as previously seen in the other species tested, could also be observed. Furthermore, the profiles showed gender-specific differences in their progressions. In addition to these results, the study demonstrated that there is a mutual influence of SKL and SRF on each other's plasma concentration. The issue of how and at what level this occurs must be clarified by further research and testing. Additional studies must also clarify the reasons for the irregular plasma profiles of SKL with regard to multiple absorption peaks and almost no elimination phases, which were previously observed only in rats.

Due to the atypical PK profiles of SKL and the male-female differences in SRF metabolism, the results obtained here will be difficult to translate to humans. In conclusion, it must be considered that the rat may not be a suitable model for predicting the pharmacokinetic behaviour of SKL and its interaction with SRF in humans.

3.3.4. Pharmacokinetic Study of Skepinone-L and Sorafenib in Monkeys

In order to assess the pharmacokinetic profile of SKL and SRF in another non-rodent species, both test items were administered orally to the cynomolgus monkey. The *in vivo* test phase was performed by the test facility CiToxLAB in Evreux (France) and sponsored by c-a-i-r biosciences GmbH in Ulm, Germany. A treatment group consisting of two male and two female monkeys received a single dose of 50 mg/kg SKL via an oral gavage. This dosage was selected based on the results of the previous bioavailability study in dogs (chapter 3.3.2). After a wash-out period, the same animals were administered a single dose of 50 mg/kg SRF. The further study design in detail, the experimental setup and the analytical method for the quantification of SKL and

SRF in plasma of cynomolgus monkeys is described in chapter 5.2.3.5 (Pharmacokinetic Study of Skepinone L and Sorafenib in Monkeys).

3.3.4.1. Pharmacokinetic Data Analysis and Parameter Calculation for Skepinone-L

Non-Compartmental Analysis

The pharmacokinetic parameters of SKL derived via NCA are given in table 41. These show that the resulted maximum concentration of 744 to 3,672 ng/mL has a relatively wide range, but with corresponding t_{max} of 1.0 to 4.0 h the time of its occurrence is roughly comparable. Although there is no clear difference in plasma profiles (Fig. 50) and calculated parameters between both genders, there seem to be slight tendencies. The plasma profiles of SKL in male monkeys show a distinct absorption peak, which slowly but clearly decreases. On the surface, they also seem to respond more strongly to treatment than the females. In particular, the profile of animal 69 shows high plasma levels of SKL and therefore deviates relatively strongly from the other curves. In females, the concentration levels of SKL appear to be lower, but the elimination phase shows little reduction in some cases. Animal 71 displays only a slight descend in SKL plasma levels after reaching C_{max} , which is reflected in the significantly high $AUC_{0-\infty}$ and the exceptionally long $t_{1/2}$ of 24.1 h. In contrast, the other animals in this study show relatively similar individual plasma half-lives of 4.5 to 6.4 hours.

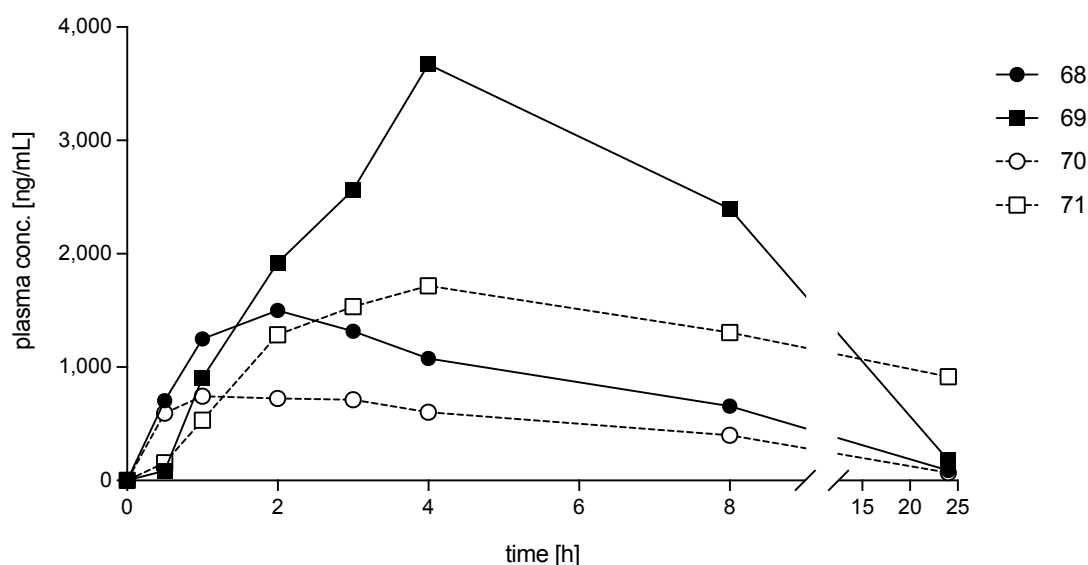


Fig. 50: Individual plasma concentration vs. time curves of SKL in male (68, 69) and female (70, 71) cynomolgus monkeys after single oral administration of 50 mg/kg SKL.

single oral administration of 50 mg/kg SKL in monkeys							
animal		C_{max} [ng/mL]	t_{max} [h]	AUC_{0-t} [ng·h/mL]	λ_z [1/h]	$t_{1/2}$ [h]	$AUC_{0-\infty}$ [ng·h/mL]
68	♂	1,502	2.0	14,079	0.1	5.5	14,779
69	♂	3,672	4.0	39,826	0.2	4.5	41,001
70	♀	744	1.0	8,336	0.1	6.4	8,972
71	♀	1,718	4.0	27,976	0.0	24.1	59,869

Tab. 41: Pharmacokinetic parameters for SKL derived by NCA of individual plasma concentration vs. time curves in male and female cynomolgus monkeys after single oral administration of 50 mg/kg SKL.

Thus, SKL can also be determined in the plasma of cynomolgus monkeys at relatively high concentrations, which indicates that it is also well absorbed in this species. The C_{max} values are relatively high, although the plasma levels achieved are slightly lower compared to plasma levels in the dog, the other non-rodent species. Due to the prolonged elimination phase and thus atypical pharmacokinetic profiles of SKL in monkeys, no compartmental analysis was performed.

3.3.4.2. Pharmacokinetic Data Analysis and Parameter Calculation for Sorafenib

Non-Compartmental Analysis

Interestingly, no secondary peaks were observed in the individual plasma concentration profiles obtained after oral administration of SRF to cynomolgus monkeys (Fig. 51).

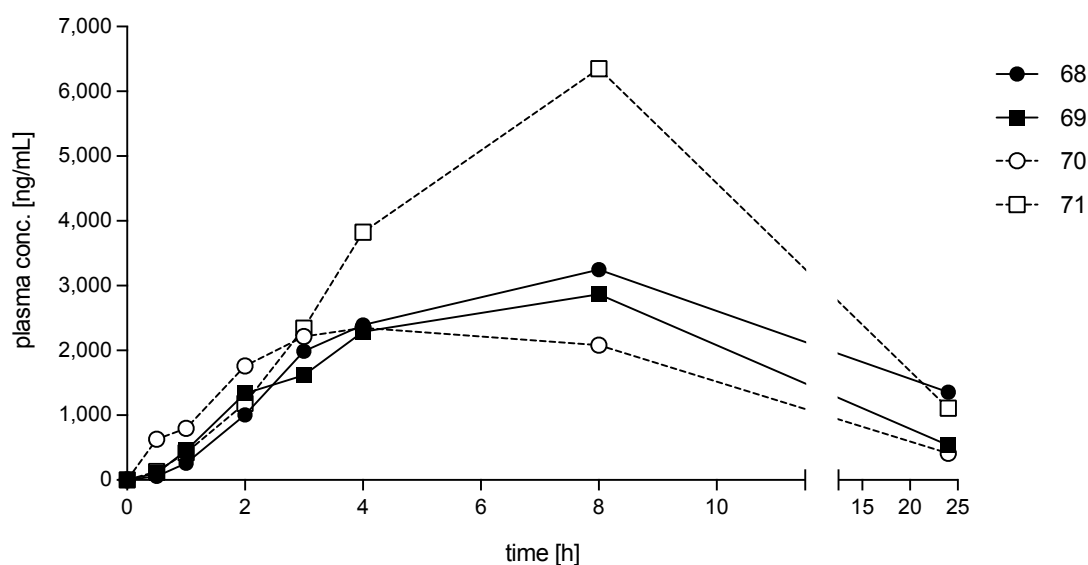


Fig. 51: Individual plasma concentration vs. time curves of SRF in male (68, 69) and female (70, 71) cynomolgus monkeys after single oral administration of 50 mg/kg SRF.

Moreover, with one exception, the profiles demonstrate very similar behaviour. Their curves ascend only slightly after 4 hours and do not show a pronounced absorption peak. In addition, their elimination phase begins relatively late and seems to descend fairly flat, so that even after 24 h a distinct quantity of SRF is still present in the plasma.

The pharmacokinetic parameters determined by NCA (Tab. 42) show that in relation to the high dose of 50 mg/kg administered, the C_{\max} achieved of 2,349 to 3,246 ng/mL is relatively low. An exception seems to be animal 71, whose maximum concentration of SRF in plasma with 6,348 ng/mL is twice to almost three times the other obtained values. It is noticeable that in all tested animals C_{\max} occurs rather late with a t_{\max} of 4 and 8 h. Due to this observed prolonged absorption phase, less than three data points were available in the terminal elimination phase. Therefore, some pharmacokinetic parameters, such as λ_z , $t_{1/2}$, and $AUC_{0-\infty}$ could not be determined through NCA for animals 68, 69 and 71.

single oral administration of 50 mg/kg SRF in monkeys							
animal		C_{\max} [ng/mL]	t_{\max} [h]	AUC_{0-t} [ng·h/mL]	λ_z [1/h]	$t_{1/2}$ [h]	$AUC_{0-\infty}$ [ng·h/mL]
68	♂	3,246	8.0	52,527	N/A	N/A	N/A
69	♂	2,866	8.0	42,007	N/A	N/A	N/A
70	♀	2,349	4.0	34,868	0.1	7.6	39,403
71	♀	6,348	8.0	85,816	N/A	N/A	N/A

Tab. 42: Pharmacokinetic parameter for SRF derived from NCA of individual plasma concentration vs. time curves in male and female cynomolgus monkeys after single oral administration of 50 mg/kg SRF. N/A = not available.

While slight tendencies were observed after administration of SKL, no gender-related differences seem to be present after administration of SRF. Both the pharmacokinetic profiles and the calculated parameters of SRF in the plasma of cynomolgus monkeys differ significantly from the results obtained in rats. In particular, the monkeys seem to respond significantly less to the treatment, which is reflected by the clearly lower plasma levels. However, it should be noted that rats received SRF via repeated administration, whereas in this present study SRF was administered as a single dose. No compartmental analysis was performed for SRF in cynomolgus monkeys, because on the one hand there was not enough usable data available and on the other hand the primary focus of the present thesis is on SKL.

3.3.5. Summary and Discussion of the Preclinical Pharmacokinetic Studies of Skepinone-L in Mice, Rats, Dogs and Monkeys

The pharmacokinetic studies of SKL *in vivo* resulted in relatively high plasma levels in all tested species. It should be emphasized that all observed plasma concentrations of SKL were significantly above the known IC₅₀ of 5 ± 2 ng/mL [111],[143] and did not decrease below for at least 8 h post dosing. In addition, the applied LOQ of the validated method of 7.81 ng/mL in rat, 10.00 ng/mL in dog and 15.63 ng/mL in human plasma was not undercut at any time in any sample.

The intravenous administration of SKL demonstrated in the applied species favourable pharmacokinetic profiles with high plasma levels, short terminal half-lives, low clearances and low to moderate V_{ss}. Unfortunately, some animals died immediately or shortly post intravenous application, but this was only observed in rats. The dose volume in relation to body weight was 0.1 mL/kg in mice, 1.0 mL/kg in dogs and 2.5 mL/kg or 5.0 mL/kg in rats. This comparatively high volume applied in rats may be the reason for the death of the animals. Following oral administration, SKL appears to be well absorbed in total, although significant differences were observed both between species and in some cases between the genders. Thus, the mean oral bioavailability of SKL in male mice was about 78 %, whereas in females it was only 41 %. However, the plasma concentration after intravenous administration is needed for the exact calculation of the oral bioavailability. Unfortunately, no data of SKL i.v. administration in female mice was available, which is why the i.v. data of male mice were used for the determination of F in females. Therefore, this result must be viewed critically on the one hand and verified on the other. In addition, oral bioavailability of SKL was analysed in dogs, as this is one of the most appropriate species for this topic. Here as well, there were clear differences between the genders, but in the opposite direction. In male dogs, the bioavailability of SKL was about 33 % in both animals tested, which can be considered as low. In the two female dogs, SKL was absorbed noticeably more with a F of 53.9 % and 65.8 % of the orally administered dose. However, due to the small number of animals in the study (2 per gender), no statistical validation of this finding is possible.

Clear differences between the tested species could be observed in t_{max} , which represents the corresponding time of occurrence of the maximum concentration. Thus, this occurs in mice after 0.5 and 0.8 h, in dogs after 2.0 to 4.0 h and in monkeys after 1.0 to 4.0 h after oral dose. C_{max} in these species appears over a relatively narrow time frame. In rats, the t_{max} following single oral administration occurred after 0.5 to 12.0 h and consequently almost the entire observation period. The mean values of the treatment groups remained between 5.0 and 6.3 h. However, these should be viewed critically due to the large individual differences between the rats. Therefore, the non-rodents show similarities to each other, while the rodents are quite different. Notably, in the rat studies, the number of treatment groups and test animals was significantly higher than in the other species. This could contribute to the large fluctuations.

There are also clear differences with regard to the terminal half-life in plasma. Following intravenous administration, $t_{1/2}$ of SKL was 3.1 and 4.3 h in mice, 3.3 to 3.9 h in dogs and 0.6 to 1.9 h in rats. After oral dosing, the half-life was 2.8 and 3.3 h in male mice and an average of 1.3 h in females. In dogs it was 3.4 to 4.5 h, with no noticeable differences either between the two genders or routes of administration. Since in both mice and dogs $t_{1/2}$ after oral administration was shorter or the same as after intravenous administration, elimination rather than absorption appears to be the rate-limiting step in the disposition of SKL in these species [11]. In the monkeys, no information can be given in this regard, as SKL was only administered orally. The $t_{1/2}$ in male cynomolgus monkeys was 4.5 and 5.5 h and in females 6.4 and 24.1 h. In the rats, however, the $t_{1/2}$ with 3.3 to 54.9 h demonstrated a broad scattering, as already observed with t_{max} . Furthermore, these half-lives are distinctly longer than those observed after i.v. administration. This could indicate that instead of elimination, the absorption of SKL is the rate-limiting factor of its disposition in rats.

This may be one of the reasons for the irregular and unexpected profiles. Because the rats seem to respond significantly different to treatment with SKL than the other species tested. Although the profiles of SKL obtained after p.o. dosing in dogs and monkeys also show irregularities in the absorption and elimination processes, no secondary peaks could be observed in these species. In mice, SKL showed a typical pharmacokinetic profile with a distinct absorption and elimination phase even after oral

administration. In contrast, the profiles of SKL in rat plasma partly showed secondary peaks or unexpected steep increases in plasma concentration. This observed multiple peak phenomena appeared to be more pronounced the higher the administered dose.

The fact that the pharmacokinetic behaviour of SKL in rats differs distinctly from that of dogs, monkeys and, above all, the other rodent genus, mice, could have a variety of reasons. For instance, the gastric emptying is slower in rats than in mice [144] which leads to SKL reaching the site of absorption faster in mice. Also, the physiology and the associated specific properties of the GIT may contribute, as rats are the only species used here that do not have a gall bladder [145]. In addition, all animals were in a fasted state for at least 12 h prior to dosing, except for the rats which had *ad libitum* access to food. This could also influence the absorption of SKL in rats and therefore its pharmacokinetic profile. Despite these numerous conjectures, the exact reasons for the irregular plasma concentration profiles of SKL in rats are not clearly understood. Therefore, the suitability of the rat as an animal model compared to the other species for the questions of the present work is only given with reservation. Despite the unexpected profiles of SKL in rats, a potential interaction in the disposition of SKL and SRF could be observed. When administered in combination, SKL seems to influence the plasma levels of SRF by decreasing them. Again, the higher the dose of SKL the more pronounced this effect. In turn, the presence of SRF increases the concentration of SKL in plasma. Further research must clarify at what level the mutual influence takes place and what consequences it could have apart from those mentioned here.

Using the add-in program PKSolver2.0, suitable two-compartment models could be generated for estimating the pharmacokinetic parameters of SKL in mouse, dog and rat plasma after intravenous administration. However, with the exception of mice, no model could be established to accurately predict the behaviour of SKL *in vivo* when administered orally. This could be due to the occurrence of multiple peaks, which is pronounced in rats and leads to atypical and thus difficult-to-predict profiles. Although, no secondary peaks can be observed in the concentration profiles of SKL in dog and monkey plasma, it seems that uncertain processes influenced the absorption and elimination behaviour of SKL in the plasma of these species. Furthermore, the possibilities to modify the compound-related properties and thus optimise the model and increase the accuracy of its prediction in the add-in program are limited.

Considering the application of SKL in humans, these preclinical studies have provided a variety of information and promising results and also some questions have been answered. It seems that at least after short treatment period, life-threatening effects are most probably not to be expected. In addition, it can be assumed that SKL would be quite well absorbed after oral administration in humans. However, the resulting low to moderate V_{ss} after intravenous injection in the animal models and the associated short half-lives indicate that more than one dose per day would be required. If the combined therapy with SKL and SRF was to be applied in humans, the pharmacokinetic interactions observed in rats should be strictly monitored. Indeed, reduced exposure of SRF, induced by the presence of SKL, could lead to fewer adverse side effects, but also involves the risk of a decreased, insufficient response to SRF treatment. In addition, it is not yet elucidated whether and to what extent the higher plasma levels of SKL contribute to the success or even failure of the treatment. How this effect caused by SRF affects the human body would also have to be thoroughly investigated.

3.4. Plasma Protein Binding of Skepinone-L *in vitro*

The binding of SKL to plasma proteins could lead to an attenuation of its pharmacological effects, since according to the free drug hypothesis [28], only unbound drug can *inter alia* bind to the therapeutic target. The low to moderate V_{ss} observed in the pharmacokinetic studies *in vivo*, the prolonged $t_{1/2}$ and the mostly barely discernible elimination phase indicate that SKL is highly bound to plasma proteins [146]. In addition, the occurrence of multiple peaks in the plasma concentration-time profiles in rats were also a distinct sign and reinforced the suspicion of the presence of binding. Thus, it was important to examine whether and to what extent SKL is bound to plasma proteins. Therefore, equilibrium dialysis of SKL was performed at concentrations of 12.5, 25.0 and 37.5 μM as described in chapter 5.2.7 (Determination of Plasma Protein Binding of Skepinone-L).

It was further suspected that potential plasma protein binding of SKL may be involved in the mutual interference of the respective plasma levels of SKL and SRF, as observed in the preclinical study in rats. In order to test this assumption, the plasma binding of SRF and its pharmacological active metabolite NOX [147] was determined both individually and in combination with SKL at varying concentrations of 12.5, 25.0 and 37.5 μM also using equilibrium dialysis.

Berry *et al.* [148] observed certain similarities in plasma binding between species for some drugs, but this is not the norm among rats, dogs, monkeys and humans. Therefore, it would be advantageous to determine the f_u in the plasma of the preclinical species used. However, fresh plasma is recommended for equilibrium dialysis [149], but this was not available of rats, dogs and monkeys. Hence, and because the application of SKL in man is the final objective, the freshly prepared pooled plasma of eight human donors was used.

	a)			b)		c)	
	SKL	+ SRF	+ NOX	SRF	+ SKL	NOX	+ SKL
c [μM]	12.5	+ 37.5	+ 37.5	12.5	+ 37.5	12.5	+ 37.5
f_b [%]	96.2	96.1	96.4	96.0	95.8	96.9	96.9
c [μM]	25.0	+ 25.0	+ 25.0	25.0	+ 25.0	25.0	+ 25.0
f_b [%]	96.4	95.9	96.4	96.2	97.2	92.0	97.1
c [μM]	37.5	+ 12.5	+ 12.5	37.5	+ 12.5	37.5	+ 12.5
f_b [%]	93.7	96.3	97.1	97.4	97.1	91.5	97.0

Tab. 43: Fraction bound (f_b) to plasma proteins of a) SKL solely and in the presence of SRF or NOX; b) SRF alone and combined with SKL; c) NOX solely and with addition of SKL. Concentrations of solo tested SKL, SRF and NOX were 12.5, 25.0 and 37.5 μM . Added concentrations of SKL, SRF and NOX were 37.5, 25.0 and 12.5 μM . The results represent mean values of duplicate analysis per combination.

The equilibrium dialysis results given in table 43 confirm that SKL is bound to plasma proteins, as previously suspected. In addition, with f_b values of 93.7 to 96.4 %, the degree of binding can be described as high [150]. No direct correlation between the concentration of SKL and the resulting f_b can be observed, therefore the binding process can be considered as concentration-independent and thus not saturable. When incubated in combination with SRF or NOX, the f_b of SKL remains within 95.0 and 97.1 %, which correlates with the values obtained in the single incubations. For all analysed variants of SKL, SRF and NOX no tendencies or dependencies could be observed with regard to the plasma-bound fraction of SKL. Thus, it appears that the plasma protein binding of SKL is not affected by the presence of either SRF or NOX in any of the concentrations and combinations tested here.

SRF is known to be extensively bound to plasma proteins with f_b above 99.5 % [142]. Thus, the plasma-bound fractions of SRF obtained here are lower, with values of 96.0 to 97.4 %. Despite these differences, it can at least be confirmed that binding to plasma of SRF appears to be independent of concentration, suggesting a non-specific and non-saturable process [151]. As already observed with the binding of SKL to plasma proteins, also the f_b of SRF does not seem to change in the presence of SKL and remains at values of 95.8 to 97.2 %. Even at a concentration ratio of SRF to SKL of 1 to 9, no effect on protein binding was observed (data not shown). These results indicate that SKL appears to have no influence on the f_b of SRF in human plasma within the concentration range tested.

The plasma protein binding of NOX does not seem to have been described in the literature so far. However, the values obtained here suggest that it is roughly comparable to the binding of SRF to proteins in human plasma. Thus, the incubation of 12.5 μM NOX resulted in an f_b of 96.9 %. However, this appeared to decrease with increasing NOX concentration. The f_b of 37.5 μM NOX was only 91.5 %. This could indicate that plasma protein binding of NOX is concentration-dependent and thus saturable. In the presence of SKL, the f_b of NOX remains constant at 96.9 to 97.1 %. Neither the concentration of NOX nor the amount of SKL added seems to have any influence. Therefore, it is difficult to interpret whether the observed decrease is concentration related. Possibly other factors, such as non-specific binding at the dialysis membrane, led to the lower values. Changes in f_b could lead to an increase in the free concentration of NOX in plasma. This in turn could increase the therapeutic efficacy but also the adverse effects of SRF. However, the similar pharmaceutical potency of NOX to SRF has so far only been described *in vitro* [100]. Moreover, the decrease in f_b of NOX does not seem to be related to SKL. Therefore, the exact cause is not of further interest in the context of this thesis.

Due to the deviations regarding the f_b of SRF between the values obtained here and those reported in the literature, it cannot be excluded that the plasma binding of SKL in human plasma could also be higher than assumed here. The reasons for the different results could be, for example, that the release of the plasma-bound analyte during protein precipitation and extraction was perhaps not complete. Also, protein breakthrough from the plasma to the buffer site could have occurred despite a

relatively small molecular weight cut-off. The anticoagulant heparin used could as well have interfered with protein binding [152]. Another cause could be the pH in the plasma, as the f_b of SRF is known to be pH-dependent and decreases in acidic milieu [100]. Unfortunately, the pH of the plasma used was not determined prior analysis. Additionally, it can unfortunately not be excluded that non-specific binding of SRF or SKL to the dialysis membrane was present.

Despite these uncertainties, at least in humans, the plasma binding of SKL and SRF can be excluded as a factor with regard to a possible mutual influence on the plasma concentrations. However, this does not explain what caused the effect observed in rats. Although it is known that the bound fraction of SRF in rat plasma is also above 99.5 % [100], it cannot be excluded that the f_b of SKL in rat plasma is lower than in human plasma. Thus, binding to plasma proteins could be increased or decreased in the presence of SRF in rats. Based on these results, a determination of the plasma-bound fraction of SKL in rat plasma would be useful to verify and confirm or refute this assumption.

3.5. Metabolic Conversion of Skepinone-L *in vitro*

It is essential to study the metabolic transformation of a drug for both, safety and efficacy. In addition to the risk that the active pharmaceutical ingredient is converted too rapidly and thus not reaching its effective concentration due to inactivation, the resulting metabolites could also be potentially toxic. The majority of drugs undergo Ph1 metabolic transformation, which is predominantly catalysed by the CYP superfamily and comprises hydrolysis, oxidations and reductions [153]. Ph2 conjugation reactions of polar and ionisable groups to Ph1 metabolites or the API itself are mediated by Ph2 enzymes, which include the UGTs [154]. Liver microsomes (LM) were selected out of numerous *in vitro* models as a test system to investigate the metabolic conversion of SKL. To assess the usability and transferability of preclinical *in vivo* studies to humans, differences between species should be investigated.

So far, SKL was known to not be metabolically degraded by CYP enzymes *in vitro* in human and rat LM [155]. Conjugated metabolites were observed *in vivo* during a pharmacokinetic study in C57BL/6 mice [121], but were not described or identified

further. Thus, there is still a lack of essential information regarding the metabolism of SKL. Therefore, *in vitro* biotransformation of SKL should be investigated using liver microsomal CYPs and UGTs. Potentially forming metabolites ought to be structurally elucidated and the respective responsible isoenzymes identified if possible.

As a combination therapy of SKL and SRF for the treatment of HCC in humans is being aspired, it was essential that metabolism-based drug-drug interactions were also investigated. Therefore, the biotransformation of SKL through activation of CYPs and UGTs should also be examined in the presence of SRF. The metabolic pathways of SRF have already been studied and elucidated in detail [94]. However, since there was the possibility that SKL influences the SRF biotransformation, both the oxidative and conjugative conversions of SRF in the presence of SKL were studied.

3.5.1. Biotransformation of Skepinone-L in Liver Microsomes

Since the metabolism rate of SKL has not been elucidated completely yet, the *in vitro* metabolic stability and conversion were examined. The rate of metabolic degradation indicates whether a drug requires higher doses at short intervals or could have tendencies to accumulate, which in turn could lead to intoxication. The remaining percentage of non-metabolised SKL after incubation in the presence of a metabolically active system over time is defined as metabolic stability. Differences between species were investigated using LMs from humans (HLM), rats (RLM), mice (MLM), dogs (DLM) and monkeys (CMLM) as test systems. Further characteristics and detailed information of the respective content of CYP and UGT activity of the LMs applied are provided in chapter 5.2.8.1 (Liver Microsomal Incubations).

3.5.1.1. CYP-mediated Biotransformation Studies

Metabolic Stability of Skepinone-L *in vitro*

CYP-mediated metabolic degradation of SKL was studied by supplementing the LMs with the required co-factors. In addition to 10 μ M SKL the incubation mixtures also contained a NADPH-regenerating system. The enzymatic reaction was stopped after 120 min and the amount of unchanged SKL was determined in percent. The relative

content calculation is based on the PAR of SKL to ISTD at the initiation and after completion of the incubation. The experimental setup in detail and the description of the LC-MS/MS method applied to determine PARs of SKL and ISTD are given in chapter 5.2.8.2. The *in vitro* metabolic stability of SKL determined in the presence of activated CYPs in HLM, RLM, MLM, DLM and CMLM are presented in following table 44. These incubations were performed as duplicates.

	HLM	RLM	MLM	DLM	CMLM
unchanged SKL [%]	95.0	82.0	89.1	76.2	71.3

Tab. 44: Metabolic stability of SKL *in vitro* after 120 min incubation by addressing microsomal CYPs of human, rat, mouse, dog and monkey LMs. The initial concentration of SKL was 10 μ M in each incubation. Results represent the mean values of two incubations per species.

Nearly no CYP-mediated biotransformation of SKL could be observed after 120 min in HLM. The highest metabolic stability after HLM was observed in MLM with 89.1 %, followed by RLM with 82.0 % and DLM with 76.2 %. In CMLM, 71.3 % of unchanged SKL remained, which means that enzymatic degradation was most pronounced here.

Some CYP isoforms are known to show strong similarities between humans and preclinical species. However, there are also isoforms that are species-specific and therefore exhibit large differences in expression, substrate specificity and catalytic activity between species. These include, for example, the CYP3A subfamily, which metabolises most substrates and thus plays a major role in the biotransformation of xenobiotics [156]. Four isoforms of CYP3A are known so far to be expressed in humans, six in mice and rats, two in dogs, and one in monkeys [157]. These isoforms show both similarities and substantial differences to the human CYP3A enzyme family. For example, the isoform expressed in monkeys is very similar to human CYP3A4 [158], but the microsomal CYP content in monkeys is significantly higher, which is also reflected in the LMs used in the present work for metabolic stability determination of SKL (Tab. 93, Ch. 5.2.8.1) In addition to the interspecies differences of the CYP isoforms, the species-specific percentage of the liver in the total body weight must also be considered. The ratio is greater in smaller animals, which leads to a higher CYP content in relation to body weight than in humans and to a faster elimination of xenobiotics [157]. Considering the species-specific CYP isoforms as well as their relative content, the interspecies differences observed with respect to the metabolic stability of SKL are not unusual. However, the values for metabolic stability

in HLM and RLM obtained in the present work differ significantly from those reported in the literature by Baur, *et.al* [155]. In those previous *in vitro* studies 100 % unchanged SKL after 180 min was described in HLM and RLM. Due to these differences, additional tests were performed in microsomes of both species. In these incubations, the SKL concentration was increased to 25, 50 and 75 μM . The further experimental setup remained unchanged. The largest deviation between the two values occurred with 1.8 % in HLM (25 μM SKL) and the smallest in RLM (75 μM) with 0.1 %.

initial SKL	HLM				RLM			
	25 μM	50 μM	75 μM	10 μM	25 μM	50 μM	75 μM	10 μM
unchanged SKL [%]	97.1	98.3	98.9	95.0*	88.7	91.9	95.0	82.0*

Tab. 45: Metabolic stability *in vitro* of SKL after 120 min incubation by addressing microsomal CYPs of human and rat LMs. The initial concentration of SKL was 25, 50 and 75 μM in the respective incubations. The results represent the mean values of two incubations per species and concentration. *results from previous incubations for comparison

The metabolic stability of SKL resulting from the additional incubations in HLM and RLM are shown in table 45. Interestingly, there seems to be a correlation, albeit weak, between these and the initial concentrations of SKL. The higher the used SKL concentration, the lower the degraded percentage. In HLM only a very slight decrease is observed, while in RLM the reduction is more pronounced in relation to the concentration. Thus, one reason for the different results with regard to SKL stability *in vitro* could be the respective initial concentration. In the present work 10 μM were utilised, whereas the amount of SKL used in the previous analysis was 100 μM . Most likely, this is due to the saturation of the enzymes involved in the presence of high substrate concentrations. In addition, purchased LMs may also differ in CYP content and catalytic activity. The final intention of the comprehensive research is the application of SKL as a therapeutic agent in humans. Therefore, the marginal difference in HLM within the results regarding the metabolic stability of SKL is acceptable. Furthermore, the appearance of SKL Ph1 metabolites could be observed. A total of five metabolites generated by CYP-mediated conversion could be found in RLMs. Their formation could also be observed in HLMs, but in some cases so low that despite a detected signal the relative amount was 0.0 %. They are designated as metabolites 1 to 5 (M#1-5) based on their retention time. Their degree of formation in percent related to the initial SKL concentration could be determined (Tab. 46) by

applying the sensitive MRM-mode. Chromatographic and MS/MS conditions are given in chapter 5.2.8.5 (Dual Activity Metabolism Assay).

	HLM			RLM		
	25 μ M	50 μ M	75 μ M	25 μ M	50 μ M	75 μ M
M#1 [%]	0.4	0.5	0.6	1.9	1.8	1.6
M#2 [%]	0.1	0.1	0.1	0.1	0.2	0.2
M#3 [%]	0.0	0.0	0.0	0.3	0.3	0.2
M#4 [%]	0.1	0.1	0.1	7.2	4.5	3.0
M#5 [%]	0.0	0.0	0.0	0.9	0.6	0.3

Tab. 46: Percentage of formed SKL Ph1 metabolites (M#1-5) after 120 min incubation by addressing microsomal CYPs of human and rat LMs. The initial concentration of SKL was 25, 50 and 75 μ M in the respective incubations. The results represent the mean values of two incubations per species.

Species-specific differences were also observed with regard to metabolite formation. Thus, M#4 is the main metabolite in RLMs with a maximum value of 7.2 %, followed by M#1 with 1.9 %. In HLMs M#1 is the most dominant product with 0.6 %. All other metabolites are lacking or were formed to a negligible percentage of 0.1 %. It is not surprising, that metabolite formation appears to decrease when LMs were exposed to a higher concentration of SKL. As described above, the higher the starting concentration, the lower the percentage of metabolites formed. On the one hand, the percentages only represent a relative content and not an actual quantity. On the other hand, the rate and extent of metabolic conversion do not increase linearly with the concentration of the parent compound. In addition, the enzymatic system will be saturated above a certain substrate concentration.

Figure 52 shows proposed structures for the SKL metabolites M#1 to 5. These were suggested based on their m/z ratios, considering that only CYPs were involved in the catalytic conversion. Thus, M#1, #2 and #3 could possibly represent products of the enzymatically catalysed hydroxylation, hydrolysis or dehydration of SKL. In addition, an NIH shift leading to the loss of one fluorine [159] could also contribute to the formation of these metabolites. These reactions may have occurred individually or in combination. Some of the hypothesised metabolic transformation reactions for the dibenzosuberone scaffold of SKL and the dioxepinone analogue have already been described by Storch, *et. al* [121].

Proposed structures for:

M#1, M#2 and M#3 ($m/z = 424.0$)

M#4 and M#5 ($m/z = 349.9$)

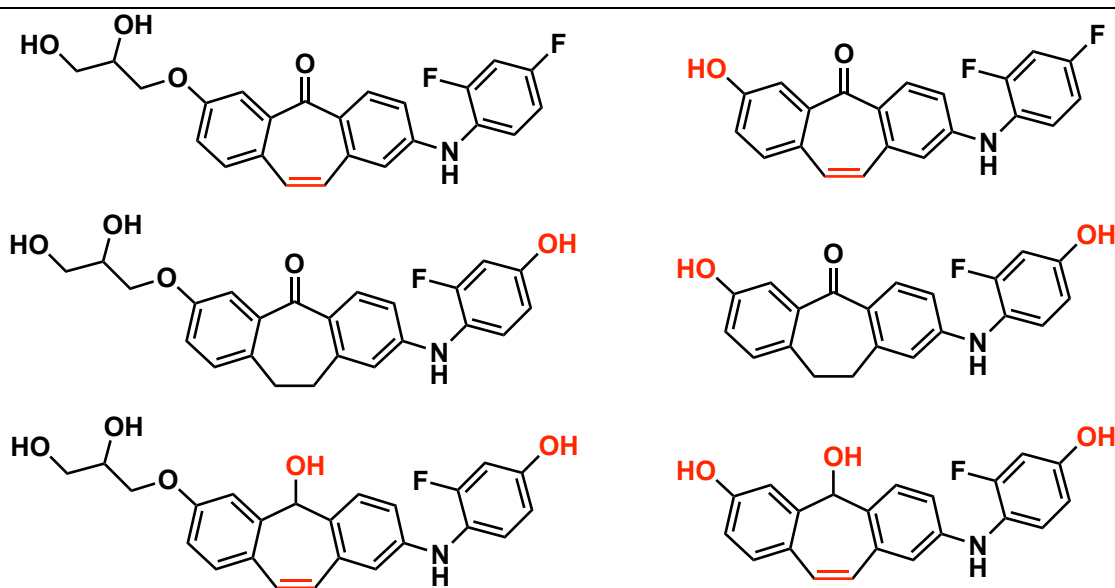


Fig. 52: Proposed structures for Ph1 metabolites of SKL after exposure to human and rat microsomal CYPs. The structures were suggested based on their m/z ratios. The structural modifications compared to SKL are marked in red. Metabolites #1, #2 and #3 were possibly formed by hydroxylation, hydrolysis, dehydration or NIH shift. In addition, M#4 and #5 might have been generated by O-dealkylation.

In addition to the transformation reactions already mentioned, the proposed structures for M#4 and #5 each involve O-dealkylation. However, this seems to occur almost exclusively in RLM. CYP2D2 is known to catalyse O-dealkylations in rats [160]. This isoform is species-specific and thus not expressed in humans or in the other species tested here, nor is any orthologue to human known to date [157]. Thus, in HLM most likely no or only marginal O-dealkylation of the glycine residue of SKL occurred. These results are consistent with the previously described metabolic behaviour of SKL if exposed to HLM by Baur, *et al.* [155]. Whether the described Ph1 metabolites of SKL are also formed in the other species was tested by co-activation of microsomal CYPs and UGTs. The detailed description follows in section 3.6.1.3.

Influence of Sorafenib on the Metabolic Stability of Skepinone-L

In order to study metabolism-based drug-drug interactions of SKL and SRF, further incubations under Ph1 conditions were performed. Therefore, the metabolic stability of 10 μM SKL combined with either 5, 10, 20 or 40 μM SRF in HLM, RLM, MLM, DLM and CMLM was examined. Further experimental setup remained unchanged and was performed as previously described.

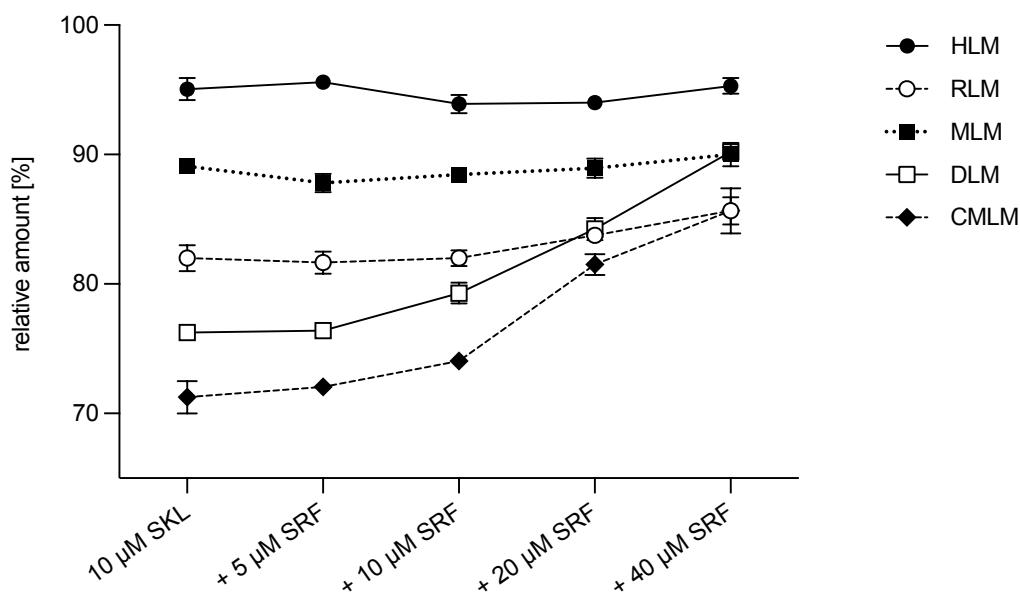


Fig. 53: Metabolic stability *in vitro* of SKL solely and in the presence of SRF after 120 min incubation by addressing microsomal CYPs of human, rat, mouse, dog and monkey LMs. The initial concentration of SKL was 10 µM in each incubation combined with either 5, 10, 20 or 40 µM SRF. Results represent the mean values of two incubations per species and concentration. The respective range of the two measured values is represented by error bars.

Figure 53 shows the amount of unchanged SKL in percent after 120 min incubation in the presence of SRF and microsomal CYPs of different species. The metabolic stability of SKL does not change significantly in the presence of SRF, regardless of concentration, in human and murine LM. In rat LM, SRF appears to have an influence at a concentration of 20 and 40 µM in terms of a slight increase with respect to the remaining SKL percentage. In dog and monkey LMs, however, an influence of SRF on the metabolic degradation of SKL is evident. The higher the SRF concentration, the more resistant SKL appears to be to metabolic degradation by CYP enzymes. Thus, in DLM, the proportion of unchanged SKL increases from 76.2 % (10 µM SKL) to 90.2 % (10 µM SKL + 40 µM SRF). For CMLM, the stability changed from 71.3 % to 85.6 %. The extent of the SRF-mediated influence on metabolic stability thus appears to be the same in DLM and CMLM.

During *in vivo* pharmacokinetic studies in rats, an increase in the C_{max} of SKL was observed when SRF was administered simultaneously. This effect did not appear to occur in humans during compassionate use. The results obtained in human and rat LMs confirm these observations. This suggests that SRF interacts with a rat specific CYP isoform which has no human orthologue with regard to substrate affinity. This also seems to apply to the biotransformation of SKL in DLM and CMLM. In their

presence SKL has relatively low metabolic stabilities of 76.2 % and 71.3 %, respectively. However, these are significantly increased up to 90.2 % and 85.6 % by simultaneous incubation with SRF. The higher the SRF concentration used, the less SKL is metabolically converted. This implies that SRF inhibits a CYP isoform that catalyses the transformation of SKL to almost the same extent in DLM and CMLM. This isoform also does not appear to be present in HLM. SRF is known to inhibit the following CYP isoforms in humans in decreasing order of potency: 2C8, 2B6, 2C9, 2C19, 2D6 and 3A4 [100]. Although their murine and rat-like orthologues are known [161], this information regarding canine and simian CYP isoforms is lacking so far. Thus, in addition to the structural elucidation of the resulting metabolites of SKL, the identification of the responsible isoforms in DLM and CMLM is also missing. But it was possible to determine interspecies differences in the influence of SRF on the metabolic transformation of SKL as well as the corresponding species. A positive finding is the high and consistent metabolic stability of SKL in HLM against CYP-induced degradation regardless of the presence or absence of SRF.

As described in the previous point, the formation of SKL Ph1 metabolites has been observed in RLM and HLM. There where clear differences between the species. Incubations of SKL in combination with SRF were performed in HLM and RLM to investigate the possible influence of SRF on the metabolite formation of SKL. The initial concentration ratio of SKL to SRF was 1 to 3, 1 to 1 and 3 to 1.

	HLM			RLM		
	SKL [μ M]	25	50	75	25	50
SRF [μ M]	75	50	25	75	50	25
M#1 [%]	1.1	1.3	1.0	1.5	1.5	1.5
M#2 [%]	0.2	0.2	0.1	0.2	0.2	0.2
M#3 [%]	0.0	0.0	0.0	0.1	0.2	0.2
M#4 [%]	0.1	0.2	0.1	0.9	1.2	1.5
M#5 [%]	0.0	0.0	0.0	0.2	0.2	0.2

Tab. 47: Percentage of formed SKL Ph1 metabolites (M#1-5) after 120 min incubation in the presence of SRF. Thereby addressing microsomal CYPs of human and rat LMs. The initial concentrations of SKL and SRF were 25+75 μ M, 50+50 μ M and 75+25 μ M in the respective incubations. The results represent the mean values of two incubations per species and concentration.

The results (Tab. 47) show, that the percentage of metabolites increases in HLM. Thus, in the presence of SRF, the percentage of M#1 increases from 0.4 % - 0.6 % to 1.0 % - 1.3 %. There seems to be no influence of SRF on any of the other metabolites in HLM. However, this increase in relation to the concentration ratios is very small and

can therefore not be considered as significant. Furthermore, no effect of SRF on the metabolic stability of SKL in HLM could be observed. In RLM a small influence on the formation of M#5 and a clear effect on M#4 was observed. For both, a more or less pronounced decrease in the percentage share can be observed in the presence of SRF. Thus, instead of 3.0 % to 7.0 % (Tab. 46) the main M#4 represents only 0.9 % to 1.5 % of the initial SKL concentration. These results confirm the assumption of a species-specific CYP isoform. This enzyme seems to have a relatively high catalytic activity with regard to SKL as a substrate, especially in DLM and CMLM. Presumably, the postulated O-dealkylation is implemented by this isoform. Interestingly, the increased metabolic stability of SKL in the presence of SRF in DLM and CMLM suggests that SRF inhibits the species-specific isoform to some extent. In RLM, the conversion rate or substrate specificity seems to be lower. In humans it either has a very low activity, is not present in the liver or is not expressed at all. Based on these results, the mouse seems to be the most similar preclinical species to humans in terms of CYP-induced transformation of SKL.

3.5.1.2. UGT-mediated Biotransformation Studies

Metabolic Stability of Skepinone-L *in vitro*

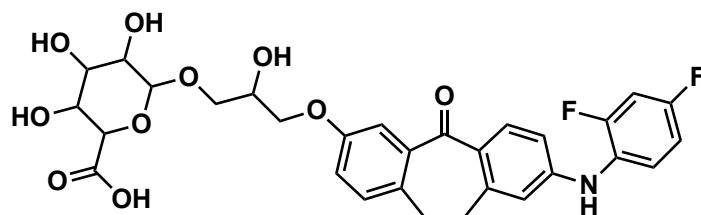
The metabolic stability determination of SKL towards UGT-mediated conjugation was performed by using microsomal uridine 5'-diphospho-glucuronosyltransferases (UGTs) of HLM, RLM, MLM, DLM and CMLM. These were activated, *i.e.*, made accessible to the substrate by rupturing the membrane with alamethicin. The incubation of 10 μ M SKL were performed, *inter alia*, in the presence of uridine diphosphate glucuronic acid (UDPGA) as glycosyl donor. The detailed description of the incubation setup and the LC-MS/MS method applied are described in chapter 5.2.8.3 (UGT-mediated Phase 2 Metabolism Studies).

	HLM	RLM	MLM	DLM	CMLM
unchanged SKL [%]	66.4	85.8	54.5	83.9	88.7

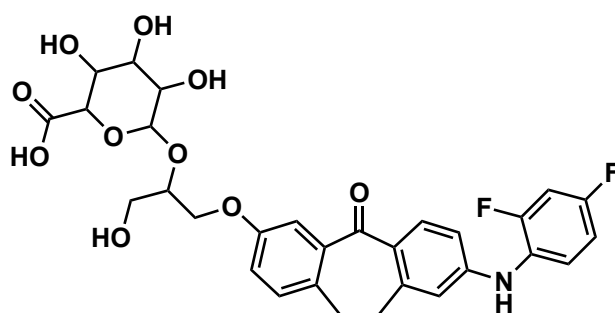
Tab. 48: Metabolic stability of SKL *in vitro* after 120 min incubation by addressing microsomal UGTs of human, rat, mouse, dog and monkey LMs. The initial concentration of SKL was 10 μ M in each incubation. Results represent the mean values of two incubations per species.

The results (Tab. 48) show that SKL was metabolically degraded by conjugation reaction in all species. This occurs strongest in HLM and MLM with values of 66.4 % and 54.5 %. In both species SKL was only metabolised to a small extent in the presence of CYPs. In RLM, DLM and CMLM the metabolic stability of SKL towards activated UGTs was almost the same at 85.8 %, 83.9 % and 88.7 %.

primary SKL-O-glucuronide (pO-Glc)



secondary SKL-O-glucuronide (sO-Glc)



SKL-N-glucuronide (N-Glc)

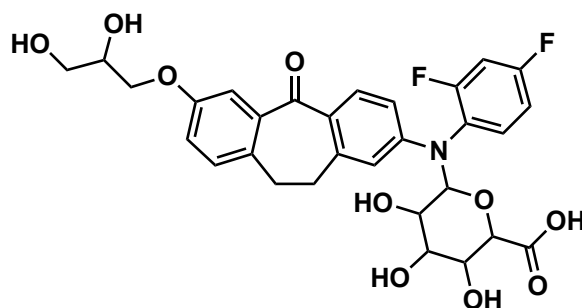


Fig. 54: Structures of the primary and secondary oxygen-linked glucuronides as well as the nitrogen-linked glucuronide of SKL. These are the conjugation products after exposure of SKL to microsomal UGTs of various species. A detailed description of the structure elucidation is given in chapter 3.5.2.4.

During incubations of SKL in the presence of activated UGTs, the formation of conjugation products was observed (Fig. 54). Three SKL-glucuronides appeared to be formed in HLM whereas two were formed in all other species tested. The structural elucidation of these glucuronides is described in the upcoming chapter 3.5.2.4. This elucidation shows that two oxygen-linked glucuronides (O-Glc) of SKL are formed *in vitro* in all species. These are described as primary SKL-O-glucuronide (pO-Glc) and secondary SKL-O-glucuronide (sO-Glc). The formation of a nitrogen-linked glucuronide (N-Glc) was observed solely in HLM.

In addition to metabolic stability the relative content of glucuronides formed in each species was determined in percent after 120 min incubation. The results (Tab. 49) reveal strong differences between the species.

	HLM	RLM	MLM	DLM	CMLM
pO-Glc [%]	3.5	1.8*	7.3	3.8	3.1
sO-Glc [%]	7.4		44.1	3.2	6.0
N-Glc [%]	5.1	-/-	-/-	-/-	-/-

Tab. 49: Percentages of formed SKL Ph2 metabolites (pO-Glc, sO-Glc, N-Glc) after 120 min incubation by addressing activated microsomal UGTs of human, rat, mouse, dog and monkey LMs. The initial concentration of SKL was 10 μ M in each incubation. The results represent the mean values of two incubations per species. *sum of both glucuronides

As already mentioned, the N-Glc is only formed in HLM. Unfortunately, a chromatographic separation of the two O-linked glucuronides was not possible in RLM. On the one hand, this was due to the low formation of these in RLM. On the other hand, the method could not be optimised because the glucuronides were not available as reference substances at the time of the analyses. Therefore, the sum of 1.8 % of the formed sO- and pO-Glcs can be given. This is very low compared to the other species. The formation of SKL's pO-Glc seems most pronounced in MLM with 7.3 %. With 3.5 % in HLM, 3.8 % in DLM and 3.1 % in CMLM there are no clear differences with respect to pO-Glc generation in these species. In contrast, glucuronide conjugation leading to sO-Glc exhibits the most interspecies differences. The least of sO-Glc is formed in DLM with 3.2 %. CMLM and HLM produced a comparable amount of 6.0 % and 7.4 % sO-Glc. The most sO-Glc was generated in MLM with 44.1 %. With regard to the biotransformation of SKL in the presence of CYPs, there seemed to be a strong similarity between HLM and MLM. This may still be the case with regard to metabolic stability towards UGT conjugation reactions. However, HLM and MLM show significantly different results in terms of metabolites formed and their relative amounts.

In addition to MLM, HLM also showed very pronounced glucuronide formation. Hence, it is essential to understand which conjugation reaction is catalysed by which human UGT-isoform. Furthermore, the elucidation of N-Glc formation occurring only in HLM is essential for the assessment of the metabolic transformation of SKL. Therefore, a reaction phenotyping of glucuronidation was performed. The experimental procedure and the identified responsible isoenzymes are described in the upcoming section 3.5.2.

Influence of Sorafenib on the Metabolic Stability of Skepinone-L

The possible interaction of SRF on the glucuronidation of SKL *in vitro* was examined in an analogous manner for CYP-mediated biotransformation (3.5.1.1).

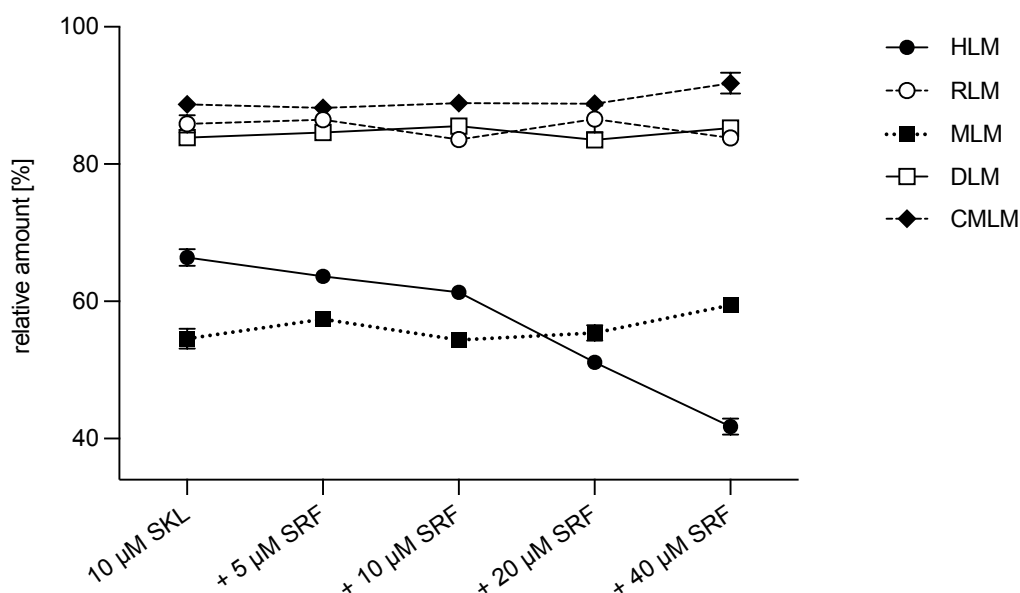


Fig. 55: Metabolic stability *in vitro* of SKL solely and in the presence of SRF after 120 min incubation by addressing activated microsomal UGTs of human, rat, mouse, dog and monkey LMs. The initial concentration of SKL was 10 µM in each incubation combined with either 5, 10, 20 or 40 µM SRF. Results represent the mean values of two incubations per species and concentration. The respective range of the two measured values is represented by error bars.

The metabolic stability of SKL in the presence of SRF in all tested species is given in figure 55. This illustrates that SRF does not appear to have any effect on the conversion of SKL via UGTs and thus its metabolic stability in RLM and DLM. In these species, there are hardly any differences between incubations with different amounts of SRF despite fluctuations in the respective amount of unchanged SKL. In MLM and CMLM only the highest SRF concentration seems to lead to a small increase in metabolic stability towards transformation by UGTs. In HLM, a noticeable influence of

SRF on the metabolic conversion of SKL is visible. The remaining percentage of unchanged parental compound decreases significantly from 66.4 % (10 μ M SKL) to 41.7 % (10 μ M SKL + 40 μ M SRF). The addition of 5 and 10 μ M SRF initially results in a relatively small decrease in SKL concentration. In the presence of 20 and 40 μ M SRF, however, a very pronounced reduction occurs. This observation in LMs of donors which were untreated prior preparation is very unusual. Co-administration of two or more compounds may induce drug-metabolizing enzymes. This could lead to increased metabolic transformation of the drug investigated. This drug-drug interaction is known for a wide variety of xenobiotics. But enzyme induction represents regulation of gene expression and can thus only occur at the mRNA level [162], which is not possible in the system used here. Preclinically, the investigation could be performed *ex vivo* with LMs from previously treated animals [163] or *in vitro* with primary hepatocytes [164]. In summary, an induction of the responsible UGT isoenzymes by means of the untreated LMs used here, as well as the relatively short incubation period, is impossible. One hypothesis is that SRF increases the catalytic activity of the responsible UGTs. This would be possible via allosteric activation. In this case, SRF would bind at a site that is distinct from the active site of the enzyme [165]. However, no description that SRF could act as an allosteric effector could be found in literature so far. Therefore, the significantly lower metabolic stability of SKL in the presence of SRF in HLM cannot be explained. The relative amounts of SKL-glucuronides formed after 120 min of simultaneous incubation of SKL and SRF (Tab. 50) show further unexpected results.

		SKL		+ SRF		
		10 μ M	5 μ M	10 μ M	20 μ M	40 μ M
pO-Glc [%]	HLM	3.5	2.4	2.8	2.0	2.2
	RLM	1.8*	1.9*	1.8*	2.4*	1.8*
	MLM	7.3	7.6	7.8	8.2	8.5
	DLM	3.8	4.5	4.8	5.0	4.7
	CMLM	3.1	3.6	2.0	2.6	2.6
sO-Glc [%]	HLM	7.4	6.2	6.0	5.5	4.8
	RLM	-/-	-/-	-/-	-/-	-/-
	MLM	44.1	47.3	47.5	46.8	45.9
	DLM	3.2	4.0	4.4	4.4	4.3
	CMLM	6.0	6.7	3.5	4.4	4.1
N-Glc [%]	HLM	5.1	5.8	7.6	9.4	13.0

Tab. 50: Percentages of formed pO-Glc, sO-Glc and N-Glc after 120 min incubation in the presence of SRF. Thereby addressing activated microsomal UGTs of human, rat, mouse, dog and monkey LMs. The initial concentration of SKL was 10 μ M in each incubation. Initial SRF concentrations were 5, 10, 20 or 40 μ M respectively. The results represent the mean values of two incubations per species and concentration. *sum of both glucuronides

The formation of pO-Glc in the presence of SRF is slightly decreasing in HLM and CMLM. However, a small but steady increase in relative pO-Glc content can be recognised in both MLM and DLM. The formation of sO-Glc also shows similar trends. Here, the decrease in HLM and CMLM is subject to less fluctuation. In MLM, there is initially an increased formation, which decreases again with higher SRF concentration. In DLM, a small increase can be observed with 5 and 10 μM SRF which remained almost unchanged with the subsequent concentrations. In RLM almost no change in the sum of the resulting metabolites was observed. With regard to the O-Glcs of SKL, the observed changes in the amounts formed in co-incubation with SRF are not distinct. In contrast, the N-Glc formation in the presence of SRF in HLM increases clearly from 5.1 % to 13.0 % in a concentration-dependent manner. At least this increased amount of N-Glc formed contributes to the reduced metabolic stability of SKL in combination with SRF in HLM.

3.5.1.3. CYP and UGT Co-Activated Biotransformation Studies

Metabolic Stability of Skepinone-L

The metabolic stability and conversion of SKL shows obvious differences between CYP- and UGT-mediated degradation in each species tested here. However, both processes occur simultaneously *in vivo* and not separately. As a low cost and time saving alternative to primary hepatocytes, both groups of enzymes were co-activated in LMs. In this so-called "dual activity" assay (DAA), microsomal UGTs were first activated as described in the previous section (3.5.1.2). The addition of the NADPH regeneration system and UDPGA made it possible to investigate simultaneous CYP- and UGT-mediated transformation. The optimal composition and handling of the incubations were determined in preliminary tests. The aim was to obtain a similar conversion rate for the coupled method compared to the individual CYP and UGT incubations. In addition to SKL and its metabolites, the DAA should also provide similar results in stability and conversion for SRF. Numerous modifications of the experimental conditions were made, since both CYP and UGT activity could be influenced by components of the reaction mixture. For example, different concentrations of MgCl_2 , as well as β -NADPH and UDPGA were tested. The potential influence of saccharolactone and bovine serum albumine (BSA) was also examined.

The final composition and optimal procedure are described in chapter 5.2.8.5. In addition, the chromatographic separation method was optimized in order to separate the three glucuronides of SKL in all species for analysis. The common test systems HLM RLM, MLM, DLM and CMLM were used.

The metabolic stabilities and the relative amounts of glucuronides obtained by the DAA of 10 μM SKL are summarised in tables 51 and 52.

	HLM	RLM	MLM	DLM	CMLM
unchanged SKL [%]	84.9	79.7	50.0	87.3	74.5

Tab. 51: Metabolic stability of 10 μM SKL after 120 min incubation by co-activation of microsomal CYPs and UGTs of human, rat, mouse, dog and monkey LMs. The results represent the mean values of two incubations per species.

	HLM	RLM	MLM	DLM	CMLM
pO-Glc [%]	3.6	1.5	20.1	3.9	1.9
sO-Glc [%]	8.3	2.8	82.6	3.9	3.1
N-Glc [%]	1.7	-/-	-/-	-/-	-/-

Tab. 52: Percentages of formed SKL Ph2 metabolites (pO-Glc, sO-Glc, N-Glc) after 120 min incubation by co-activation of microsomal CYPs and UGTs of human, rat, mouse, dog and monkey LMs. The initial concentration of SKL was 10 μM in each incubation. The results represent the mean values of two incubations per species.

These results show that SKL appears to have the highest metabolic stability of 87.3 % in DLM and 84.9 % in HLM when CYPs and UGTs were simultaneous activated. RLM and CMLM are also similar to each other with values of 79.7 % and 74.5 %. With 50 %, the highest metabolic conversion of SKL has occurred in MLM.

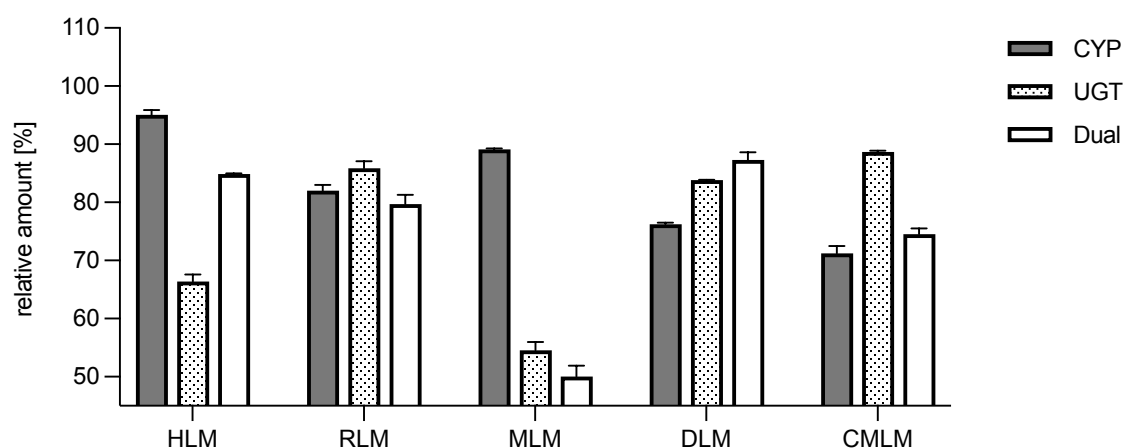


Fig. 56: Metabolic stability of SKL obtained after 120 min by addressing microsomal CYPs, UGTs either solely or co-activated of human, rat, mouse, dog and monkey LMs. The initial concentration of SKL was 10 μM in each incubation. The results represent the mean values of two incubations per species. The range of the two measured values is represented by error bars.

Directly compared (Fig 56), SKL shows in HLM a slightly lower stability during DAA than under Ph1 conditions. But related to UGT-mediated degradation it is significantly higher. Considering the resulting O-Glcs (Fig. 57) it is noticeable that their relative proportion increases slightly in the DAA compared to the UGT incubations. During co-activation the formation of N-Glc seems to be significantly reduced, which in turn explains the higher metabolic stability. This implies that the UGT isoform responsible for N-Glc formation is less active under DAA conditions.

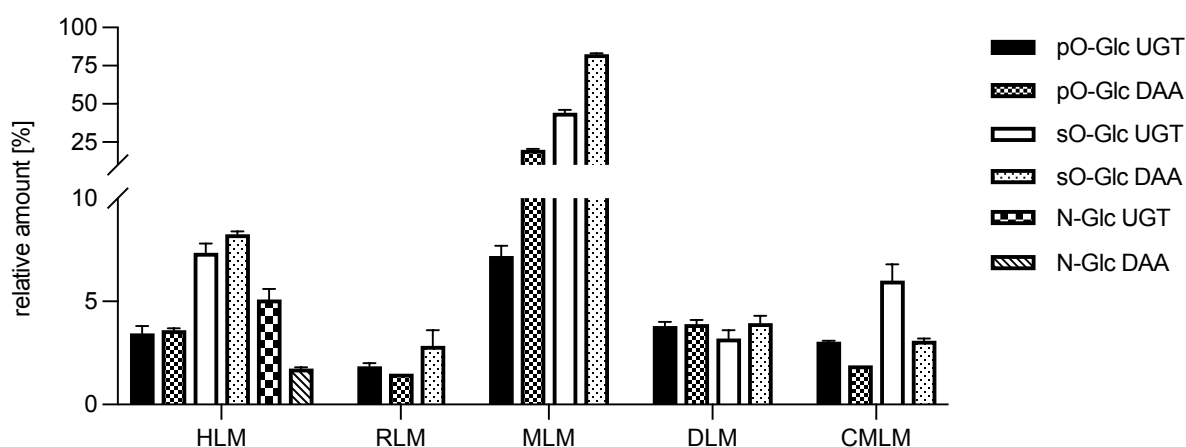


Fig. 57: Percentages of formed pO-Glc, sO-Glc and N-Glc obtained after 120 min incubation. Either by activated microsomal UGTs or co-activated CYPs and UGTs of human, rat, mouse, dog and monkey LMs. The initial concentration of SKL was 10 μ M in each incubation. The results represent the mean values of two incubations per species. The respective range of the two measured values is represented by error bars.

In RLM, the remaining amount of SKL after DAA is the lowest of all three analyses at 79.7 %. However, it is similar to the CYP (82.0 %) and UGT conditions (85.8 %). Since it was not possible to separate the glucuronides under Ph2 conditions, a direct comparison between the two different assays was not possible. However, the differences between the percentages formed are very little, which is in alignment with the hardly changed amount of remaining SKL. In MLM, almost no CYP-mediated degradation of SKL could be observed. However, there was a high conversion in the presence of UGTs. This is most pronounced under DAA conditions. The metabolic stability decreased slightly by 4.5 to 50.0 %, but the relative amounts of the two glucuronides increased significantly. The pO-Glc increased by 12.8 to 20.1 %, while the sO-Glc even rose by 38.5 to 82.6 %. Based on these relative quantities, it is obvious that the SKL glucuronides are very different from SKL in terms of ion yields. It has also not yet been clarified whether there is a linear relationship between concentration and signal intensity under the SKL-specific device parameters. To clarify

these questions, the glucuronides must be available and analysed as pure substances. In DLM, co-activation of both enzyme systems resulted in increased metabolic stability of SKL, although the glucuronide concentration slightly increased. Possibly, the conjugation reaction prevented metabolic degradation by CYPs resulting in an overall higher amount of unchanged SKL. In CMLM, the amount of SKL remaining after DAA was significantly lower than after Ph2, and thus comparable to CYP-mediated conversion. Glucuronide formation was also divided in half.

In summary, the results obtained by DAA enables assumptions about the metabolic pathway of SKL *in vitro* in the species tested here. The examination of SKL in HLM initially showed a strong transformation with activated UGTs but was significantly reduced under DAA. This indicates that SKL has a high metabolic stability under *in vivo*-like conditions. In contrast, the degradation of SKL by co-activation is even more pronounced in MLM. Thus, in this rodent species, the main metabolic pathway of SKL appears to be via conjugation with glucuronic acid. In DLM SKL seemed to be metabolised mainly by CYPs. However, coupled transformation resulted in increased metabolic stability. In CMLM, the DAA confirmed the assumption that the metabolic degradation of SKL was primarily mediated by CYPs. These observations from the DAA clearly show that co-activation is much more meaningful than analyses of CYP- or UGT-mediated degradation alone in assessing the metabolic stability and metabolite formation of SKL. Moreover, it is not possible to draw conclusions from one species to another, nor is there a homogeneous picture within a genus such as rodent or non-rodent.

Influence of Sorafenib on the Metabolic Stability of Skepinone-L

The study of SKL and SRF drug-drug interactions was also performed by performing an DAA. The procedure was conducted as described previous in this section (3.5.1.3). The metabolic stabilities of SKL in the presence of SRF obtained by DAA are shown in figure 58.

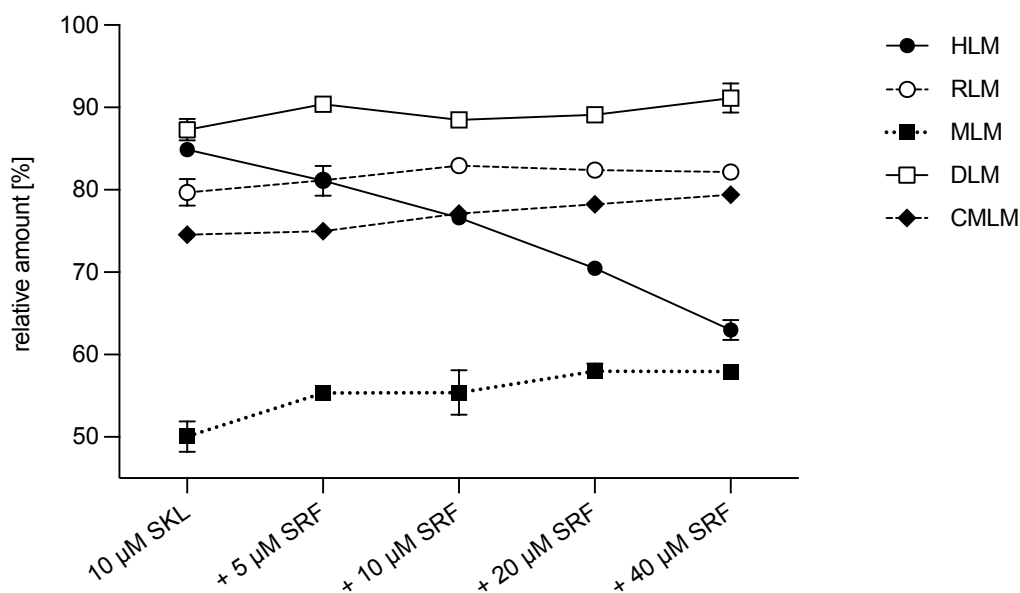


Fig. 58: Metabolic stability *in vitro* of SKL solely and in the presence of SRF after 120 min incubation by co-activation of microsomal CYPs and UGTs of human, rat, mouse, dog and monkey LMs. The initial concentration of SKL was 10 µM in each incubation combined with either 5, 10, 20 or 40 µM SRF. Results represent the mean values of two incubations per species and concentration. The respective range of the two measured values is represented by error bars.

These are very similar to the results after UGT-mediated degradation. Despite some fluctuations no effect of SRF on the degradation of SKL in RLM and DLM could be observed. In MLM, SRF appears to suppress metabolic conversion in a concentration-dependent manner. Thus, the percentage of unchanged SKL increases from 50.0 % to 57.9 %. An impact on the SKL concentration can also be observed in CMLM, but it is slightly lower with an overall change of 4.5 to 79.4 %. In summary, SRF appears to contribute to the increase in metabolic stability of SKL in the animal species tested here. HLM again shows a contrary result. Here, the amount of SKL decreases almost linearly from 84.9 % without SRF to a final 63.2 % in the presence of SRF.

		SKL	+ SRF			
		10 µM	5 µM	10 µM	20 µM	40 µM
M#1 [%]	HLM	0.0	0.3	0.4	0.5	0.7
	RLM	0.7	0.6	0.6	0.9	0.5
	CMLM	0.7	0.9	1.2	2.3	2.7
M#2 [%]	HLM	0.0	0.0	0.0	0.0	0.0
	RLM	0.2	0.3	0.2	0.3	0.2
	CMLM	0.2	0.3	0.3	0.7	0.7
M#4 [%]	HLM	0.0	0.0	0.0	0.0	0.0
	RLM	0.0	0.0	0.0	0.0	0.0
	CMLM	0.3	0.3	0.3	0.0	0.0

Tab. 53: Percentage of formed SKL Ph1 metabolites after 120 min incubation in the presence of SRF. Thereby addressing co-activated microsomal CYPs and UGTs of human, rat and monkey LMs. The initial concentration of SKL was 10 µM in each incubation. Initial SRF concentrations were 5, 10, 20 or 40 µM respectively. The results represent the mean values of two incubations per species.

Table 53 shows the relative amounts of SKL Ph1 metabolites in the absence or presence of SRF. In contrast to the CYP assay significantly fewer CYP-modified products were formed under DAA conditions. In MLM and DLM no formation of the metabolites investigated here could be observed. Moreover, M#3 and M#5 did not seem to be formed in any species.

In HLM, only the conversion of SKL to M#1 could be observed. This seemed to be slightly increased by the presence of SRF. Although this is consistent with the observation from section 3.6.1.1, the relative amounts and differences are marginal. While M#4 was the main metabolite in RLM under Ph1 conditions, it was not observed during DAA. Thus, only M#1 and M#2 appeared to be formed in RLM. The addition of SRF does not seem to have any influence on their formation. Most metabolites appeared to be formed in CMLM. The formation of M#1 and M#2 seemed to be enhanced in the presence of SRF, whereas the formation of M#4 was suppressed. However, only M#1 showed a comparatively significant change of 2.0 %, whereas all others remained below 1.0 %. In summary, hardly any of the Ph1 metabolites M#1 to M#5 of SKL under DAA conditions were formed in all species tested here. Glucuronidation seems to be the main pathway of SKL metabolism.

Regarding the formation of conjugated metabolites, the DAA results (Tab. 54) are similar to those obtained in Ph2 (3.5.1.2).

		SKL		+ SRF		
		10 μ M	5 μ M	10 μ M	20 μ M	40 μ M
pO-Glc [%]	HLM	3.6	3.4	2.8	2.9	2.8
	RLM	1.5	1.9	1.8	1.6	1.7
	MLM	20.1	19.0	17.6	18.1	18.5
	DLM	3.9	3.9	3.7	3.3	3.0
	CMLM	1.9	1.9	1.7	2.1	2.2
sO-Glc [%]	HLM	8.3	7.5	6.1	6.0	6.1
	RLM	2.8	2.7	3.5	2.0	1.8
	MLM	82.6	79.6	76.1	74.3	65.7
	DLM	3.9	4.1	3.7	3.8	3.3
	CMLM	3.1	3.0	2.7	3.5	3.8
N-Glc [%]	HLM	1.7	3.3	4.3	7.6	12.9

Tab. 54: Percentages of formed pO-Glc, sO-Glc and N-Glc after 120 min incubation of SKL in the presence of SRF. Thereby addressing co-activated microsomal CYPs and UGTs of human, rat, mouse, dog and monkey LMs. The initial concentration of SKL was 10 μ M in each incubation. Initial SRF concentrations were 5, 10, 20 or 40 μ M respectively. The results represent the mean values of two incubations per species.

Apart from minor deviations and fluctuations, either no change or only a slight decrease in the concentration of pO-Glc could be observed in the presence of SRF in all species. The formation of sO-Glc shows similar tendencies, but partly more pronounced. Thus, the presence of 40 μM SRF in HLM led to 2.2 % less sO-Glc. In MLM, the formation even decreased by 16.9 %. In RLM, DLM and CMLM increases in concentration are also occasionally observed. However, their differences compared to the percentage share without SRF do not exceed 1.0 % and can therefore not be considered as significant. The N-Glc formation in the absence of SRF was initially 1.7 %, which was significantly lower than the 5.1 % generated in UGT-mediated transformation assay. However, a clear SRF-dependent increase in concentration could also be observed in DAA. The analysis with 40 μM SRF reaches with 12.9 % almost the same concentration as under Ph2 conditions.

Metabolic Stability and Glucuronidation of Skepinone-L in Female Human Liver Microsomes

The metabolic transformation of many marketed drugs is characterised by gender-specific differences [166]. These are due to the different expression levels of hepatic drug-metabolising enzymes in males and females [167]. *In vivo* pharmacokinetic studies of SKL in preclinical animal species have been performed in both sexes, whereas *in vitro* metabolism has only been studied in male microsomes. Therefore, it should be examined whether the metabolic transformation of SKL *in vitro*, glucuronidation in particular, is also subject to gender-specific differences. For this purpose, a DAA as described previously was performed with SKL in the presence of SRF in female HLM.

		SKL	+ SRF	
		10 μM	20 μM	40 μM
unchanged	♀	84.8	79.7	74.8
SKL [%]	♂	84.9	70.5	63.0
pO-Glc [%]	♀	2.1	1.7	1.8
	♂	3.6	2.9	2.8
sO-Glc [%]	♀	3.6	3.3	3.1
	♂	8.3	6.0	6.1
N-Glc [%]	♀	0.9	1.7	3.9
	♂	1.7	7.6	12.9

Tab. 55: Metabolic stability of SKL and percentages formed pO-Glc, sO-Glc and N-Glc after 120 min in the presence of SRF. Thereby addressing co-activated microsomal CYPs and UGTs of female and male human LMs. The initial concentration of SKL was 10 μM in each incubation. Initial SRF concentrations were 20 and 40 μM respectively. The results represent the mean values of two incubations per sex.

The presence of SRF led to a decrease in concentration of SKL in both. With 79.7 % and 74.8 % in the presence of 20 μ M and 40 μ M SRF, this was significantly less pronounced in female HLMs. Gender-specific differences can also be seen with regard to glucuronidation. The formation of the three SKL glucuronides is reduced by about half in female HLMs. The suppressive effect on oxygen-linked glucuronidation on the one hand and the enhancing effect on the formation of N-Glc on the other hand could also be observed in female HLMs in the presence of SRF. However, this is significantly less pronounced than in male HLMs.

These results are not surprising as the HLMs that were used are characterised by their CYP content and UGT activities. Table 94 (Ch. 5.2.8.1) clearly shows that both content and activities are significantly lower in female than in male HLMs. Since this is comparable to the conditions *in vivo*, it can be assumed that both genders show clear differences with regard to the extent of metabolic transformation of SKL. In both genders, sO-Glc was formed the most, followed by pO-Glc and N-Glc. Thus, they differ only in the amount of unchanged SKL and the quantity of metabolites formed. Therefore, it can be assumed that the gender-related differences are reflected in a higher metabolic stability and lower metabolite formation in females, no further investigations of the metabolic transformation of SKL *in vitro* using female LMs were performed.

N-Glucuronide Formation in the Presence and Absence of Alamethicin

N-Glc formation increases significantly in the presence of SRF in a concentration-dependent manner. As already explained, the peptide alamethicin is used to activate microsomal UGTs in order to study glucuronidation. Since enzyme induction is not possible in the system used, other factors must lead to the increased formation of N-Glc. Although it is assumed that alamethicin has no direct effect on a specific UGT isoform and its protein structure [168], an interaction with SRF cannot be excluded. This assumption was investigated by performing an UGT-mediated biotransformation assay in HLM according to the description given (Ch. 5.2.8.3). Incubations of 25 μ M SKL with and without 75 μ M SRF were performed in the presence and absence of alamethicin. The PARs obtained after 120 min of the generated SKL-glucuronides are shown in figure 59.

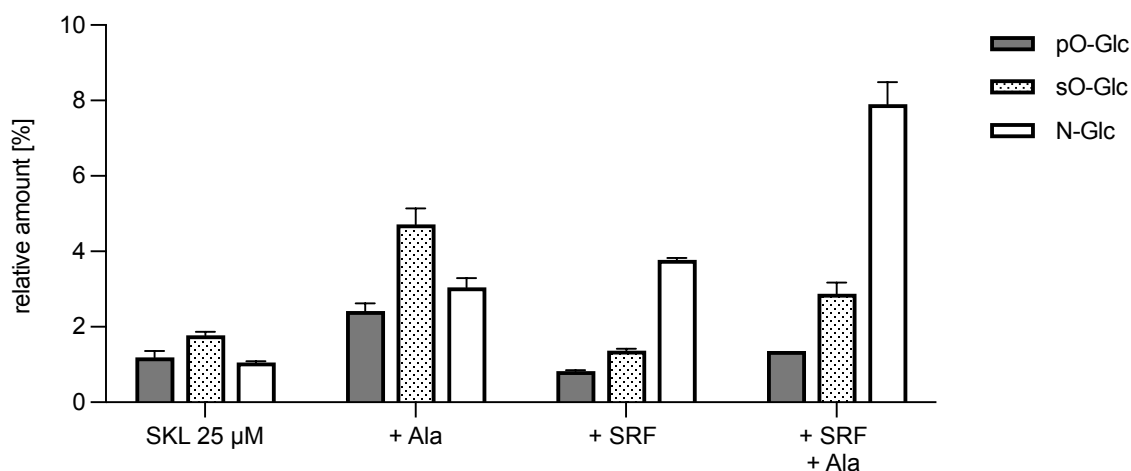


Fig. 59: Formation of pO-Glc, sO-Glc and N-Glc in HLM after 120 min. Incubations of 25 µM SKL were performed in non-activated and activated (+Ala) microsomal UGTs each in the absence or presence (+SRF) of 75 µM SRF. The results represent the mean values of two incubations per analysis. The respective range of the two measured values is represented by error bars.

The incubation of 25 µM SKL without activation of microsomal UGTs resulted in 1.2 % pO-Glc, 1.8 % sO-Glc and 1.1 % N-Glc. In the presence of alamethicin a distinct increase in the concentrations of all glucuronides was observed. But their relation to each other remained unchanged. Thus, sO-Glc was formed mainly in this analysis with 4.7 %, followed by N-Glc at 3.0 % and pO-Glc with 2.4 %.

The simultaneous incubation of SKL and SRF without alamethicin clearly shows a changed ratio of relative amounts. Thus, only 0.8 % pO-Glc and 1.4 % sO-Glc were formed in the presence of SRF. The main product is now N-Glc with 3.8 %. The co-incubation of SKL and SRF with the addition of alamethicin resulted in the same tendencies. The formation of only 1.4 % pO-Glc and 2.9 % sO-Glc was observed. N-Glc was again the most conjugated product with 7.9 %. In addition, the formation of the nitrogen-linked SRF-glucuronide was determined. But its relative amount showed no significant change with values of 0.2 % in the absence and 0.3 % in the presence of alamethicin (data not shown).

This clearly demonstrates that the increased formation of N-Glc in the presence of SRF is not due to alamethicin. Indeed, an effect of alamethicin on the formation of glucuronides can be observed. However, this is not due to the interaction of alamethicin with SRF. Through pore-forming in the microsomal membrane, the latency period until the substrate reaches the enzyme is eliminated. Thus, alamethicin does not seem to interact with SKL, SRF or the UGTs, but merely performs its function. This

suggests that SRF influences the UGT-mediated conversion of SKL which seems to be based on the specific induction of the N-Glc formation.

Influence of Regorafenib on the Metabolic Stability of Skepinone-L

Regorafenib (RGF) has high structural similarities to SRF (Fig. 60). RGF belongs also to small molecule multi-kinase inhibitors and is approved for the second-line treatment of HCC [169].

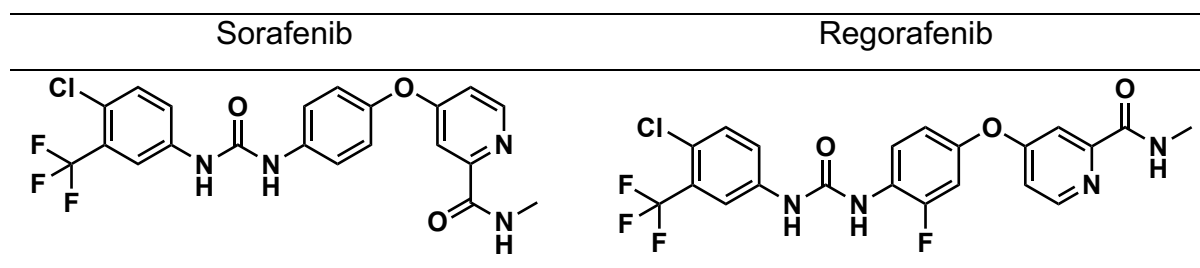


Fig. 60: Structures of multi-kinase inhibitors Sorafenib (SRF) and Regorafenib (RGF).

Due to the structural similarity and potency [170] a combined therapy of SKL and RGF for the treatment of HCC in human could also be considered. Therefore, DAA was used to investigate whether the enhancing effect on the formation of SKL N-Glc is induced only by SRF or also by RGF. For this purpose, 10 μ M SKL were incubated in HLM with different concentrations of RGF.

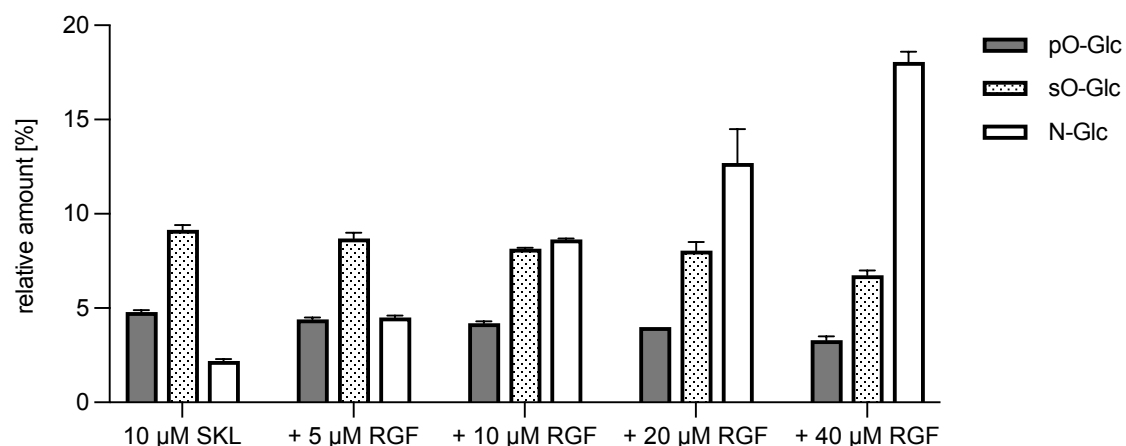


Fig. 61: Formation of pO-Glc, sO-Glc and N-Glc in HLM after 120 min in the presence of RGF. Thereby addressing co-activated CYPs and UGTs of human LM. The initial concentration of SKL was 10 μ M in each incubation. Initial RGF concentrations were 5, 10, 20 or 40 μ M respectively. The results represent the mean values of two incubations per analysis. The respective range of the two measured values are represented by error bars.

Figure 61 clearly illustrates that the presence of RGF also influences the metabolic conversion of SKL by conjugation with glucuronic acid. Thus, the formation of pO-Glc

decreases from 4.8 % without RGF to 3.3 % with 40 μM RGF. The sO-Glc shows a decrease of 2.4 % from 9.2 % to 6.8 %. In contrast, SKL N-Glc is formed more when RGF is added. This was already observed in incubations with SRF. Its percentage share increases in dependence of the concentration of RGF added. Without RGF only 2.2 % of N-Glc was formed. In contrast, the presence of 40 μM RGF resulted in 18.1 %. Thus, the inducing effect on the N-Glc formation could also be observed in the presence of RGF. This allows the conclusion that not a single substance but rather a class of compounds initiates the underlying processes.

Influence of Sorafenib on Glucuronide Formation of Trifluoperazine

The previous study shows that the observed influence on the SKL N-Glc formation does not seem to be only dependent on SRF. The same effect occurred in the presence of RGF which is structurally similar to SRF. Thus, the question should now be clarified whether the increased N-linked glucuronidation is directly related to SKL. It could also be possible that SRF affects the nitrogen-bound glucuronidation of each substrate of the responsible UGT isoform. In the following section (3.5.2) the reaction phenotyping of SKL glucuronidation is described. Among other things, this shows that a known substrate of the UGT isoform that catalyses the N-glucuronidation of SKL is trifluoperazine (TFP) [171].

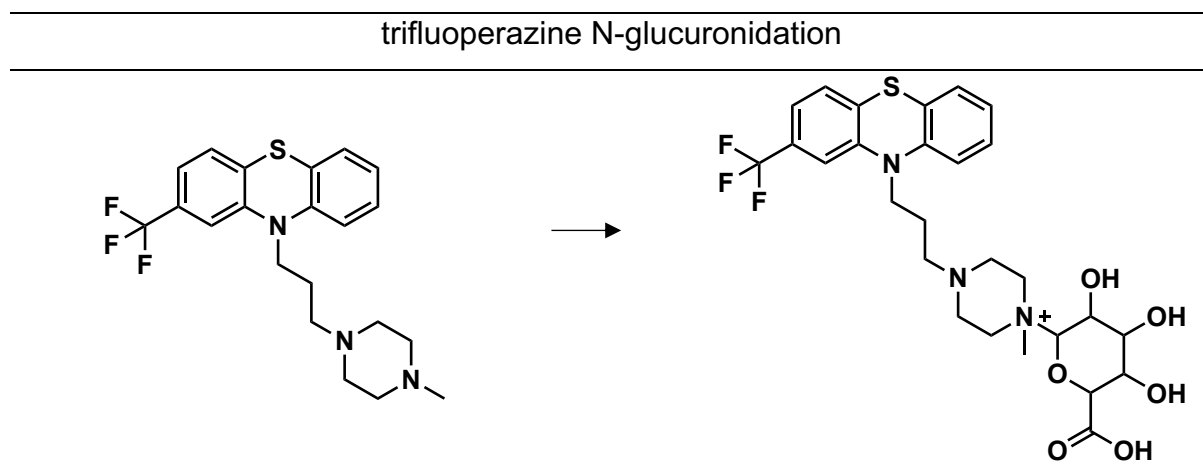


Fig. 62: Structures of (left) trifluoperazine and (right) trifluoperazine-N-glucuronide.

DAA was used to investigate the potential effect of SRF on TFP-N-glucuronide formation in HLM. This was conducted analogously to the procedure described previously. The chromatographic and MS/MS conditions are given in table 102 (Ch. 5.2.8.5). The added concentrations of SRF were 10 and 40 μM .

	TFP	+ SRF	
	10 μ M	10 μ M	40 μ M
unchanged TFP [%]	44.0	39.3	42.4
TFP-N-Glc [%]	7.6	6.6	5.8

Tab. 56: Metabolic stability of TFP and percentages of formed TFP- N-Glc after 120 min incubation in the presence of SRF. Thereby addressing co-activated CYPs and UGTs of human LM. The initial concentration of TFP was 10 μ M in each incubation. Initial SRF concentrations were 10 or 40 μ M respectively. The results represent the mean values of two incubations per analysis.

Table 56 surprisingly shows a decrease in TFP-N-Glc formation. The initial 7.6 % were reduced to 5.8 % in the presence of 40 μ M SRF. However, the observed amount of unchanged TFP shows inhomogeneous values. It is possible that TFP is additionally metabolised by microsomal CYPs or other UGT isoforms which could influence both metabolic stability and N-Glc formation. Therefore, the influence of SRF on TFP-N-glucuronidation was investigated on the recombinant UGT isoenzyme (upcoming section 3.5.3.5).

3.5.2. Biotransformation of Sorafenib in the Presence of Skepinone-L in Liver Microsomes

The metabolic transformation of SRF has been extensively investigated and elucidated since it is already approved for the treatment of HCC in humans under the trade name Nexavar® [100, 172]. However, there is a lack of data on whether and to what extent the biotransformation of SKL and SRF is influenced by their simultaneous presence. An interaction of SRF on the metabolic conversion of SKL *in vitro* could be observed as described in the previous chapter. Since interactions are usually based on reciprocity, the investigation of a possible influence of SKL on the *in vitro* transformation of SRF should also be examined. For this purpose, the metabolic stability of SRF was first determined in the test system of the respective species. Subsequently, co-incubations with different amounts of SKL were performed. Any differences that may occur with regard to metabolic stability and the formation of metabolites can most likely be attributed to the presence of SKL.

The *in vitro* studies also included CYP- and UGT-mediated biotransformation as well as metabolic transformation with co-activation of both enzyme systems. LMs from humans, rats, mice, dogs and monkeys served as test systems.

3.5.2.1. Influence of Skepinone-L on the CYP-mediated Biotransformation of Sorafenib

The study of the CYP-mediated transformation of SRF was performed in analogy to the metabolic stability determination of SKL (3.5.1.1). The results obtained by duplicate determination are shown in figure 63.

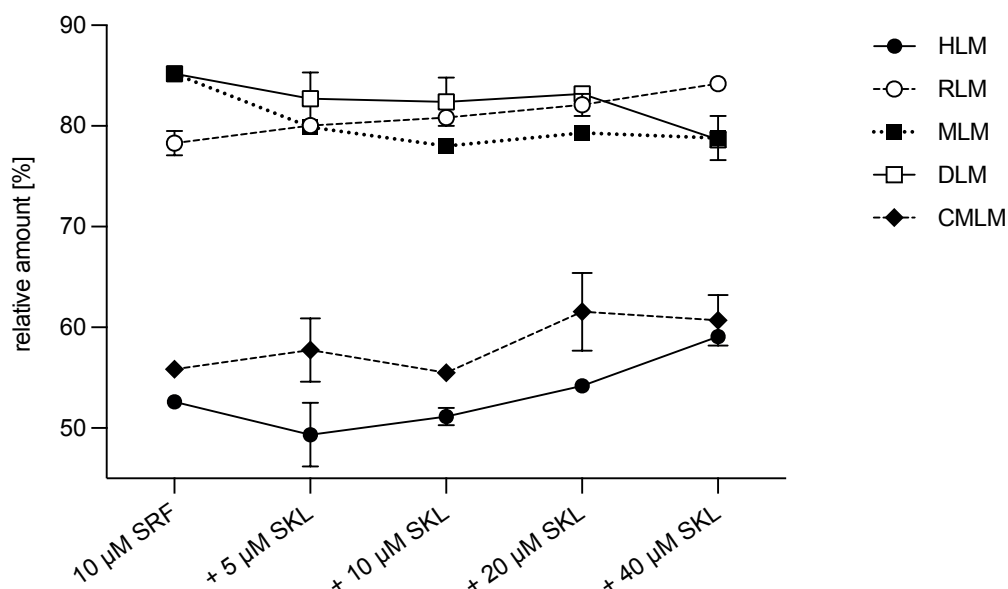


Fig. 63: Metabolic stability *in vitro* of SRF solely and in the presence of SKL after 120 min incubation by addressing microsomal CYPs of human, rat, mouse, dog and monkey LMs. The initial concentration of SRF was 10 µM in each incubation combined with either 5, 10, 20 or 40 µM SKL. Results represent the mean values of two incubations per species. The respective range of the two measured values are represented by error bars.

The results show that SKL seems to have an influence on the metabolic stability of SRF *in vitro* under CYP conditions. Thus, in each of the species tested here, there is a shift in the relative amount of unchanged SRF. In HLM, RLM and CMLM an overall increase in unchanged SRF can be observed in association with SKL. Up to 6.5 % more SRF in HLM and up to 5.9 % more SRF in RLM were detected. In the presence of 40 µM SKL in CMLM the increase in concentration of SRF is 4.9 %, despite some clear fluctuations. In contrast, the metabolic stability of SRF seems to decrease by addition of SKL in MLM and DLM. With a reduction of 4.9 % in MLM and 6.5 % in DLM this decrease is quite pronounced despite slight variations. As already mentioned, increased metabolic transformation through enzyme induction is actually not possible in the system used here. Therefore, the reasons for the reduced metabolic stabilities of SRF in the presence of SKL are still unclear.

The potential influence of SKL on the formation of primary SRF Ph1 metabolites NOX, HOM and DES was additionally examined (Tab. 57).

		SRF		+ SKL		
		10 μ M	5 μ M	10 μ M	20 μ M	40 μ M
NOX [%]	HLM	11.1	11.2	11.9	11.0	8.7
	RLM	0.4	0.4	0.4	0.4	0.6
	MLM	0.8	1.4	2.3	3.4	4.2
	DLM	0.1	0.1	0.1	0.2	0.2
	CMLM	7.7	9.1	7.2	9.9	8.4
HOM [%]	HLM	4.9	4.7	5.3	5.5	4.5
	RLM	1.7	1.5	1.4	1.3	1.3
	MLM	3.0	2.4	2.2	2.4	2.0
	DLM	2.7	2.7	3.7	3.9	4.0
	CMLM	3.3	4.2	3.4	5.6	6.7
DES [%]	HLM	0.6	0.6	0.7	0.7	0.6
	RLM	0.3	0.3	0.2	0.2	0.3
	MLM	0.6	0.5	0.5	0.6	0.5
	DLM	0.2	0.3	0.3	0.3	0.4
	CMLM	0.9	1.0	0.9	1.2	1.3

Tab. 57: Percentages of formed oxidative metabolites NOX, HOM and DES of SRF after 120 min incubation in the presence of SKL. Thereby addressing microsomal CYPs of human, rat, mouse, dog and monkey LMs. The initial concentration of SRF was 10 μ M in each incubation. Initial SKL concentrations were 5, 10, 20 or 40 μ M respectively. The results represent the mean values of two incubations per species.

The metabolic transformation of 10 μ M SRF mediated by CYP enzymes observed here, reflects roughly the findings reported in literature [172]. Thus, NOX, which is also pharmacologically active [93], was formed most in HLM and CMLM with 11.1 % and 7.7 %, respectively. In contrast, it occurred only slightly in RLM, MLM and DLM with a maximum of 0.8 %. In these species, the formation of HOM was predominant with 3.0 % in MLM, 2.7 % in DLM and 1.7 % in RLM. It represents the second most abundant metabolite in HLM with 4.9 %. The minor metabolite was DES, which was formed only in small amounts (0.2 to 0.9 %) in each species tested here. In the scientific discussion of Nexavar® (SRF), the *in vitro* metabolite profile of the rhesus monkey is considered to be most similar to that of humans [100]. In this study the closest correlation in *in vitro* metabolite formation to humans was observed in CMLM, too. The addition of SKL does not seem to have any significant effect on the metabolite formation of SRF in HLM. The relative amount of HOM shows both slight increases and decreases. In contrast, the amount of DES remained almost unchanged. After an initial increase, only NOX shows a decrease in the presence of 40 μ M SKL. However, this is less than the increase in metabolic stability. In RLM, the amounts of NOX and DES remained almost unchanged. The formation of HOM showed a very slight

decrease after the addition of SKL. This does not correlate directly with the increased amount of unchanged SRF in terms of relative amounts, either. The percentages of DES also remained unchanged in MLM. For HOM, a decrease by a total of 1.0 % to 2.0 % could be observed. The relative amounts of NOX obtained show a significant increase. Only 0.8 % was formed without SKL but in the presence of 40 μ M SKL this amount was 4.2 %. This increase also explains the decrease in the metabolic stability of SRF in MLM in the presence of SKL. Similar trends can be observed in DLM. However, the amount of NOX remained almost unchanged, whereas the amount of HOM formed increased from 2.7 % to 4.0 %. DES also showed an increase from 0.2 % to 0.4 %. Particularly unexpected results with regard to metabolite formation in the presence of SKL can be observed in CMLM. Despite fluctuations, an increase of about 5 % in unchanged SRF was observed. However, the three Ph1 metabolites also appeared to be formed more frequently, which contrasts with the increased metabolic stability of SRF. However, the relative amounts of NOX and DES formed showed some fluctuations. Moreover, the difference to the analysis without SKL is not very pronounced and is -0.5 % to 2.2 % for NOX and 0.1 % to 0.4 % for DES. In contrast there was a plus of HOM with 3.4 % in the presence of 40 μ M SKL. One of the reasons for the increased metabolic stabilities of SRF and the reduced formation of metabolites in the presence of SKL may be the affinity to the substrate. Another reason could be the inhibition of the corresponding CYP isoform. Furthermore, alterations in solubility and thus availability in the incubation mixture could influence the results.

SRF is known to undergo metabolic transformation by hydroxylation and N-oxidation selectively catalysed by human CYP3A4 [92]. Interestingly, the major metabolite NOX is known to inhibit this isoform [147]. CYP3A8 in CMLM shows the strongest similarity to human 3A4. Both murine and canine CYP3A isoforms show some parallels to humans. Although six CYP3A isoforms are expressed in rats, there are many discrepancies in the biotransformation of numerous xenobiotics between rats and humans [157]. This explains the differences in the resulting Ph1 metabolites of SRF in the species tested here. Another secondary biotransformation pathway, where NOX is enzymatically reduced to SRF was described by Gillani et al. [93]. The formation of SRF due to the reduction of previously formed NOX could influence the results of the microsomal incubations. Therefore, the CYP-mediated conversion of NOX in HLM was investigated. Within 180 min, neither the formation of SRF nor a significant

degradation of NOX could be observed in any of the three incubation mixtures (Data not shown). Consequently, an enzymatically induced reduction of NOX to SRF under the conditions used here in HLM can be excluded. Thus, the underlying processes regarding the increased metabolite formation of SRF in the presence of SKL remain unclear.

3.5.2.2. Influence of Skepinone-L on the UGT-mediated Biotransformation of Sorafenib

A potential influence of SKL on the UGT-mediated conjugation of SRF should be examined since N-glucuronidation of SRF accounts for 15 % of elimination in humans [173]. Therefore, Ph2 incubations of 10 μ M SRF solely and in combination with either 5, 10, 20 or 40 μ M SKL in HLM, MLM, DLM and CMLM were performed. Further experimental setup and the chromatographic conditions are described in chapter 5.2.8.3. UGT1A9 is known to be the responsible UGT isoform of SRF N-glucuronidation [174]. In rats no glucuronidation of SRF occurs because *Ugt1a9* is a pseudogene [46], thus no functional protein is expressed. For this reason, the possible interaction of SKL on the Ph2 metabolism of SRF was not studied in RLM.

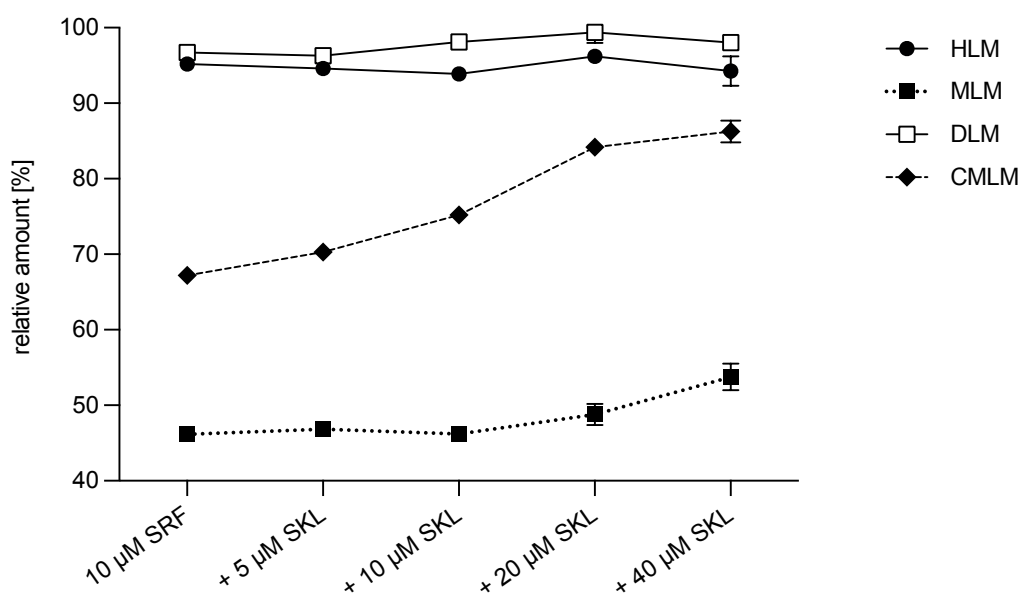


Fig. 64: Metabolic stability *in vitro* of SRF solely and in the presence of SKL after 120 min incubation by addressing activated microsomal UGTs of human, mouse, dog and monkey LMs. The initial concentration of SRF was 10 μ M in each incubation combined with either 5, 10, 20 or 40 μ M SKL. Results represent the mean values of two incubations per species and concentration. The respective range of the two measured values are represented by error bars.

Figure 64 illustrates that SRF has a high metabolic stability in HLM and DLM towards UGT-mediated transformation. In both species only very small changes in percentages of remaining SRF occurred in the presence of SKL. As observed for SKL, SRF was heavily degraded in MLM. Starting with the addition of 20 μM SKL, the amount of SRF increased by 7.6 % to 53.8 % at 40 μM . The metabolic degradation of SRF in CMLM by UGTs is not quite as pronounced but nevertheless clearly observable. However, the addition of SKL led to a significant increase in stability. Thus, after 120 min, only 67.2 % of the initial 10 μM SRF remained unchanged. In contrast, the addition of 40 μM SKL resulted in a stability of 86.2 %. Table 58 shows the relative amounts of SRF-glucuronide (SRF-Glc) formed in HLM, MLM, DLM, and CMLM.

		SRF	+ SKL			
		10 μM	5 μM	10 μM	20 μM	40 μM
SRF-Glc [%]	HLM	0.9	1.4	0.7	0.9	0.7
	MLM	17.5	16.5	15.5	15.2	13.3
	DLM	0.0	0.0	0.0	0.0	0.0
	CMLM	9.0	8.1	5.9	4.6	3.0

Tab. 58: Percentages of formed SRF-N-glucuronide after 120 min incubation in the presence of SKL. Thereby addressing activated microsomal UGTs of human, mouse, dog and monkey LMs. The initial concentration of SRF was 10 μM in each incubation. Initial SKL concentrations were 5, 10, 20 or 40 μM respectively. The results represent the mean values of two incubations per species.

In HLM the SRF-Glc was formed only at a very low level of 0.7 % to 1.4 %. There seems to be no interaction with SKL. However, the amounts obtained here *in vitro* are below the 15 % of the applied dose reported for *in vivo*. These data include glucuronidated NOX in addition to SRF-Glc [173]. This cannot be formed in the absence of CYP enzymes. Moreover, *in vivo-in vitro* correlations usually require the determination as well as consideration of numerous factors and are therefore not hardly predictable. A high SRF-Glc formation occurred in MLM agrees with the observed metabolic stability. This is not surprising since the mRNA expression level of *Ugt1a9* is very high in mouse liver [175]. As the concentration of co-incubated SKL increases, the amount of SRF-Glc appears to decrease. In the absence of SKL 17.5 % SRF-Glc was formed, which steadily impaired upon addition. Thus, only 13.3 % SRF-Glc was formed in the presence of 40 μM SKL. Despite *UGT1A9* is functionally present in dogs no formation of SRF-Glc was observed in DLM. This result is consistent with descriptions from the literature. Thus, the specific substrate propofol is not glucuronidated in canine liver despite the expression of the responsible UGT isoform [46]. However, no comprehensive study of canine UGT expression levels has

been performed to date. CMLM also showed significant glucuronidation of SRF at 9.0 %. This was significantly reduced after the addition of SKL. Incubation of SRF in the presence of 40 μ M SKL resulted in a formation of only 3.0 % SRF-Glc. These results imply that SKL inhibits the specific UGT isoform responsible for SRF glucuronidation *in vitro* in MLM and CMLM. In HLM, no influence of SKL on SRF-Glc formation could be observed. The sum of the relative amounts of remaining SRF and formed SRF-Glc show high differences to the assumed value of 100 %, especially in MLM. Possibly, the formation of additional, non-detected glucuronides occurred in MLM and CMLM. Most likely, the difference is due to the specific ion yields generated by the ESI-source of SRF and its N-glucuronide. The latter was not available as a pure substance. Therefore, this assumption could unfortunately not be verified. Overall, the UGT-mediated transformation of SRF in the presence of SKL seems reasonable.

3.5.2.3. Influence of Skepinone-L on the CYP and UGT Co-Activated Biotransformation of Sorafenib

The metabolic conversion of SRF also showed clear differences between the CYP and UGT-mediated incubation assays in all species tested. However, both processes are not separated *in vivo*. In addition, there is the possibility that oxidative products are subsequently conjugated with glucuronic acid. This is already known for the Ph1 major metabolite NOX [173]. Therefore, the metabolic transformation of SRF in the presence of SKL in HLM, RLM, MLM, DLM and CMLM under DAA reaction conditions was examined.

The obtained relative stabilities of SRF after 120 min DAA are shown in figure 68. The percentage of unchanged SRF in co-activated conditions increases in the presence of SKL in all species, or remains almost unchanged, despite some fluctuations. A particularly strong increase by addition of SKL was observed in HLM. Although this effect was already evident in the Ph1 incubation system, the overall change was only 6.5 %. However, in DAA conditions an increase of almost 18 % was observed. The stability of SRF in MLM and DLM even showed a decrease of 4.9 % and 6.5 % following Ph1 incubations in the presence of SKL. In contrast, the stabilities obtained after performing DAA did not change significantly by addition of SKL in both species.

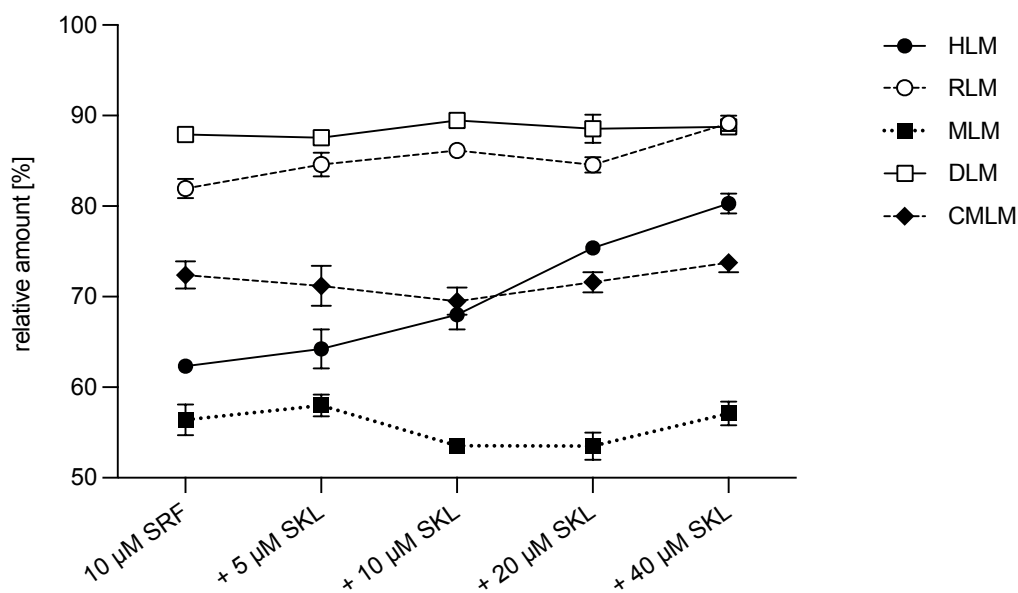


Fig. 65: Metabolic stability *in vitro* of SRF solely and in the presence of SKL after 120 min incubation by co-activation of microsomal CYPs and UGTs of human, rat, mouse, dog and monkey LMs. The initial concentration of SRF was 10 µM in each incubation combined with either 5, 10, 20 or 40 µM SKL. Results represent the mean values of two incubations per species. The respective range of the two measured values are represented by error bars.

		SRF		+ SKL		
		10 µM	5 µM	10 µM	20 µM	40 µM
NOX [%]	HLM	10.8	11.2	11.4	10.6	7.8
	RLM	0.2	0.2	0.3	0.2	0.2
	MLM	0.4	0.9	1.3	2.4	3.9
	DLM	0.0	0.0	0.0	0.0	0.0
	CMLM	6.3	6.5	6.1	6.3	5.1
HOM [%]	HLM	4.9	5.2	5.3	5.2	4.3
	RLM	2.9	2.6	2.3	2.3	1.9
	MLM	4.1	4.0	3.7	3.1	2.8
	DLM	2.1	2.1	2.6	2.6	2.8
	CMLM	4.0	4.1	3.8	4.8	4.7
DES [%]	HLM	0.2	0.2	0.2	0.2	0.2
	RLM	0.1	0.2	0.1	0.1	0.2
	MLM	0.3	0.4	0.4	0.4	0.4
	DLM	0.0	0.0	0.0	0.0	0.0
	CMLM	0.4	0.4	0.3	0.3	0.3
SRF-Glc [%]	HLM	0.1	0.2	0.1	0.1	0.1
	RLM	0.0	0.0	0.0	0.0	0.0
	MLM	5.8	5.6	5.2	4.5	4.1
	DLM	0.0	0.0	0.0	0.0	0.0
	CMLM	1.1	1.0	0.7	0.7	0.5

Tab. 59: Percentages of formed NOX, HOM, DES and SRF-Glc after 120 min incubation of SRF in the presence of SKL. Thereby addressing co-activated microsomal CYPs and UGTs of human, rat, mouse, dog and monkey LMs. The initial concentration of SRF was 10 µM in each incubation. Initial SKL concentrations were 5, 10, 20 or 40 µM respectively. The results represent the mean values of two incubations per species.

The relative amounts of SRF metabolites formed under DAA conditions are given in table 59. They show some differences compared to the individual Ph1 and Ph2

studies, too. NOX was formed less in all species, but the tendencies remained unchanged with the addition of SKL. Thus, the relative amount decreased significantly by 3.0 % in HLM and slightly by 1.2 % in CMLM in the presence of 40 μ M SKL. In RLM the minor amount of NOX produced remained unchanged with the addition of SKL. No NOX was formed during SRF incubation in DLM under DAA conditions. In contrast, the presence of SKL with SRF in MLM appeared to enhance the level of NOX generated. Thus, the relative quantity increased significantly from 0.4 % (without SKL) to 3.9 % (40 μ M SKL). In HLM the percentage of HOM formed after DAA is the same as after single oxidative metabolism reaction studies. Although quite marginal, both increases and decreases were seen in the presence of SKL. In RLM and MLM a plus of 1 % HOM was formed than under CYP conditions but decreased to the same extent in the presence of SKL. Significant increases in HOM concentrations by addition of SKL in the Ph1 assay were observed in DLM and CMLM (Tab. 57, section 3.5.2.1). These effects were less significant in DAA. However, the tendency is visible in DLM, whereas the content of HOM fluctuated in CMLM. DES is formed even less under DAA conditions in all species than in the Ph1 incubation reaction system. In DLM, no formation is observed. The addition of SKL did not lead to a significant change in concentration in any species.

The formation of SRF-Glc in DAA is significantly lower than in the absence of the NADPH-regeneration system. Only 5.8 % of 10 μ M SRF in MLM were glucuronidated instead of 17.5 %. In CMLM conjugation decreased from 9.0 % to 1.1 %. Despite this significantly lower formation, the previously observed influence of SKL also occurred in DAA. Thus, in both species, the relative amount of SRF-Glc decreased in the presence of SKL. This effect was not as pronounced as in the UGT reaction incubation system due to the lower initial concentration formed. It was not possible to detect the glucuronidation of NOX in any of the tested species. The coupled oxidative-conjugative reaction analysis of the metabolic transformation of SRF in the presence of SKL shows that there are not only advantages. Differences in SRF transformation observed during DAA were less pronounced than in the individual CYP- and UGT-mediated analyses. Thus, the separate incubation reaction systems seemed to be more appropriate for examining the interaction of SKL on the biotransformation of SRF. It is possible to identify minor differences as well as trends in metabolite formation more clearly. Regardless of the assay used, a change in the metabolic

stability and metabolite formation of SRF was observed in all species tested linking to the presence of SKL. The conversion of SRF to NOX appeared to be reduced by SKL in HLM and CMLM. In contrast, an increase was observed in MLM. On the one hand the presence of SKL led to a lower formation of HOM in HLM, RLM and MLM and on the other hand to an increased formation in DLM and CMLM. Only the relative content of DES formed in all species did not seem to be influenced by SKL. The transformation of all CYP-mediated reaction products of SRF is only catalysed by the human CYP3A4 isoform [94]. Apart from the unlikely induction in the given test system, selective inhibition of individual metabolites is also not possible. This would result in a reduced formation of all SRF Ph1 metabolites. It is possible that more than one CYP isoform is involved in the conversion of SRF into its different metabolites in the preclinical species. However, no increase in concentration resulting from the induction of the corresponding enzyme is possible, meaning that this observation remains unexplained. Regarding the glucuronidation of SRF, the addition of SKL seems to reduce the formation of SRF-Glc in a concentration-dependent manner. This suggests an inhibition of UGT1A9. However, this is mainly observed in MLM and CMLM. Mouse *Ugt1a9* and monkey UGT1A9 are functional, but they are also subject to inter-species differences in terms of substrate specificity and catalytic activity [176],[177]. Therefore, further studies must clarify whether and to what extent human UGT1A9 is inhibited by SKL. There are obvious differences in the formation of SRF metabolites between the individual Ph1 and Ph2 studies and the coupled oxidative-conjugative reaction analyses. However, it can be assumed that the DAA setup corresponds closely to the actual situation *in vivo*. For this, it remains to be noted that SKL significantly increases the metabolic stability of SRF in HLM. This could be advantageous with regard to the intended combination therapy.

3.5.2.4. Structure Elucidation of Skepinone-L Glucuronides

In the previous chapters, it was already mentioned that the *in vitro* glucuronidation of SKL results in the generation of three products. The formation of pO-Glc and sO-Glc was observed in all species tested here, while N-Glc appears to be formed only in human LM. The identification and structural elucidation of these SKL glucuronides is described below.

During preliminary experiments of SKL in HLM in the presence of UDPGA as well as activated UGTs, the formation of initially two conjugation products was observed. The mass spectrum of the reaction products obtained using full scan mode is shown in figure 66. This illustrates that the compounds formed have an m/z ratio of 601.9 to 603.0. SKL has a molecular weight of 425.43 g/mol and conjugation with glucuronic acid would result in the theoretical m/z ratios of 601.2, 602.2 and 603.2. Therefore, the obtained m/z ratios allow the conclusion that these are glucuronides of SKL.

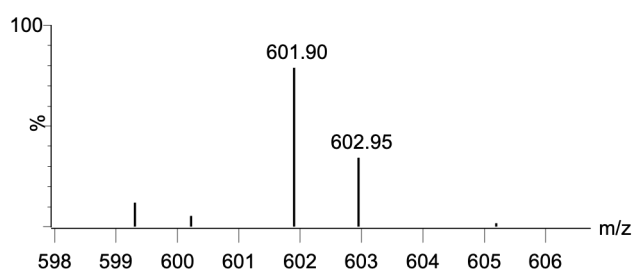


Fig. 66: Mass spectrum of postulated SKL-glucuronides with m/z values of 601.90 and 602.95 acquired in full scan mode.

Figure 67 shows the superimposed chromatograms resulted from different UGT reaction mixtures. The analysis a_1 of SKL shows two clear product peaks after 60 min in the Ph2 incubation system. These increase in intensity after 120 min incubation, as the chromatogram of a_2 shows. In contrast, no peaks could be detected at the same retention time after 120 min incubation in b, without UDPGA or c, the absence of SKL. These results of the different reaction mixtures as well as the obtained mass spectrum of the reaction products clearly show that the metabolites formed are most likely glucuronides of SKL.

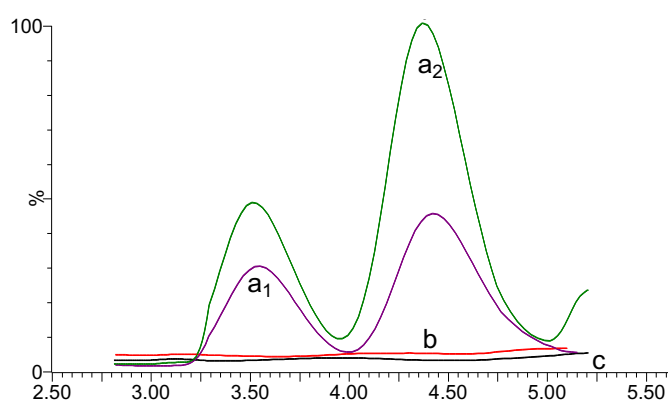


Fig. 67: Chromatograms of intensity over time resulted from preliminary incubations of SKL after 60 min (a_1 , purple) and 120 min (a_2 , green) in the presence of human microsomal UGTs. In addition, the results after 120 min Ph2 incubation in the absence of UDPGA (b, red) and without SKL (c, black) are shown.

Subsequently, the analytical method was optimised to achieve a baseline separation of the two glucuronides formed. For this purpose, SKL was incubated at a high concentration of 75 μM in the Ph2 reaction system in well available and relatively low-cost RLM. Figure 68 illustrates the SKL glucuronides formed after 120 min. Multiple reaction monitoring analysis ensured that both occurring peaks were glucuronides of SKL. Unlike in the previous experiments, these are clearly separated from each other with retention times of 9.9 and 11.3 min.

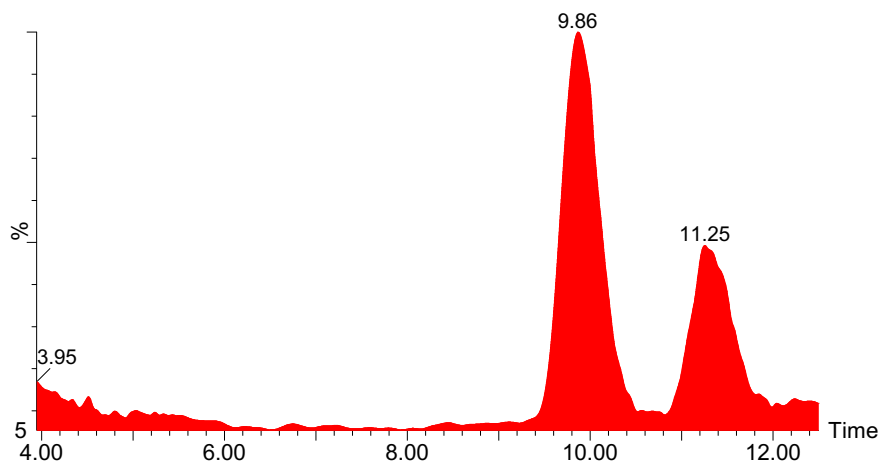


Fig. 68: LC-MS/MS chromatogram of SKL-glucuronides eluting at 9.9 and 11.3 min. Metabolite formation was analysed after 120 min Ph2 incubation of 75 μM SKL in rat LM.

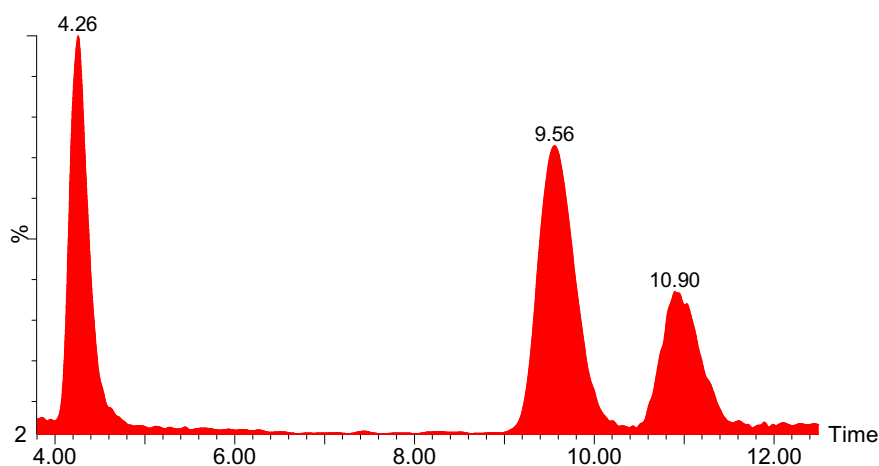


Fig. 69: LC-MS/MS chromatogram of SKL-glucuronides eluting at 4.3, 9.9 and 11.3 min. Metabolite formation was analysed after 120 min Ph2 incubation of 75 μM SKL in human LM.

The same conditions were used for the incubation of 75 μM SKL in HLM. Surprisingly, the chromatogram obtained (Fig. 69) shows a third peak at a retention time of 4.3 min. Based on its m/z ratio and further control incubations, it can be assumed that the third peak is also a glucuronide of SKL. In the chromatogram obtained from the preliminary experiment, there was therefore obviously an insufficient separation of the three

metabolites. This initially led to the erroneous assumption that only two, instead of three SKL glucuronides are formed *in vitro*. However, one of these three glucuronides do not seem to be formed in RLM.

SKL possesses three possible binding sites for the conjugation of glucuronic acid (Fig. 70a). Thus, oxygen-bound glucuronides could be formed at the glycerol residue of SKL in both primary (1) and secondary (2) positions. The third possibility would be the formation of a tertiary nitrogen-bound (3) SKL glucuronide. The chromatogram (Fig. 70b) obtained after Ph2 incubations of SKL in HLM, show that the three glucuronides (i), (ii) and (iii) were formed. These share the same m/z ratio but differ in their retention behaviour. Chromatographic separation indicates that (i) exhibits marked differences in polarity compared to (ii) and (iii). The latter two have similar retention times and are thus probably structurally very similar to each other.

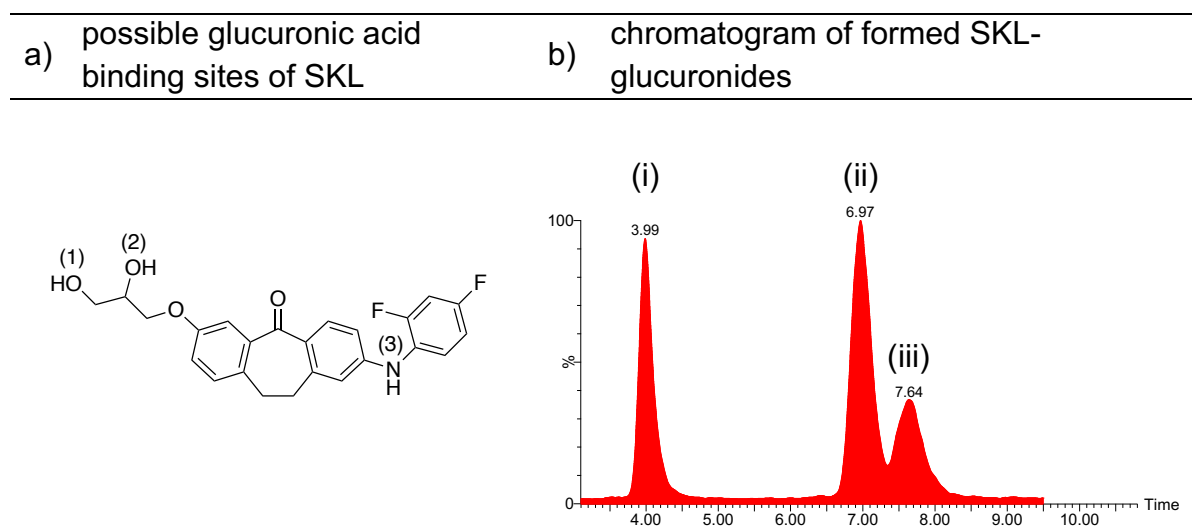


Fig. 70: Possible binding sites of SKL (a) for conjugation with glucuronic acid to form (1) primary- or (2) secondary oxygen-linked as well as tertiary nitrogen-bound (3) glucuronides. LC-MS/MS chromatogram (b) of formed glucuronides (i), (ii) and (iii) obtained after 120 min Ph2 incubation of 75 μ M SKL in HLM.

The respective binding site of the glucuronic acid can provide information about the UGT isoforms involved. This in turn is important for the investigation of drug-drug interactions or adverse side effects due to genetic polymorphism. Therefore, the structure elucidation of the in total three different SKL glucuronides was essential.

For this purpose, structural analogues of SKL were incubated in the presence of activated human liver microsomal UGTs. In order to obtain sufficient glucuronides, the

initial substrate concentration was 100 μM and the incubation time 6 h. Further experimental setup and the applied chromatographic conditions are given in table , chapter 5.2.7.4. Figure 71 shows the structures of the SKL derivatives examined and the resulted LC-MS/MS chromatogram of their glucuronides respectively.

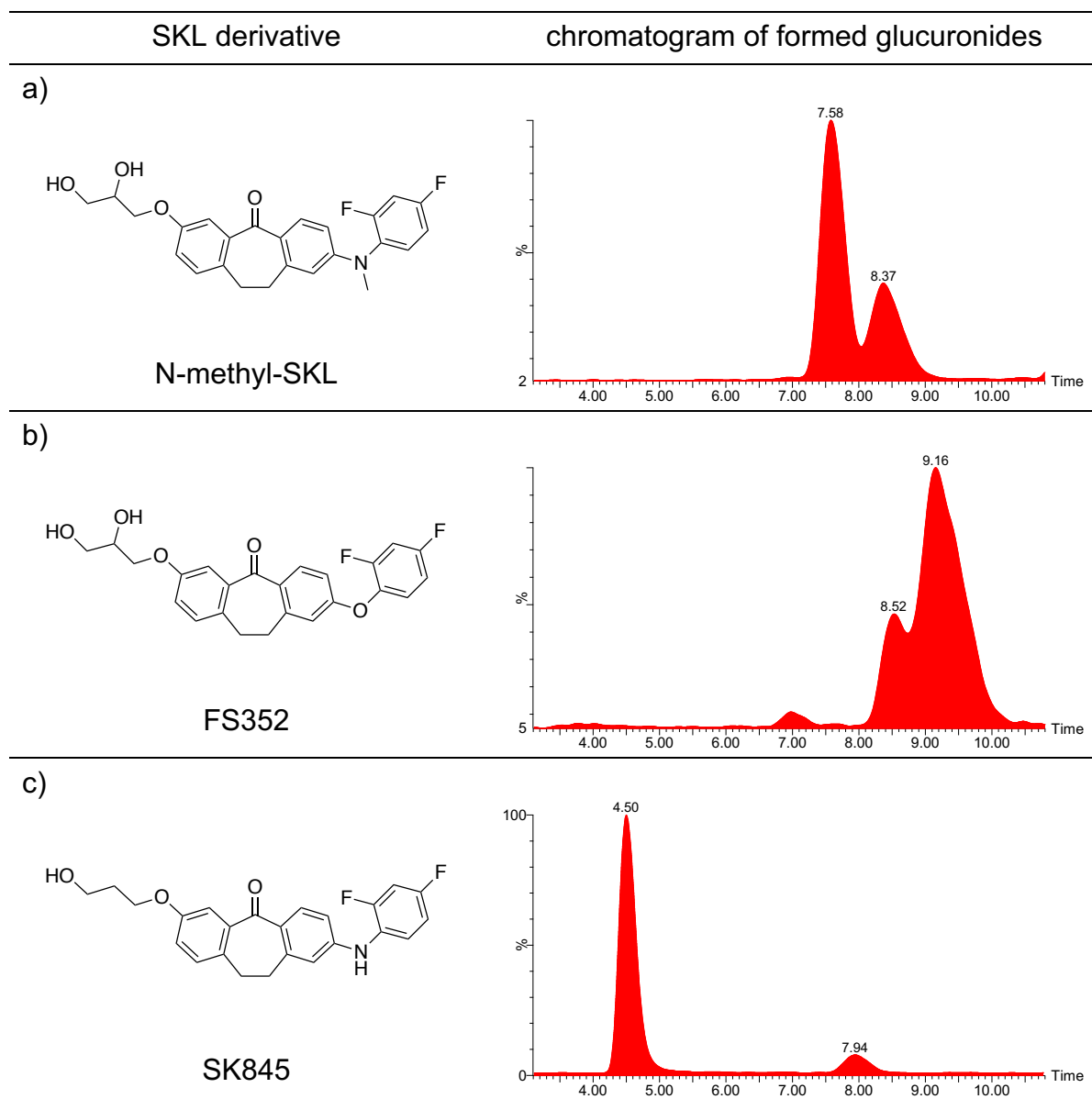


Fig. 71: Structures of SKL derivatives and their corresponding LC-MS/MS chromatogram of formed glucuronides after 6 h Ph2 incubations of 100 μM substrate in HLM. Blocking of the nitrogen binding site by a methyl group (a) as well as the exchange by oxygen (b) led to the formation of two glucuronides each. c) The absence of the secondary oxygen of the glycerol residue of SKL also results in the formation of two glucuronides.

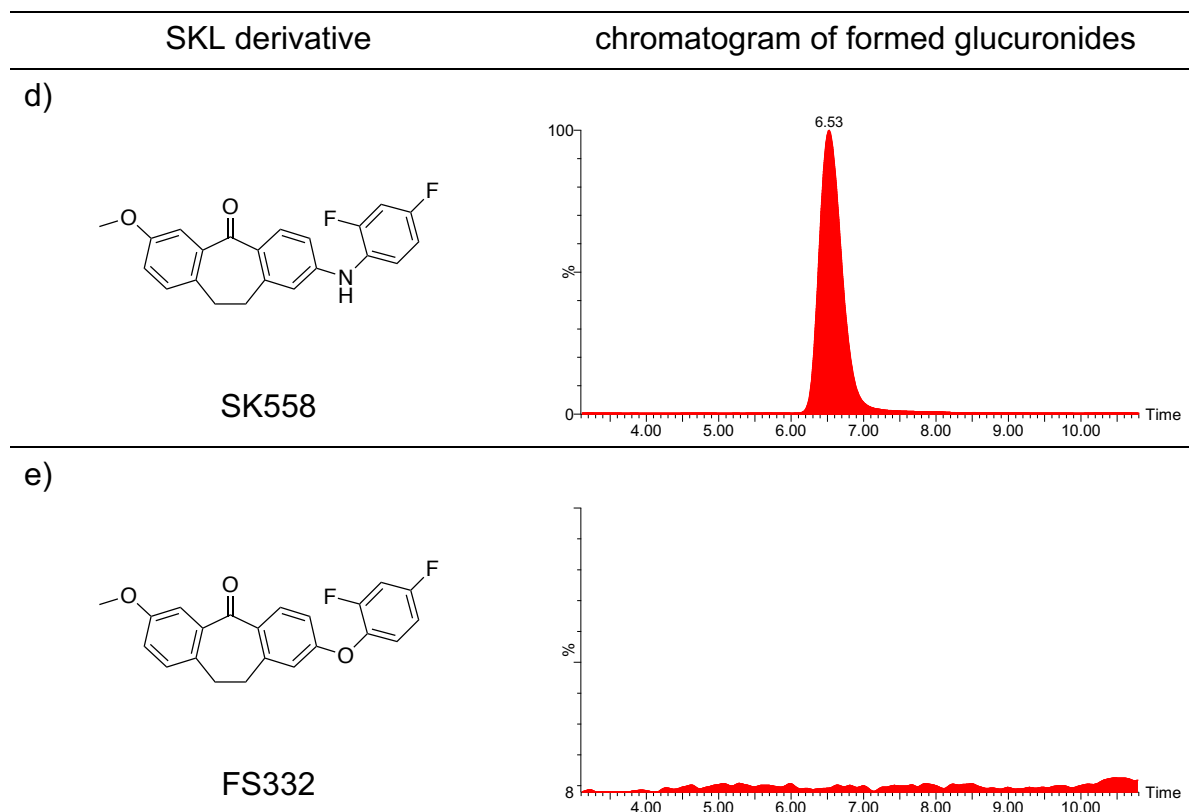


Fig. 72 (Continuation of fig.71): Structures of SKL derivatives and their corresponding LC-MS/MS chromatogram of formed glucuronides after 6 h Ph2 incubations of 100 μ M substrate in HLM. Only one glucuronide is formed (d) when the glycerol residue is replaced by a methyl group. e) The replacement of nitrogen by oxygen and of the glycerol residue by a methyl group suppresses any glucuronide formation.

The derivative glucuronides differ structurally and thus also in their physicochemical properties from the SKL glucuronides. It was therefore to be expected that they have different retention behaviour. Nevertheless, due to the number of glucuronides formed, as well as the difference in their retention times, both similarities and differences to SKL could be assessed.

Compared to SKL, N-methyl-SKL (Fig. 71a) and FS352 (Fig. 71b) have only two hypothetical binding sites. This is due to the methylation of the nitrogen or its replacement by oxygen. This leaves only the primary and secondary hydroxy group of the glycerol residue as conjugation sites. The resulting chromatograms confirm these assumptions. After incubation of both SKL derivatives, the formation of two glucuronides can be observed. These show similar retention behaviour to each other, comparable to the SKL glucuronides (ii) and (iii) from figure 73b. The SKL derivative SK845 (Fig. 71c) has a hydroxypropoxy residue instead of a glycerol residue, and thus two possible binding sites. Whereby one would result in an oxygen bound glucuronide

and the other in a nitrogen-linked one. The related chromatogram shows the formation of two conjugation products. Compared to the results of the previous structural analogues, these glucuronides appear to show very different retention behaviour and thus have different polarities. The first eluting peak is comparable to the SKL glucuronide (i) (Fig. 70b). In contrast, the metabolite with higher retention time is most likely (ii) or (iii) shown in figure 70b. Of the three possible binding sites in SKL, its derivative SK558 (Fig. 72d) only possesses the nitrogen since the glycerol residue has been replaced by a methyl group. As expected, this results in the formation of only one glucuronide. If, on the other hand, none of the three possibilities of conjugation with glucuronic acid postulated for SKL are present, as in the case of FS332 (Fig. 72e), glucuronide formation is completely suppressed.

The incubations of the SKL structural analogues led to the result that the binding sites postulated for SKL are actually conjugated with glucuronic acid *in vitro*. Thus, a total of three SKL glucuronides were apparently formed *in vitro* by UGT-mediated conjugation. In two of them, the glucuronic acid is bound via oxygen. The third conjugate product is most likely the glucuronide bound to the nitrogen. The analytical separation of the conjugation products (ii) and (iii) (Fig. 70b) was challenging in the preliminary stage. This suggests strongly similar physicochemical properties to each other, which could be based on close structural similarities. This indicates separate glucuronidation at the primary and secondary hydroxyl group of the glycerol moiety. Therefore, the first eluting peak (i) with a retention time of 4.0 min is most likely the tertiary nitrogen bound SKL glucuronide. However, Ph2 incubations of SKL demonstrated that the N-linked glucuronide is not generated in LMs of rat, mouse, dog and monkey. Thus, it seems to occur in human LM only.

The formation of the three SKL glucuronides in HLM could be confirmed in the research group "Clinical Pharmacogenomics and Cancer" of the IKP Stuttgart (Germany) under the direction of Prof. M. Schwab. In figure 73 a representative LC-MS/MS chromatogram generated there after UGT-mediated conversion of SKL in HLM is given. In addition, two of the three SKL glucuronides could be chemically synthesised by this research group. Thus, it was possible to confirm the hypothesised structures of at least the two O-linked glucuronides. The exact binding site of the

glucuronic acid and the elution order could also be identified using the pure substances.

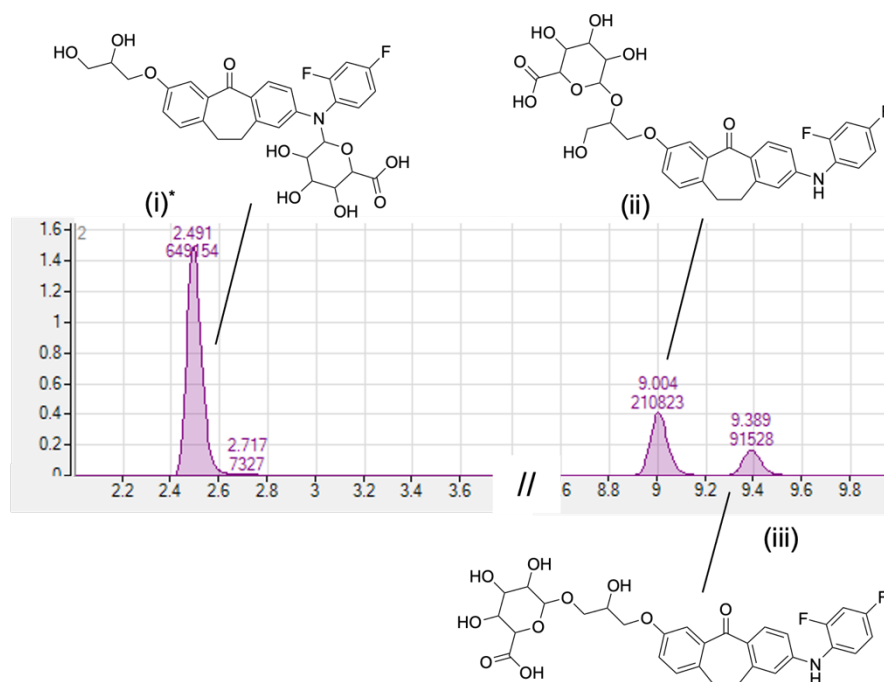


Fig. 73: LC-MS/MS chromatogram and the related structures of SKL-glucuronides. First the N-Glc (i) elutes after 2.9 min followed by the sO-Glc (ii) after 9.0 min and the pO-Glc (iii) after 9.4 min. Metabolite formation was analysed after Ph2 incubation of 100 μ M SKL in human LM. LC-MS/MS chromatogram with the kind permission of the Clinical Pharmacogenomics and Cancer research group (IKP Stuttgart). *structure of the N-Glc and peak assignment not verified

Thus, the substance was identified from peak (ii) (Fig. 70b, 73) as the secondary SKL glucuronide (sO-Glc) and metabolite (iii) is the primary bound glucuronide of SKL (pO-Glc). Consequently, the first eluting substance (i) must be the postulated nitrogen-linked glucuronide (N-Glc), as previously assumed. Unfortunately, this could not be verified by means of pure substance, since a chemical synthesis of N-Glc has not been possible so far. The enzymatic *in vitro* synthesis using liver microsomes was not economically justifiable due to the low yield in contrast to the incubation components to be used in large quantities.

3.5.2.5. Intensity of Oxygen-linked Skepinone-L Glucuronides

The relative amounts of glucuronides formed during the LM incubations of SKL exceeded the theoretically possible 100 % in some cases. This suggested that under the chromatographic conditions applied, the conjugates possess significantly higher ion yields than SKL itself. It was possible to verify this for pO-Glc and sO-Glc on the

basis of the available reference substances. For this purpose, blank plasma was spiked with exactly equal amounts of both O-linked glucuronides and SKL itself and processed as described earlier. The final concentration of all analytes was 10 μM each. The chromatogram obtained by LC-MS/MS analysis is shown in figure 74.

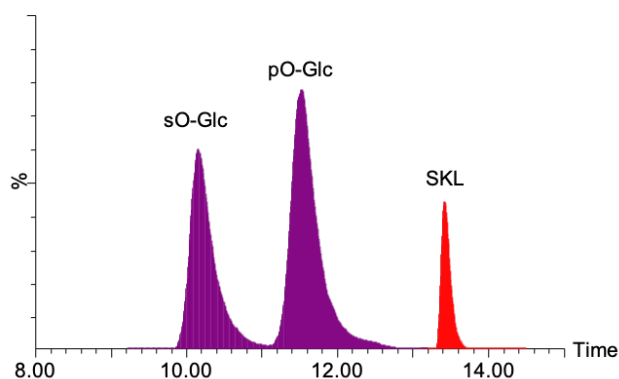


Fig. 74: LC-MS/MS chromatogram of sO-Glc, pO-Glc and SKL at 10 μM each in order to compare their specific ion yields.

This demonstrates clearly that the peak areas of the glucuronides significantly exceed those of SKL despite equal concentrations. Thus, the sO-Glc eluting at 10.25 min shows a peak area 3.3-times larger than SKL. The area of pO-Glc even exceeds that of SKL by 4.6-times. Thus, the assumption of strongly different ion yields of SKL and its O-glucuronides is confirmed. Unfortunately, this could not be verified for the N-Glc as this was not available as a pure substance.

3.5.2.6. Inhibitory Activity of Oxygen-Linked Skepinone-L Glucuronides against p38 α Mitogen-Activated Protein Kinase

In general, glucuronidation leads to the metabolic deactivation of endogenous and exogenous compounds [42]. In contrast to Ph1 reaction products, glucuronides are therefore commonly considered to be pharmaceutically inactive. However, some glucuronides are known to exhibit pharmaceutical activity comparable to that of their parent compound [178]. The previous results suggest that SKL undergoes metabolic conversion mainly by glucuronic acid conjugation reactions. The resulting glucuronides seem to represent the major *in vitro* metabolites, in almost all species tested here. Moreover, in human liver microsomal incubations, pO-Glc, sO-Glc and N-Glc appear to be the only metabolites of SKL that were formed in significant amounts. Since SKL is a selective and highly potent inhibitor of p38 α MAP

kinase [111], it should be examined whether its glucuronides also possess inhibitory properties. However, this could only be performed for pO-Glc and sO-Glc, as N-Glc was not available as pure substance. The inhibitory activity of pO-Glc and sO-Glc was tested by performing an enzyme-linked immunosorbent assay (ELISA). Here, the remaining activity of p38 α MAP kinase in the presence of the potential inhibitors is determined photometrically. The concentrations of glucuronides used to study the kinase reaction were 0.001, 0.01, 0.1 and 1.0 μ M, respectively. The well-known p38 α MAP kinase inhibitor SB203580 served as reference and assay control. The further experimental set-up and procedure were performed in accordance with the description by Goettert *et al.* [179]. The concentration-response diagram (Fig. 75) shows the inhibitory effect of pO-Glc and sO-Glc compared to the reference SB203580. Both glucuronides appear to inhibit p38 α MAP kinase potently to a similar extent. Thus, the calculated IC₅₀ for pO-Glc is 3.7 nM and for sO-Glc 4.1 nM. These excellent inhibitory activities are similar to unchanged SKL which possesses an IC₅₀ of 5 ± 2 nM [143]. The stability of pO-Glc and sO-Glc in the ELISA kinase buffer for 14 h at 37°C was examined and confirmed as described in chapter 5.2.9 (p38 α -Mitogen-Activated Protein Kinase Assay). Thus, it can be excluded that SKL was present in the assay as a result of hydrolytic cleavage. Hence, there was no influence of the parent compound on the IC₅₀ values of pO-Glc and sO-Glc.

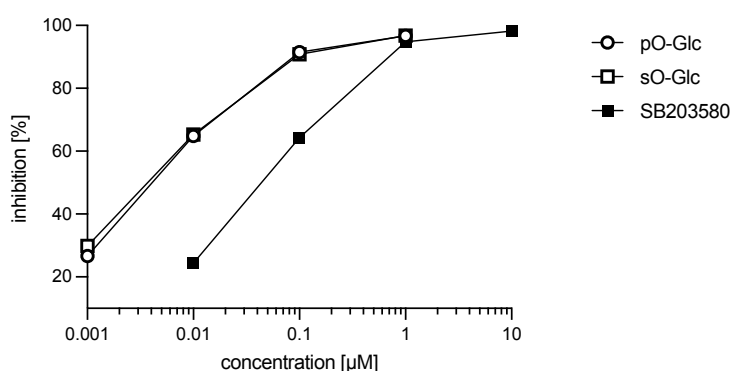


Fig. 75: Inhibitory activities of pO-Glc and sO-Glc towards p38 α MAP kinase determined by an enzyme-linked immunosorbent assay in accordance with Goettert *et al.* [179].

Due to the structural and physicochemical similarity of both glucuronides, a comparable inhibitory activity was expected. Nevertheless, both IC₅₀ obtained are unexpected, since, as already mentioned, glucuronidation results predominantly in inactivation and enhanced excretion of the parent drug. To explain this supposed contradiction, the binding of SKL to the ATP-pocket of p38 α MAP kinase must be

examined more closely. It is known that SKL induces a glycine-flip at the hinge region and interacts with the hydrophobic regions I (HR I) and II (HR II) [111]. As shown schematically in figure 76, the pinone core of SKL forms two hydrogen bonds with methionine (Met109) and glycine (Gly110) [155]. Another hydrogen bond is formed by the terminal OH-group of the 2,3-dihydroxypropoxy moiety of SKL with the backbone carbonyl of Gly110. In addition, the secondary amine of SKL forms a water-mediated hydrogen bond with phenylalanine (Phe169), among others [111].

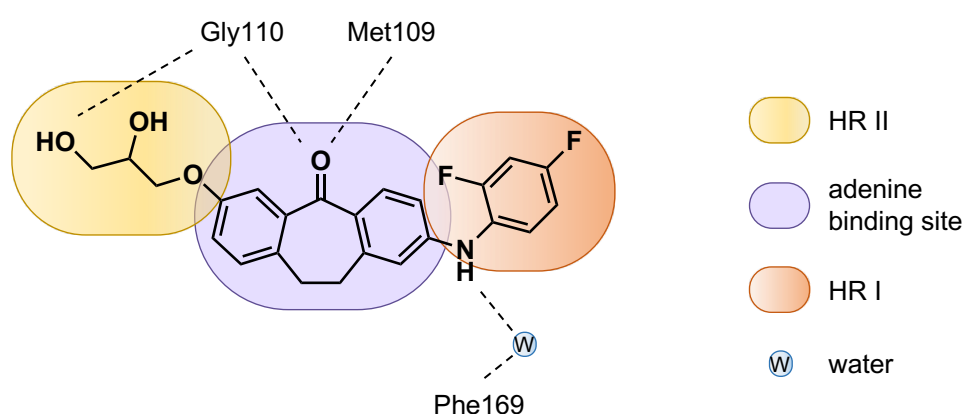


Fig. 76: Graphical representation of the binding mode of SKL in the ATP-binding pocket of p38 α MAP kinase. SKL forms polar interactions with the hinge region and addresses the hydrophobic regions I (HR I) and II (HR II). Two hydrogen bonds are formed with the carbonyl group of the SKL-pinone core and the amide nitrogens of Met109 and Gly110. An additional hydrogen bond engages the backbone carbonyl of Gly110 and the terminal OH of the 2,3-dihydroxypropoxy moiety of SKL. The secondary amine of SKL is linked via a water-bridged hydrogen bond to the backbone amide of Phe169. Graphic adapted from [155] and [111].

Since the glucuronyl-residue of pO- and sO-Glc is solvent exposed, it has no or only a minor influence on the binding of the SKL scaffold in the active kinase. Thus, the two O-bound glucuronides of SKL can also induce the glycine-flip and interact with HR I and HR II. This explains why their inhibitory activities are similar to unchanged SKL. In contrast the structural motif of the postulated N-Glc, which addresses the HR I is strongly changed compared to SKL. Thus, the metabolite has both a different molecular surface and increased hydrophilic properties at this structural element. Therefore, a linear binding of N-Glc into the binding pocket of the active p38 α MAP kinase and an induction of the glycine-flip is highly unlikely. Hence, it can be assumed that the N-Glc has no inhibitory activity towards the p38 α MAP kinase.

The formation of pharmaceutically active metabolites can have both advantages and disadvantages. On the one hand, the reaction products can serve as templates for the

development of new drug candidates or even as drug candidates themselves. In addition, the presence of active metabolites can increase the therapeutic efficacy of the active pharmaceutical ingredient. However, this can also result in increased adverse effects or even toxicity [180]. For a better assessment of the disadvantages, knowledge of the UGT isoforms involved in the glucuronidation of SKL is essential. This is because these could be subject to genetic polymorphisms [181] and thus lead to high intervariability. Furthermore, there is the possibility that sorafenib is an inhibitor of these UGTs. This would be crucial for potential drug-drug interactions in terms of the aimed combination therapy of SKL and SRF. In addition, if possible, upcoming *in vivo* studies should examine whether and to which quantity the SKL-glucuronides circulate in plasma. If they are immediately excreted, their inhibitory activity against p38 α MAP kinase would not be decisive for the efficacy and side effects of SKL.

3.5.2.7. Kinetic Analysis of *in vitro* Skepinone-L Glucuronidation

The kinetic analysis of the *in vitro* glucuronidation of SKL included the determination of the Michealis-Menten constant K_m and the maximum reaction velocity V_{max} . These were needed to identify the UGT isoenzymes involved in the conjugation reactions. If several isoforms catalyse the conversion of SKL, their substrate affinity can be distinguished on the basis of K_m . The aim is to identify those with a high affinity, as these are already involved in glucuronidation at lower substrate concentrations and are therefore of clinical relevance. Prior to the determination of K_m and V_{max} , the optimal protein concentrations and the required incubation time were defined on the basis of preliminary experiments, as described in chapter 5.2.7.6. The kinetic parameters were evaluated by measuring the turnover rate of the enzyme in the presence of different SKL concentrations. This was conducted in the Ph2 incubation reaction system in HLM, RLM, MLM, DLM and CMLM. The detailed experimental procedure can be found in chapter 5.2.7.6 (Kinetic Analysis of Skepinone-L Glucuronidation in Liver Microsomes). Since only pO-Glc and sO-Glc were available as pure substances, no calibration could be carried out for N-Glc in HLM. However, it was very important to be able to represent its formation and compare it with the O-glucuronides in order to assess the affinities. Therefore, its quantification was performed using the calibration function of the sO-Glc.

The respective kinetic constants were calculated by nonlinear regression using GraphPadPrism9.0. For the graphical representation of the experimental data, the corresponding Michaelis-Menten diagram was created for each species. This represents the reaction rate of the enzymatic conversion as a function of the substrate concentration. The double reciprocal Lineweaver-Burk plot was used for extended graphical interpretation.

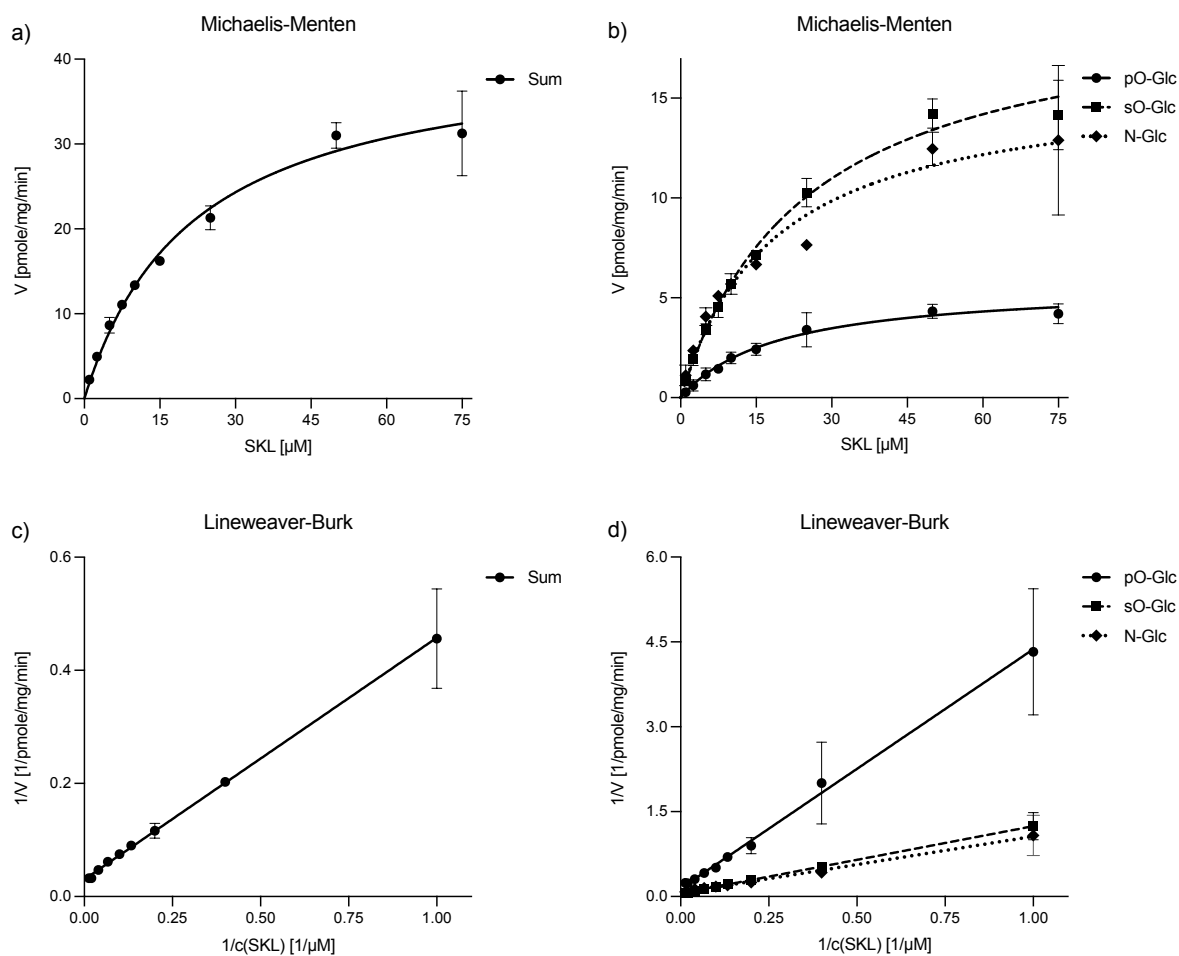


Fig. 77: Graphical representation of the glucuronidation kinetic of SKL in HLM. Michaelis-Menten plot of (a) the sum of the formed glucuronides and (b) pO-Glc, sO-Glc and N-Glc individually. Lineweaver-Burk plot of (c) the sum of the formed glucuronides and (d) pO-Glc, sO-Glc and N-Glc individually. Each value represents the mean of triplicate experiments. The respective standard deviation is indicated by error bars.

The glucuronidation of SKL seems to correspond to Michaelis-Menten kinetics in HLM. This is evident from the obtained hyperbolic curve of the Michaelis-Menten plot (Fig. 77a), as well as the straight line observed in the Lineweaver-Burk plot (Fig. 77c). The individual saturation curves of the glucuronides (Fig. 77b) reveal distinct differences in the kinetics of their formation. Thus, the conversion reaction to pO-Glc

saturates significantly faster than for sO-Glc. Since the quantification of N-Glc was performed by applying the calibration function of sO-Glc, no conclusion can be derived about its actual conversion rate. However, the formation of N-Glc is the only one to show deviations from the hyperbolic curve which could be an indication of allosterism.

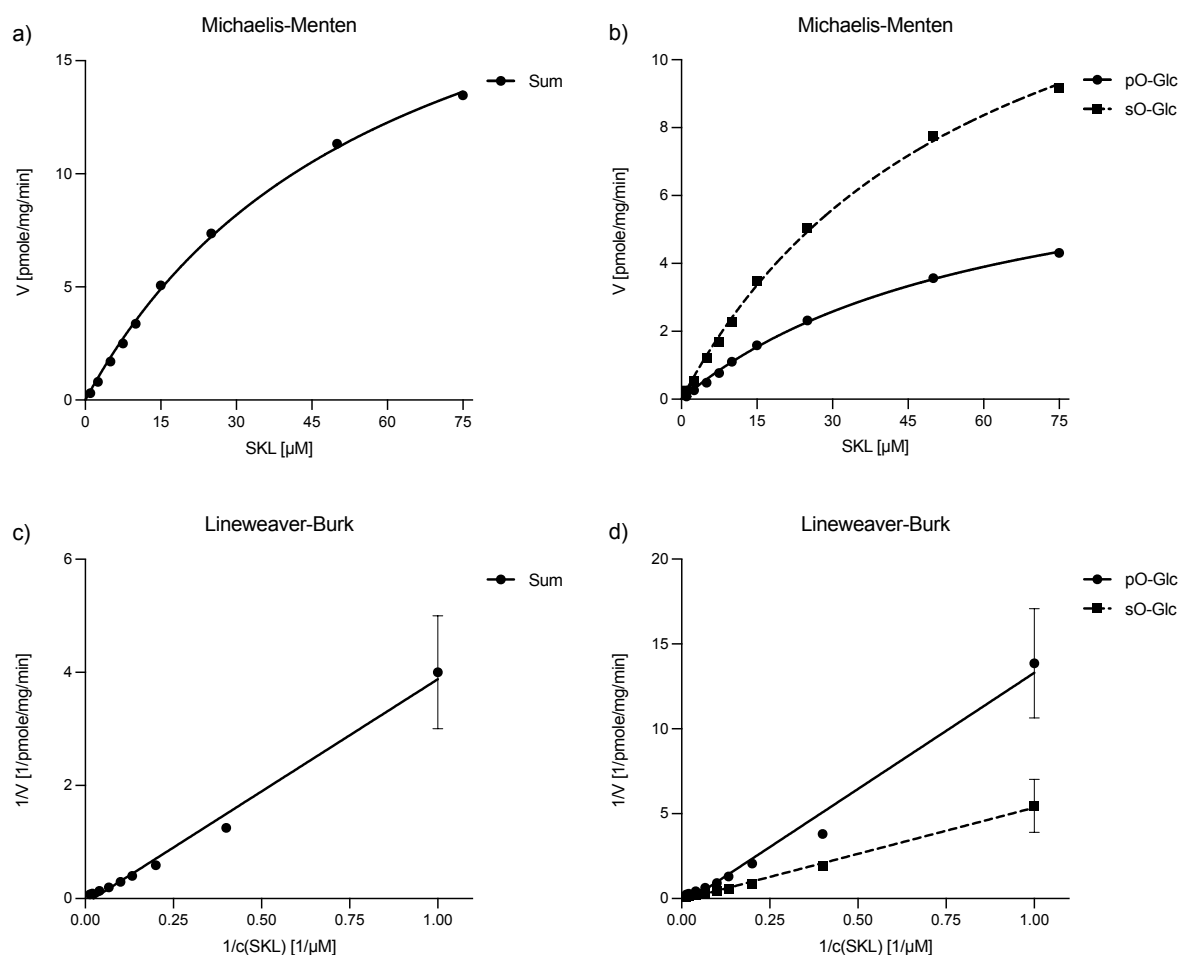


Fig. 78: Graphical representation of the glucuronidation kinetic of SKL in RLM. Michaelis-Menten plot of (a) the sum of the formed glucuronides and (b) pO-Glc and sO-Glc individually. Lineweaver-Burk plot of (c) the sum of the formed glucuronides and (d) pO-Glc and sO-Glc individually. Each value represents the mean of triplicate experiments. The respective standard deviation is indicated by error bars.

In RLM the glucuronidation of SKL seems to proceed significantly slower than in HLM. Moreover, none of the saturation curves of the Michaelis-Menten plots (Fig. 78a,b) show a clear asymptotic approximation to the substrate concentration. This indicates that with the concentration of SKL applied, complete saturation and thus the maximum reaction rate has not yet been reached. The double reciprocal application of the sum (Fig. 78c) results in a slightly concave curve. However, positive cooperativity can be ruled out as a reason for this, since the corresponding Michaelis-Menten plot does not

display a sigmoidal curve. Thus, the glucuronidation of SKL in RLM did not follow Michaelis-Menten kinetics. The single plot of both metabolites (Fig. 78d) shows that this mainly applies to the formation of pO-Glc.

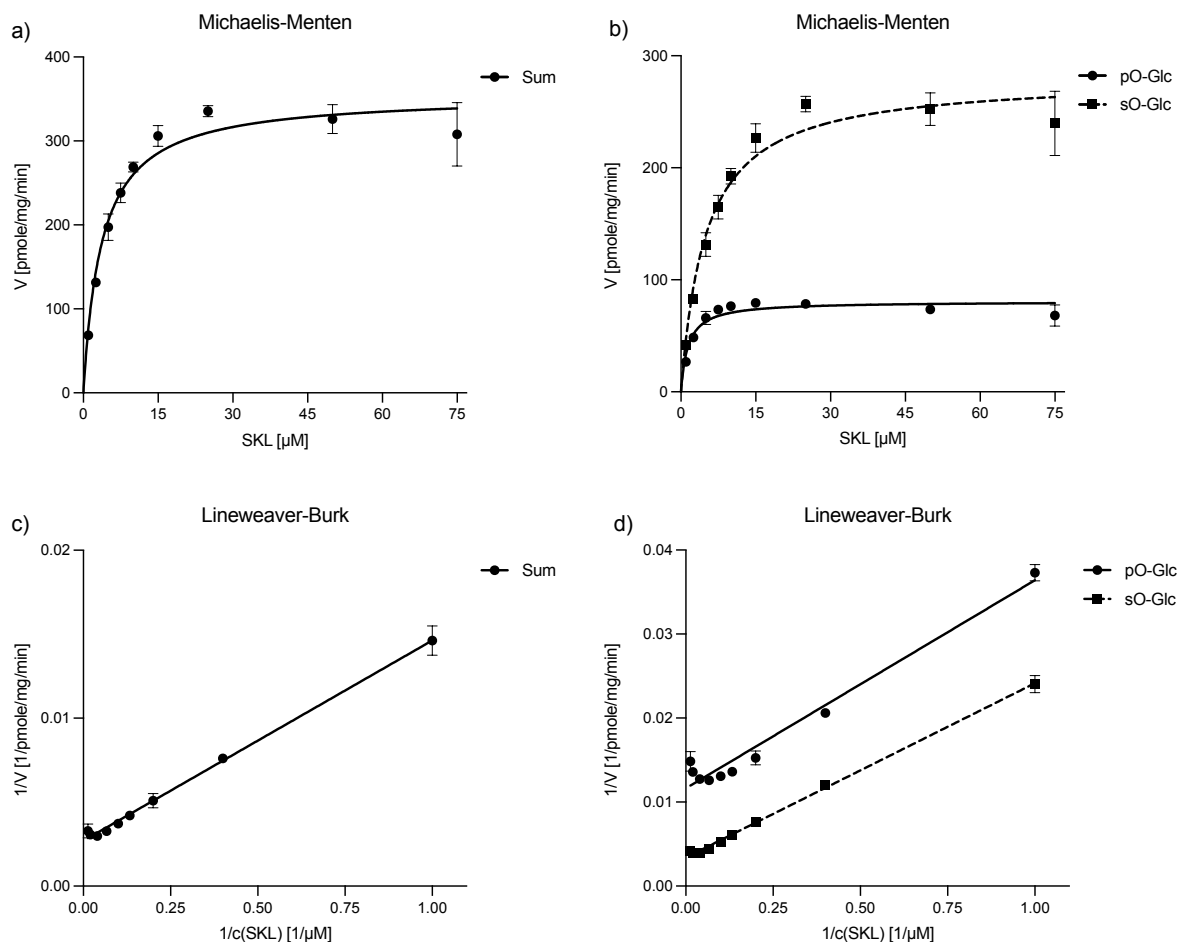


Fig. 79: Graphical representation of the glucuronidation kinetic of SKL in MLM. Michaelis-Menten plot of (a) the sum of the formed glucuronides and (b) pO-Glc and sO-Glc individually. Lineweaver-Burk plot of (c) the sum of the formed glucuronides and (d) pO-Glc and sO-Glc individually. Each value represents the mean of triplicate experiments. The respective standard deviation is indicated by error bars.

The kinetic of SKL glucuronidation in MLM seems to follow the Michaelis-Menten at least up to a substrate concentration of about 25 μM . However, figure 79a clearly shows that in the presence of higher SKL concentrations the reaction rate decreases after reaching V_{max} . Product or substrate inhibition of the enzymes involved might be the reason for this observation. It seemed to affect the formation of pO-Glc and sO-Glc equally (Fig. 79b). The obtained bell shape of the plot according to Lineweaver-Burk (Fig. 79c,d) additionally indicates a substrate or product excess.

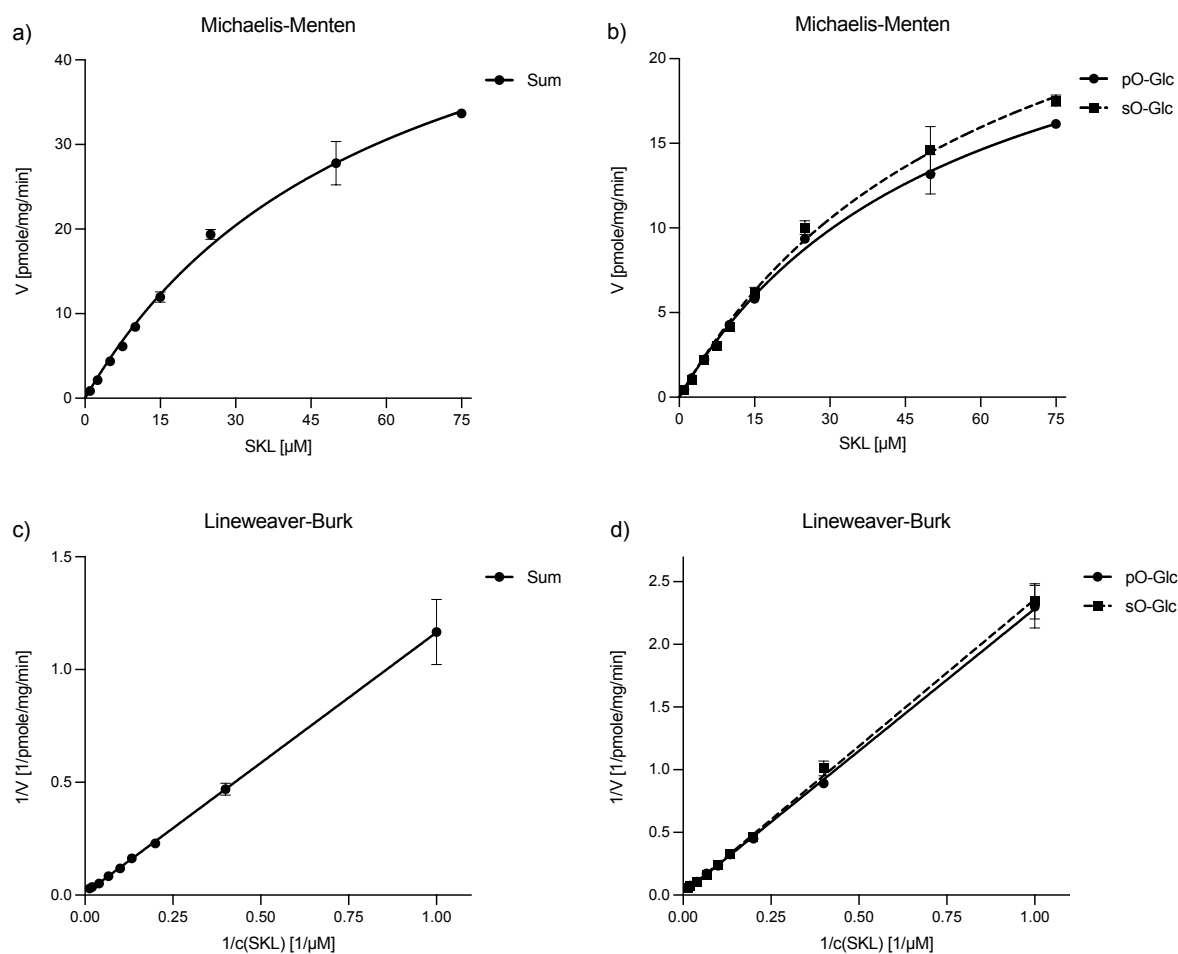


Fig. 80: Graphical representation of the glucuronidation kinetic of SKL in DLM. Michaelis-Menten plot of (a) the sum of the formed glucuronides and (b) pO-Glc and sO-Glc individually. Lineweaver-Burk plot of (c) the sum of the formed glucuronides and (d) pO-Glc and sO-Glc individually. Each value represents the mean of triplicate experiments. The respective standard deviation is indicated by error bars.

In DLM, the glucuronidation of SKL also seems to correspond the Michaelis-Menten kinetics. However, the diagrams (a) and (b) from figure 80 indicate that complete saturation and the associated V_{max} were not achieved with the substrate concentration applied. In HLM, RLM and MLM the pO-Glc formation rate was significantly lower than that of sO-Glc. In contrast, visually, only a minor difference between the turnover rates of SKL to pO-Glc and sO-Glc in DLM (Fig. 80b,d) could be observed.

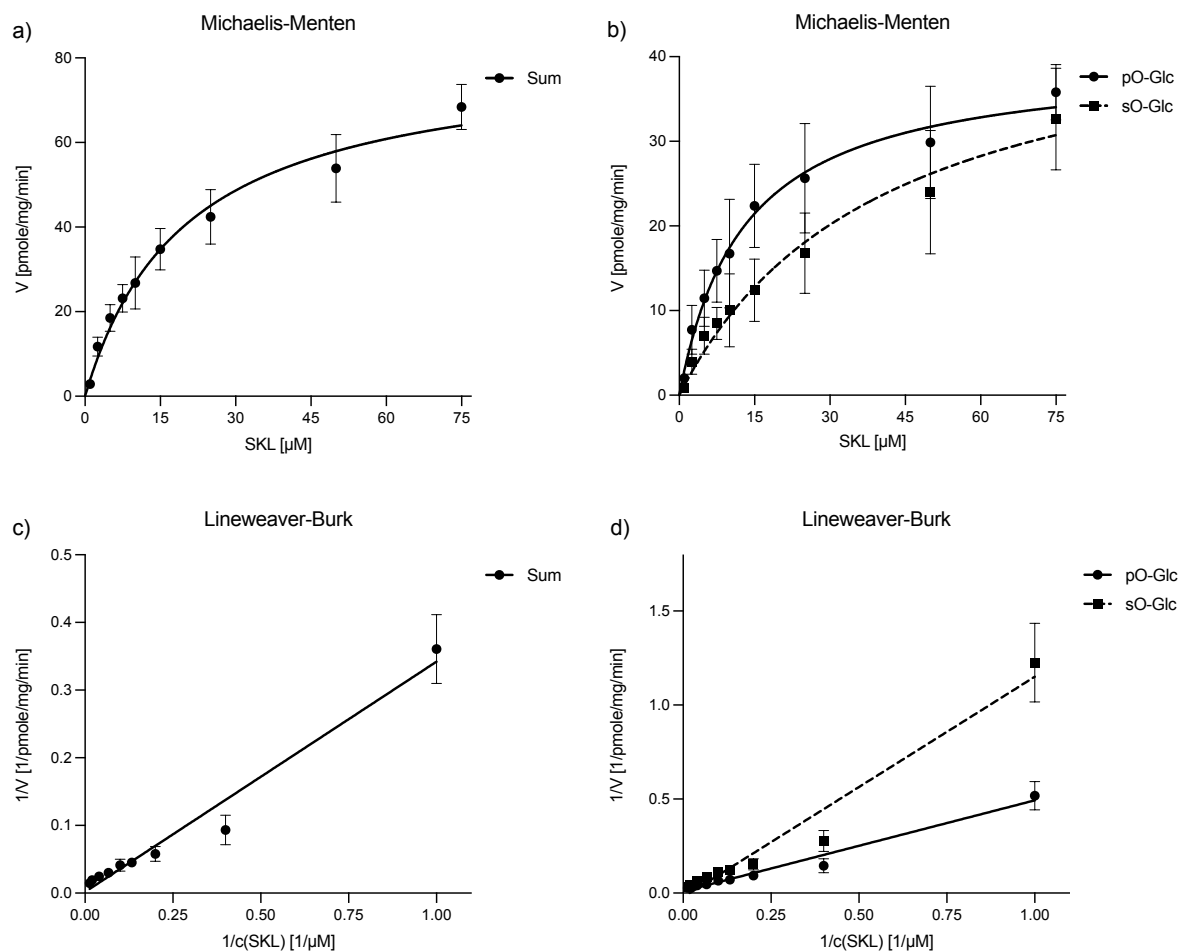


Fig. 81: Graphical representation of the glucuronidation kinetic of SKL in CMLM. Michaelis-Menten plot of (a) the sum of the formed glucuronides and (b) pO-Glc and sO-Glc individually. Lineweaver-Burk plot of (c) the sum of the formed glucuronides and (d) pO-Glc and sO-Glc individually. Each value represents the mean of triplicate experiments. The respective standard deviation is indicated by error bars.

Both the Michaelis-Menten (Fig. 81a) and the Lineweaver-Burk (Fig. 81c) plot indicate an atypical kinetic for the glucuronidation of SKL in CMLM. The saturation curves of both O-glucuronides (Fig. 81b,c) show a similar course as previously observed for N-Glc formation in HLM. This could indicate positive cooperativity, but the Michaelis-Menten plot does not exhibit a sigmoidal curve. Therefore, allosteric effects could be a possible reason. In contrast to the other species tested, the amount and rate of conversion of pO-Glc formation in CMLM exceeds that of sO-Glc. However, the formation reaction of sO-Glc does not seem to be completely saturated. The kinetic analysis of SKL glucuronidation is thus subject to significant species-specific differences. In addition to the above graphical representations of the experimental data, this is also reflected through the calculated kinetic parameters K_m and V_{max} (Tab. 60).

microsomes	glucuronide	K_m [μM]	V_{max} [pmol/mg/min]	R^2 (Lineweaver-Burk)
HLM	sum	21.4	41.7	0.9636
	pO-Glc	19.2	5.7	0.7948
	sO-Glc	24.8	20.1	0.9005
	N-Glc	18.5	15.9	0.7502
RLM	sum	59.9	24.5	0.8562
	pO-Glc	62.7	8.0	0.8657
	sO-Glc	59.3	16.6	0.8254
MLM	sum	3.7	355.4	0.9900
	pO-Glc	1.4	80.7	0.9544
	sO-Glc	5.0	280.8	0.9896
DLM	sum	59.0	60.6	0.9866
	pO-Glc	54.8	28.0	0.9848
	sO-Glc	63.0	32.7	0.9886
CMLM	sum	20.1	81.2	0.9070
	pO-Glc	12.9	39.9	0.9024
	sO-Glc	40.5	47.3	0.8857

Tab. 60: Kinetic parameters of the glucuronidation reaction of SKL in HLM, RLM, MLM, DLM and CMLM. K_m and V_{max} were determined for the sum and each individual glucuronide. The corresponding R^2 were derived from the Lineweaver-Burk plots.

The obtained K_m values of SKL glucuronidation in sum ranged from 3.7 to 59.9 μM and V_{max} values from 24.5 to 355.4 pmol/mg/min. By far the strongest substrate affinity with 1.4 μM for pO-Glc and 5.0 μM for sO-Glc formation was observed in MLM. The conversion rate of 80.7 pmol/mg/min (pO-Glc) and 280.8 pmol/mg/min (sO-Glc) was also clearly fastest in MLM. The K_m values of 62.7 and 59.3 μM for the formation of pO- and sO-Glc in RLM are very similar to those observed in DLM (54.8 μM for pO-Glc, 63.0 μM for sO-Glc). In addition, they correspond to the highest values for K_m , indicating a lower affinity towards SKL as substrate. However, RLM and DLM differ significantly in their respective conversion rates. In RLM, V_{max} with values of 8.0 pmol/mg/min for pO-Glc and 16.6 pmol/mg/min for sO-Glc formation was significantly slower than the V_{max} observed in DLM (28.0 pmol/mg/min for pO-Glc, 32.7 pmol/mg/min for sO-Glc). In HLM, K_m of 19.2 μM for pO-Glc and 24.8 μM for sO-Glc indicate a relatively strong substrate affinity. However, the corresponding V_{max} of 5.7 pmol/mg/min (pO-Glc) and 20.1 pmol/mg/min (sO-Glc) are slow and comparable to those obtained in RLM. In HLM, RLM and DLM, the K_m values of the respective pO-Glc and sO-Glc are relatively similar to each other. While in DLM the corresponding V_{max} are also comparable, in HLM and RLM SKL is converted to sO-Glc at a significantly higher rate than to pO-Glc.

Overall, the kinetic parameters obtained correlate with the results of the *in vitro* metabolism studies. However, the dissimilarities and thus the complexity of interspecies scaling and *in vitro* extrapolation were also exemplified. For example, microsomal UGTs of both rodent species show completely different affinities and conversion rates of SKL. The highest similarity of the tested species to HLM was observed in CMLM. However, the most significant difference between HLM and the animal species is the formation of the postulated N-Glc.

3.5.3. Glucuronidation of Skepinone-L in Recombinant Isoenzymes

3.5.3.1. Identification of Skepinone-L Metabolizing UGT Isoforms

UGT-mediated glucuronidation appears to be the major metabolic pathway for SKL *in vitro*. The results obtained so far show significant species-related differences in glucuronidation. Particularly noticeable is the formation of three glucuronides in HLM, in contrast to all other species tested here, in which only two SKL glucuronides are formed. This indicates the involvement of different isoforms, some of which are probably only expressed in humans. To predict adverse effects due to drug-drug interactions and genetic polymorphism, the UGT isoforms involved must be determined. For this purpose, human recombinant UGTs (rUGTs) 1A1, 1A3, 1A4, 1A6, 1A9, 2B7, 2B10 and 2B15 were initially screened for glucuronidation of SKL. They were selected based on their expression in hepatic tissue and their important role in hepatic glucuronidation of xenobiotics [46]. The initial screening for glucuronidation was performed with a SKL concentration that correlated approximately with the K_m in HLM and one ten times that value. Thus, incubations of 10 and 100 μM SKL in the presence of each rUGT were performed as described in chapter 5.2.8.1 (Glucuronidation Reaction by Recombinant UGTs). The enzymatic reactions were stopped after 60 min.

Reaction phenotyping indicated that rUGT1A1, 1A3 and 2B7 contribute for the formation of both SKL O-glucuronides. This enzymatic conversion can be described as a bi-reaction, since one enzyme forms two products. As illustrated in figure 91, the responsibility of each isoform seems to be dependent from the substrate concentration. Regarding the SKL concentration of 10 μM , which corresponds roughly

the estimated K_m value in HLM, rUGT2B7 seems to be the only isoform involved in the O-linked conjugation. Interestingly, no difference in the formed amount of pO-Glc via rUGT2B7 between both substrate concentrations could be observed.

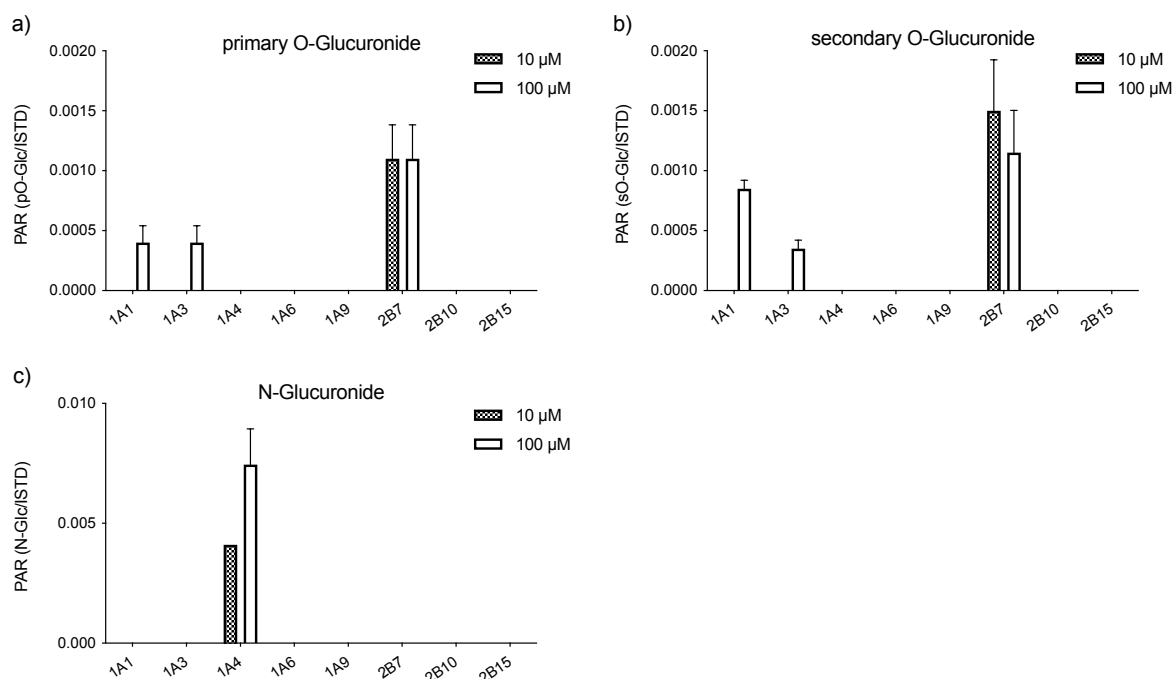


Fig. 82: Formation of (a) the primary SKL-O-glucuronide, (b) the secondary SKL-O-glucuronide and (c) the N-glucuronide *in vitro* after 60 min incubation of 10 μM and 100 μM SKL in the presence of recombinant UGTs expressed as peak area ratio (area glucuronide vs. area ISTD). Reaction phenotyping indicates that in a concentration-dependent manner rUGT1A1, 1A3 and 2B7 contribute for the formation of pO-Glc and sO-Glc, whereas rUGT1A4 could be identified as solely responsible for N-Glc formation.

In contrast, sO-Glc formation seemed to decrease at 100 μM initial SKL concentration. In addition, overlapping substrate selectivity could be observed at high substrate concentration. At high SKL levels, rUGT1A1 and 1A3 appear to catalyse the O-linked glucuronidation. However, rUGT1A1 seems to be more involved in the formation of sO-Glc than rUGT1A3. Thus, for SKL O-linked glucuronidation *in vitro*, UGT2B7 appears to be the main enzyme responsible. UGT1A1 and 1A3 can be considered as minor pathways. With respect to N-Glc formation, figure 82c shows that only rUGT1A4 appears to exhibit catalytic activity. The higher substrate concentration led to an increased level of glucuronide production. None of the other isoforms tested here appear to contribute to the formation of N-Glc, regardless of the SKL concentration applied. Figure 83 summarises the results obtained in terms of structural elucidation and identification of the main responsible UGT isoform for each SKL glucuronide formed *in vitro*.

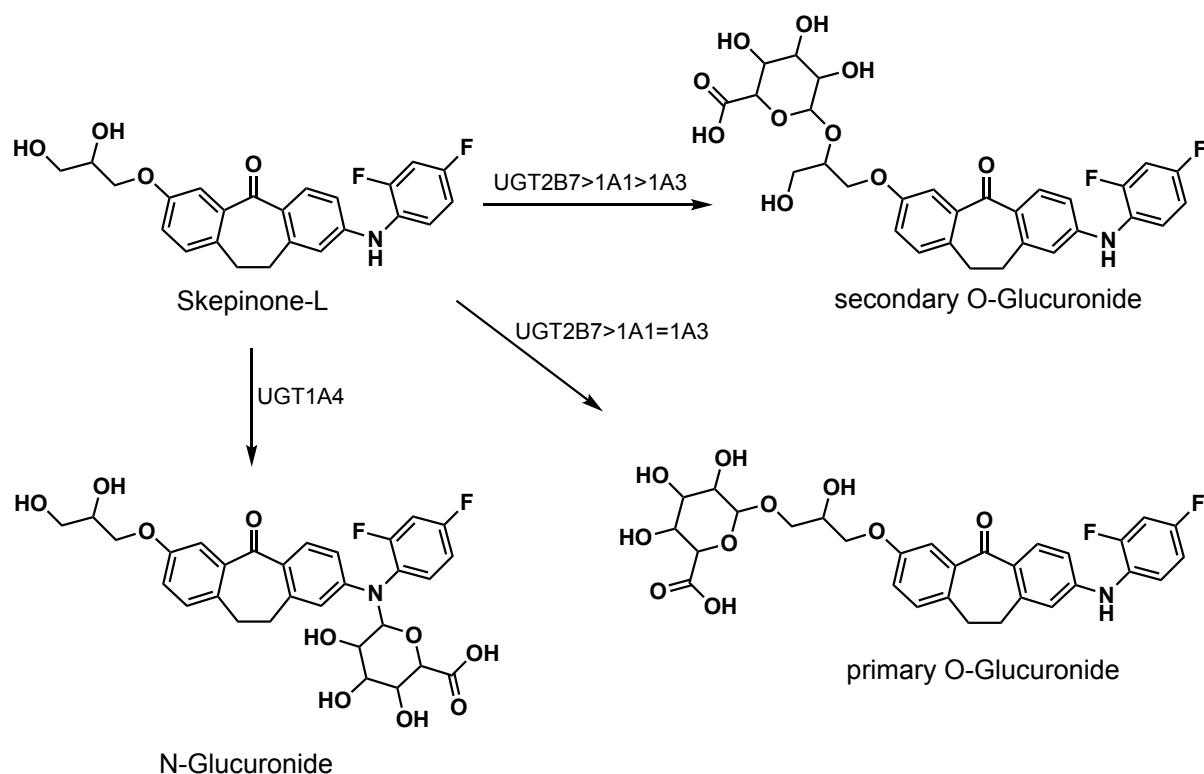


Fig. 83: Summarised results of the structural elucidation of pO-Glc, sO-Glc and postulated N-Glc as well as the respective contributing UGT-isoenzymes.

UGT2B7 is known to be one of the major drug metabolizing human hepatic UGTs. Besides the liver it is also expressed in the intestine, kidney, brain and several additional organs and tissues [182]. Genetic polymorphism which could significantly affect the clearance and efficacy of therapeutic drugs has been reported for UGT2B7 [183], [184]. Known orthologues for the *UGT2B7* gene are, amongst others, present in rats (*Ugt2b15*), mice (*Ugt2b36*, *Ugt2b35*) and dogs [185]. However, there were significant differences between the species with regard to the obtained K_m and V_{max} values as well as the amounts of conjugation products formed *in vitro*. An interesting fact is that UGT2B7 catalyses the conjugation of two products from one substrate. The *in vitro* metabolism studies showed that in terms of the relative amounts of glucuronides formed, the sO-Glc was preferentially formed over the pO-Glc. However, the kinetic analysis of glucuronidation showed lower K_m for pO-Glc than for sO-Glc. In contrast the associated turnover rate of pO-Glc formation was significantly lower than that of sO-Glc formation. This in turn explains the relative amounts formed during the microsomal incubations. These results lead to the hypothesis that UGT2B7 has at least two independent substrate binding sites, or active centres. These could exhibit varying affinities for SKL and differ in the respective catalysed conjugation

reaction. The structure and number of these centres could vary between the UGT2B7 orthologues, which could result in the inter species differences with regard to pO-Glc and sO-Glc formation observed *in vitro*. UGT1A1 is also responsible for the glucuronidation of numerous drugs. It is mainly located in the liver but can also be found within the colon, small intestine and stomach [186, 187]. More than 100 different variants have been described for the human *UGT1A1* gene, which, *inter alia*, result in reduced or increased activity of the enzyme [188]. The functional *UGT1A1* is also abundant in rat, mouse, dog and monkey and the human UGT1A1 is considered to be their orthologue [46]. Interestingly, SRF is known to be a very potent inhibitor of UGT1A1 [174]. This could explain the decrease of pO-Glc and sO-Glc formation observed in the presence of SRF during the *in vitro* metabolism studies. The third UGT isoform identified to contribute to SKL O-linked glucuronidation is UGT1A3. Its substrates include bile acids [189] and with only 6.5 % of all hepatic UGTs it is one of the less abundant [190]. As for almost every UGT-coding gene genetic polymorphism has also been reported for *UGT1A3* [191]. In mice *Ugt1a3* is a pseudogene [192] and also no UGT1A3 present in monkeys has been reported so far [46]. In all species, the relative proportion of sO-Glc formed *in vitro* is significantly higher than that of pO-Glc. The incubations of SKL on the recombinant isoenzyme also result in higher PARs for sO-Glc compared to pO-Glc. Thus, the conjugation at the secondary hydroxy group of SKL seems to be catalysed preferentially by UGT2B7 compared to the primary one. UGT1A4 accounts for about 26 % of the total UGT-mediated conjugation reactions [193]. In addition to O-glucuronidation reactions, it contributes to the glucuronic acid conjugation to amines, forming N-linked products [194]. This shows that the binding of glucuronic acid to the nitrogen of the difluorophenylamino-moiety of SKL is quite possible. Thus, the thesis of the postulated N-Glc is supported, even if it is not available as a pure substance. Moreover, the identification of rUGT1A4 as the only responsible isoform explains why N-Glc formation *in vitro* was only observed in human LM. *Ugt1a4* is a pseudogene in both rats and mice and is therefore not expressed as a functional enzyme. In dogs and monkeys, UGT1A4 is formed, but there are distinct species-specific differences with regard to substrate specificity [46].

In addition to UGT1A4, UGT1A3, 1A9 and 2B10 also catalyse the glucuronidation of amines [195]. It is therefore interesting that UGT1A4 is the only one of the isoforms tested that is involved in the N-glucuronidation of SKL. Furthermore, UGT1A3 and 1A4 share about 93 % homology, thus possess overlapping substrate specificity [196]. This accounts for both O- and N-linked glucuronidation. Therefore, it is also interesting that UGT1A3 but not 1A4 seems to be involved in sO- and pO-Glc formation. In summary, a total of four of the UGT isoforms tested are involved in the conjugation reaction of SKL. At the clinically more relevant lower SKL concentration, even only UGT2B7 and 1A4. However, all involved isoforms are subjects to genetic polymorphisms [197], which may lead to interindividual differences in the degradation of SKL and the formation of its glucuronides. In addition, their expression can be induced *in vivo*, e.g., by anti-cancer drugs, which has already been described for UGT2B7 [198] and 1A4 [199] in liver cell models. This can lead to an increase in metabolic degradation and thus to drug resistance. Some severe diseases, for example of the liver and intestine, can also alter the expression of UGTs [49]. Downregulation of both expression levels and activity in the context of HCC has been described for UGT1A1, 1A4 and 2B7 [200]. It is highly likely that this results in influencing the metabolism of specific isoform targeting substrates, such as SKL. This could possibly help to understand why N-Glc was not detectable in all human plasma samples. The *in vivo* formation of pO-Glc and sO-Glc could also be influenced or altered by downregulation or induction of the responsible isoforms.

However, the glucuronidation of SKL and the associated formation of both O-linked reaction products does not represent the norm. Contrary to the actual purpose, the conjugation of SKL does not result in its complete inactivation. Both pO-Glc and sO-Glc appear to have almost the same pharmacological potency as SKL (Ch. 3.5.2.6) *in vitro*. Thus, drug resistance caused by non-genetic regulatory factors could possibly be circumvented. However, further studies must resolve which factors are responsible for the presence and absence of N-Glc in human plasma. It also remains to be clarified whether and to what extent these factors affect the pharmacological effect of SKL. Thus, the identification of the UGT isoforms involved also shows that the *in vitro* - *in vivo* correlation as well as the scaling from preclinical species to human possess a high complexity.

3.5.3.2. Kinetic Analysis of *in vitro* Skepinone-L Glucuronidation with Recombinant UGT Isoenzymes

The kinetic parameters for SKL glucuronidation were previously determined in the enzyme mixture represented by LMs. Therefore, K_m and V_{max} should also be ascertained in the presence of the major contributing UGT isoforms for each known glucuronide. Thus, incubations of SKL in the presence of rUGT2B7 and 1A4 were performed as described in the previous section 3.5.3.1.

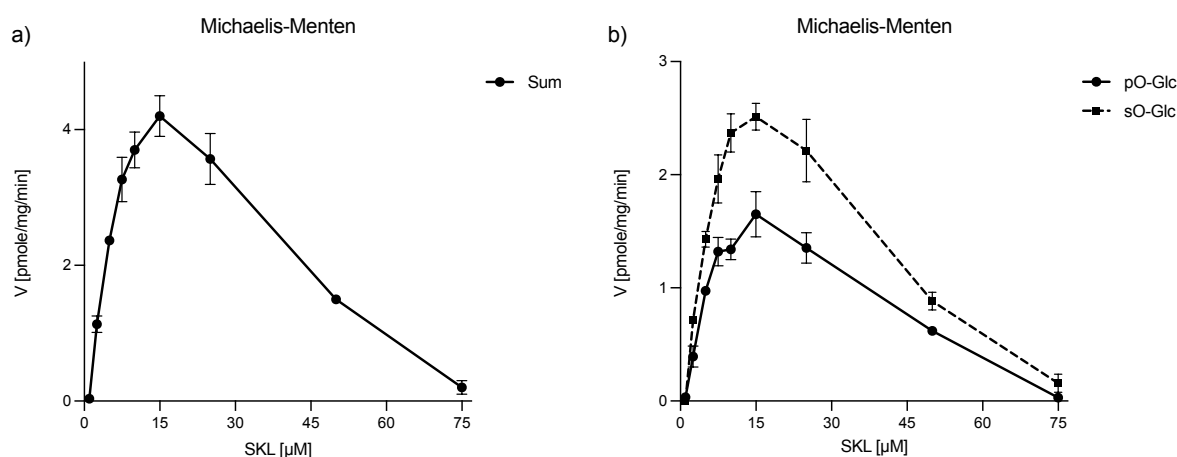


Fig. 84: Graphical representation of the glucuronidation kinetic of SKL with rUGT2B7. Michaelis-Menten plot of (a) the sum of the formed glucuronides and (b) pO-Glc and sO-Glc individually. Each value represents the mean of triplicate experiments. The respective standard deviation is indicated by error bars.

The kinetic of SKL glucuronidation in the presence of rUGT2B7 shows a similar behaviour as previously observed in MLM. Thus, a clear reduction of the reaction velocity is observed from about 15 μM SKL. However, the rate decreases at the isoenzyme with increasing substrate concentration results in an almost complete standstill of the enzymatic reaction (Fig. 84). Hence, the rUGT2B7-mediated glucuronidation of SKL is affected either by product or substrate inhibition, and thus does not follow Michaelis-Menten kinetics. Therefore, neither K_m nor V_{max} could be determined, and due to the atypical course, no Lineweaver-Burk plot could be generated. Nevertheless, the kinetic analysis of SKL conjugation reaction catalysed by UGT2B7 illustrates the involvement of UGT1A1 and 1A3 in the formation of pO-Glc and sO-Glc at higher substrate concentrations. In MLM, a clear decrease of the turnover rate was observed, but not as pronounced as at rUGT2B7. In addition, reaction velocity also appeared to decrease in HLM, but only to a very small extent.

Accordingly, the formation of SKL O-glucuronides seems to be mediated mainly via UGT1A1 and 1A3 from higher SKL concentrations. The ratios of the formed amounts of pO-Glc and sO-Glc also illustrate the involvement of other UGT isoforms besides UGT2B7 in HLM. Thus, on average, about 3-fold more sO-Glc than pO-Glc was formed in HLM. In contrast, the amounts of sO-Glc and pO-Glc formed in the presence of rUGT2B7 showed a significantly lower ratio of only 1 to 1.5.

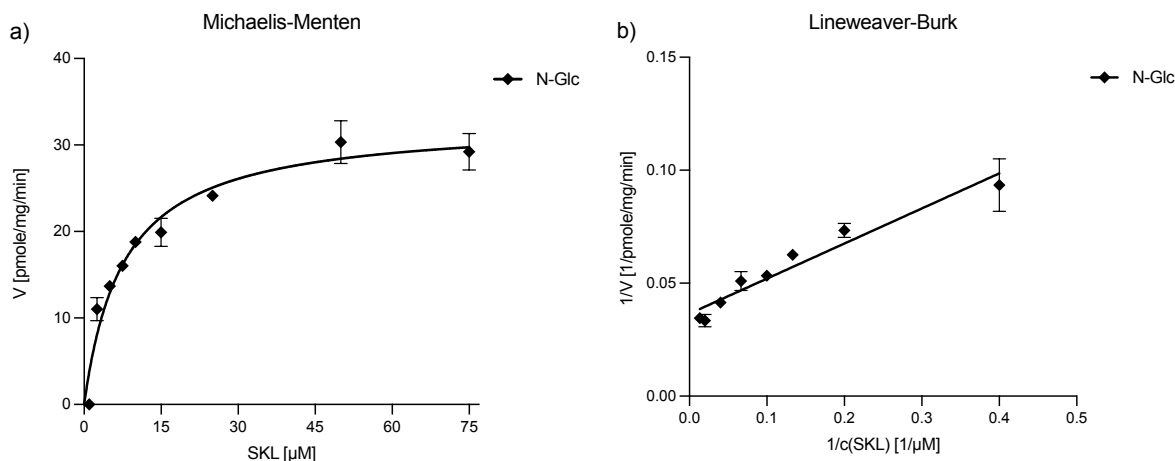


Fig. 85: Graphical representation of the glucuronidation kinetic of SKL with rUGT1A4. (a) Michaelis-Menten plot and (b) Lineweaver-Burk plot of the formed N-Glc. Each value represents the mean of triplicate experiments. The respective standard deviation is indicated by error bars.

Figure 85 shows the graphical representation of the kinetic analysis of SKL glucuronidation by rUGT1A4. However, it should be noted that the postulated N-Glc was unfortunately not available as pure substance. Therefore, the calibration function of sO-Glc was used for its quantification. Thus, the kinetic parameters K_m and V_{max} with 7.7 μM and 32.8 pmol/mg/min most likely do not represent the actual values and only serve as an approximation. Both the Michaelis-Menten (Fig. 85a) and the Lineweaver-Burk plot (Fig. 85b) leave scope for interpretation as to whether the formation of N-Glc mediated by rUGT1A4 is based on Michaelis-Menten kinetics. It might also be a biphasic process, which could be due to positive cooperativity. However, both the rapid increase in the reaction rate from 2.5 μM SKL and the hyperbolic and thus non-sigmoidal course of the curve contradict this. Interestingly, N-Glc was formed in almost equal amounts in both HLM and rUGT. Both rUGT1A4 and HLM-UGT1A4 had similar catalytic activities with 1,100 pmol/mg/min (Tab. 103, Ch. 5.2.8) and 1,150 pmol/mg/min (Tab. 92, Ch. 5.2.7.1). However, the final protein concentrations were 0.5 mg/mL within HLM and 0.25 mg/mL with rUGT1A4

incubations. Thus, N-Glc was formed in HLM in smaller quantities compared to the formed amount by rUGT1A4. The glucuronidation of SKL in HLM is known to result in the conjugated products pO-Glc and sO-Glc in addition to N-Glc. Thus, less substrate is available to UGT1A4, which could explain the lower amount of N-Glc formed in HLM. To fully clarify which of the three SKL glucuronides is preferentially generated, the actual K_m of N-glucuronidation must be known. Thus, the substrate affinities of the enzymes involved could be compared.

3.5.3.3. Inhibition Analysis of rUGT2B7

Results obtained in the previous section (Fig. 84) show that higher values of the substrate concentration led to decreased product formation. The conjugation reaction catalysed by rUGT2B7 nearly stopped at the highest SKL-concentration of 75 μM . These findings indicate the existence of either substrate or product inhibition *in vitro* of UGT2B7. Several incubations were performed to elucidate if UGT2B7 is inhibited by either SKL, pO-Glc or sO-Glc. A chemical probe substrate of UGT2B7 is 7-hydroxy-4-trifluoromethylcoumarin (HTMC) [201] which served therefore as activity control. The analysis of HTMC-Glc formation was performed by incubating 0.5 mg/mL rUGT2B7 in the presence of 10 μM HTMC at 37°C for 60 min. Prior, the isoenzyme was pre-incubated for 5 min on ice in the presence of the respective test compounds. Thus, rUGT2B7 was pre-incubated with either 10 or 100 μM SKL, 0.1 or 1.0 μM sO-Glc as well as with 0.1 or 1.0 μM pO-Glc. For the intended enzymatic inhibition, 200 μM of the non-enzyme-selective inhibitor diclofenac (DCF) were added [202]. Pre-incubation with DMSO served as positive control. Each reaction was started by adding HTMC and stopped with ACN which contained ISTD. Further experimental setup and the chromatographic conditions applied were as described in chapter 5.2.8.3 (Inhibition of rUGT2B7).

Figure 86 shows that in all incubations the conjugation product HTMC-Glc could be observed. However, the substrate itself appeared to be only present when incubated with 200 μM DCF or 100 μM SKL. In all but these two incubations, the PARs of the glucuronide formed are nearly the same as that of the positive control (10 μM HTMC). Thus, the presence of neither 10 μM SKL nor even pO-Glc and sO-Glc each at both concentrations appeared to influence the formation of HTMC-Glc. In contrast to

200 μM diclofenac and 100 μM SKL, where significantly less HTMC-Glc was formed. Since the incubation with diclofenac served as a control of inhibition, the decrease in reaction product was expected. However, diclofenac does not appear to be a highly potent inhibitor of UGT2B7, at least at the concentration used. Eventually, the pre-incubation period was too short to completely stop the enzymatic reaction. In addition, perhaps the incubation period should have been shorter to completely avoid glucuronide formation. As observed with diclofenac, the isoenzyme retained some of its activity in the presence of 100 μM SKL.

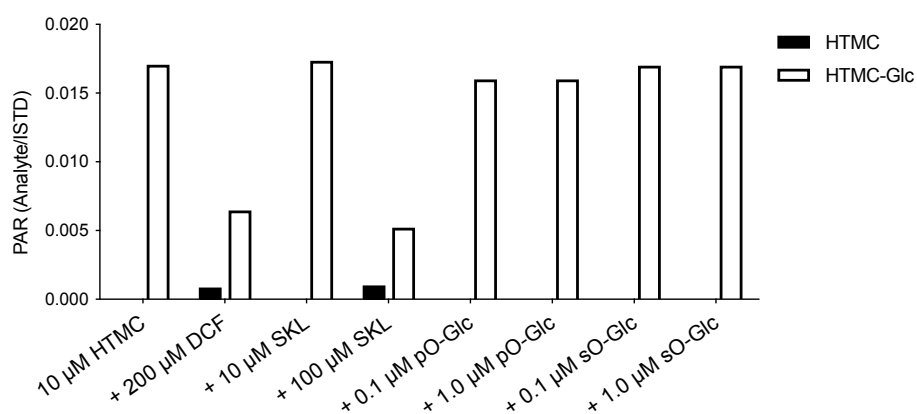


Fig. 86: Formation of HTMC-Glc (white) *in vitro* after 60 min incubation of 10 μM HTMC (black) with rUGT2B7. Pre-incubations of rUGT2B7 with 200 μM DCF, 10 μM or 100 μM SKL, 0.1 μM or 1.0 μM pO-Glc and 0.1 μM or 1.0 μM sO-Glc served to assess their inhibitory activity.

Although inhibition with known and postulated inhibitors was thus apparently incomplete, the results clearly show that rUGT2B7 is inhibited by SKL in a concentration-dependent manner. Since the formation of HTMC-Glc was not reduced by either the pO-Glc or the sO-Glc, it appears that there is no product inhibition but rather a substrate inhibition. The exact SKL concentration at which this occurs must be determined in further experiments. But based on the kinetic analyses with the isoenzyme, it can be estimated that the inhibition seems to start between 10 and 15 μM SKL. Catalysis of both the primary and secondary hydroxyl groups of SKL seems to be reduced to the same extent.

The result that SKL appears to be both a substrate and an inhibitor of UGT2B7 could help to explain the high SKL concentrations in rat plasma. It is possible that the rat isoform Ugt2b15 is already inhibited by lower SKL concentrations. The longer exposure of 14 days in total could also lead to downregulation of the enzymatic activity. Thus, it cannot be excluded that the increased SKL concentration after

simultaneous administration with SRF is not exclusively due to the combinatorial treatment. During the kinetic analyses in LM, almost every species showed an atypical course of the Michaelis-Menten plot. The increase flattened steadily with increasing SKL concentration but did not reach a plateau even in the presence of very high concentrations. These observations could also be due to substrate inhibition. At the isoenzyme, the inhibitory effect of SKL on rUGT2B7 appeared to be relatively strong. In contrast, only a small impact of substrate inhibition on the reaction rate could be observed in HLM. This suggests that the conjugation of SKL *in vivo* is not very affected by the inhibition of UGT2B7 through SKL. However, based on the results to date, it is not possible to clearly predict the extent to which substrate inhibition could influence the plasma concentrations of SKL *in vivo* in humans.

3.5.3.4. Influence of Sorafenib on Skepinone-L Glucuronide Formation in the Presence of Recombinant UGT Isoenzymes

As described in chapter 3.3.3.7 simultaneous administration of SKL and SRF in rats showed a significant increase in SKL plasma-concentration compared to SKL monotherapy. A correlation between the metabolic stability of SKL and the presence of SRF was also observed during *in vitro* incubations of SKL in HLM, RLM, MLM, DLM and CMLM. Except for HLM, a mostly significant rise in the relative amounts of unchanged SKL could be observed with increasing SRF concentrations. This is due to the reduced formation of both O-linked glucuronides. This also occurs in HLM, but the presence of SRF seemed to induce the formation of the postulated N-Glc. This in turn resulted in a decrease in the metabolic stability of SKL after co-incubation with SRF. Since the processes underlying these observations could only be assumed, it should be investigated whether the effect of SRF on the metabolic conversion of SKL *in vitro* and *in vivo* occurs at the level of the involved UGT isoforms UGT2B7, 1A1 and 1A4.

rUGT2B7

The conjugation of glucuronic acid to SKL is mainly catalysed by UGT2B7 resulting in pO-Glc and sO-Glc. Therefore, it should be investigated whether this influence of SRF on the O-glucuronide formation of SKL observed in LM is also present at the rUGT. For this purpose, the metabolic conversion of 10 μ M SKL solely or in combination with

10 and 40 μM SRF by rUGT2B7 was investigated as described (Ch. 5.2.8.1). These incubations were performed as duplicates.

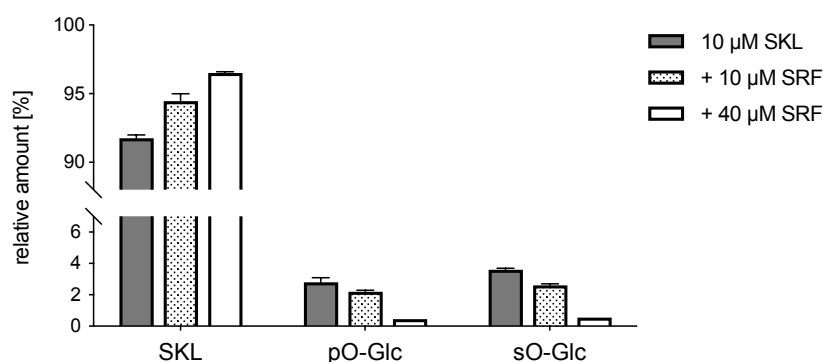


Fig. 87: Metabolic stability of SKL solely and in the presence of 10 μM and 40 μM SRF after 60 min incubation with rUGT2B7. In addition, corresponding relative amounts of formed pO-Glc and sO-Glc are given. Results represent the mean values of two incubations per concentration. The respective range of the two measured values is represented by error bars.

Figure 87 presents the results of the rUGT2B7-incubations of 10 μM SKL alone or with the addition of 10 and 40 μM SRF. There is a distinct correlation between the metabolic stability of SKL and the added concentration of SRF. This was 91.7 % without SRF and increased via 94.4 % to 96.5 % with addition of SRF. This increase in unchanged SKL is reflected by the reduced formation of pO-Glc and sO-Glc. Their relative amounts also show a clear trend in the presence of SRF. Thus, the formation of pO-Glc decreases from 2.8 % to 2.2 % and finally to 0.5 %. The relative quantity of sO-Glc was 3.6 % without SRF, with 10 μM it already dropped to 2.6 % and the addition of 40 μM SRF reduced the formation to 0.5 %. These results clearly show that the activity *in vitro* of UGT2B7 with respect to the conversion of SKL is influenced by SRF. As far as is known, SRF itself is not a substrate of this isoform. Thus, SRF seems to have a certain inhibition capacity towards UGT2B7.

rUGT1A1

Another UGT isoform involved in the conversion of SKL is UGT1A1. However, compared to UGT2B7, it seems to play a minor role in the formation of pO-Glc and sO-Glc. Moreover, with an IC_{50} of 70 nM, SRF represents a highly potent inhibitor of this isoform [203]. Therefore, the interaction of SRF on the biotransformation of SKL with UGT1A1 should be investigated, or rather the expected inhibition should be confirmed. For this purpose, the incubation of SKL with rUGT1A1 was performed as described for rUGT2B7.

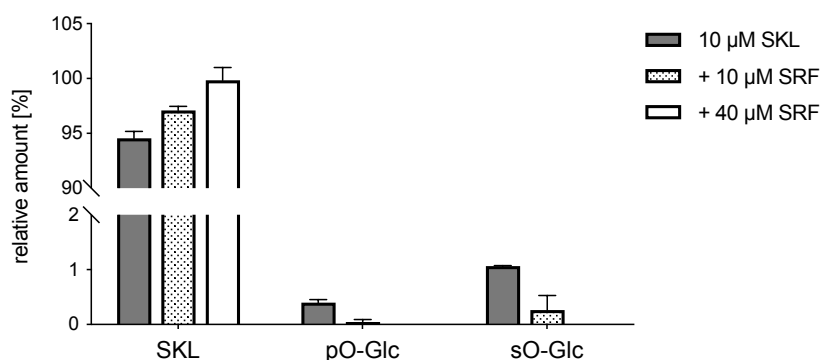


Fig. 88: Metabolic stability of SKL solely and in the presence of 10 μ M and 40 μ M SRF after 60 min incubation with rUGT1A1. In addition, corresponding relative amounts of formed pO-Glc and sO-Glc are given. Results represent the mean values of two incubations per concentration. The respective range of the two measured values is represented by error bars.

The results obtained (Fig 88) are in line with expectations. Thus, the conversion of 10 μ M SKL to 0.4 % pO-Glc and 1.1 % sO-Glc catalysed by rUGT1A1 is significantly lower than that of rUGT2B7. The addition of 10 μ M SRF already strongly reduced the formation of both glucuronides. In the presence of 40 μ M SRF, no enzymatically catalysed conversion of SKL was observed. This is further illustrated by the increasing metabolic stability of SKL in the presence of SRF. Thus, the UGT1A1-mediated formation of O-linked glucuronides is relatively strongly influenced or inhibited by the addition of SRF. However, this isoform only seems to be involved in the conversion of SKL at very high substrate concentrations, which is why the expected influence of SRF *in vivo* is most likely not very substantial.

rUGT1A4

A significant decrease in the relative amounts of pO-Glc and sO-Glc was also observed in HLM during co-incubation with SRF. However, the metabolic stability of SKL also declined. This was due to the formation of N-Glc, which seemed to be induced by the addition of SRF in a concentration-dependent manner. As already mentioned, enzyme induction is not possible in the test system used. Therefore, incubation of SKL on the responsible isoenzyme rUGT1A4 could help to elucidate the underlying processes. The experimental setup corresponded to the description for the incubations with rUGT2B7.

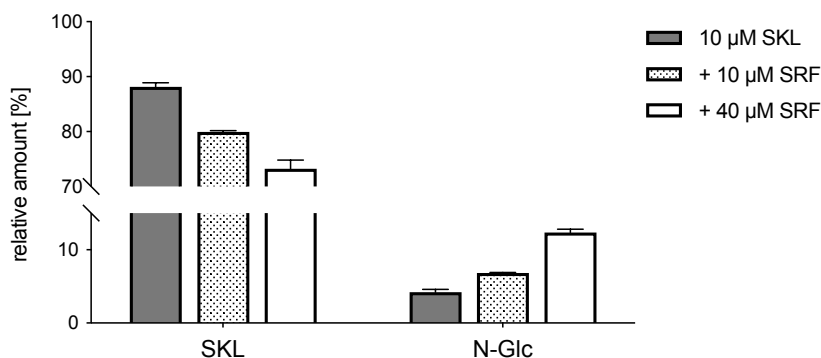


Fig. 89: Metabolic stability of SKL solely and in the presence of 10 µM and 40 µM SRF after 60 min incubation with rUGT1A4. In addition, the corresponding relative amount of formed N-Glc is given. Results represent the mean values of two incubations per concentration. The respective range of the two measured values is represented by error bars.

Figure 89 clearly shows that in the presence of SRF, the metabolic stability of SKL decreases and at the same time the amount of N-Glc formed increases. Thus, SRF affects the N-glucuronidation of SKL in the same manner at the isoenzyme as previously observed in HLM. A direct, concentration-dependent interaction of SRF and UGT1A4 thus appears to be present. Clearly, this rules out induction by increasing the enzyme concentration as a cause. Interactions of SRF with other components of the LM can also be excluded. This result is highly interesting and unexpected, since SRF with an IC_{50} of 16.1 µM has a significantly higher inhibitory effect towards UGT1A4 compared to UGT2B7 [203]. Thus, the activating or enhancing effect on UGT1A4 of SRF seems to exceed its inhibitory activity.

3.5.3.5. Influence of Sorafenib on Glucuronide Formation of Trifluoperazine in the Presence of rUGT1A4

As already described (Ch. 3.5.1.3), UGT1A4 catalyses with high affinity the glucuronidation of TFP to TFP-N-Glc. It should be examined whether SRF induces the formation of N-glucuronides of other substrates besides SKL. Incubations in HLM showed a contradictory and not entirely consistent result in this respect. No direct correlation between the metabolic stability of TFP and the presence of SRF could be observed. Moreover, the relative amounts of TFP-N-Glc decreased upon co-incubation with SRF. However, an influence of microsomal CYPs as well as other UGT isoforms or further components of the LM incubations could not be excluded. Therefore, the influence of SRF on TFP-N glucuronidation on the rUGT1A4 was

investigated. This was conducted analogously to the procedure described for rUGT2B7.

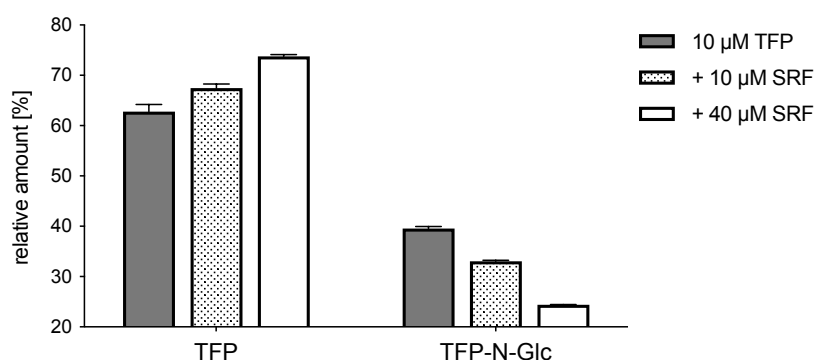


Fig. 90: Metabolic stability of TFP solely and in the presence of 10 μ M and 40 μ M SRF after 60 min incubation with rUGT1A4. In addition, the corresponding relative amount of formed TFP-N-Glc is given. Results represent the mean values of two incubations per concentration. The respective range of the two measured values is represented by error bars.

The N-linked glucuronidation of TFP decreased significantly in the presence of SRF (Fig. 90). Thus, 39.6 % of 10 μ M TFP was glucuronidated by rUGT1A4 within 60 min. In the presence of 10 μ M SRF, the relative amount of TFP-N-Glc was reduced to 33.0 %. Only 24.4 % was formed during co-incubation with 40 μ M SRF. These results correlate with the amount of unchanged TFP obtained. This increased from 62.8 % via 67.4 % to 73.8 % respectively. The results thus illustrate the inhibitory activity of SRF towards rUGT1A4. The inducing effect of SRF on N-Glc formation must therefore be based on a mutual interaction of SRF (or RGF), SKL and UGT1A4.

3.5.4. Summary and Discussion of *in vitro* Metabolism Studies of Skepinone-L

The *in vitro* metabolism studies show that the metabolic transformation of SKL has large interspecies differences. In HLM SKL appears to be stable against CYP-mediated degradation with a metabolic stability of 95.0 %. Despite this low degradation it was possible to observe the formation of five Ph1 metabolites. The relative quantities formed amounted from 0.0 % to 1.3 % of the initial SKL concentration which is very low and can thus be considered as negligible. In contrast, SKL was highly susceptible towards UGT-mediated conjugation reaction in the Ph2 incubation system in HLM. Only 66.4 % of the initial 10 μ M SKL remained unchanged. The formation of three glucuronides was observed. Their structures and accordingly the binding site of the

glucuronic acid could be elucidated and thus identified as pO-Glc, sO-Glc and N-Glc. The metabolic stability of SKL during the simultaneous activation of both enzyme systems was 84.9 %. This value is clearly higher than under Ph2 conditions but still lower than in the Ph1 reaction system. Two of the five Ph1 metabolites of SKL did not appear to be formed in the DAA. The formation of the remaining ones was very low (0.0 % to 0.7 %). The kinetic parameters determined show that glucuronide formation of SKL in HLM follows Michaelis-Menten kinetics. The amounts of pO-Glc and sO-Glc formed showed almost no differences between the UGT and DA assay. Compared to 5.1 % N-Glc formed in the Ph2 incubation reaction system, its formation during DAA was significantly lower (1.7 %). The presence of SRF had no effect on the CYP-mediated transformation of SKL in HLM. Under UGT and DAA conditions a decrease of the metabolic stability of SKL was observed. The higher the SRF concentration the more pronounced the reduction. In addition to the relative amount of unchanged SKL, pO-Glc and sO-Glc were formed less when SKL was co-incubated with SRF. However, the N-Glc formation seemed to be induced by the presence of SRF and RGF. Thus, not a single substance but rather a class of compounds seems to be responsible for this induction. However, studies of the N-glucuronidation of TFP in the presence of SRF showed that the enhancing effect only appears to occur in connection with SKL as a substrate. In addition to the influence of SRF on the biotransformation of SKL, an effect of SKL on the conversion of SRF can also be observed. Thus, the presence of SKL results in a higher metabolic stability of SRF under Ph1 conditions and in DAA. The increase in unchanged SRF is mainly due to the decrease in the formation of NOX. This suggests that SKL exhibits inhibitory activity towards CYP3A4.

The metabolic stability of SKL in RLM was 82.0 % under CYP, 85.8 % under UGT conditions and 79.7 % in DAA. Accordingly, SKL in RLM is metabolically degraded to almost the same extent in the Ph1 and Ph2 incubation reaction systems. As in HLM the formation of five Ph1 metabolites was also observed in RLM. Based on the m/z ratios obtained and their retention behaviour, the oxidative reactions of SKL in HLM and RLM most likely resulted in the same metabolites. The UGT-mediated glucuronidation of SKL led to the formation of pO-Glc and sO-Glc in RLM. However, they were formed in significantly lower relative amounts compared to HLM. The conversion of SKL to its glucuronides in RLM did not appear to follow Michaelis-Menten Kinetics. Co-incubation with SRF led to a slightly higher stability of SKL under

CYP conditions. In both the UGT and DA assays no effect on the biotransformation of SKL was observed regardless of the SRF-concentration applied. SKL appears to influence the metabolic transformation of SRF in RLM in each incubation system. Thus, an increase of remaining SRF and consequently increased metabolic stability was observed. Although this increase was only slight, it seemed to be related to the presence of SKL. In contrast to HLM the increased metabolic stability of SRF in the presence of SKL was due to the reduced formation of HOM. Thus, different CYP isoforms are most likely responsible for the conversion of SRF in RLM than in HLM. A potential interaction of SKL on the glucuronidation of SRF in RLM was not investigated as the responsible UGT isoform is not expressed in rats and no glucuronide formation was observed during preliminary studies. In MLM SKL showed a high stability of 89.1 % in the Ph1 incubation reaction system. In contrast with remaining 54.5 % and 50.0 % UGT-mediated metabolic degradation was prominent in Ph2 and DAA systems. Glucuronidation resulted in pO-Glc and sO-Glc whereas the latter being formed with a marked preference. During kinetic analysis of glucuronide formation of SKL in MLM a decrease in V_{max} was observed in the presence of higher substrate concentrations. This suggests substrate or product inhibition of the involved UGT isoforms. The influence of SRF on the metabolic conversion of SKL in MLM was not entirely consistent under UGT conditions. On the one hand the presence of SRF led to a higher metabolic stability of SKL. On the other hand, there was also an increase in the amount of pO-Glc formed, while the relative amount of sO-Glc remained unchanged. The proportion of unchanged SKL also increased in the DAA in the presence of SRF. However, this time a clear decrease in the amounts of both glucuronides formed was observed. The influence of SKL on the metabolic conversion of SRF also appeared to be inhomogeneous. Co-incubation with SKL resulted in increased formation of NOX in the CYP and DA assays. In contrast the formation of HOM seemed to be reduced and DES unchanged. This was also reflected in the decrease in metabolic stability of SRF in the presence of SKL. Furthermore, SKL in MLM appeared to possess an inhibitory effect towards glucuronidation of SRF in both Ph2 and co-activated conditions.

CYP-mediated degradation led to the lowest metabolic stability of SKL in DLM with 76.2 %. Under UGT conditions 83.9 % and after DAA 87.3 % of the initial concentration of 10 μ M SKL remained unchanged. As conjugation products pO-Glc

and sO-Glc were identified. They were formed in almost equal relative amounts of 3.8 % and 3.2 %. The kinetic analysis of their formation showed that it seemed to correspond to the Michaelis-Menten kinetic. The metabolic stability of SKL towards CYP-mediated degradation appeared to be slightly enhanced by the co-incubation of SRF. In contrast, no clear correlation was observed between the presence of SRF and the remaining amount of SKL in the Ph2 and DAA incubation reaction systems. SRF also did not seem to have a significant influence on the glucuronide formation of SKL in both the UGT and DA assays in DLM. CYP-mediated degradation of SRF was enhanced by the presence of SKL and led to increased formation of HOM, while NOX and DES remained unchanged. This was also observed to a lesser extent in DAA. Although the corresponding UGT isoform should be theoretically present no formation of SRF-N-Glc in DLM could be observed. In CMLM, SKL was metabolically degraded mainly by CYP enzymes. The Ph2 and DA assay showed that the UGT-mediated conjugation reaction represents the minor metabolic pathway of SKL. Under UGT conditions the presence of SRF slightly reduced the formation of the two glucuronides pO-Glc and sO-Glc. The metabolic stability of SKL with 74.5 % during co-activation of both enzyme systems was comparable to the 71.3% under Ph1 conditions. In addition, the formation of three SKL Ph1 metabolites was observed during DAA. The presence of SRF seemed to influence their formation. An increased formation of M#1 and M#2 as well as a decreased formation of M#3 could be observed. The amounts of pO-Glc and sO-Glc formed remained unchanged during the simultaneous incubation of SKL with SRF. The kinetic analysis of their formation showed an atypical behaviour which does not correspond to Michaelis-Menten kinetics. CYP-mediated transformation of SRF was marginal affected by co-incubation with SKL. A slight increase of HOM and DES formation was observed by increasing SKL concentration. In contrast to the other species tested, incubation with activated UGTs in CMLM showed a significant SRF-N-Glc formation at 9.0 %. This was reduced to 3.0 % by the presence of SKL and led to a significant increase of SRF's metabolic stability. Any effect of SKL on the remaining amount of unchanged SRF could be observed under DAA conditions. However, the formation of SRF-N-Glc and NOX appeared to be reduced while DES remained unchanged, and HOM appeared to be increased. In almost each species reduced metabolite formation and consequently increased metabolic stability of SKL and SRF could be observed during their co-incubation. These findings can be explained by inhibitory activities and different substrate affinities. However, the

simultaneous incubation of SKL and SRF partly resulted in increased formation of single metabolites and decreased metabolic stability. This stimulatory effect seemed to be particularly pronounced by SRF on the formation of N-Glc in HLM. The possible causes and correlations of the increased metabolic transformation of SKL and SRF are discussed in more detail below.

Reaction phenotyping results indicated that UGT2B7, 1A1, 1A3 and 1A4 were the responsible isoforms for the glucuronidation of SKL. Contributors to the formation of pO-Glc and sO-Glc were UGT2B7, 1A1 and 1A3. The latter two are only involved at high substrate concentrations. The kinetic of SKL-glucuronidation in the presence of rUGT2B7 showed that V_{max} decreased pronouncedly starting at a SKL concentration of about 15 μM and finally stopped at 100 μM . Thus, rUGT2B7 is inhibited either by SKL or its glucuronides. Analysis of HTMC glucuronidation was used to determine whether the substrate or product was responsible for inhibition of UGT2B7. For this purpose, rUGT2B7 was pre-incubated with diclofenac and different concentrations of SKL, pO-Glc and sO-Glc. These analyses clearly showed that SKL inhibits rUGT2B7 in high concentrations. Thus, substrate inhibition was present. The influence of SRF on the formation of pO-Glc and sO-Glc was investigated on rUGT2B7 and rUGT1A1. The higher the SRF concentration, the lower the formation of both glucuronides and the more unchanged SKL remained. SRF thus appears to have significant inhibitory activity against rUGT2B7. Independent of SKL concentration, rUGT1A4 was identified as the sole isoform responsible for N-glucuronidation observed exclusively in HLM. The enzymatic conversion of SKL to N-Glc follows the Michaelis-Menten kinetic. Co-incubation of SKL and SRF with rUGT1A4 clearly showed an influence of SRF on the N-Glc formation. The more concentrated SRF was, the lower the metabolic stability of SKL and the higher the relative amount of N-Glc formed. However, the same experimental conditions with TFP as substrate led to a significant decrease in TFP-N-Glc formation. Thus, the enhancing effect of SRF on N-glucuronidation is dependent on SKL as substrate. The identification of isoforms involved in the metabolic transformation of SKL may help to elucidate the detailed processes of metabolism-based drug-drug interactions between SKL and SRF and explain the results obtained.

A recent article by Karbownik et al. [204] describes that SRF significantly increases the plasma levels of tapentadol *in vivo* when both are administered in combination.

The reason for this is that SRF inhibits the glucuronidation of tapentadol, which is a substrate of UGT1A9 and 2B7. However, this article did not elucidate which and to what extent the two isoforms involved are inhibited by SRF. A detailed UGT inhibition screen of several kinase inhibitors, including SRF, was conducted by Miners et al. [203]. Their studies showed that the inhibitory potency of SRF towards UGT2B7 can be described as moderate with an IC_{50} of about 52 μ M. The results of UGT2B7-mediated transformation *in vitro* of SKL solely and with the addition of SRF are therefore in agreement with the descriptions in the literature. Despite the low inhibitory capacity of SRF towards UGT2B7, its activity is nevertheless expected to be strongly influenced due to the additionally present substrate inhibition of SKL. Thus, the co-therapy of SKL with SRF could result in a significant reduction of the O-glucuronidation of SKL, which in turn would increase SKL exposure. Therefore, it would be advisable to determine in future *in vivo* studies the amount of pO-Glc and sO-Glc formed in plasma as well as in urine and faeces. This could provide insights into how pronounced the impact of SRF on the metabolic conversion of SKL is and what were the consequences on both the therapeutic effect and any side reactions of SKL.

In terms of UGT1A4-mediated N-glucuronidation of SKL, two marked observations emerged whose underlying mechanisms need to be clarified. The first topic involves the stimulatory effect of SRF on N-Glc formation *in vitro*. The increased conversion was observed both with HLM and the isoenzyme rUGT1A4 and appeared to be dependent on SKL as substrate. Enzyme induction is not possible in the test system used as no nucleus and thus no expression was present. Thus, a direct interaction of SRF with UGT1A4 must exist, which results in the increased formation of N-Glc. In addition to negative regulation through inhibition the enzymatic activity can also be increased by ligand binding. This is described as allosteric regulation [205]. The regulatory molecule has a different binding site on the enzyme than the substrate. Distal binding induces a conformational change of the active site which alters e.g., the affinity to the substrate or the conversion rate [206]. However, several substrate binding sites or effector binding sites must be present on the enzyme. The purification and crystallisation of membrane-bound proteins such as mammalian UGTs is very difficult, which is why their three-dimensional structure has not yet been fully elucidated [207]. With the application of two-site models Zhou et. al [194] were able to

show that UGT1A4 appears to possess several aglycone binding sites. In addition, the activation *in vitro* of the catalytic activity of UGT1A4 by a phosphatidylinositol 3-kinase inhibitor was recently described by Gao et. al [208], also assuming a mechanistic two-site model.

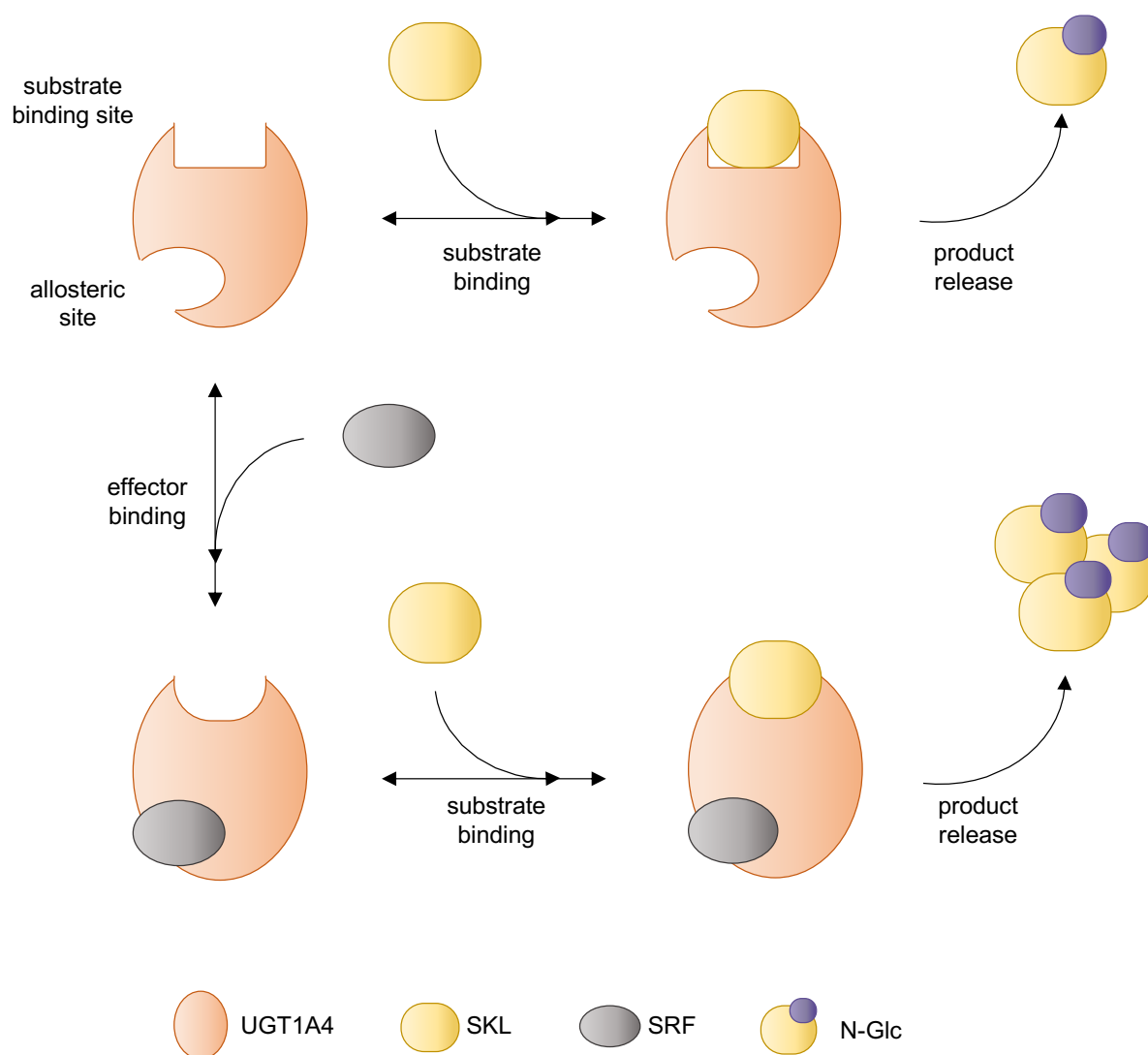


Fig. 91: The binding of SRF to the allosteric site of UGT1A4 leads to conformational changes of the substrate binding site. This alters the functional activity and results in increased N-Glc formation compared to that in the absence of SRF. Graphic adapted from [206].

Based on this information and the results obtained in the present work, it is postulated that SRF acts as a heterotropic allosteric effector with respect to the UGT1A4-mediated conversion of SKL. This means that SRF is not a substrate of UGT1A4 but nevertheless alters its functional activity. As shown schematically in figure 91, the binding of SRF occurs outside the active site, which changes the conformation of the substrate binding site. This structural change thus has an increasing effect on the formation of N-Glc and the associated metabolic degradation of SKL. Thus, SRF

seems to positively regulate the glucuronidation reaction of SKL. Whether this occurs by increasing the affinity for SKL as a substrate or the turnover rate must be clarified in further studies.

The conversion of the neuroleptic TFP is also catalysed by UGT1A4. However, this glucuronidation reaction is affected in a negative way by the presence of SRF. To date, the underlying mechanism of this SRF-induced inhibition has not been elucidated in detail. There might be a competitive inhibition in which SRF and TFP compete for the same binding site on the enzyme [209]. However, it could also be a case of negative allosteric regulation. In this model, the binding of SRF would trigger a conformational change of the active site, which would reduce or prevent the conversion of TFP to TFP-N-Glc by decreasing the affinity or catalytic activity. However, if the mechanism of inhibition remains unclear, this can only be speculated.

Numerous new insights into the metabolic *in vitro* transformation of SKL were gained through the metabolism studies performed in the present work. The isoenzymes involved were identified and their kinetic parameters determined. In addition, metabolism-based drug-drug interactions of SKL and SRF were detected and suggestions for the underlying mechanisms were proposed.

3.6. Excretion of Skepinone-L *in vivo*

In addition to metabolism, the excretion of a substance is also part of its pharmacokinetic evasion phase. This ends with the final removal from the organism. The xenobiotic can be excreted both intact and chemically modified in the form of its metabolites. While hydrophilic substances are mainly excreted in the urine, biliary excretion is the main route of elimination of lipophilic substances. The route of excretion can therefore provide further information on the pharmacokinetic behaviour. Since diseases of the corresponding elimination sites can influence the excretion and thus the therapeutic efficacy or toxicity of a drug, knowledge of the corresponding excretion pathways is essential. Drug-drug interactions can also affect the retention time of a substance in the organism.

Since SKL has lipophilic properties ($\log D_{\text{predict}} = 4.25$) and a molecular weight greater than 300 g/mol, the absorbed but chemically unchanged portion will most likely be excreted mainly via the bile [210]. This route of elimination includes, in addition to direct excretion in faeces, the possibility of resorption and thus enterohepatic recycling [139]. This could increase exposure, which in turn would have to be taken into account in the dosing interval [211]. As described in chapter 3.5, conjugation with glucuronic acid is the main pathway of metabolic conversion of SKL *in vitro*. The resulting glucuronides are most likely excreted renally in the urine due to their hydrophilic properties. To investigate these assumptions, SKL and its glucuronides were quantitatively determined in mouse faeces.

3.6.1. Skepinone-L and its Glucuronides in Mouse Faeces

For the quantitative determination of SKL and its glucuronides, the faeces of mice excreted over 24 hours were collected. At the time of sampling, these animals had already been treated with 10 mg/kg/day SKL for 10 months. Since the administration was oral, the amount of SKL consumed within 24 hours was also determined. In total, the faeces of three groups (I, II, III) of 5 mice each (C57BL/6) were examined. Groups I and II consisted of females and group III of males. The exact procedure for extracting SKL and its glucuronides from mouse faeces as well as the analytical method used are described in chapter 5.2.10.

group		within 24 h			% of administered SKL dose in faeces		
		food [g]	SKL [mg]	faeces [g]	SKL	pO-Glc	sO-Glc
I	♀	10.16	1.016	1.047	7.1	0.06	0.06
II	♀	10.73	1.073	1.443	8.5	0.10	0.10
III	♂	12.21	1.221	1.525	15.0	0.21	0.29

Tab. 61: Overview of the amount of food, thus SKL eaten within 24 h by each of the three groups examined. Further, the amount of excreted faeces and the percentages of SKL, pO-Glc and sO-Glc from the administered dose contained therein are given.

The results (Tab. 61) show that the mouse faeces contained SKL as well as pO-Glc and sO-Glc. The total quantity of SKL in the faeces of group I was 72 µg, 91 µg of II and 184 µg of group III. This corresponds to a percentage share of 7.1 % (I), 8.5 % (II) and 15.0 % (III) of the administered SKL dosage. The determined amount of pO-Glc was 0.9 to 3.6 µg which corresponds to 0.06 % to 0.21% of the ingested SKL dose. The quantity of sO-Glc excreted in faeces was marginally higher at 0.9 to 5.0 µg which

corresponds to 0.6 % to 0.29 % of the administered dosage of SKL. The very low amounts of O-glucuronides in the faeces confirms the assumption that they are mainly excreted via the kidneys due to their polar properties. The percentage of unchanged SKL excreted in faeces is relatively low. Accordingly, at least 85 % of the administered dose would have to be metabolically converted. Within the scope of the *in vitro* metabolism studies conducted in the present work, a low metabolic stability as well as very high relative amounts of glucuronides formed in MLM were observed for SKL. This correlates with the determined percentages in mouse faeces. To verify whether the remaining 85 % of the applied SKL quantity is actually excreted as glucuronides, the analysis of mouse urine is necessary. Since this was unfortunately not available within the experimental setup used in the present work, further investigations must be performed. However, both the results of the *in vitro* metabolism studies and the determination of the SKL concentration in mouse faeces lead to the conclusion that the mouse does not have comparable behaviour to humans regarding the metabolic conversion of SKL. Thus, extrapolation from mice to humans to predict the pharmacokinetics of SKL is not directly possible, and mice are rather unsuitable as an animal model for this question.

4. CONCLUSION

In the present study, the ADME profile of SKL was comprehensively investigated and elucidated. A selective LC-MS/MS method was developed for the reliable quantification of SKL and SRF both individually and simultaneously from plasma of rats, dogs, monkeys and humans. This method was validated according to the FDA "bioanalytical method validation" and ICH "validation of analytical procedures" guidelines with respect to sensitivity, linearity, accuracy, precision and reproducibility. The results of the validation were always within the acceptance criteria, so that the method clearly fulfilled all requirements.

The analysis of the plasma samples from the pharmacokinetic studies of SKL in rats, dogs and monkeys was performed with the method developed. The obtained plasma concentration-time profiles (Previous section 3.3) were used to calculate the pharmacokinetic parameters by both non-compartmental and two-compartmental analysis. These parameters (Tab. 62 and 63, upcoming section 4.1) show that the absorption of SKL was extensive in all species, which led to partly very high C_{max} . This is also illustrated by the mean pharmacokinetic profiles of SKL in rats, dogs and monkeys obtained after p.o. administration (Fig. 92).

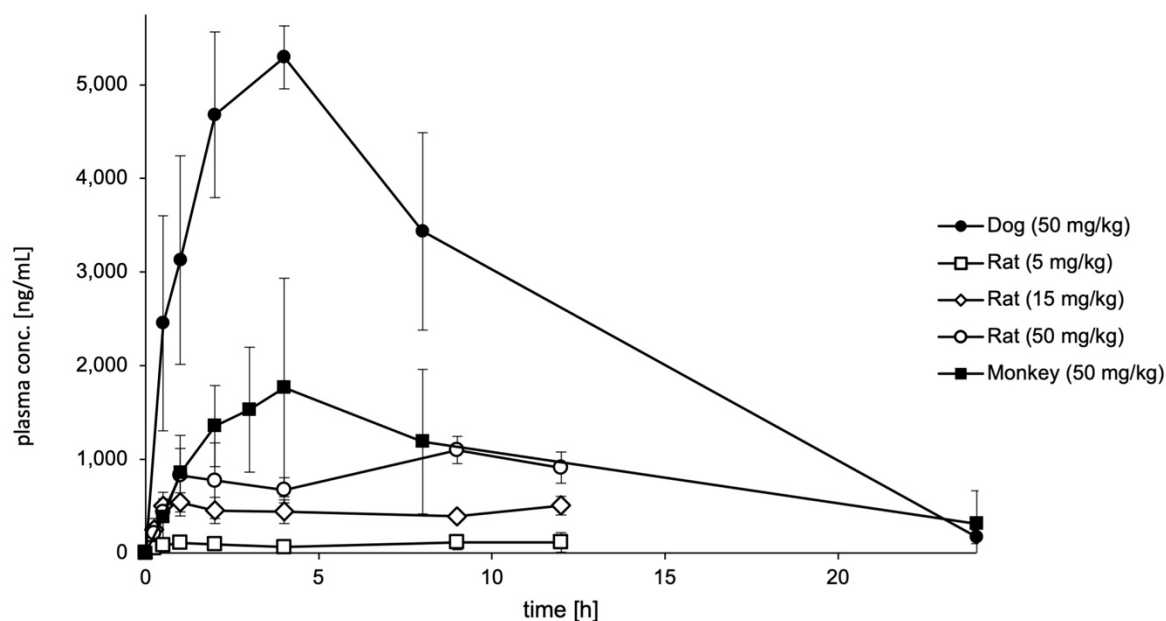


Fig. 92: Mean plasma concentration vs. time profiles of SKL following p.o. administration of 50 mg/kg SKL in dogs, 5, 15 and 50 mg/kg SKL in rats and 50 mg/kg SKL in monkeys. The respective standard deviation is represented by error bars.

During the combined treatment of SKL and SRF in rats a positive influence of SRF on the pharmacokinetic behaviour of SKL after repetitive oral administration was observed (Tab. 64, upcoming section 4.1). The parameters derived from the plasma profiles indicated that SKL was strongly bound to plasma proteins *in vivo*. However, a mutual influence of SRF and SKL on each other's plasma protein binding could not be observed.

The metabolic profile of SKL was elucidated by incubations in LM of different species. Both CYP-mediated degradation and UGT-mediated degradation were analysed individually and in combination. There were clear differences between the species. SKL was stable against CYP-mediated degradation in HLM, RLM and MLM, whereas strong oxidative degradation was observed in DLM and CMLM. In contrast, UGT-mediated transformation showed an opposite picture. In RLM, DLM and CMLM, SKL was metabolically stable, whereas in HLM and MLM, a very strong conjugation of SKL with glucuronic acid was observed. Incubations using both enzyme systems simultaneously confirmed that SKL is almost exclusively subject to UGT-mediated degradation in human microsomes. Co-incubations of SKL and SRF showed a mutual influence on metabolic transformation in all species. Thus, the presence of SRF in the presence of CYP enzymes led to increased stability of SKL in all LM. Interestingly,

UGT-mediated degradation was only affected in human liver microsomes, where a significant decrease in the stability of SKL was observed. In the dual system, the presence of SRF in all animal species led predominantly to an increase in the remaining relative proportion of SKL, whereas in HLM there was repeatedly increased metabolic degradation.

While two glucuronides were formed in all animal species, the formation of three conjugation products was observed in human microsomes. By means of incubations with derivatives of SKL, it was possible to elucidate the structures of all three glucuronides (po-Glc, sO-Glc and N-Glc). During this work it was found that the N-Glc was exclusively formed in HLM, and its formation was even increased by the presence of SRF. This was identified as the main reason for the increased degradation of SKL. Following the structural elucidation of the metabolites, the isoenzymes involved in the catalytic conversion were identified. These were determined by reaction phenotyping with 8 recombinant UGT isoenzymes. The isoenzymes involved as well as the resulting structures of the SKL-glucuronides are shown in the following figure 93.

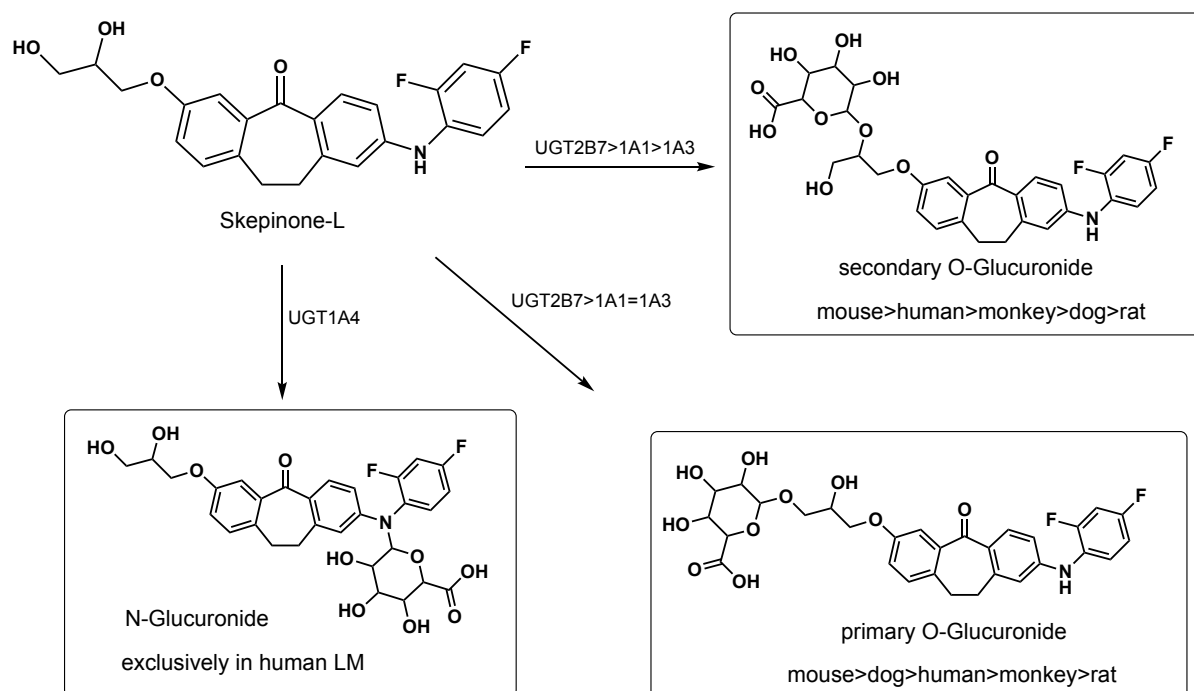


Fig. 93: Schematic pathway of the metabolic conversion of SKL into its glucuronides, the contributing isoenzymes and the respective species.

Studies with RGF and TFP revealed that the inducing effect of SRF on N-Glc formation is due to regulations directly on the isoenzyme. This is most likely an allosteric activation of UGT1A4 by SRF. However, this positive regulation appears to apply only

to SKL as a substrate, inhibiting the conversion of other substrates. Due to their high polarity, glucuronides of SKL are supposed to be excreted preliminary via the kidney and thus the urine, while unchanged SKL most likely leaves the organism via faeces.

4.1. Synopsis of Results

4.1.1. Pharmacokinetic behaviour of Skepinone-L *in vivo*

single bolus injection of SKL

species		dose (SKL) [mg/kg]	C ₀ [ng/mL]	t _{1/2} [h]	AUC _{0-t} [ng·h/mL]	V _{ss} [L/kg]	Cl [L/h/kg]
mouse	♂	0.4	186; 218	3.1; 4.3	291; 327	3.3; 3.5	1.2; 1.4
dog	♂	5	2,912; 3,782	3.3; 3.9	12,948; 18,254	1.4; 1.6	0.3; 0.4
	♀	5	2,137; 2,715	3.7	10,600; 14,306	1.6; 2.2	0.4; 0.5
rat	♂	3	4,288	1.4	11,085	0.9	0.4
		5*	3,573	1.9	7,776	1.6	0.6
		10	5,341; 9,710	0.6; 1.9	4,677; 16,405	1.2; 1.4	0.6; 1.5

Tab. 62: Summary of the pharmacokinetic parameters of SKL in mice, dogs and rats following intravenous administration. *only one value for each parameter available in this dose group

single oral administration of SKL

species		dose (SKL) [mg/kg]	C _{max} [ng/mL]	t _{max} [h]	t _{1/2} [h]	AUC _{0-t} [ng·h/mL]
mouse	♂	1.2	188; 206	0.5	2.8; 3.3	670; 773
	♀	10	1,346	0.8	1.3	3,095
dog	♂	50	4,969; 5,257	4.0	3.9; 4.1	41,976; 61,249
	♀	50	5,099; 6,025	2.0; 4.0	3.4; 4.5	69,832; 76,021
rat	♂	5	175	5.0	8.6	1,112
		15	586	4.5	35.0; 37.7	5,217
		50	1,210	6.3	54.9*	10,011
monkey	♂	50	1,502; 3,672	2.0; 4.0	4.5; 5.5	14,079; 39,826
	♀	50	744; 1,718	1.0; 4.0	6.4; 24.1	8,336; 27,976

Tab. 63: Summary of the pharmacokinetic parameters of SKL in mice, dogs, rats, monkeys and humans following single oral administration. *only one value available

repetitive oral administration of SKL in rats

gender	SKL dose [mg/kg]	SRF dose [mg/kg]	C _{max} [ng/mL]	t _{max} [h]	t _{1/2} [h]	AUC _{0-t} [ng·h/mL]
♂	15	-/-	1,310	6.7	8.4	16,398
	15	25	5,410	2.7	3.1	58,928
	50	-/-	1,933	9.0	11.1	32,293
	50	25	11,415	1.3	8.5	123,196
	50*	25	7,133	1.7	9.0	82,994
♀	15	-/-	2,015	3.8	13.9	42,428
	15	25	6,792	1.0	9.0	72,001
	50	-/-	5,277	4.0	18.4	81,942
	50	25	13,970	2.3	7.6	164,996
	50*	25	13,798	1.7	12.3	178,453

Tab. 64: Summary of the pharmacokinetic parameters of SKL in rats following repetitive oral administration of SKL solely and combined with SRF. * treatment order: SRF first, SKL second

4.1.2. Pharmacokinetic behaviour of Sorafenib *in vivo*

single oral administration of SRF

species	dose (SRF) [mg/kg]	C _{max} [ng/mL]	t _{max} [h]	t _{1/2} [h]	AUC _{0-t} [ng·h/mL]
monkey ♂	50	2,866; 3,246	8.0	N/A	42,007; 52,527
monkey ♀	50	2,349; 6,348	4.0; 8.0	7.6*	34,868; 85,816

Tab. 65: Summary of the pharmacokinetic parameters of SRF in monkeys following single oral administration. *only one value available

repetitive oral administration of SRF in rats

gender	SRF dose [mg/kg]	SKL dose [mg/kg]	C _{max} [ng/mL]	t _{max} [h]	t _{1/2} [h]	AUC _{0-t} [ng·h/mL]
♂	25	-/-	16,578	5.0	16.4	250,141
	25	15	16,283	7.3	20.6	285,009
	25	50	13,718	2.7	23.0	240,040
	25*	50*	25,289	6.7	17.2	439,002
♀	25	-/-	28,625	3.3	34.7	489,594
	25	15	25,284	4.0	30.4	460,585
	25	50	16,000	5.7	84.2	327,473
	25*	50*	32,049	3.3	40.3	601,501

Tab. 66: Summary of the pharmacokinetic parameters of SRF in rats following repetitive oral administration of SRF solely and combined with SKL. *treatment order: SRF first, SKL second

4.1.3. Metabolic Stability and Transformation of Skepinone-L *in vitro*

metabolic stability of SKL [%] in liver microsomes

microsomes	SKL 10 µM			with	SRF 5 µM			10 µM			20 µM			40 µM		
	CYP	UGT	DAA		CYP	UGT	DAA	CYP	UGT	DAA	CYP	UGT	DAA	CYP	UGT	DAA
HLM	95.0	66.4	84.9		95.6	63.7	81.1	94.1	61.3	76.6	94.0	51.1	70.5	95.3	41.7	63.0
RLM	82.0	85.8	79.7		81.6	86.4	81.2	82.0	83.6	82.9	83.7	86.6	82.4	85.6	83.8	82.1
MLM	89.1	54.5	50.0		87.8	57.4	55.3	88.4	56.4	55.4	89.0	55.4	58.0	89.7	59.4	57.9
DLM	76.2	83.9	87.3		76.4	84.6	90.4	79.3	85.6	88.5	84.2	83.6	89.1	90.2	85.2	91.2
CMLM	71.3	88.7	74.5		72.1	88.2	75.0	74.0	88.9	77.1	81.5	88.8	78.2	85.6	91.8	79.4

Tab. 67: Metabolic stability [%] of 10 µM SKL after 120 min incubation solely and in the presence of 5, 10, 20 or 40 µM SRF. Incubations were performed in HLM, RLM, MLM, DLM and CMLM. In each, the microsomal CYP and UGT enzyme systems were activated, either individually or in combination (DAA).

SKL-metabolite formation [%] in liver microsomes

metabolite	microsomes	SKL 10 µM		with	SRF 5 µM		10 µM		20 µM		40 µM	
		UGT	DAA		UGT	DAA	UGT	DAA	UGT	DAA	UGT	DAA
pO-Glc [%]	HLM	3.5	3.6		2.4	3.4	2.8	2.8	2.0	2.9	2.2	2.8
	RLM	1.8*	1.5		1.9*	1.9	1.8*	1.8	2.4*	1.6	1.8*	1.7
	MLM	7.3	20.1		7.6	19.0	7.8	17.6	8.2	18.1	8.5	18.5
	DLM	3.8	3.9		4.5	3.9	4.8	3.7	5.0	3.3	4.7	3.0
	CMLM	3.1	1.9		3.6	1.9	2.0	1.7	2.6	2.1	2.6	2.2
sO-Glc [%]	HLM	7.4	8.3		6.2	7.5	6.0	6.1	5.5	6.0	4.8	6.1
	RLM	-/-	2.8		-/-	2.7	-/-	3.5	-/-	2.0	-/-	1.8
	MLM	44.1	82.6		47.3	79.6	47.5	76.1	46.8	74.3	45.9	65.7
	DLM	3.2	3.9		4.0	4.1	4.4	3.7	4.4	3.8	4.3	3.3
	CMLM	6.0	3.1		6.7	3.0	3.5	2.7	4.4	3.5	4.1	3.8
N-Glc [%]	HLM	5.1	1.7		5.8	3.3	7.6	4.3	9.4	7.6	13.0	12.9

Tab. 68: Formation of SKL metabolites [%] after 120 min incubation of 10 µM SKL solely and in the presence of 5, 10, 20 or 40 µM SRF. Incubations were performed in HLM, RLM, MLM, DLM and CMLM. In each, the UGT enzyme system was activated, individually or in co-activation with the microsomal CYPs (DAA). *sum amount formed [%] of pO- and sO-Glc

metabolic stability and metabolite formation [%] of SKL in the presence of recombinant UGTs

analyte	SKL 10 μ M			with	SRF 10 μ M			40 μ M		
	rUGT1A1	rUGT1A4	rUGT2B7		rUGT1A1	rUGT1A4	rUGT2B7	rUGT1A1	rUGT1A4	rUGT2B7
	SKL [%]	94.5	88.2		91.7	97.1	79.9	94.4	99.9	73.2
pO-Glc [%]	0.4	0.0	2.2	0.0	0.0	2.2	0.0	0.0	0.5	
sO-Glc [%]	1.1	0.0	2.6	0.3	0.0	2.6	0.0	0.0	0.6	
N-Glc [%]	0.0	4.2	0.0	0.0	6.9	0.0	0.0	12.4	0.0	

Tab. 69: Metabolic stability and metabolite formation of SKL [%] after 60 min incubation of 10 μ M SKL solely and in the presence of 10 or 40 μ M SRF. Incubations were performed with rUGT1A1, rUGT1A4 and rUGT2B7.

4.1.4. Influence of Skepinone-L on the Metabolic Stability and Transformation of Sorafenib *in vitro***metabolic stability of SRF [%] in liver microsomes**

microsomes	SRF 10 μ M			with	SKL 5 μ M			10 μ M			20 μ M			40 μ M		
	CYP	UGT	DAA		CYP	UGT	DAA	CYP	UGT	DAA	CYP	UGT	DAA	CYP	UGT	DAA
	HLM	52.6	95.2		62.4	49.3	95.6	64.2	51.2	93.9	68.0	54.2	96.2	75.4	59.1	94.3
RLM	78.3	-/-	82.0	80.1	-/-	83.1	80.9	-/-	86.2	82.1	-/-	84.5	84.2	-/-	89.2	
MLM	83.2	46.2	56.4	79.4	46.8	58.0	78.5	46.2	53.5	79.3	48.8	53.5	78.3	53.8	57.1	
DLM	85.2	96.7	87.9	82.7	96.3	87.6	82.4	98.1	89.5	83.2	99.4	88.6	78.7	98.0	88.7	
CMLM	55.8	67.2	72.4	57.7	70.3	71.2	55.5	75.2	69.5	61.5	84.2	71.6	60.7	86.2	73.8	

Tab. 70: Metabolic stability [%] of 10 μ M SRF after 120 min incubation solely and in the presence of 5, 10, 20 or 40 μ M SKL. Incubations were performed in HLM, RLM, MLM, DLM and CMLM. In each, the microsomal CYP and UGT enzyme systems were activated, either individually or in combination (DAA).

oxidative SRF-metabolite formation [%] in liver microsomes

metabolite	microsomes	SRF		SKL		10 µM		20 µM		40 µM	
		10 µM	DAA	5 µM	DAA	CYP	DAA	CYP	DAA	CYP	DAA
NOX [%]	HLM	11.1	10.8	11.2	11.2	11.9	11.4	11.0	10.6	8.7	7.8
	RLM	0.4	0.2	0.4	0.2	0.4	0.3	0.4	0.2	0.6	0.2
	MLM	0.8	0.4	1.4	0.9	2.3	1.3	3.4	2.4	4.2	3.9
	DLM	0.1	0.0	0.1	0.0	0.1	0.0	0.2	0.0	0.2	0.0
	CMLM	7.7	6.3	9.1	6.5	7.2	6.1	9.9	6.3	8.4	5.1
HOM [%]	HLM	4.9	4.9	4.7	5.2	5.3	5.3	5.5	5.2	4.5	4.3
	RLM	1.7	2.9	1.5	2.6	1.4	2.3	1.3	2.3	1.3	1.9
	MLM	3.0	4.1	2.4	4.0	2.2	3.7	2.4	3.1	2.0	2.8
	DLM	2.7	2.1	2.7	2.1	3.7	2.6	3.9	2.6	4.0	2.8
	CMLM	3.3	4.0	4.2	4.1	3.4	3.8	5.6	4.8	6.7	4.7
DES [%]	HLM	0.6	0.2	0.6	0.2	0.7	0.2	0.7	0.2	0.6	0.2
	RLM	0.3	0.1	0.3	0.2	0.2	0.1	0.2	0.1	0.3	0.2
	MLM	0.6	0.3	0.5	0.4	0.5	0.4	0.6	0.4	0.5	0.4
	DLM	0.2	0.0	0.3	0.0	0.3	0.0	0.3	0.0	0.4	0.0
	CMLM	0.9	0.4	1.0	0.4	0.9	0.3	1.2	0.3	1.3	0.3

Tab. 71: Formation of SRF oxidative metabolites [%] after 120 min incubation of 10 µM SRF solely and in the presence of 5, 10, 20 or 40 µM SKL. Incubations were performed in HLM, RLM, MLM, DLM and CMLM. In each, the CYP enzyme system was activated, individually or in co-activation with the microsomal UGTs (DAA).

SRF-glucuronide formation [%] in liver microsomes

metabolite	microsomes	SRF		SKL		10 µM		20 µM		40 µM	
		10 µM	DAA	5 µM	DAA	UGT	DAA	UGT	DAA	UGT	DAA
SRF-Glc [%]	HLM	0.9	0.1	1.4	0.2	0.7	0.1	0.9	0.1	0.7	0.1
	MLM	17.5	5.8	16.5	5.6	15.5	5.2	15.2	4.5	13.3	4.1
	DLM	0.0	0.0	0.0	0.0	0.0	0.0	0.0	0.0	0.0	0.0
	CMLM	9.0	1.1	8.1	1.0	5.9	0.7	4.6	0.7	3.0	0.5

Tab. 72: Formation of SRF-Glc [%] after 120 min incubation of 10 µM SRF solely and in the presence of 5, 10, 20 or 40 µM SKL. Incubations were performed in HLM, MLM, DLM and CMLM. In each, the UGT enzyme system was activated, individually or in co-activation with the microsomal CYPs (DAA).

4.2. Outlook

In summary, a lot of knowledge and information regarding the ADME profile of SKL has been gained through the present work. This in turn has led to some new questions that need to be clarified in future studies. For example, it should still be determined whether and to what extent SKL is an inhibitor of CYP3A4 and UGT1A9. In addition, the chemical synthesis of N-Glc is still needed to verify the postulated structure and to examine whether it is pharmacologically active. Since SKL has no prerequisite for the formation of potentially toxic acyl glucuronides, a toxic effect from N-Glc is not to be expected. Furthermore, the quantitative determination of glucuronides in human urine and faeces after oral administration is required to fully elucidate the excretion route of SKL. In addition, the potential influence of SRF on the biotransformation and thus excretion of SKL *in vivo* should be investigated by urine and faeces analyses after simultaneous administration. To test the hypothetical allosteric activation of UGT1A4 by SRF dependent on SKL as substrate, incubations on the isoenzyme at different SKL concentrations are still required. In addition, it would be interesting to clarify whether the positive regulatory influence of SRF is only present with SKL as a substrate or if this also applies to the conversion of other substrates and would be of pharmacological benefit.

4.3. Summary

The results obtained in the present thesis regarding the pharmacokinetics and biotransformation of SKL *in vitro* and *in vivo* as well as the identified interactions of SKL and SRF clearly show that a successful completion of the clinical trials of the targeted combinatory therapy with SKL and SRF can be expected with a high degree of probability. Thus, in conclusion, the proposition of a promising therapeutic approach for the treatment of HCC can be confirmed from a pharmacological perspective.

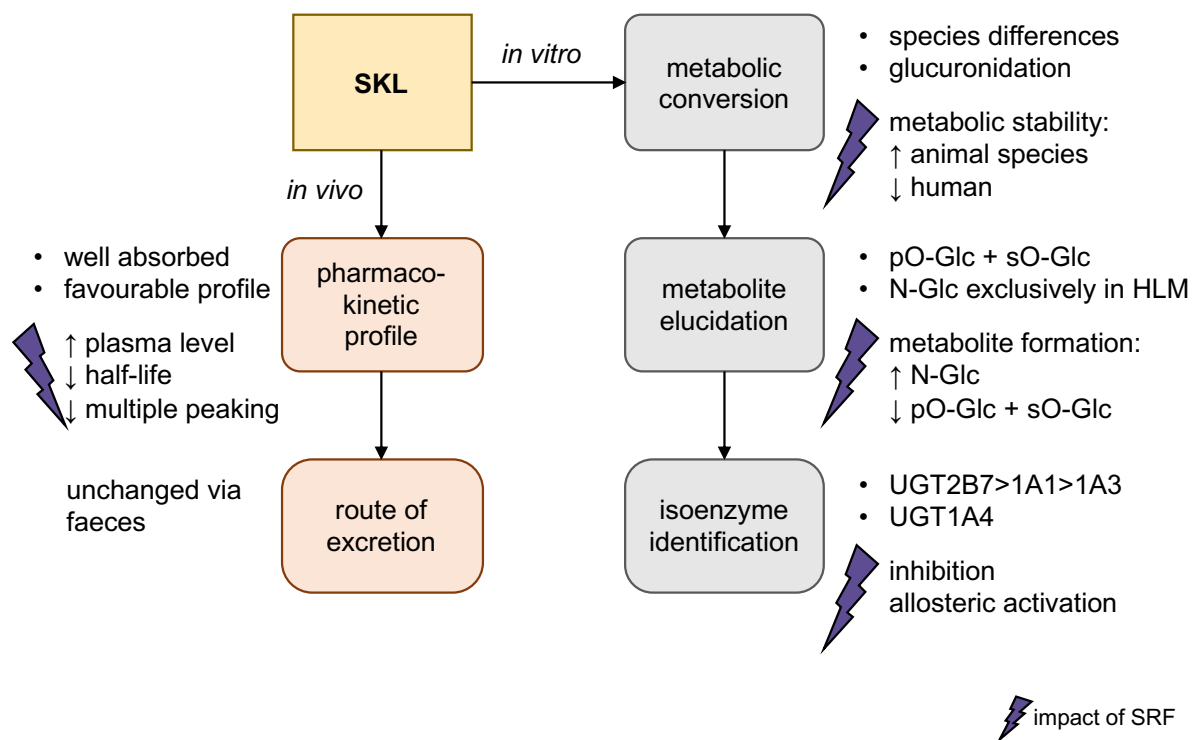


Fig. 94: Schematic representation of the obtained results regarding the pharmacokinetic profile of SKL *in vitro* and *in vivo* and the influence of SRF.

5. MATERIAL AND METHODS

5.1. Material

5.1.1. Biological Material

Beagle dog plasma	Envigo, Horst (NL)
C57BL/6 mouse plasma	Envigo, Horst (NL)
Cynomolgus monkey plasma	CiToxLab, Evreux (FR)
Human plasma	blood donation centre, Tübingen
Sprague Dawley rat plasma	Envigo, Horst (NL)

5.1.2. Chemicals and Reagents

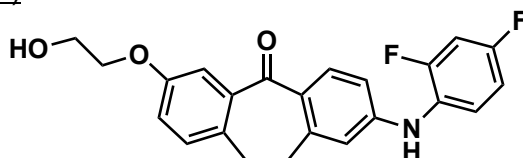
Acetonitrile	Fisher Scientific, Loughborough (GB)
Alamethicin	Sigma Aldrich, St. Louis (US)
Bovine serum albumin	VWR International, Darmstadt
Dimethylsulfoxide	Carl Roth, Karlsruhe
Formic acid	Carl Roth, Karlsruhe
Glucose-6-phosphate	Sigma Aldrich, St. Louis (US)
Glucose-6-phosphate dehydrogenase	Roche Diagnostics, Mannheim
Heparin sodium injection	Braun Melsungen, Melsungen
Hydroxy-4-(trifluoromethyl)coumarin	Tokyo Chemical Industry, Tokyo (JP)
Magnesium chloride hexahydrate	VWR International, Darmstadt
Methylcellulose	Sigma Aldrich, St. Louis (US)
N-Methylpyrrolidone	Sigma Aldrich, St. Louis (US)
Nicotinamide adenine dinucleotide-phosphate	Sigma Aldrich, St. Louis (US)

Polyethylene glycol 400	Sigma Aldrich, St. Louis (US)
Polysorbate 80	VWR International, Darmstadt
Propylene glycol	VWR International, Darmstadt
Saccharic acid 1,4-lactone monohydrate	Sigma Aldrich, St. Louis (US)
Trifluoperazine dihydrochloride	Sigma Aldrich, St. Louis (US)
Trizma® Base	Sigma Aldrich, St. Louis (US)
Trizma® hydrochloride	Sigma Aldrich, St. Louis (US)
Uridine 5'-diphosphoglucuronic acid-trisodium salt	Sigma Aldrich, St. Louis (US)
Ultra pure Water	in-house ELGA PureLab Ultra purification system

5.1.3. Test and Reference Compounds

FS112 (Internal Standard)

Structure:



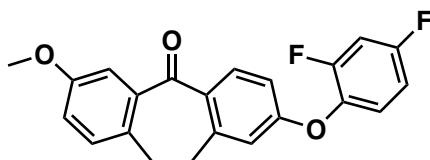
IUPAC nomenclature: 2-((2,4-difluorophenyl)amino)-7-(2-hydroxyethoxy)-10,11-dihydro-5H-dibenzo[a,d][7]annulen-5-one

Chemical formula: $C_{23}H_{19}F_2NO_3$

Molecular weight: 395.41 g/mol

FS332

Structure:



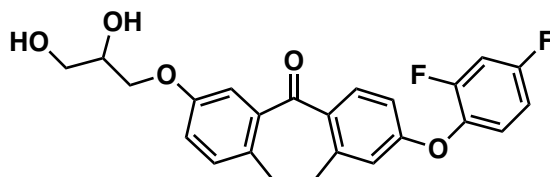
IUPAC nomenclature: 2-(2,4-difluorophenoxy)-7-methoxy-10,11-dihydro-5H-dibenzo[a,d][7]annulen-5-one

Chemical formula: $C_{22}H_{16}F_2O_3$

Molecular weight: 366.36 g/mol

FS352

Structure:



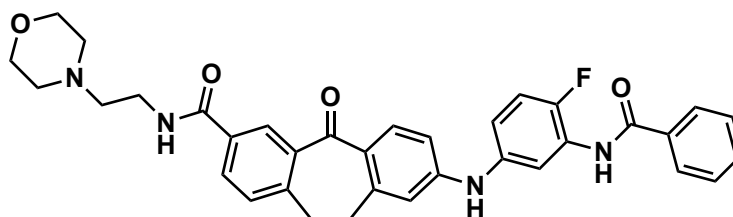
IUPAC nomenclature: 2-(2,4-difluorophenoxy)-7-(2,3-dihydroxypropoxy)-10,11-dihydro-5H-dibenzo[a,d][7]annulen-5-one

Chemical formula: $C_{24}H_{20}F_2O_5$

Molecular weight: 426.42 g/mol

FS694

Structure:



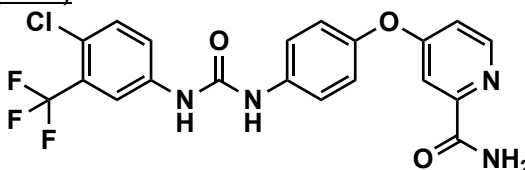
IUPAC nomenclature: 8-((3-benzamido-4-fluorophenyl)amino)-N-(2-morpholinoethyl)-5-oxo-10,11-dihydro-5H-dibenzo[a,d][7]annulene-3-carboxamide

Chemical formula: $C_{35}H_{33}FN_4O_4$

Molecular weight: 592.67 g/mol

N-Desmethyl Sorafenib (DES)

Structure:



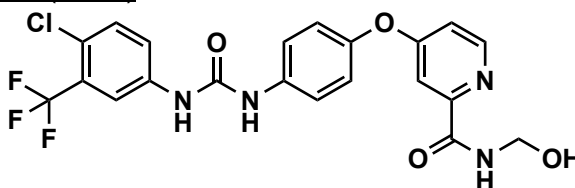
IUPAC nomenclature: 4-(4-(3-(4-chloro-3-(trifluoromethyl)phenyl)ureido)phenoxy)picolinamide

Chemical formula: $C_{20}H_{14}ClF_3N_4O_3$

Molecular weight: 450.80 g/mol

N-Hydroxymethyl Sorafenib (HOM)

Structure:



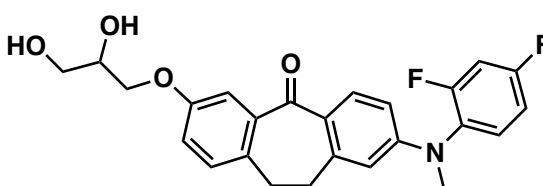
IUPAC nomenclature: 4-(4-(3-(4-chloro-3-(trifluoromethyl)phenyl)ureido)phenoxy)-N-(hydroxymethyl)picolinamide

Chemical formula: $C_{21}H_{16}ClF_3N_4O_4$

Molecular weight: 480.83 g/mol

N-Methyl-Skepinone-L

Structure:



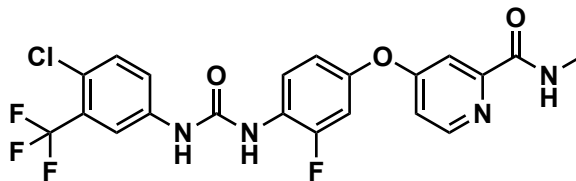
IUPAC nomenclature: 2-((2,4-difluorophenyl)(methyl)amino)-7-(2,3-dihydroxy-propoxy)-10,11-dihydro-5H-dibenzo[a,d][7]annulene-5-one

Chemical formula: $C_{25}H_{23}F_2NO_4$

Molecular weight: 439.46 g/mol

Regorafenib (RGF)

Structure:



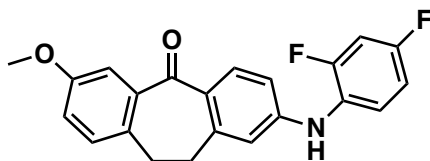
IUPAC nomenclature: 4-(4-(3-(4-chloro-3-(trifluoromethyl)phenyl)ureido)-3-fluorophenoxy)-N-methylpicolinamide

Chemical formula: $C_{21}H_{15}ClF_4N_4O_3$

Molecular weight: 482.82 g/mol

SK558

Structure:



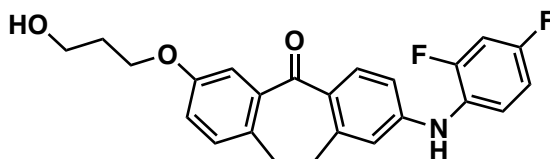
IUPAC nomenclature: 2-((2,4-difluorophenyl)amino)-7-methoxy-10,11-dihydro-5H-dibenzo[a,d][7]annulen-5-one

Chemical formula: $C_{22}H_{17}F_2NO_2$

Molecular weight: 365.38 g/mol

SK845

Structure:



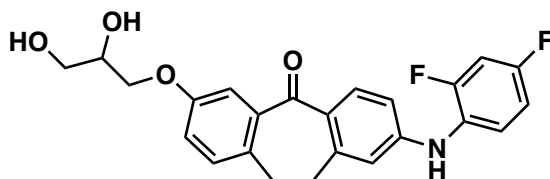
IUPAC nomenclature: 2-((2,4-difluorophenyl)amino)-7-(3-hydroxypropoxy)-10,11-dihydro-5H-dibenzo[a,d][7]annulen-5-one

Chemical formula: $C_{24}H_{21}F_2NO_3$

Molecular weight: 409.43 g/mol

Skepinone-L (SKL)

Structure:



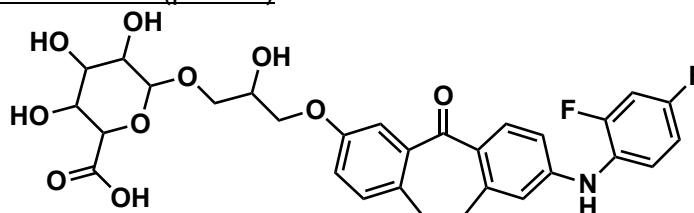
IUPAC nomenclature: 2-((2,4-difluorophenyl)amino)-7-(2,3-dihydroxypropoxy)-10,11-dihydro-5H-dibenzo[a,d][7]annulen-5-one

Chemical formula: $C_{24}H_{21}F_2NO_4$

Molecular weight: 425.43 g/mol

Skepinone-L primary O-Glucuronide (pO-Glc)

Structure:



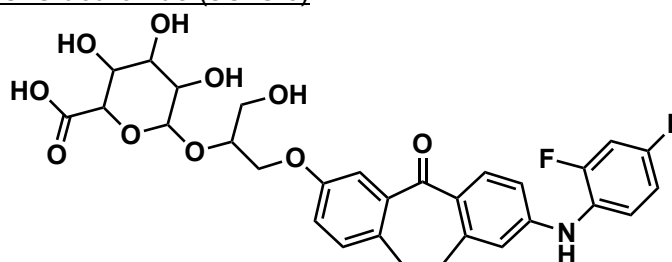
IUPAC nomenclature: 6-(3-((8-((2,4-difluorophenyl)amino)-5-oxo-10,11-dihydro-5H-dibenzo[a,d][7]annulen-3-yl)oxy)-2-hydroxypropoxy)-3,4,5-trihydroxytetrahydro-2H-pyran-2-carboxylic acid

Chemical formula: $C_{30}H_{29}F_2NO_{10}$

Molecular weight: 601.56 g/mol

Skepinone-L secondary O-Glucuronide (sO-Glc)

Structure:



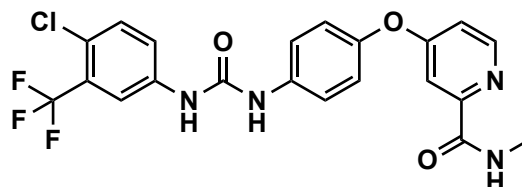
IUPAC nomenclature: 6-((1-((8-((2,4-difluorophenyl)amino)-5-oxo-10,11-dihydro-5H-dibenzo[a,d][7]annulen-3-yl)oxy)-3-hydroxypropan-2-yl)oxy)-3,4,5-trihydroxytetrahydro-2H-pyran-2-carboxylic acid

Chemical formula: $C_{30}H_{29}F_2NO_{10}$

Molecular weight: 601.56 g/mol

Sorafenib (SRF)

Structure:



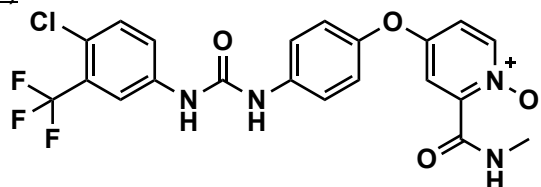
IUPAC nomenclature: 4-(4-(3-(4-chloro-3-(trifluoromethyl)phenyl)ureido)phenoxy)-N-methylpicolinamide

Chemical formula: $C_{21}H_{16}ClF_3N_4O_3$

Molecular weight: 464.83 g/mol

Sorafenib-N-Oxide (NOX)

Structure:



IUPAC nomenclature: 4-(4-(3-(4-chloro-3-(trifluoromethyl)phenyl)ureido)phenoxy)-2-(methylcarbamoyl)pyridine 1-oxide

Chemical formula: $C_{21}H_{16}ClF_3N_4O_4$

Molecular weight: 480.83 g/mol

5.1.4. Consumables

Micro inserts	Macherey-Nagel, Dueren
Pipette Tips	Eppendorf, Hamburg
Reaction tubes	Eppendorf, Hamburg
RED plate with inserts	Thermo Scientific Pierce, Rockford (US)
Vacutainer Li-Heparine	Sarstedt, Nümbrecht
Vials and caps	Macherey-Nagel, Dueren

5.1.5. Apparatus

Alliance 2695 separations module	Waters, Eschborn
Analytical balance MSA6.6S	Sartorius, Göttingen
Centrifuge Universal 32-R	Hettich, Tuttlingen
Incubator	Heidolph, Schwabach
pH meter	Mettler-Toleda, Gießen
Pipets	Eppendorf, Hamburg
Quattro micro™ API with an ESI-probe	Waters, Eschborn
Thermo Shaker	Eppendorf, Hamburg
Ultra sonic bath	Bandelin, Berlin
Vortex mixer	Heidolph, Schwabach

5.2. Methods

5.2.1. Descriptive Statistic

The following location parameter and dispersion characteristics of the descriptive statistic were used to summarize the data obtained during method validation. In addition, they were utilised to present the collected pharmacokinetic data and results [216].

arithmetic mean:
$$\bar{x} = \frac{1}{n} \sum_{i=1}^n x_i = \frac{x_1+x_2+\dots+x_n}{n} \quad (\text{Eq. 7})$$

standard deviation (s.d.):
$$s = + \sqrt{\frac{1}{n-1} \sum_{i=1}^n (x_i - \bar{x})^2} \quad (\text{Eq. 8})$$

coefficient of variation (CV):
$$v = \frac{s}{\bar{x}} \cdot 100\% \quad (\text{Eq. 9})$$

5.2.2. Method Validation of Skepinone-L and Sorafenib in Plasma

Chromatographic Conditions

LC-MS/MS analysis is performed on a triple quadrupole mass spectrometer combined to an LC device for chromatographic separation of SKL, SRF and ISTD (FS112).

Analytical column:	Waters Symmetry® C18, 5µm, 4.6x150mm
Column temperature:	40°C
Sample temperature:	4°C
Eluent:	A: 90% H ₂ O / 10% ACN (v/v) + 0.1% formic acid B: ACN + 0.1% formic acid isocratic mode: 30% A / 70% B
Flow rate:	0.4 mL/min
Injection volume:	20 µL
Retention time [min]:	SKL: 5.0 – 5.8 SRF: 7.1 – 7.2 FS112: 5.7 – 6.7

The relatively wide range in retention time is due to exchange of capillaries and pre-column holder between the validation in rat, dog and monkey plasma.

MS/MS Conditions

Ionisation:	ESI (+)
Source temperature:	100°C
Desolvation temperature:	280°C
Desolvation gas flow:	550 L/h
Cone gas flow:	50 L/h
Collision gas:	argon 5.0
Collision cell pressure:	<1e ⁻⁴ mbar
Detection:	MRM-mode

For increased sensitivity and enhanced selectivity, CID with argon as collision gas is applied to generate product ions from precursor ions. Further instrumental adjustments and monitored pairs of m/z values detected via MRM-mode are utilized as given in following table 75.

	SKL	SRF	FS112
cone voltage [V]	51	51	51
collision energy [V]	29	29	29
precursor ion [M+H] ⁺	426.3	465.0	396.3
product ion	257.6	252.5	257.6

Tab. 73: Instrumental parameters for the mass spectral analysis of SKL, SRF and FS112 in dog, rat, monkey and human plasma using MRM-mode.

5.2.2.1. Sample Preparation

The precipitation of plasma proteins is initiated by adding 50 μ L ISTD solution at a concentration of 2000 ng/mL FS112 in ACN to 50 μ L plasma (sample or blank). In order to achieve optimal precipitation, samples are blend for 10 s through a vortex-inducing-mixer followed by 20 min incubation at 4°C. The samples are then centrifuged at 4°C and 19,800 relative centrifugal force for 20 min. The supernatant is transferred into a micro volume HPLC-vial insert and directly used for LC-MS analysis.

5.2.2.2. Vehicle and Dose Formulation Preparation

The vehicle used for preparation of SKL and SRF dose formulation is composed as follows:

- 45 % v/v polyethylene glycol 400 (PEG400)
- 30 % v/v 1,2-propylene glycol (1,2-PG)
- 20 % v/v deionized water
- 5 % N-Methyl-2-pyrrolidone (NMP)

For dose formulation preparation, the test compound (SKL or SRF) is exactly weighed into a previously tared glass vial. Then the corresponding volume of NMP is added and blend on a vortex-inducing-mixer. After complete dissolution, remaining vehicle is pipetted and the glass container is placed in an ultrasonic bath for 10 min to remove eventual occurring bubbles of air.

5.2.2.3. Stock Solutions, Calibration Standards and QC Samples

Stock solutions for SKL (SS1-SKL; SS2-SKL), SRF (SS1-SRF; SS2-SRF) and FS112 (SS-FS112) are prepared in 1.5 mL glass vials. The reference substances are weighed exactly and are dissolved in the corresponding solvent, whose volume is determined by each initial weight. The sets of 9 till 10 calibration standards are generated from SS1-SKL and SS1-SRF and were diluted in rat, dog and human blank plasma. SS2-SKL and SS2-SRF are used to prepare the 5 QC samples in each rat, dog, monkey and human blank plasma. Detailed dilution procedures for stock solutions, calibration standards and QC samples in plasma of each applied species are described in tables 76 to 84. Calibration standards and QC samples are prepared freshly prior use and mixed with an equal volume of ISTD solution to achieve the desired analyte concentrations.

Validation in Rat Plasma

stock solution	SKL or SRF [mg]	dissolved in	final concentration [mg/mL]
SS1-SKL	0.816	1.020 mL ACN	0.800
SS2-SKL	0.792	0.990 mL ACN	0.800
SS1-SRF	1.100	1.375 mL vehicle*	0.800
SS2-SRF	0.900	1.125 mL vehicle*	0.800
SS-FS112	0.620	1.550 mL ACN	0.400

Tab. 74: Initial weight and preparation of SKL, SRF and FS112 stock solutions for validation and analysis in rat plasma. * Vehicle: 45% PEG400; 30% 1,2-PG; 20% H₂O; 5% NMP (v/v)

The ISTD solution with a FS112 concentration of 2,000.00 ng/mL is prepared by pipetting 250 µL of SS-FS112 in a 50 mL volumetric flask and filling up with ACN.

calibration standard	SKL [ng/mL]	SRF [ng/mL]	dilution procedure (diluent: rat plasma)	
C _{SKL/SRF} -4000	4,000.0	4,000.0	20.0 µL SS1-SKL+ 20.0 µL SS1-SRF	ad 1.00 mL
C _{SKL/SRF} -2000	2,000.0	2,000.0	500 µL C _{SKL/SRF} -4000	ad 1.00 mL
C _{SKL/SRF} -1000	1,000.0	1,000.0	500 µL C _{SKL/SRF} -2000	ad 1.00 mL
C _{SKL/SRF} -500	500.0	500.0	500 µL C _{SKL/SRF} -1000	ad 1.00 mL
C _{SKL/SRF} -250	250.0	250.0	500 µL C _{SKL/SRF} -500	ad 1.00 mL
C _{SKL/SRF} -125	125.0	125.0	500 µL C _{SKL/SRF} -250	ad 1.00 mL
C _{SKL/SRF} -62.5	62.50	62.50	500 µL C _{SKL/SRF} -125	ad 1.00 mL
C _{SKL/SRF} -31.3	31.25	31.25	500 µL C _{SKL/SRF} -62.5	ad 1.00 mL
C _{SKL/SRF} -15.6	15.63	15.63	500 µL C _{SKL/SRF} -31.3	ad 1.00 mL

Tab. 75: Preparation of SKL/SRF calibration standards in rat plasma.

QC sample	SKL [ng/mL]	SRF [ng/mL]	dilution procedure (diluent: rat plasma)	
QC _{SKL/SRF} -3960	3,960.0	3,960.0	19.8 µL SS2-SKL+ 19.8 µL SS2-SRF	ad 1.00 mL
QC _{SKL/SRF} -1980	1,980.0	1,980.0	500 µL QC _{SKL/SRF} -3960	ad 1.00 mL
QC _{SKL/SRF} -990	990.0	990.0	500 µL QC _{SKL/SRF} -1980	ad 1.00 mL
QC _{SKL/SRF} -198	198.0	198.0	100 µL QC _{SKL/SRF} -990	ad 0.50 mL
QC _{SKL/SRF} -19.8	19.80	19.80	50 µL QC _{SKL/SRF} -198	ad 0.50 mL

Tab. 76: Preparation of SKL/SRF quality control samples for validation and analysis in rat plasma.

Validation in Dog Plasma

stock solution	SKL [mg]	dissolved in	final concentration [mg/mL]
SS1-SKL	0.800	1.000 mL ACN	0.800
SS2-SKL	0.796	0.995 mL ACN	0.800
SS-FS112	0.340	0.850 mL ACN	0.400

Tab. 77: Initial weight and preparation of SKL and FS112 stock solutions for validation and analysis in dog plasma.

The ISTD solution with a FS112 concentration of 2,000.00 ng/mL is prepared by pipetting 250 µL of SS-FS112 in a 50 mL volumetric flask and filling up with ACN.

calibration standard	SKL [ng/mL]	dilution procedure (diluent: dog plasma)	
C _{SKL} -4000	4,000.0	50.0 µL SS1-SKL	<i>ad</i> 5.00 mL
C _{SKL} -3000	3,000.0	1500 µL C _{SKL} -4000	<i>ad</i> 2.00 mL
C _{SKL} -2000	2,000.0	1000 µL C _{SKL} -3000	<i>ad</i> 1.50 mL
C _{SKL} -1000	1,000.0	500 µL C _{SKL} -2000	<i>ad</i> 1.00 mL
C _{SKL} -500	500.0	500 µL C _{SKL} -1000	<i>ad</i> 1.00 mL
C _{SKL} -250	250.0	500 µL C _{SKL} -500	<i>ad</i> 1.00 mL
C _{SKL} -100	100.0	400 µL C _{SKL} -250	<i>ad</i> 1.00 mL
C _{SKL} -50	50.0	500 µL C _{SKL} -100	<i>ad</i> 1.00 mL
C _{SKL} -25	25.0	500 µL C _{SKL} -50	<i>ad</i> 1.00 mL
C _{SKL} -10	10.0	200 µL C _{SKL} -25	<i>ad</i> 0.50 mL

Tab. 78: Preparation of SKL calibration standards in dog plasma.

QC sample	SKL [ng/mL]	dilution procedure (diluent: dog plasma)	
QC _{SKL} -3921.6	3,921.57	10.0 µL SS2-SKL	<i>ad</i> 1.010 mL
QC _{SKL} -1960.8	1,960.78	500 µL QC _{SKL} -3921.6	<i>ad</i> 1.000 mL
QC _{SKL} -980.4	980.39	500 µL QC _{SKL} -1960.8	<i>ad</i> 1.000 mL
QC _{SKL} -196.1	196.08	100 µL QC _{SKL} -980.4	<i>ad</i> 0.500 mL
QC _{SKL} -19.6	19.61	50 µL QC _{SKL} -196.1	<i>ad</i> 0.500 mL

Tab. 79: Preparation of SKL quality control samples for validation and analysis in dog plasma.

Validation in Human Plasma

stock solution	SKL or SRF [mg]	dissolved in	final concentration [mg/mL]
SS1-SKL	0.820	1.025 mL ACN	0.800
SS2-SKL	0.652	0.815 mL ACN	0.800
SS1-SRF	0.141	0.704 mL ACN	0.200
SS2-SRF	0.127	0.635 mL ACN	0.200
SS-FS112	0.868	0.868 mL ACN	1.000

Tab. 80: Initial weight and preparation of SKL, SRF and FS112 stock solutions for validation in human and analysis in monkey and human plasma.

The ISTD solution with a FS112 concentration of 2,000.00 ng/mL is prepared by pipetting 100 µL of SS-FS112 in a 50 mL volumetric flask and filling up with ACN.

calibration standard	SKL [ng/mL]	SRF [ng/mL]	dilution procedure (diluent: human plasma)	
C _{SKL/SRF} -4000	4,000.0	4,000.0	10.0 µL SS1-SKL+ 40.0 µL SS1-SRF	<i>ad</i> 1.00 mL
C _{SKL/SRF} -2000	2,000.0	2,000.0	500 µL C _{SKL/SRF} -4000	<i>ad</i> 1.00 mL
C _{SKL/SRF} -1000	1,000.0	1,000.0	500 µL C _{SKL/SRF} -2000	<i>ad</i> 1.00 mL
C _{SKL/SRF} -500	500.0	500.0	500 µL C _{SKL/SRF} -1000	<i>ad</i> 1.00 mL
C _{SKL/SRF} -250	250.0	250.0	500 µL C _{SKL/SRF} -500	<i>ad</i> 1.00 mL
C _{SKL/SRF} -125	125.0	125.0	500 µL C _{SKL/SRF} -250	<i>ad</i> 1.00 mL
C _{SKL/SRF} -62.5	62.50	62.50	500 µL C _{SKL/SRF} -125	<i>ad</i> 1.00 mL
C _{SKL/SRF} -31.3	31.25	31.25	500 µL C _{SKL/SRF} -62.5	<i>ad</i> 1.00 mL
C _{SKL/SRF} -15.6	15.63	15.63	250 µL C _{SKL/SRF} -31.3	<i>ad</i> 0.50 mL

Tab. 81: Preparation of SKL/SRF calibration standards in human plasma.

QC sample	SKL [ng/mL]	SRF [ng/mL]	dilution procedure (diluent: human or monkey plasma)	
QC _{SKL/SRF} -3960	3,960.0	3,960.0	9.9 µL SS2-SKL+ 39.6 µL SS2-SRF	ad 1.00 mL
QC _{SKL/SRF} -1980	1,980.0	1,980.0	500 µL QC _{SKL/SRF} -3960	ad 1.00 mL
QC _{SKL/SRF} -990	990.0	990.0	500 µL QC _{SKL/SRF} -1980	ad 1.00 mL
QC _{SKL/SRF} -198	198.0	198.0	100 µL QC _{SKL/SRF} -990	ad 0.50 mL
QC _{SKL/SRF} -19.8	19.80	19.80	50 µL QC _{SKL/SRF} -198	ad 0.50 mL

Tab. 82: Preparation of SKL/SRF quality control samples for validation in human plasma and analysis in cynomolgus monkey and human plasma.

5.2.2.4. Quantification and Data Evaluation

SKL, SRF and ISTD FS112 were evaluated using the MRM detection and scanning mode for three mass pairs of precursor- and product ion combinations. A desktop computer and the MassLynx™4.1 software supported data acquisition and analysis. Calibration and quantification of SKL and SRF in plasma of various species was done by establishing linear regression functions after 1/x weighting of PAR (analyte/ISTD) versus corresponding analyte concentrations. Further data processing was performed using Microsoft® Excel 2013.

5.2.3. Pharmacokinetic Studies of Skepinone-L *in vivo*

No animal experiments were performed within the present dissertation. Only plasma samples from different animal species were analysed in this thesis. These samples originated from externally commissioned and externally conducted *in vivo* experiments.

5.2.3.1. Animal Treatment Conditions of Pharmacokinetic Studies

The preliminary pharmacokinetic study of SKL in mice was planned, commissioned and financed by the department of Pharmaceutical and Medicinal Chemistry from Tübingen University. The bioavailability study of SKL in dogs and the pharmacokinetic studies of SKL and SRF in rats and monkeys were planned, commissioned and financed by c-a-i-r biosciences GmbH from Ulm, Germany.

The following tables 83 till 87 provide a brief overview of treatment for each tested species. Besides the routes of administration, the corresponding doses of all

administered compounds and the duration, if applicable, is given. In addition, the gender and number of all tested animals are listed.

SKL in mice – treatment summary				
	dose [mg/kg]	route	m	f
SKL	0.4	i.v.	2*	-/-
	1.2	p.o.	2*	-/-
	10	p.o.	-/-	3

Tab. 83: Treatment summary of C57BL/6 mice with SKL in the preclinical PK study.
i.v. = intravenous; p.o. = per oral; m = male; f = female; *two sets of animals, one consisted of 9 mice

SKL in dogs – treatment summary				
	dose [mg/kg]	route	m	f
SKL	5	i.v.	2	2
	50	p.o.	2	2
	50	capsule	2	2

Tab. 84: Treatment summary of beagle dogs with SKL in the bioavailability study.
i.v. = intravenous; p.o. = per oral; m = male; f = female

SKL in rats part I – treatment summary				
	dose [mg/kg]	route	m	f
SKL	3	i.v.	3	-/-
	5	i.v.	3	-/-
	10	i.v.	3	-/-
	5	p.o.	3	-/-
	15	p.o.	3	-/-
	50	p.o.	3	-/-

Tab. 85: Summary of treatment of Sprague Dawley rats with SKL during the PK studies part I.
i.v. = intravenous; p.o. = per oral; m = male; f = female

SKL and SRF in rats part II– treatment summary					
	dose [mg/kg]	route	duration [days]	m	f
SKL	15	p.o.	7	6	6
	50	p.o.	7	6	6
SRF	25	p.o.	7	6	6
	25	p.o.	7	3	3
SKL + SRF	15 + 25	p.o.	7	3	3
	50 + 25	p.o.	7	6	6

Tab. 86: Summary of treatment of Sprague Dawley rats with SKL and SRF during the PK studies part II. i.v. = intravenous; p.o. = per oral; m = male; f = female

SKL and SRF in monkeys – treatment summary				
	dose [mg/kg]	route	m	f
SKL	50	p.o.	2	2
SRF	50	p.o.	2	2

Tab. 87: Summary of treatment of cynomolgus monkeys with SKL and SRF during the PK study.
i.v. = intravenous; p.o. = per oral; m = male; f = female

5.2.3.2. Preliminary Study of Skepinone-L in Mice

Part I of the preliminary study in mice was performed and analysed by Synovo GmbH in Tübingen, Germany. Cassette dosing was applied in this study, using two cassettes, C#1 and C#2. Each consisted of six compounds, where only SKL is considered in the present work. C#1 and C#2 were administered both intravenous and oral to a total of four sets of animals, where one set consisted of nine male C57BL/6 mice. The dosing of SKL was 0.4 mg/kg for i.v. and 1.2 mg/kg for p.o. administration.

Vehicle i.v.: 63 % serum; 36 % PEG400; 1 % Tween 80

Vehicle p.o.: 63 % hypromellose (0.5 % in H₂O); 36 % PEG400; 1 % Tween 80

For determination of SKL-plasma levels blood samples were taken at 5, 15, 30 and 60 min as well as at 2.0, 4.0, 8.0 and 24.0 h post i.v.-dosing and at 0.25, 0.5, 1.0, 2.0, 4.0, 8.0 and 24.0 h after p.o. administration. It should be noted that the number mice from which blood samples were taken at each time point ranged between three and nine.

The *in vivo* section of the preliminary pharmacokinetic study in mice part II was performed at the Department of Physiology, University Hospital Tübingen, Germany. Dose formulation, sample preparation and analysis were conducted in-house (Department of Pharmaceutical and Medicinal Chemistry, Tübingen University). In this study, 10 mg/kg SKL was administered to three female C57BL/6 mice per oral gavage.

Vehicle: 57 % PEG400; 37 % methylcellulose (0.5 % in H₂O); 6 % Tween 80

Blood samples from the tail vein were taken shortly before and 15, 30, 60, 120, 240, 480 as well as 1,440 min after administration. 20.0 µL blood were immediately vortex-mixed for 30 s with 80.0 µL heparin solution, followed by addition of 100 µL ice cooled ISTD solution (500 ng/mL FS694 in ACN). The samples were then ultrasonically treated on ice for 10 min, centrifuged at 1°C and 19,800 relative centrifugal force for 15 min. The supernatant was transferred into a micro volume HPLC-vial insert and directly analysed via LC-MS/MS.

Chromatographic Conditions

The injection volume, column, sample temperature and eluent were used as described in chapter 5.2.2.

Analytical column:	Phenomenex Synergi™ Max-RP, 4µm, 4.6x150mm						
Gradient mode:							
t [min]	0.0	0.5	4.0	10.5	11.0	12.0	16.5
% B	0.0	0.0	60	80	100	0.0	stop

Flow rate: 0.5 mL/min
Retention time [min]: SKL: 13.9 – 14.0
FS694: 5.7 – 5.8

MS/MS Conditions

Ionisation: ESI (+)
Source temperature: 100°C
Desolvation temperature: 350°C
Desolvation gas flow: 600 L/h
Cone gas flow: 40 L/h
Collision gas: argon 5.0
Collision cell pressure: $1e^{-4}$ mbar
Detection: MRM-mode

	SKL	FS694
cone voltage [V]	50	50
collision energy [V]	29	29
precursor ion [M+H] ⁺	426.3	593.6
product ion	257.6	506.0

Tab. 88: Instrumental parameters for the mass spectral analysis of SKL and FS694 in mouse plasma applying MRM-mode.

5.2.3.3. Bioavailability Study of Skepinone-L in Dogs

The *in vivo* phase of the bioavailability study of SKL in dogs was performed at the Research Toxicology Centre (RTC) in Baugy, France. The study was conducted on a single group of four beagle dogs in total (two male and two female). SKL was administered by the intravenous route with a dosage of 5 mg/kg and after a wash-out period by the oral route with 50 mg/kg SKL. The vehicle and dose formulations were prepared by RTC prior use according to the preparation procedure description (Ch. 5.2.2.2). Blood samples from the cephalic vein were collected shortly before and 5, 15, 30 min and 1, 2, 4, 8 and 24 h after intravenous administration. Following oral administration, blood samples were taken before treatment and at 0.5, 1, 2, 4, 8 and 24 h after treatment. The collected blood samples were transferred into tubes containing lithium heparin as anticoagulant, centrifuged at 1,900 g for 10 min at room temperature. The plasma was frozen and stored at -20°C until dispatch on dry ice. Complete analysis of the received plasma samples was performed in-house

(Department of Pharmaceutical and Medicinal Chemistry, Tübingen University) using the developed and validated method in dog plasma as described in chapter 5.2.2.

5.2.3.4. Pharmacokinetic Study of Skepinone-L and Sorafenib in Rats

The *in vivo* section to investigate the PK profiles of SKL and SRF in Sprague Dawley rats was performed at the RTC in Pomezia, Italy. Part I of this study consisted of six treatment groups (Tab. 22, Ch. 3.3.3.1), each of three male rats. SKL was administered once to three groups orally by gavage at dose levels of 5, 15 and 50 mg/kg. Remaining treatment groups received SKL per intravenous bolus injection with a single dosage of 3, 5 and 10 mg/kg. Time points for blood sampling from the tail vein were 0.25, 0.5, 1, 2, 4, 9 and 12 h after oral and 5, 15 min and 1, 2, 4 and 9 h after intravenous administration. Three groups were treated in part II, were each group consisted of six male and six female rats (Tab. 29, Ch. 3.3.3.3). A fourth group with three animals of each gender served as control group. In the first phase of this study part, two groups received repeated oral administration of SKL on seven consecutive days, at dose levels of 15 and 50 mg/kg/day, respectively. The third group was treated in the same manner with the reference item SRF at a dose of 25 mg/kg/day. On the seventh day, blood samples were taken from three male and three female rats of each treatment group, which were then sacrificed. In the second phase, 25 mg/kg/day SRF or a combination of SRF and 15 or 50 mg/kg/day SKL was administered orally to the remaining animals for further 7 days of treatment.

Depending on the treatment group, blood was collected pre-dose and at 0.5, 1, 2, 4, 9, 12 and 24 h after dosing, at the seventh or fourteenth day of treatment. All blood samples were transferred into tubes containing heparin as anticoagulant and centrifuged at room temperature. The plasma was frozen at -20°C and dispatched on dry ice. RTC prepared vehicles and dose formulations for both study parts, according to the preparation procedure description (Ch. 5.2.2.2). Complete analysis of received plasma samples was performed in-house (Department of Pharmaceutical and Medicinal Chemistry, Tübingen University) using the developed and validated method in rat plasma as described in chapter 5.2.2.

5.2.3.5. Pharmacokinetic Study of Skepinone-L and Sorafenib in Monkeys

CiToxLAB in Evreux (France) was the test facility which performed the *in vivo* phase to assess the pharmacokinetic profiles of SKL and SRF in cynomolgus monkeys. One treatment group, consisting of two male and two female monkeys, was used in this study. First, they received a single dose of 50 mg/kg SKL by oral gavage. After a wash-out period 50 mg/kg SRF were administered also by the oral route. Blood samples for plasma level determination of SKL and SRF were collected pre-dose and at 0.5, 1, 2, 3, 4, 8 and 24 h after dosing. Collected venous blood samples were transferred into tubes containing lithium heparin and centrifuged at 3,000 g and 4°C for 10 min. The plasma was stored at -20°C and dispatched on dry ice. Vehicle and dose formulations were prepared freshly prior use by CiToxLAB according to the preparation procedure as described previously (Ch. 5.2.2.2). Plasma analysis and pharmacokinetic analysis of the received plasma samples were performed in-house (Department of Pharmaceutical and Medicinal Chemistry, Tübingen University) using the developed and validated method in human plasma as described in chapter 5.2.2.

5.2.4. Pharmacokinetic Data Analysis

5.2.4.1. Non-Compartmental Analysis

Based on the individual and calculated mean plasma concentrations, the primary pharmacokinetic parameter were determined by non-compartmental analysis (NCA) calculation. The evaluation was done with PKSolver2.0, an add-in program for pharmacokinetic data analysis in Microsoft® Excel [15]. For this purpose, an NCA-model was selected which described the plasma concentration of the administered drug after either intravenous bolus injection or extravascular application.

The terminal elimination slope λ_z is calculated by using the regression of three terminal data points from the semi-logarithmic graph. The AUC, a primary pharmacokinetic parameter, expresses the intensity of drug exposure and acts as a distinguishing marker of linear and non-linear pharmacokinetic [217]. As described as follows, the linear trapezoidal method was used to calculate the AUC from zero to the last sampling time point (AUC_{0-t}). The last observed plasma concentration ($C_{t \text{ last}}$) and

the slope of the terminal elimination λ_z provide the basis for the AUC extrapolation from time zero to infinity ($AUC_{0-\infty}$).

$$AUC_{(0-t)} = \sum_{i=1}^n \frac{(C_i + C_{i+1})}{2} \cdot \Delta t \quad (\text{Eq. 10})$$

$$AUC_{(0-\infty)} = AUC(t_0 - t_{\text{last}}) + \frac{C_{t_{\text{last}}}}{\lambda_z} \quad (\text{Eq. 11})$$

The AUMC from time zero to the last sampling time point was also determined by using the linear trapezoidal method and the extrapolation from zero to infinity as described as follows.

$$AUMC_{(0-\infty)} = AUMC(t_0 - t_{\text{last}}) + \left(\frac{C_{t_{\text{last}}} \cdot t}{\lambda_z} + \frac{C_{t_{\text{last}}}}{\lambda_z^2} \right) \quad (\text{Eq. 12})$$

The time required to reduce the plasma concentration by half is defined as the terminal plasma half-life $t_{1/2}$ and is related to the terminal elimination rate [21]. Since the kinetics of SKL can be described as non-linear, the calculation of the apparent volume of distribution V is performed at the time of steady state (SS) following intravenous bolus injection [22]. The total body clearance (Cl) is the sum of all occurring renal and non-renal excretion processes and describes the drug elimination rate from the body. To determine V_{ss} and Cl after extravascular administration the drug bioavailability (F) must be known [218].

$$\text{terminal plasma half-life:} \quad t_{1/2} = \frac{\ln 2}{\lambda_z} \quad (\text{Eq. 13})$$

$$\text{volume of distribution:} \quad V_{ss} = \frac{D^{iv} \cdot AUMC_{0-\infty}^{iv}}{(AUC_{0-\infty}^{iv})^2} \quad (\text{Eq. 14})$$

$$\text{total body clearance:} \quad Cl = \frac{D^{iv}}{AUC_{0-\infty}^{iv}} \quad (\text{Eq. 15})$$

$$\text{bioavailability:} \quad F = 100 \cdot \frac{AUC_{0-\infty}^{po} \cdot D^{iv}}{AUC_{0-\infty}^{iv} \cdot D^{po}} \quad (\text{Eq. 16})$$

5.2.4.2. Compartmental Analysis

Compartmental data analysis was also performed with the add-in program PKSolver2.0. For this purpose, the arithmetic mean of the observed plasma concentrations was calculated using descriptive statistics and plotted versus time in a semi-logarithmic graph. To select the most appropriate pharmacokinetic model, the decline of the concentration was visually assessed if the decrease was either mono- or multi-exponential. Since the elimination of SKL *in vivo* could be described as

biphasic, the two-compartment model seemed to be the most suitable one and obeys following equations:

$$\text{intravenous bolus input: } C(t) = A \cdot e^{-\alpha t} + B \cdot e^{-\beta t} \quad (\text{Eq. 17})$$

$$\text{extravascular input: } C(t) = A \cdot e^{-\alpha t} + B \cdot e^{-\beta t} - (A + B) \cdot e^{-k_a t} \quad (\text{Eq. 18})$$

In order to adapt these equations to the observed plasma concentration curves, the model parameters were calculated by nonlinear regression. The optimization of these model equations was mathematically a minimization of the weighted sum of squares (WSS) and was calculated from the differences (w_i) of the observed (C_i) and predicted (\hat{C}_i) concentrations.

$$WSS = \sum_{i=1}^n w_i \cdot (C_i - \hat{C}_i)^2 \quad (\text{Eq. 19})$$

To obtain the absolute minimum of the WSS-function, PKSolver2.0 uses the generalized reduced gradient algorithm for nonlinear optimization [15].

5.2.5. Pharmacokinetic Model Assessment

In addition to the coefficient of correlation R^2 and the visual assessment, further criteria were used to assess the precision of the estimated pharmacokinetic parameters of the selected model. Of the numerous model diagnostic possibilities which were provided by PKSolver2.0, the Akaike's information criterion (AIC) and Schwarz criterion (SC) can be considered as the most important ones [219]. They are used to compare different PK models of the same weighting type and are calculated as follows:

$$AIC = n \cdot \ln(WSS) + 2p \quad (\text{Eq. 20})$$

$$SC = n \cdot \ln(WSS) + p \cdot \ln(n) \quad (\text{Eq. 21})$$

where the number of measurement points (n), the WSS and the number of estimated parameters (p) were considered [15]. The smaller the AIC or SC value, the better the model is suited for the respective mathematical description of the data.

5.2.6. Determination of Plasma Protein Binding of Skepinone-L

In order to determine the affinity of SKL to bind to plasma proteins an equilibrium dialysis was performed. In addition, it was researched whether the potential binding

affinity of SKL is influenced in any manner by the presence of SRF, NOX or HOM. For these purposes, RED plates with inserts purchased from Thermo Scientific™ Pierce, Rockford (USA), were used.

Equilibrium dialysis is a common technique for determining the fraction of new chemical entities bound to plasma proteins. This method consists of two chambers which are separated by a semi-permeable membrane. The molecular-weight cut-off of dialysis membranes allows small molecules to diffuse but restricts the passage of proteins. In the present study, membranes with 8 kDa cut-off were used. The protein chamber contained human plasma pooled from eight donors processed within a maximum of 4 hours after blood donation. The second compartment was protein-free and contained phosphate-buffered saline (PBS) consisting of 10 mM phosphate-buffer, 2.7 mM KCl and 137 mM NaCl.

For each analysis (n = 2) 200 μ L human plasma spiked with analyte was added to the sample compartment and 350 μ L PBS to the buffer compartment. Pre-conditioning of the RED membrane inserts was not necessary. In order to verify the state of equilibrium, the sample compartment of the control analysis contained buffer instead of plasma spiked with analyte. Immediately after the sample transfer the plates were covered with sealing tape and incubated in a shaking-incubator for 4 h at 37°C and 750 rpm. Afterwards, 75 μ L from both the plasma and the buffer compartment were pipetted in separate microcentrifuge tubes containing the equal volume of either blank buffer or blank plasma, thus all samples had the same plasma to buffer ratio. Protein precipitation and analyte release was performed by adding 300 μ L chilled ACN containing the ISTD (15 μ M FS112). The samples were vortex-mixed for 30 s, incubated for 30 min at 4°C and centrifuged for 20 min at 19,800 relative centrifuge force and 4°C. The supernatant was directly used for LC-MS/MS analysis.

The percentages of the fraction unbound (f_u) and the percentage of compound bound to plasma proteins (f_b) and was calculated using following equations:

$$f_u = \frac{\text{PAR buffer compartment}}{\text{PAR plasma compartment}} * 100 \quad (\text{Eq. 22})$$

$$f_b = 100 - f_u \quad (\text{Eq. 23})$$

The plasma protein-bound fraction of SKL, SRF and NOX was determined both separately and combined in varying concentrations of 12.5, 25.0 and 37.5 μM . This corresponds to 5,318, 10,636 and 15,953 ng/mL SKL, to 5,810, 11,621 and 17,431 ng/mL SRF and to 6,010, 12,020 and 18,030 ng/mL NOX.

Chromatographic Conditions

The analytical column, injection volume, column and sample temperature, flow rate and eluent used were the same as described in chapter 5.2.2, except that the isocratic composition consisted of 33 % solvent A.

Retention time [min]: SKL: 5.2 – 5.3
 SRF: 7.9 – 8.0
 NOX: 5.7 – 5.8
 FS112: 6.1 – 6.2

MS/MS Conditions

Instrumental parameters were applied as described previously (Ch. 5.2.2). Further adjustments and monitored pairs of m/z values detected via MRM-mode were utilized as following (Tab. 89).

	SKL	SRF	NOX	FS112
cone voltage [V]	51	51	40	51
collision energy [V]	29	29	29	29
precursor ion $[M+H]^+$	426.3	465.0	481.0	396.3
product ion	257.6	252.5	286.2	257.6

Tab. 89: Instrumental parameters for the mass spectral analysis using MRM in order to determine the degree of binding to plasma proteins of SKL, SRF, NOX and FS112.

5.2.7. Metabolism and Biotransformation *in vitro*

5.2.7.1. Liver Microsomal Incubations

Since the biotransformation of drugs takes place predominantly in the liver, microsomes are a frequently used test system for investigating metabolic transformation *in vitro*. They require little equipment, and the experiments are relatively quick, simple and low-cost. However, they have neither cytosolic nor organelle-associated enzymes, and require the addition of relevant co-factors. Pooled liver microsomes of different species were purchased from Sekisui Xenotech (Kansas City, USA) and Sigma Aldrich (Steinheim, Germany). These microsomes were

characterized in protein content (Tab. 90) and used to study the *in vitro* metabolism of SKL by conducting Ph1, Ph2 and DA incubation assays.

species	race	abbreviation	catalogue No.	gender	protein content [mg/mL]
human	Caucasian, African	HLM	H1000	m	20
	American, Hispanic	fHLM	H1500	f	20
rat	Sprague Dawley	RLM	M9066	m	20
mouse	CD-1	MLM	M1000	m	20
dog	beagle	DLM	D1000	m	20
monkey	cynomolgus	CMLM	P2000	m	20

Tab. 90: Overview of purchased and for *in vitro* metabolism studies of SKL and SRF applied liver microsomes of male and female humans, male Sprague Dawley rats, CD-1 mice, beagle dogs and cynomolgus monkeys.

Further, the CYP content expressed in nmol per mg protein of purchased LMs is specified as well as the activity of UGT isoforms 1A1, 1A4, 1A9 and 2B7 of human LMs. Table 91 summarises the lot of LM used in each assay and its characteristics regarding CYP content and UGT activity.

LM	lot	CYP content [nmol/mg protein]	UGT activity [pmole/mg protein/min]				incubation assay		
			1A1	1A4	1A9	2B7	Ph1	Ph2	DA
HLM	1210270	0.428	1210	1150	4570	4060	X	X	X
fHLM	1210079	0.402	833	818	4210	3720	--	--	X
RLM	SLBN0707V	0.770	N/A	N/A	N/A	N/A	X	X	--
	SLBS4975	0.650	--	--	--	--	--	--	X
MLM	1610148	1.166	N/A	N/A	N/A	N/A	X	X	X
DLM	1310086	0.579	N/A	N/A	N/A	N/A	X	X	X
CMLM	1110329	1.258	N/A	N/A	N/A	N/A	X	X	X

Tab. 91: Characteristic CYP content and UGT activity of applied LMs in the corresponding incubation assay. N/A = not available; X = lot used in incubation-assay; -- = lot not used in incubation-assay

5.2.7.2. CYP-mediated Phase 1 Metabolism Studies

CYP-mediated Ph1 biotransformation of SKL and SRF was studied using pooled LM from humans, mice, rats, dogs and monkeys. The incubations were performed in the presence of a nicotinamide adenine dinucleotide phosphate (NADPH)-regenerating system, which consisted of 5 mM glucose-6-phosphate (G6P), 5 U/mL glucose-6-phosphate dehydrogenase (G6PDH) and 1 mM NADP⁺. The analytes, the regeneration system and 4 mM MgCl₂ x 6 H₂O in 0.1 M Tris-HCl buffer (pH 7.4 at 37°C) were preheated for 5 min at 37°C and 750 rpm in an incubator. The incubation mix was split into 50 µL aliquots and the reaction was started by adding the respective

LM. Thereby the microsomal protein content was standardized to 1.0 mg/mL. To follow the course of potential metabolic degradation, reaction tubes were quenched after 0, 10, 20, 30, 60, 90 and 120 min by adding 150 μ L ice cooled ISTD (FS112) at a concentration of 30 μ M in ACN. The samples were vortexed immediately for 30 s and incubated at 4°C for 30 min to ensure that precipitation of proteins and salts is complete. Afterwards the mixture was centrifuged for 20 min at 19,800 relative centrifugal force and 4°C. The supernatant was directly used for LC-MS/MS analysis. All incubations in the present thesis were performed at least as duplicates, mostly as triplicates, and incubations with heat-inactivated LM were used to demonstrate that the analyte reduction that occurred resulted only from metabolic degradation.

reagent	solvent	stock solution concentration	final concentration
Tris-HCl pH 7.4 (37°C) [mM]	H ₂ O	100.0	-/-
MgCl ₂ [mM]	Tris-HCl	80.0	4.0
β -NADPH [mM]	Tris-HCl	20.0	1.0
G6P [mM]	Tris-HCl	100.0	5.0
G6PDH [U/mL]	Tris-HCl	100.0	5.0
analyte [μ M]	DMSO	1,000.0	10.0
LM [mg/mL protein]	-/-	20.0	1.0

Tab. 92: Composition of the Ph1 incubation assays for the determination of metabolic stability and analysis of metabolite formation of SKL and SRF *in vitro* in LM from humans, mice, rats, dogs and monkeys.

Incubations of 10 μ M SKL alone and in the presence of 5, 10, 20 and 40 μ M SRF were performed to study whether the Ph1 metabolism of SKL *in vitro* is influenced by SRF. The influence of SKL on the biotransformation of SRF was examined by microsomal incubations containing 10 μ M SRF alone and with additional 5, 10, 20 and 40 μ M SKL. Changes and deviations from the procedure described here are mentioned with the respective results in chapter 3.5.

Chromatographic Conditions

The analytical column, column and sample temperature, flow rate and eluent used were the same as described in chapter 5.2.2.

Injection volume: 15 μ L

Gradient mode:

t [min]	0.00	0.10	2.25	4.00	4.50	10.0
% B	45.0	45.0	87.0	87.0	45.0	stop

Retention time [min]:	SKL: 7.2 – 7.3
	SRF: 8.7 – 8.8
	NOX: 7.6 – 7.7
	HOM: 7.9 – 8.0
	DES: 8.1 – 8.2
	FS112: 8.0 – 8.1

The chromatographic conditions used for the analysis of the SKL Ph1 metabolites M#1 to M#5 are the same as for the determination of the UGT-mediated metabolism reaction and are given in the upcoming section 5.2.7.3.

Retention time [min]:	M#1: 6.4 – 6.5
	M#2: 7.6 – 7.7
	M#3: 9.5 – 9.6
	M#4: 10.0 – 10.1
	M#5: 11.8 – 11.9

MS/MS Conditions

Instrumental parameters were applied as described previously (Ch. 5.2.2). Further adjustments and the pairs of *m/z* values detected by MRM-mode are given in the following tables 93 and 94.

	SKL	SRF	NOX	HOM	DES	FS112
cone voltage [V]	51	51	40	55	51	51
collision energy [V]	29	29	29	27	29	29
precursor ion [M+H] ⁺	426.1	465.0	481.0	462.8	451.0	396.3
product ions	257.7	252.5	259.0	268.0	256.0	257.6
	378.1	424.9	286.0	406.0	406.0	
	407.2	446.9	462.8	451.0		

Tab. 93: Instrumental parameters for the mass spectral analysis using MRM to determine the metabolic degradation of SKL and SRF.

	M#1	M#2	M#3	M#4	M#5
cone voltage [V]	51	51	51	51	51
collision energy [V]	29	25	25	25	25
precursor ion [M+H] ⁺	424.0	424.0	424.0	349.9	349.9
product ions	203.4	358.9	203.4	202.9	194.0
	255.9	387.9	255.9	215.8	215.8
	358.9		358.9	256.0	221.8
	387.9		387.9	332.5	332.5

Tab. 94: Instrumental parameters for the mass spectral analysis using MRM to determine Ph1 metabolites of SKL.

5.2.7.3. UGT-mediated Phase 2 Metabolism Studies

In vitro glucuronidation of SKL was examined by utilising microsomal uridine 5'-diphospho-glucuronosyltransferases (UGTs). The active site of these membrane-bound enzymes protrudes into the inside of the endoplasmic reticulum. Therefore, the

membrane is disrupted using a pore-forming agent to enhance substrate access for maximum enzyme activity [168]. For this purpose, pooled LM with a final protein concentration of 1.0 mg/mL were pre-incubated for 30 min on ice in 0.1 M Tris-HCl buffer in the presence of 50 µg/mg protein alamethicin. Subsequently, the LMs thus activated were tempered up to 37°C for 5 min with 5 mM uridine diphosphate glucuronic acid (UDPGA) as glycosyl donor, 5 mM saccharolactone to inhibit microsomal β-glucuronidases [220] and 5 mM MgCl₂ as another essential cofactor.

After splitting this incubation mixture into 50 µL aliquots, conjugation reaction was started by addition of analyte and was performed in an incubator at 37°C and 750 rpm. After 0, 10, 20, 30, 60, 90 and 120 min the reaction was stopped with 150 µL of ice cooled ISTD (30 µM FS112 in ACN) to monitor time dependent glucuronide formation. One incubation without analyte and one without UDPGA served to demonstrate that occurring products are glucuronides of the test compound. Sample preparation for LC-MS/MS analysis was performed as described in section 5.2.7.2. A potential influence of SKL on the biotransformation of SRF and *vice versa* was also to be investigated under Ph2 conditions. For this purpose, incubations of the analyte to be tested were carried out in the presence of different concentrations of the other substance analogous to the previous section (5.2.7.3).

reagent	solvent	stock solution concentration	final concentration
Tris-HCl pH 7.4 (37°C) [mM]	H ₂ O	100.0	-/-
MgCl ₂ [mM]	Tris-HCl	80.0	5.0
UDPGA [mM]	Tris-HCl	40.0	5.0
saccharolactone [mM]	Tris-HCl	40.0	5.0
alamethicin [mg/mL]	DMSO	10.0	50.0
			[µg/mg protein]
analyte [µM]	DMSO	1,000.0	10.0
LM [mg/mL protein]	-/-	20.0	1.0

Tab. 95: Composition of Ph2 incubation assay to determine conjugative metabolite formation of SKL and SRF *in vitro* in LM from humans, mice, rats, dogs and monkeys.

Chromatographic Conditions

The analytical column, flow rate, column and sample temperature as well as eluent used were the same as described in chapter 5.2.2.

Injection volume: 15 µL

Gradient mode:

t [min]	0.00	7.50	7.65	11.0	11.01	16.20
% B	40.0	40.0	80.0	80.0	40.0	stop

Retention time [min]:	SKL: 13.4 – 13.5
	pO-Glc: 11.5 – 11.6
	sO-Glc: 10.1 – 10.2
	N-Glc: 4.2 – 4.3
	SRF: 15.5 – 15.6
	SRF-Glc: 7.1 – 7.2
	FS112: 14.0 – 14.1

MS/MS Conditions

Instrumental parameters were applied as previously described (Ch. 5.2.2). Specific MRM settings were used for SKL, SRF and FS112 as presented in section 5.2.7.2. Further adjustments and the pairs of *m/z* values of the remaining analytes detected by MRM-mode are given in the following table 96.

	pO-Glc	sO-Glc	N-Glc	SRF-Glc
cone voltage [V]	51	51	51	51
collision energy [V]	29	29	29	29
precursor ions [M+H] ⁺	426.1	426.1	426.1	465.0
	602.8	602.8	602.8	641.1
product ions	257.6	257.6	257.6	252.5
	351.0	351.0	351.0	424.9
	378.3	378.3	426.1	446.9
	426.1	426.1		465.0

Tab. 96: Instrumental parameters for the mass spectral analysis using MRM to analyse the formed glucuronides of SKL and SRF.

5.2.7.4. UGT-mediated Metabolism Studies of Skepinone-L Analogues

Structural elucidation of SKL glucuronides was performed by incubations of SKL analogues in HLM. Therefore 100 μ M of N-methyl-SKL, FS352, SK845, SK558 and FS332 were incubated in the presence of activated microsomal UGTs for 6 h. Further procedure and the composition of the reaction mixture was as described in the previous section 5.2.7.3.

Chromatographic Conditions

The analytical column, flow rate, column and sample temperature as well as eluent used were the same as described in chapter 5.2.2.

Gradient mode:

N-methyl-SKL	t [min]	0.00	4.75	5.00	10.00	10.10	16.20
	% B	50.0	50.0	65.0	65.0	50.0	stop
FS352	t [min]	0.00	5.00	5.25	10.00	10.10	16.20
	% B	50.0	50.0	70.0	70.0	50.0	stop

FS332	t [min]	0.00	5.00	5.25	9.50	11.0	11.01	16.70
	% B	50.0	50.0	85.0	90.0	90.0	50.0	stop
SK558	t [min]	0.00	5.00	5.50	8.50	10.0	10.01	16.50
	% B	50.0	50.0	85.0	90.0	90.0	50.0	stop
SK845	t [min]	0.00	5.00	5.25	10.00	10.10	16.50	
	% B	50.0	50.0	70.0	70.0	50.0	stop	

Retention time [min]:

N-methyl-SKL	FS352	FS332	SK558	SK845
11.3	11.6	15.4	13.7	12.3

MS/MS Conditions

Instrumental parameters were applied as described in chapter 5.2.2. Further adjustments and monitored pairs of m/z values detected via MRM-mode are given in the following tables 97 and 98.

	N-methyl-SKL	N-methyl-SKL-Glc.	FS352	FS352-Glc	FS332	FS332-Glc
cone voltage [V]	51	51	35	35	40	40
collision energy [V]	29	29	24	24	25	25
precursor ions [M+H] ⁺	440.1	440.1	427.1	427.1	367.0	367.0
product ions		616.0		603.1		544.1
	231.8	231.8	259.0	259.0	259.0	259.0
	271.8	271.8	336.0	336.0	305.0	305.0
	347.6	347.6	378.8	378.8	323.6	323.6
	391.9	391.9	390.5	390.5	335.5	335.5
		440.1		427.1		367.0

Tab. 97: Instrumental parameters for the mass spectral analysis of N-methyl-SKL, FS352, FS332 as well as their respective glucuronides applying MRM.

	SK558	SK558-Glc	SK845	SK845-Glc
cone voltage [V]	45	45	45	45
collision energy [V]	25	25	28	28
precursor ions [M+H] ⁺	366.0	366.0	410.0	410.1
product ions		542.0		586.1
	209.2	209.2	257.8	257.8
	230.0	230.0	335.7	335.7
	257.6	257.6	351.8	351.8
	347.8	347.8	391.5	391.5
		366.0		410.1

Tab. 98: Instrumental parameters for the mass spectral analysis of SK558 and SK845 as well as their respective glucuronides using MRM.

5.2.7.5. Dual-Activity Metabolism Assay

In order to study the simultaneous oxidative conjugative reaction dual activity metabolism assays (DAA) with pooled LM were performed. The incubation mixture consisted of an adapted combination of the Ph1 and Ph2 metabolism studies ingredients (Tab. 99). Additionally, it contained 0.1 % bovine serum albumin (BSA) to antagonise inhibitory long-chain fatty acids [221] and thus influence the activities of CYP and UGT enzymes [222].

The incubation mixture consisted of two separately prepared parts. As described for Ph2 metabolism studies, LMs were pre-incubated with alamethicin in Tris-buffer on ice for 30 min, which represented part A. All remaining components were contained in solution part B, except the analyte. Both parts were tempered to 37°C for 5 min. Immediately after addition of analyte to part A the enzymatic reaction was started by mixing both parts and subsequently splitting the incubation mixture into aliquots of 50 µL. The further procedure, also with regard to study the drug-drug interactions of SKL and SRF, RGF and TFP was as described in chapter 5.2.7.3.

reagent	solvent	stock solution concentration	final concentration	mixture part
Tris-HCl pH 7.4 (37°C) [mM]	H ₂ O	100.0	-/-	A / B
MgCl ₂ [mM]	Tris-HCl	80.0	4.0	B
UDPGA [mM]	Tris-HCl	100.0	5.0	B
saccharolactone [mM]	Tris-HCl	100.0	5.0	B
β-NADPH [mM]	Tris-HCl	20.0	1.0	B
G6P [mM]	Tris-HCl	100.0	2.5	B
G6PDH [U/mL]	Tris-HCl	100.0	5.0	B
BSA [%]	Tris-HCl	5.0 (w/v)	0.1 (v/v)	B
alamethicin [mg/mL]	DMSO	10.0	50.0	A
			[µg/mg protein]	
analyte [µM]	DMSO	1,000.0	10.0	A
LM [mg/mL protein]	-/-	20.0	1.0	A

Tab. 99: Composition of mixture parts A and B for the dual-activity assay to determine oxidative-conjugative metabolite formation of SKL and SRF *in vitro* in LM from humans, mice, rats, dogs and monkeys. In addition, the DAA mixture was used to study the metabolic transformation of RGF and TFP in the presence of SKL or SRF in HLM.

Chromatographic Conditions

Chromatographic conditions applied for analysis of SKL, SRF and FS112 in DAA were the same as used in UGT-mediated Ph2 metabolism studies. The retention times of these analytes and their glucuronides were as described previously (Ch. 5.2.7.3). The separation method outlined there was additionally used for the analysis of RGF.

Retention time [min]: RGF: 14.9 – 15.0
 NOX: 13.8 – 13.9
 HOM: 14.2 – 14.3
 DES: 14.6 – 14.7

In order to determine glucuronidation of TFP during DAA studies the gradient was as follows. The analytical column, flow rate, column and sample temperature as well as eluent used were the same as described in chapter 5.2.2.

Injection volume: 15 μ L

Gradient mode:

t [min]	0.00	0.50	2.25	4.40	4.50	11.50
% B	33.0	33.0	87.0	87.0	33.0	stop

Retention time [min]: SRF: 9.1 – 9.2
 TFP: 5.8 – 5.9
 TFP-Glc: 6.2 – 6.3
 FS112: 8.5 – 8.6

MS/MS Conditions

Instrumental settings were applied as described in chapter 5.2.2. Specific MRM parameters for SKL, SRF, NOX, HOM, DES and FS112 were used as given in chapter 5.2.8.2. The adjustments applied in section 5.2.7.3 for the glucuronides of SKL and SRF were adopted for the DAA. The pairs of m/z values of the remaining analytes detected by MRM following DAA are given in the table 100.

	RGF	TFP	TFP-Glc
cone voltage [V]	51	51	30
collision energy [V]	29	29	33
precursor ions [M+H] ⁺	483.0	408.0	584.2
product ions	270.2	141.0	113.1
	287.7	247.8	141.0
	423.9	259.6	279.8
	442.3	279.8	408.0
	465.2		

Tab. 100: Instrumental parameters for the mass spectral analysis using MRM to analyse RGF, TFP and TFP-Glc.

5.2.7.6. Kinetic Analysis of Skepinone-L Glucuronidation in Liver Microsomes

Linearity Determination of Glucuronide Formation

The conversion of substrate over time must be linear in order to determine K_m and V_{max} . The optimal protein concentration and incubation time were therefore

ascertained in advance. For this purpose, incubations of 100, 10 and 1 μM SKL in HLM, RLM, MLM, DLM and CMLM were performed applying Ph2 conditions (Ch. 5.2.8.3). Protein concentrations were 0.10, 0.25, 0.50 and 1.00 mg/mL, respectively. The reactions were stopped after 10, 20, 40 and 60 min by addition of ISTD in ACN. The chromatographic conditions used were as described previously (Ch. 5.2.7.3).

Determination of K_m and V_{max}

To determine K_m and V_{max} the conjugation of SKL with glucuronic acid was examined as described in chapter 5.2.7.3, including sample preparation and chromatographic conditions. However, the reaction mixture displayed there has been changed somewhat. Besides the modified protein contents, this mixture contained 10 mM UDPGA and 0.1% BSA. SKL was incubated at nine different concentrations in HLM, RLM, MLM, DLM and CMLM. Table 101 shows the final concentrations of SKL as well as the respective protein contents and incubation times. The Ph2-incubations for each SKL concentration were performed as triplicate.

	HLM	RLM	MLM	DLM	CMLM
SKL [μM]	1.0 / 2.5 / 5.0 / 7.5 / 10 / 15 / 25 / 50 / 75				
protein [mg/mL]	1.00	1.00	0.25	1.00	0.50
time [min]	30	20	20	20	20

Tab. 101: Concentrations of SKL, liver microsomal protein content of each species and incubation time applied to determine K_m and V_{max} .

Calculation of the kinetic constants K_m and V_{max} from experimental data were performed via nonlinear regression using the enzyme kinetics model of GraphPadPrism9.0.

5.2.8. Incubations with Recombinant UGTs

The complete elucidation of the metabolic transformation of a xenobiotic also requires the identification of the involved isoforms of the catalysing enzyme family. Incubations with recombinant human UGTs (rUGTs) were used to identify the isoforms involved in the glucuronidation of SKL. Recombinant enzymes were purchased from Corning (Woburn, USA). SupersomesTM were prepared from insect cells infected with baculovirus containing human UGT cDNA. Table 102 summarises the general

information about the applied isoforms and their characteristic protein content and glucuronidation activities.

UGT	catalogue No.	lot No.	protein content [mg/mL]	glucuronidation activity [pmol/mg protein/min]	specific substrate
1A1	456411	8047001	5.0	870	estradiol
1A3	456413	6197002	5.0	190	estradiol
1A4	456414	7179004	5.0	1,100	TFP
1A6	456416	6216001	5.0	4,000	HTMC
1A9	456419	6307002	5.0	4,600	HTMC
2B7	456427	7193001	5.0	2,400	HTMC
2B10	453323	7326001	5.0	9.7	amitriptyline
2B15	456435	6271006	5.0	1,700	HTMC

Tab. 102: Overview of purchased and for *in vitro* glucuronidation studies of SKL applied UGT isoforms. TFP = trifluoperazine, HTMC = hydroxytrifluoromethylcoumarin

5.2.8.1. Glucuronidation Reaction by Recombinant UGTs

Glucuronidation reaction of SKL in the presence of rUGTs was performed in accordance with the UGT Corning-Supersomes™ guidelines. SKL was incubated with 0.5 mg/mL of the respective isoform in 0.1 M Tris-HCl buffer in the presence of 25 µg/mL alamethicin, 10 mM MgCl₂ and 5 mM UDPGA at 37°C. The exact composition of the reaction mixture is given in table 103. The substrate concentration and the incubation time varied depending on the objective. To avoid deactivation of the respective human rUGT, no further agitation after initial mixing and no pre-incubation of the reaction mixture were performed. The enzymatic reaction was stopped by adding ice cooled ISTD in ACN. The function of the isoenzyme was verified by control incubations with rUGT-specific substrate (Tab. 102), with known inhibitor as well as without protein. Sample preparation for LC-MS/MS analysis was performed as described in section 5.2.7.2. A potential influence of SRF on the SKL-glucuronidation was also to be investigated in the presence of the respective human rUGT isoform. For this purpose, rUGT-mediated glucuronidation of SKL were examined in the presence of different SRF concentrations. Each glucuronidation reaction incubation was performed as duplicate.

reagent	solvent	stock solution concentration	final concentration
Tris-HCl pH 7.5 (37°C) [mM]	H ₂ O	100.0	-/-
MgCl ₂ [mM]	Tris-HCl	500.0	10.0
UDPGA [mM]	Tris-HCl	100.0	5.0
alamethicin [mg/mL]	DMSO	10.0	0.025
analyte [μM]	DMSO	1,000.0	1.0 – 100 0
rUGT [mg/mL protein]	-/-	5.0	0.5

Tab. 103: Composition of glucuronidation reaction mixture with human rUGTs to determine conjugative metabolite formation of SKL *in vitro*.

Chromatographic conditions and MS/MS parameters applied for SKL, SRF and TFP analysis were the same as described in chapter 5.2.7.5.

5.2.8.2. Kinetic Analysis of Skepinone-L Glucuronidation in Recombinant UGTs

The determination of the kinetic parameters was also performed in the presence of the respective major responsible rUGT isoform. As previously described (Ch. 5.2.7.6) for the analysis in LM, the optimal protein concentration and analysis duration were determined in preliminary experiments. The incubations of SKL with rUGT2B7 and 1A4 for the determination of K_m and V_{max} were performed with 0.5 mg/mL protein each and stopped after 20 min. The incubation reaction mixture used is described in the previous chapter. Sample preparation for LC MS/MS analysis was performed as described in section 5.2.7.2 by applying the chromatographic conditions displayed in chapter 5.2.7.3.

5.2.8.3. Inhibition of rUGT2B7

Several incubations with rUGT2B7 were used to clarify whether SKL, pO-Glc or sO-Glc are inhibitors of this isoform. For this purpose, the glucuronidation of the chemical probe substrate HTMC was investigated. The sample preparation was performed analogously to the description in chapter 5.2.7.2 and the composition of the incubation mixture is shown in section 5.2.8.1.

Chromatographic Conditions

The analytical column, flow rate, column and sample temperature as well as eluent used were the same as described in chapter 5.2.2. Injection volume and LC gradient were given in chapter 5.2.7.3.

MS/MS Conditions

Instrumental parameters were applied as described previously (Ch. 5.2.2). Specific MRM settings used for SKL, pO-Glc, sO-Glc and ISTD FS112 are presented in chapter 5.2.7.3 UGT. Further adjustments and the pairs of m/z values of HTMC and HTMC-Glc detected by MRM-mode are given in the following table 104.

	HTMC	HTMC-Glc
cone voltage [V]	51	51
collision energy [V]	29	29
precursor ions [M+H] ⁺	231.0	231.4 407.0
product ions	161.3 166.8 229.0 230.6	161.3 166.8 230.6 231.4

Tab. 104: Instrumental parameters for the mass spectral analysis using MRM in order to analyse HTMC and HTMC-Glc.

5.2.9. p38 α Mitogen-Activated Protein Kinase Assay

In order to assess the inhibitory activity of pO-Glc and sO-Glc towards p38 α MAP kinase, an ELISA as described by Goettert et al. [179] was performed.

Stability of Oxygen-linked Skepinone-L Glucuronides

Hitherto, very little was known about the properties, especially the stability in solution, of the newly discovered SKL-glucuronides. O-linked glucuronides are generally less predisposed to chemical hydrolysis than other glucuronides [223]. However, it is possible that pO-Glc and sO-Glc were unstable in the kinase buffer used in the ELISA during the test period. This could result in the hydrolysis of the glucuronide-SKL conjugates into glucuronic acid and SKL. The presence of highly potent SKL could result in misrepresented IC₅₀ values for the glucuronides. In order to exclude this, both glucuronides were incubated in ELISA kinase buffer for a total of 14 h at 37°C. The exact composition of the kinase buffer can be found in the description by Goettert *et. al.* [179]. Changes in the peak areas of sO-Glc and pO-Glc over the

incubation duration as well as a possible formation of SKL were investigated by LC-MS/MS using the method described in section 5.2.7.5. Neither a decrease in the peak areas nor a SKL signal could be detected over the duration of the entire experiment. Thus, the pO-Glc as well as the sO-Glc can be considered stable in the ELISA kinase buffer under assay conditions. Consequently, the presence of SKL and a possible influence on the determined IC₅₀ can be excluded.

5.2.10. Extraction of Skepinone-L from Mouse Faeces

In order to investigate the route of excretion of SKL and its glucuronides, their quantities in mouse faeces were determined. To extract SKL and its glucuronides from mouse faeces, it was first shredded with metal beads using a vortex mixer. For extraction the exactly weighed faeces was suspended with 0.5 mL H₂O and 1.0 mL ISTD in ACN (FS112, 30 μ M). After 10 min ultra-sonication at room temperature the suspensions were incubated for 4 h at 1,000 rpm in a shaker. Subsequently, the samples were centrifuged for 10 min at room temperature and 19,800 relative centrifugal force. 1,000 μ L of the supernatant were filtered (0.45 μ m) and analysed by LC-MS/MS. The mouse faeces consisted mainly of the carrier of the oral formulation. Therefore, this carrier was spiked with 2 μ g each of pO-Glc and sO-Glc and processed accordingly to the samples. Since almost no SKL could be detected, pO-Glc and sO-Glc appeared to be stable during the sample preparation. Chromatographic conditions and instrumental parameters to analyse the faeces samples were applied as described in chapter 5.2.7.1.

6. LIST OF PUBLICATIONS

During the preparation of the thesis, the following publications were contributed to:

- 1.) Heider F, Ansideri F, Tesch R, Pantsar T, Haun U, Döring E, Kudolo M, Poso A, Albrecht W, Laufer SA, Koch P. Pyridinylimidazoles as dual glycogen synthase kinase 3 β /p38 α mitogen-activated protein kinase inhibitors. *J Med Chem.* **2019**; 175:309-329.
- 2.) Opretzka LCF, Espírito-Santo RFD, Nascimento OA, Abreu LS, Alves IM, Döring E, Soares MBP, Velozo EDS, Laufer SA, Villarreal CF. Natural chromones as potential anti-inflammatory agents: Pharmacological properties and related mechanisms. *Int Immunopharmacol.* **2019**; 72:31-39.
- 3.) Forster M, Chaikuad A, Dimitrov T, Döring E, Holstein J, Berger BT, Gehringer M, Ghoreschi K, Müller S, Knapp S, Laufer SA. Development, Optimization, and Structure-Activity Relationships of Covalent-Reversible JAK3 Inhibitors Based on a Tricyclic Imidazo[5,4- d]pyrrolo[2,3- b]pyridine Scaffold. *J Med Chem.* **2018**; 61(12):5350-5366.

- 4.) Juchum M, Günther M, Döring E, Sievers-Engler A, Lämmerhofer M, Laufer S. Trisubstituted Imidazoles with a Rigidized Hinge Binding Motif Act As Single Digit nM Inhibitors of Clinically Relevant EGFR L858R/T790M and L858R/T790M/C797S Mutants: An Example of Target Hopping. *J Med Chem.* **2017**; 60(11):4636-4656.
- 5.) Heider F, Haun U, Döring E, Kudolo M, Sessler C, Albrecht W, Laufer S, Koch P. From 2-Alkylsulfanylimidazoles to 2-Alkylimidazoles: An Approach towards Metabolically More Stable p38 α MAP Kinase Inhibitors. *Molecules.* **2017**; 22(10):1729.
- 6.) Walter NM, Wentsch HK, Bührmann M, Bauer SM, Döring E, Mayer-Wrangowski S, Sievers-Engler A, Willemsen-Seegers N, Zaman G, Buijsman R, Lämmerhofer M, Rauh D, Laufer SA. Design, Synthesis, and Biological Evaluation of Novel Type I $^{1/2}$ p38 α MAP Kinase Inhibitors with Excellent Selectivity, High Potency, and Prolonged Target Residence Time by Interfering with the R-Spine. *J Med Chem.* **2017**; 60(19):8027-8054.
- 7.) Günther M, Lategahn J, Juchum M, Döring E, Keul M, Engel J, Tumbrink HL, Rauh D, Laufer S. Trisubstituted Pyridinylimidazoles as Potent Inhibitors of the Clinically Resistant L858R/T790M/C797S EGFR Mutant: Targeting of Both Hydrophobic Regions and the Phosphate Binding Site. *J Med Chem.* **2017**; 60(13):5613-5637.
- 8.) Muth F, El-Gokha A, Ansideri F, Eitel M, Döring E, Sievers-Engler A, Lange A, Boeckler FM, Lämmerhofer M, Koch P, Laufer SA. Tri- and Tetrasubstituted Pyridinylimidazoles as Covalent Inhibitors of c-Jun N-Terminal Kinase 3. *J Med Chem.* **2017**; 60(2):594-607.
- 9.) Muth F, Günther M, Bauer SM, Döring E, Fischer S, Maier J, Drückes P, Köppler J, Trappe J, Rothbauer U, Koch P, Laufer SA. Tetra-substituted pyridinylimidazoles as dual inhibitors of p38 α mitogen-activated protein kinase and c-Jun N-terminal kinase 3 for potential treatment of neurodegenerative diseases. *J Med Chem.* **2015**; 58(1):443-56.

7. APPENDIX

7.1. Primary Calibration Lines during Method Validation

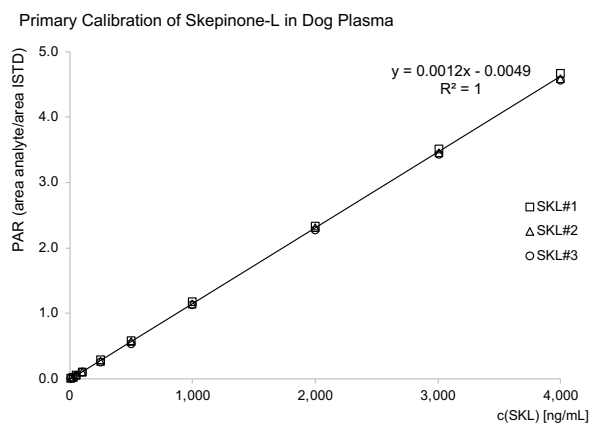


Fig. 95: Primary calibration line for the determination of SKL in dog plasma at a range of 10.00 to 4,000.00 ng/mL.

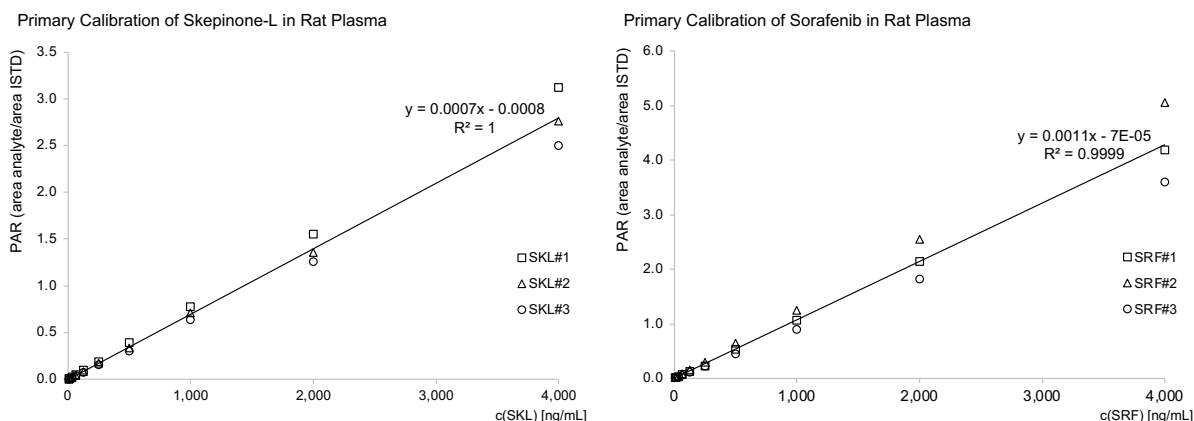


Fig. 96: Primary calibration lines for the determination of SKL (left) and SRF (right) in rat plasma at a range of 7.81 to 4,000.00 ng/mL.

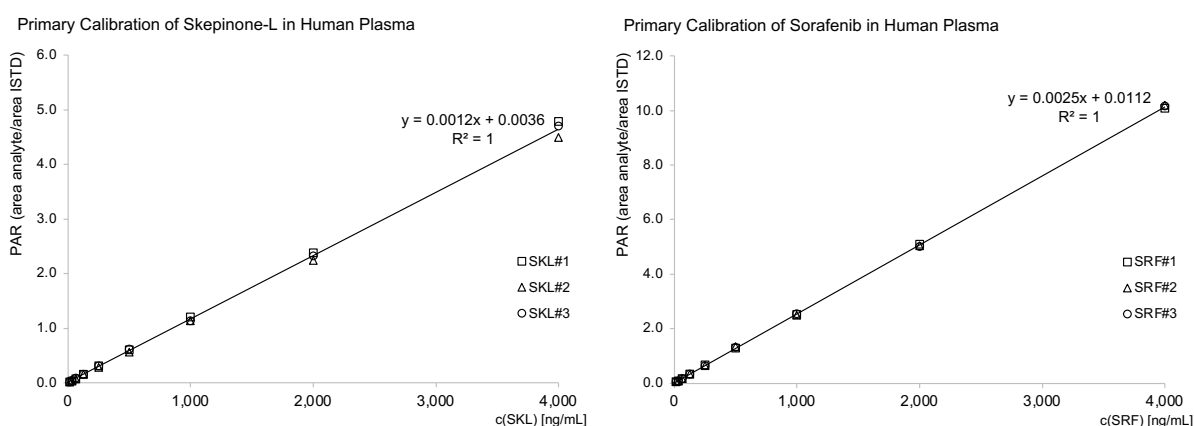


Fig. 97: Primary calibration lines for the determination of SKL (left) and SRF (right) in human plasma at a range of 15.63 to 4,000.00 ng/mL.

7.2. Plasma Concentrations of Skepinone-L and Sorafenib *in vivo*

Preliminary Study of SKL in Mice:

SKL [ng/mL] in male mouse plasma after cassette dosing								
time [h]	cassette 1				cassette 2			
	i.v.	n	p.o.	n	i.v.	n	p.o.	n
0.08	178.16	9	-/-	-/-	175.70	9	-/-	-/-
0.25	163.65	3	138.23	9	114.48	3	119.03	9
0.50	163.17	3	205.91	3	107.72	3	187.78	3
1.00	73.31	6	182.19	3	69.30	6	168.42	3
2.00	39.88	3	110.60	6	41.27	3	105.89	6
4.00	13.14	3	64.32	3	12.59	3	41.14	3
8.00	4.09	3	16.25	3	4.21	3	15.66	3
24.00	0.45	3	0.44	3	0.13	3	0.60	3

Tab. 105: Individual and mean concentrations of SKL [ng/mL] in mouse plasma of male C57BL/6 mice after 0.4 mg/kg i.v. and 1.2 mg/kg p.o. administration of cassette 1 and 2. n = number of samples

SKL [ng/mL] in female mouse plasma after p.o. administration

time [h]	animal			mean
	1	2	3	
0.00	0.00	0.00	0.00	0.0
0.25	635.38	415.48	616.48	525.4
0.50	1,191.14	1,101.33	1,103.81	1,146.2
1.00	1,338.47	1,595.90	1,078.46	1,467.2
2.00	652.4	681.48	538.63	666.9
4.00	136.02	274.76	124.62	205.4
8.00	29.37	37.51	17.52	33.4
24.00	0.00	0.00	0.00	0.0

Tab. 106: Individual and mean concentrations of SKL [ng/mL] in mouse plasma of female C57BL/6 mice after single p.o. administration of 10 mg/kg SKL.

Bioavailability Study of SKL in Dogs:**SKL [ng/mL] in dog plasma after i.v. administration**

time [h]	4 (male)	5 (male)	6 (female)	7 (female)
0.00	0.00	0.00	0.00	0.00
0.08	2,864.80	3,365.44	2,022.35	2,579.35
0.25	2,772.69	2,664.22	1,811.18	2,327.55
0.50	2,658.94	2,238.03	1,530.93	2,271.76
1.00	2,444.96	2,001.77	1,493.77	2,129.00
2.80	1,732.52	1,420.39	1,236.35	1,525.93
4.00	1,522.64	1,133.78	751.86	1,154.54
8.00	644.02	349.89	363.21	458.85
24.00	42.71	15.59	17.21	29.69

Tab. 107: Individual concentrations of SKL in plasma of male and female beagle dogs after single intravenous administration of 5 mg/kg SKL.

SKL [ng/mL] in dog plasma after p.o. administration

time [h]	4 (male)	5 (male)	6 (female)	7 (female)
0.00	0.00	0.00	0.00	0.00
0.50	3,071.52	1,676.50	1,075.94	3,996.88
1.00	3,691.45	2,479.43	1,723.04	4,621.24
2.00	4,599.63	3,538.48	4,551.21	6,025.03
4.00	5,256.50	4,968.63	5,098.93	5,851.79
8.00	3,272.95	1,787.01	4,506.20	4,174.52
24.00	151.96	142.77	103.98	296.13

Tab. 108: Individual concentrations of SKL [ng/mL] in dog plasma of male and female Beagle dogs after single oral (p.o.) administration of 50 mg/kg SKL.

SKL [ng/mL] in dog plasma after p.o. administration (capsule)

time [h]	4 (male)	5 (male)	6 (female)	7 (female)
0.00	0.00	0.00	0.00	0.00
0.50	10.83	440.90	157.31	0.00
1.00	5.60	366.19	576.80	696.77
2.00	85.85	1,705.03	1,605.85	713.79
4.00	376.99	3,086.89	2,011.78	707.42
8.00	6,323.07	1,063.09	722.85	444.40
24.00	914.08	44.83	23.98	418.64

Tab. 109: Individual concentrations of SKL [ng/mL] in dog plasma of male and female Beagle dogs after single oral (p.o.) administration of 50 mg/kg SKL per capsule.

Pharmacokinetic Study of Skepinone-L and Sorafenib in Rats:

Part I:

SKL [ng/mL] in rat plasma after 5 mg/kg p.o. administration

time [h]	8	9	10	mean
0.00	0.00	0.00	0.00	0.0
0.25	27.09	84.52	44.45	52.0
0.50	32.01	106.86	105.72	81.5
1.00	79.05	137.80	115.43	110.8
2.00	55.12	149.73	78.17	94.3
4.00	46.69	100.08	41.95	62.9
9.00	199.94	127.40	12.03	113.1
12.00	258.89	71.23	13.11	114.4

Tab. 110: Individual and mean concentrations of SKL [ng/mL] in rat plasma of male Sprague Dawley rats after single oral (p.o.) administration of 5 mg/kg SKL.

SKL [ng/mL] in rat plasma after 15 mg/kg p.o. administration

time [h]	11	12	13	mean
0.00	0.00	0.00	0.00	0.0
0.25	414.61	192.24	145.05	250.6
0.50	603.43	491.92	402.91	499.4
1.00	572.99	650.35	401.41	541.6
2.00	455.78	626.17	281.95	454.6
4.00	439.71	600.40	291.20	443.8
9.00	381.99	378.25	413.68	391.3
12.00	387.37	631.56	502.82	507.3

Tab. 111: Individual and mean concentrations of SKL [ng/mL] in rat plasma of male Sprague Dawley rats after single oral (p.o.) administration of 15 mg/kg SKL.

SKL [ng/mL] in rat plasma after 50 mg/kg p.o. administration

time [h]	14	15	16	mean
0.00	0.00	0.00	0.00	0.0
0.25	272.33	194.48	161.66	209.5
0.50	361.57	424.24	525.91	437.2
1.00	436.10	619.81	1,426.87	827.6
2.00	384.31	605.58	1,330.04	773.3
4.00	485.32	741.96	792.06	673.1
9.00	954.93	1,247.65	N/A	1,101.3
12.00	803.00	787.02	1,147.57	912.5

Tab. 112: Individual and mean concentrations of SKL [ng/mL] in rat plasma of male Sprague Dawley rats after single oral (p.o.) administration of 50 mg/kg SKL. N/A = not available

SKL [ng/mL] in rat plasma after 3 mg/kg i.v. administration

time [h]	17	18	19	mean
0.00	0.00	0.00	0.00	0.0
0.08	5,600.36	4,485.61	1,409.24	3,831.7
0.25	3,659.10	4,585.94	1,332.89	3,192.6
1.00	3,796.61	2,426.53	870.49	2,364.5
2.00	N/A	3,704.03	693.56	2,198.8
4.00	1,021.69	1,341.04	333.82	898.9
9.00	35.85	59.86	41.21	45.6

Tab. 113: Individual and mean concentrations of SKL [ng/mL] in rat plasma of male Sprague Dawley rats after single intravenous (i.v.) administration of 3 mg/kg SKL. N/A = not available

SKL [ng/mL] in rat plasma after 5 mg/kg i.v. administration

time [h]	23	24	25	mean
0.00	0.00	0.00	0.00	0.0
0.08	3,339.73	3,159.27	5,276.31	3,925.1
0.25	2,917.75	3,896.06	3,538.27	3,450.7
1.00	1,764.00	*	*	-/-
2.00	1,135.05			-/-
4.00	682.83			-/-
9.00	94.36			-/-

Tab. 114: Individual and mean concentrations of SKL [ng/mL] in rat plasma of male Sprague Dawley rats after single intravenous (i.v.) administration of 5 mg/kg SKL. N/A = not available; *= rat died

SKL [ng/mL] in rat plasma after 10 mg/kg i.v. administration

time [h]	21	22	mean
0.00	0.00	0.00	0.0
0.08	7,875.79	5,086.33	6,481.1
0.25	5,180.97	4,613.34	4,897.2
1.00	2,434.69	4,003.17	3,218.9
2.00	*	N/A	-/-
4.00		1,346.64	-/-
9.00		215.86	-/-

Tab. 115: Individual and mean concentrations of SKL [ng/mL] in rat plasma of male Sprague Dawley rats after single intravenous (i.v.) administration of 10 mg/kg SKL. N/A = not available; *= rat died

Part II-A:

SKL [ng/mL] in male rat plasma after 15 mg/kg/day

time [h]	32	33	34	mean
0.00	45.83	48.00	47.86	47.2
0.50	1,052.73	346.42	857.44	752.2
1.00	987.88	499.03	1,031.72	839.5
2.00	1,610.97	435.68	965.06	1,003.9
4.00	1,104.19	307.62	1,347.09	919.6
9.00	1,010.83	804.50	1,515.37	1,110.2
12.00	504.41	749.87	751.92	668.7
24.00	128.61	430.00	41.28	200.0

Tab. 116: Individual and mean concentrations of SKL [ng/mL] in rat plasma of male Sprague Dawley rats after repetitive oral administration of 15 mg/kg/day.

SKL [ng/mL] in female rat plasma after 15 mg/kg/day

time [h]	38	39	40	mean
0.00	65.51	485.16	154.27	235.0
0.50	1,467.17	1,412.04	2,065.80	1,648.3
1.00	1,869.64	1,560.75	2,055.83	1,828.7
2.00	2,211.54	1,112.64	1,540.57	1,621.6
4.00	1,470.05	1,105.70	690.56	1,088.8
9.00	1,045.81	1,767.93	787.64	1,200.5
12.00	759.19	906.87	352.19	672.8
24.00	233.68	351.86	1,367.96	651.2

Tab. 117: Individual and mean concentrations of SKL [ng/mL] in rat plasma of female Sprague Dawley rats after repetitive oral administration of 15 mg/kg/day.

SKL [ng/mL] in male rat plasma after 50 mg/kg/day

time [h]	44	45	46	mean
0.00	1,031.89	371.83	669.68	691.1
0.50	1,810.81	1,359.65	1,517.68	1,562.7
1.00	1,709.97	1,566.47	1,613.43	1,630.0
2.00	1,832.24	1,719.26	1,909.12	1,820.2
4.00	1,801.96	1,482.95	1,688.43	1,657.8
9.00	2,117.56	1,732.15	1,948.58	1,932.8
12.00	1,864.55	1,328.11	929.06	1,373.9
24.00	250.25	939.96	583.8	591.3

Tab. 118: Individual and mean concentrations of SKL [ng/mL] in rat plasma of male Sprague Dawley rats after repetitive oral administration of 50 mg/kg/day.

SKL [ng/mL] in female rat plasma after 50 mg/kg/day

time [h]	50	51	52	mean
0.00	1,498.38	513.35	1,263.11	1,091.6
0.50	4,870.64	1,296.63	2,403.67	2,857.0
1.00	5,959.12	1,669.72	3,620.54	3,749.8
2.00	5,678.79	2,903.05	4,095.54	4,225.8
4.00	5,777.06	3,197.00	3,192.25	4,055.4
9.00	4,895.42	5,775.13	3,253.25	4,641.3
12.00	2,248.43	4,987.78	2,952.19	3,396.1
24.00	1,886.95	2,221.73	2,320.90	2,143.2

Tab. 119: Individual and mean concentrations of SKL [ng/mL] in rat plasma of female Sprague Dawley rats after repetitive oral administration of 50 mg/kg/day.

SRF [ng/mL] in male rat plasma after 25 mg/kg/day

time [h]	56	57	58	mean
0.00	12,386.79	11,821.78	10,829.97	11,679.5
0.50	13,498.77	13,168.10	12,723.01	13,130.0
1.00	16,530.31	21,823.85	14,688.41	17,680.9
2.00	17,328.63	29,304.91	20,360.88	22,331.5
4.00	18,440.35	32,998.52	20,802.98	24,080.6
9.00	16,782.41	30,913.07	18,650.58	22,115.4
12.00	15,139.04	16,326.29	24,429.09	18,631.5
24.00	7,742.61	17,548.85	9,848.60	11,713.4

Tab. 120: Individual and mean concentrations of SRF [ng/mL] in rat plasma of male Sprague Dawley rats after repetitive oral administration of 25 mg/kg/day.

SRF [ng/mL] in female rat plasma after 25 mg/kg/day

time [h]	62	63	64	mean
0.00	22,762.68	22,601.64	20,385.71	21,916.7
0.50	22,790.04	28,152.91	21,640.80	24,194.6
1.00	26,999.80	31,278.29	24,685.51	27,654.5
2.00	36,960.41	32,436.67	25,007.84	31,468.3
4.00	35,143.43	33,768.49	25,418.57	31,443.5
9.00	30,690.84	28,014.39	20,432.32	26,379.2
12.00	28,254.43	24,932.58	18,588.43	23,925.1
24.00	21,732.51	22,156.22	16,598.04	20,162.3

Tab. 121: Individual and mean concentrations of SRF [ng/mL] in rat plasma of female Sprague Dawley rats after repetitive oral administration of 25 mg/kg/day.

SRF [ng/mL] in male rat plasma after 25 mg/kg/day

time [h]	26	27	28	mean
0.00	886.26	11,704.63	6,997.06	6,529.3
0.50	2,100.38	13,111.10	7,803.75	7,671.7
1.00	16,260.23	5,297.13	10,541.49	10,699.6
2.00	10,232.21	13,331.24	17,514.40	13,692.6
4.00	16,982.57	10,750.69	12,345.17	13,359.5
9.00	11,350.42	15,238.74	12,020.27	12,869.8
12.00	8,058.97	12,978.55	10,021.60	10,353.0
24.00	5,261.96	7,594.23	7,255.97	6,704.1

Tab. 122: Individual and mean concentrations of SRF [ng/mL] in rat plasma of male Sprague Dawley rats after repetitive oral administration of 25 mg/kg/day SRF.

SRF [ng/mL] in female rat plasma after 25 mg/kg/day

time [h]	29	30	31	mean
0.00	13,032.16	13,438.71	13,431.79	13,300.9
0.50	15,804.54	16,551.10	13,866.76	15,407.5
1.00	22,221.35	16,944.60	19,001.92	19,389.3
2.00	34,715.02	24,946.43	21,438.94	27,033.5
4.00	32,097.03	26,251.51	24,907.89	27,752.1
9.00	24,189.20	17,850.91	18,273.49	20,104.5
12.00	26,831.94	16,253.21	17,739.64	20,274.9
24.00	19,883.08	13,990.19	13,056.73	15,643.3

Tab. 123: Individual and mean concentrations of SRF [ng/mL] in rat plasma of female Sprague Dawley rats after repetitive oral administration of 25 mg/kg/day.

Part II-B:

SKL and SRF [ng/mL] in male rat plasma after 15 mg/kg/day SKL + 25 mg/kg/day SRF

time [h]	35		36		37	
	SKL	SRF	SKL	SRF	SKL	SRF
0.0	180.10	9,148.92	129.18	8,396.49	351.34	6,426.25
0.5	2,443.55	11,612.72	3,638.24	10,364.79	1,864.62	7,090.23
1.0	5,618.53	15,715.09	3,661.19	10,382.76	4,502.03	11,397.17
2.0	6,121.05	17,173.78	4,431.64	14,886.51	4,442.15	11,044.31
4.0	5,745.59	13,933.04	3,283.24	12,262.26	5,676.39	16,171.08
9.0	3,895.83	17,479.23	3,417.16	15,199.42	3,642.76	10,788.92
12.0	2,440.88	16,115.22	1,614.82	8,316.79	1,570.30	11,358.06
24.0	186.99	12,274.57	134.57	7,405.21	66.91	5,510.80

Tab. 124: Individual concentrations of SKL and SRF [ng/mL] in rat plasma of male Sprague Dawley rats after simultaneous repetitive oral administration of 15 mg/kg/day SKL and 25 mg/kg/day SRF.

SKL and SRF [ng/mL] in female rat plasma after 15 mg/kg/day SKL + 25 mg/kg/day SRF

time [h]	41		42		43	
	SKL	SRF	SKL	SRF	SKL	SRF
0.0	440.16	13,554.35	380.26	11,145.17	296.09	18,253.86
0.5	5,219.78	15,091.86	3,365.50	14,241.39	7,354.88	29,133.95
1.0	6,847.58	17,351.79	5,455.91	14,926.46	8,073.10	25,369.52
2.0	5,381.83	19,728.87	5,002.47	19,002.47	6,614.86	29,342.02
4.0	4,993.59	23,298.30	4,254.70	21,458.60	4,874.03	31,095.08
9.0	4,548.13	21,542.28	3,379.78	15,043.91	2,174.54	24,503.20
12.0	3,316.11	19,448.76	3,090.58	14,683.79	2,053.52	22,920.14
24.0	257.39	14,190.77	853.40	11,195.77	1,169.51	17,730.38

Tab. 125: Individual concentrations of SKL and SRF [ng/mL] in rat plasma of female Sprague Dawley rats after simultaneous repetitive oral administration of 15 mg/kg/day SKL and 25 mg/kg/day SRF.

SKL and SRF [ng/mL] in male rat plasma after 50 mg/kg/day SKL + 25 mg/kg/day SRF

time [h]	47		48		49	
	SKL	SRF	SKL	SRF	SKL	SRF
0.0	285.82	6,026.97	333.34	8,305.82	887.16	6,284.95
0.5	4,748.35	7,007.67	11,936.67	11,436.58	8,401.58	8,026.56
1.0	6,458.31	8,514.21	14,450.64	13,862.12	8,961.30	10,138.54
2.0	6,044.54	9,275.84	7,531.36	10,471.59	13,336.14	14,307.76
4.0	5,826.95	7,907.81	12,267.14	17,570.70	6,625.02	12,406.82
9.0	5,699.28	7,247.61	7,294.79	14,579.68	6,405.94	12,099.08
12.0	3,960.15	5,847.96	4,798.54	12,716.46	5,398.97	11,849.57
24.0	2,470.40	5,273.86	1,197.29	9,084.46	265.24	7,283.53

Tab. 126: Individual concentrations of SKL and SRF [ng/mL] in rat plasma of male Sprague Dawley rats after simultaneous repetitive oral administration of 50 mg/kg/day SKL and 25 mg/kg/day SRF.

SKL and SRF [ng/mL] in male rat plasma after 50 mg/kg/day SKL + 25 mg/kg/day SRF

time [h]	59		60		61	
	SKL	SRF	SKL	SRF	SKL	SRF
0.0	2,728.33	5,738.93	1,140.24	6,019.44	729.48	3,228.30
0.5	7,090.22	8,446.41	3,607.89	6,075.33	2,391.85	3,494.26
1.0	2,935.05	3,941.99	5,154.91	6,787.84	8,028.02	10,075.20
2.0	7,621.87	9,824.32	5,748.45	7,660.39	2,915.27	4,636.17
4.0	6,391.46	8,980.24	5,409.99	8,408.54	2,938.15	4,909.92
9.0	5,920.25	10,386.65	4,085.66	8,144.17	2,883.18	4,269.43
12.0	4,570.35	11,559.74	2,997.11	6,678.65	2,739.39	3,306.99
24.0	1,788.02	7,651.14	1,396.70	5,210.81	869.55	2,949.10

Tab. 127: Individual concentrations of SKL and SRF [ng/mL] in rat plasma of male Sprague Dawley rats after simultaneous repetitive oral administration of 50 mg/kg/day SKL and 25 mg/kg/day SRF.

SKL and SRF [ng/mL] in female rat plasma after 50 mg/kg/day SKL + 25 mg/kg/day SRF

time [h]	53		54		55	
	SKL	SRF	SKL	SRF	SKL	SRF
0.0	1,649.20	10,097.23	1,527.49	11,142.05	1,325.23	12,946.31
0.5	12,384.11	12,364.01	10,274.64	12,756.41	3,224.50	11,817.14
1.0	13,067.41	13,419.02	16,647.21	14,710.48	5,827.55	13,096.56
2.0	14,870.98	14,085.89	15,676.16	15,514.36	8,436.06	13,497.67
4.0	12,383.69	16,615.73	14,681.19	15,449.01	10,390.89	15,426.93
9.0	6,982.03	15,437.97	9,376.91	15,956.79	7,525.36	13,635.14
12.0	5,554.57	12,819.92	5,723.33	14,952.17	6,560.57	13,129.42
24.0	2,095.47	11,572.50	2,214.90	14,859.65	1,584.45	8,023.59

Tab. 128: Individual concentrations of SKL and SRF [ng/mL] in rat plasma of female Sprague Dawley rats after simultaneous repetitive oral administration of 50 mg/kg/day SKL and 25 mg/kg/day SRF.

SKL and SRF [ng/mL] in female rat plasma after 50 mg/kg/day SKL + 25 mg/kg/day SRF

time [h]	65		66		67	
	SKL	SRF	SKL	SRF	SKL	SRF
0.0	1000.41	10942.60	2048.92	9497.98	1247.36	12754.02
0.5	8979.83	11675.60	12432.84	11809.94	7494.37	12566.77
1.0	12440.56	12848.69	16749.52	12965.42	10105.14	13754.78
2.0	13292.43	14072.88	17995.80	15230.48	9564.76	14037.57
4.0	12949.33	13809.46	14444.07	15111.08	7173.63	14015.34
9.0	9694.83	13609.27	9806.28	17736.61	6245.28	13469.41
12.0	7029.08	12595.98	6068.66	14996.68	5481.09	12005.05
24.0	3820.11	11012.41	3993.92	12797.28	3147.23	9936.56

Tab. 129: Individual concentrations of SKL and SRF [ng/mL] in rat plasma of female Sprague Dawley rats after simultaneous repetitive oral administration of 50 mg/kg/day SKL and 25 mg/kg/day SRF.

Pharmacokinetic Study of Skepinone-L and Sorafenib in cynomolgus monkeys:**SKL [ng/mL] in monkey plasma after 50 mg/kg p.o. administration**

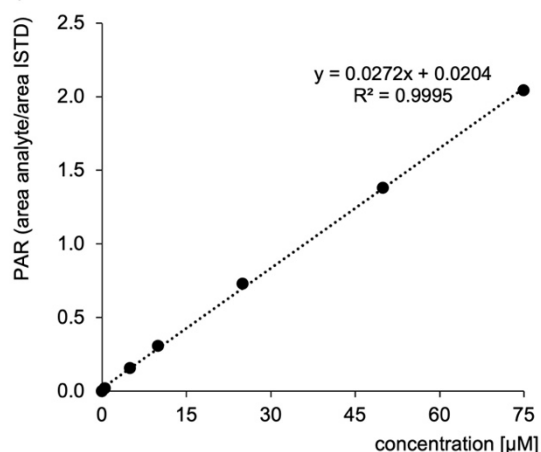
time [h]	68 (male)	69 (male)	70 (female)	71 (female)
0.0	0.00	0.00	0.00	0.00
0.5	703.74	87.19	592.89	156.94
1.0	1,248.71	904.22	744.10	531.36
2.0	1,501.39	1,921.92	723.71	1,285.97
3.0	1,317.67	2,565.36	712.35	1,532.99
4.0	1,076.77	3,671.86	602.86	1,718.27
8.0	657.72	2,399.21	398.62	1,305.07
24.0	87.82	180.63	69.07	916.74

Tab. 130: Individual concentrations of SKL in plasma of male and female cynomolgus monkeys after single oral administration of 50 mg/kg SKL.**SRF [ng/mL] in monkey plasma after 50 mg/kg p.o. administration**

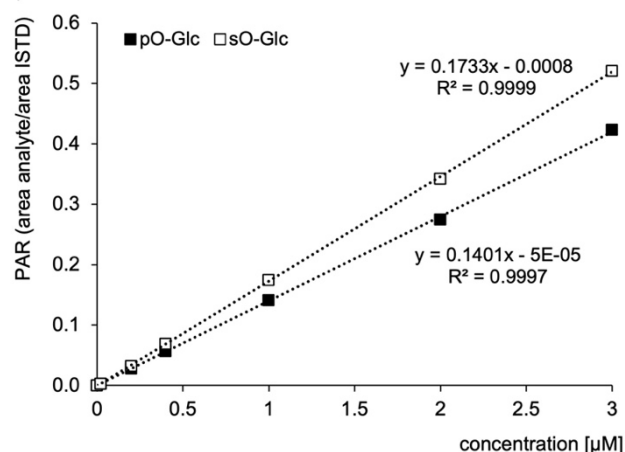
time [h]	68 (male)	69 (male)	70 (female)	71 (female)
0.0	0.00	0.00	0.00	0.00
0.5	58.02	103.79	627.47	130.87
1.0	258.11	456.29	800.18	421.78
2.0	1,005.82	1,334.39	1,759.61	1,181.13
3.0	1,988.19	1,616.72	2,216.93	2,345.80
4.0	2,393.62	2,290.24	2,348.92	3,824.20
8.0	3,246.43	2,866.31	2,080.42	6,347.96
24.0	1,357.74	534.16	412.64	1,108.43

Tab. 131: Individual concentrations of SRF in plasma of male and female cynomolgus monkeys after single oral administration of 50 mg/kg SRF.**7.3. Calibration Lines during Kinetic Analysis of Skepinone-L Glucuronidation**

a) Calibration Line of SKL in HLM



b) Calibration Line of SKL-Glucuronides in HLM

**Fig. 98:** Calibration lines for the determination of SKL (a) and its glucuronides pO-Glc and sO-Glc (b) in human LM to determine V_{max} and K_m .

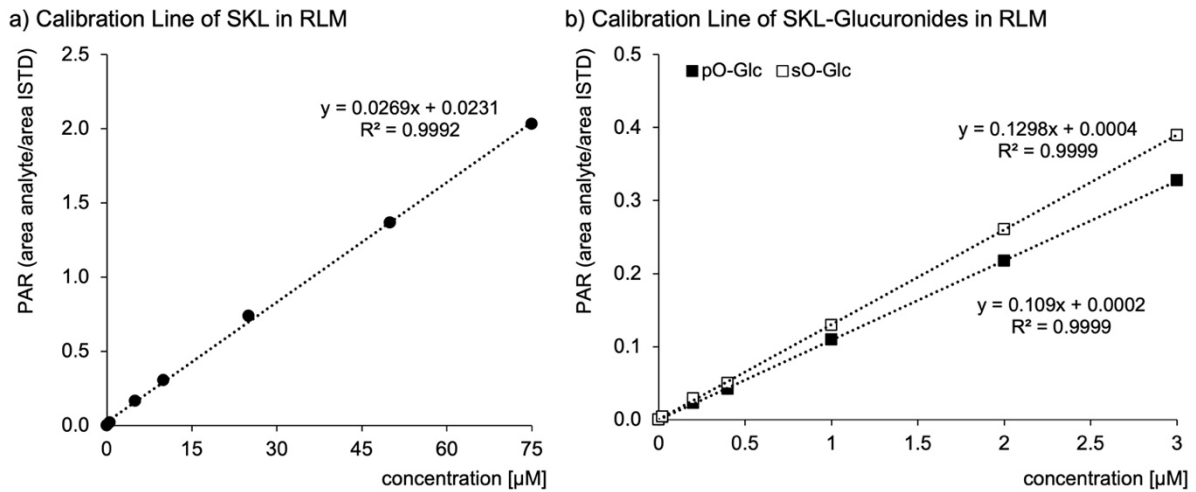


Fig. 99: Calibration lines for the determination of SKL (a) and its glucuronides pO-Glc and sO-Glc (b) in rat LM to determine V_{\max} and K_m .

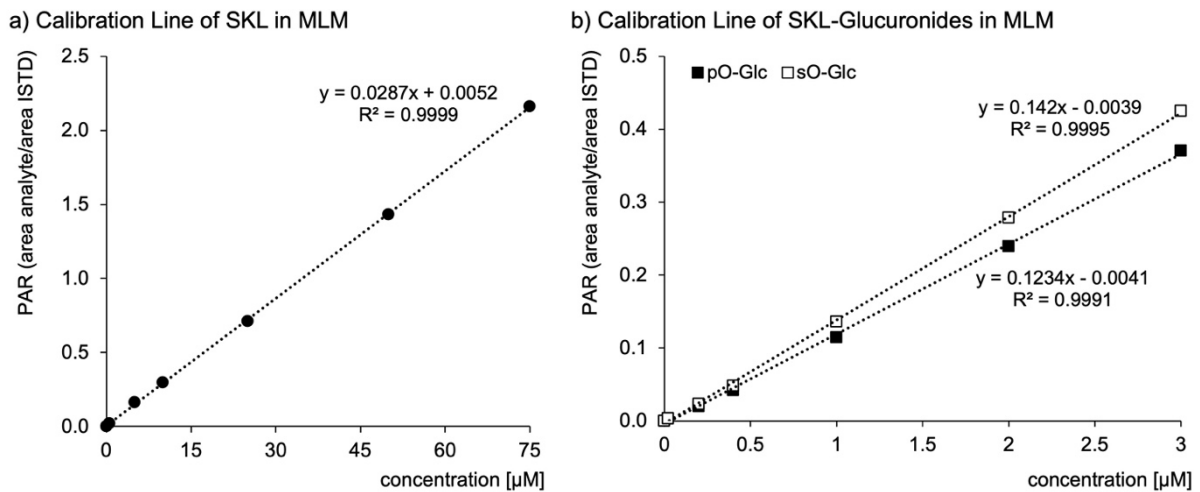


Fig. 100: Calibration lines for the determination of SKL (a) and its glucuronides pO-Glc and sO-Glc (b) in mouse LM to determine V_{\max} and K_m .

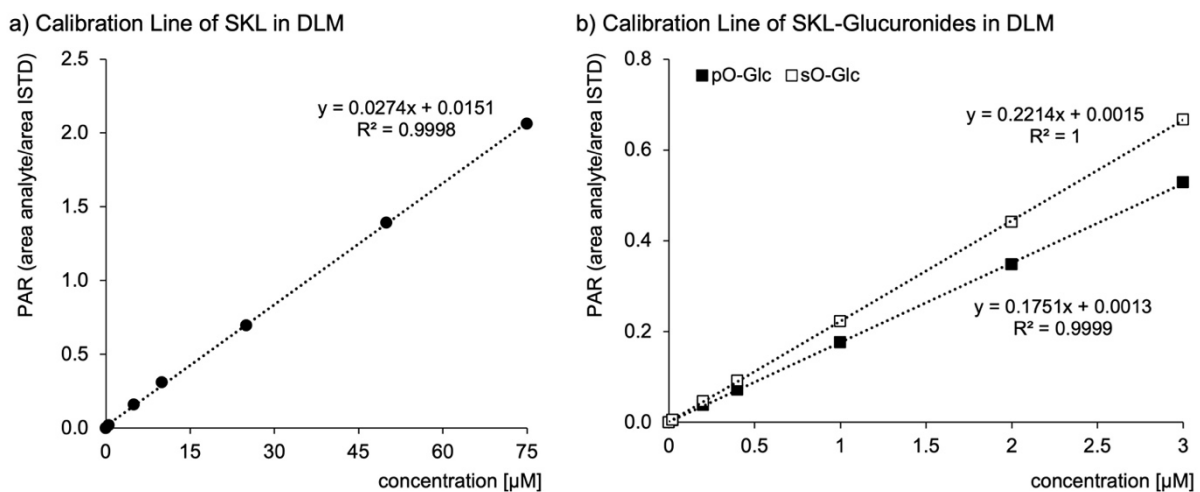


Fig. 101: Calibration lines for the determination of SKL (a) and its glucuronides pO-Glc and sO-Glc (b) in dog LM to determine V_{\max} and K_m .

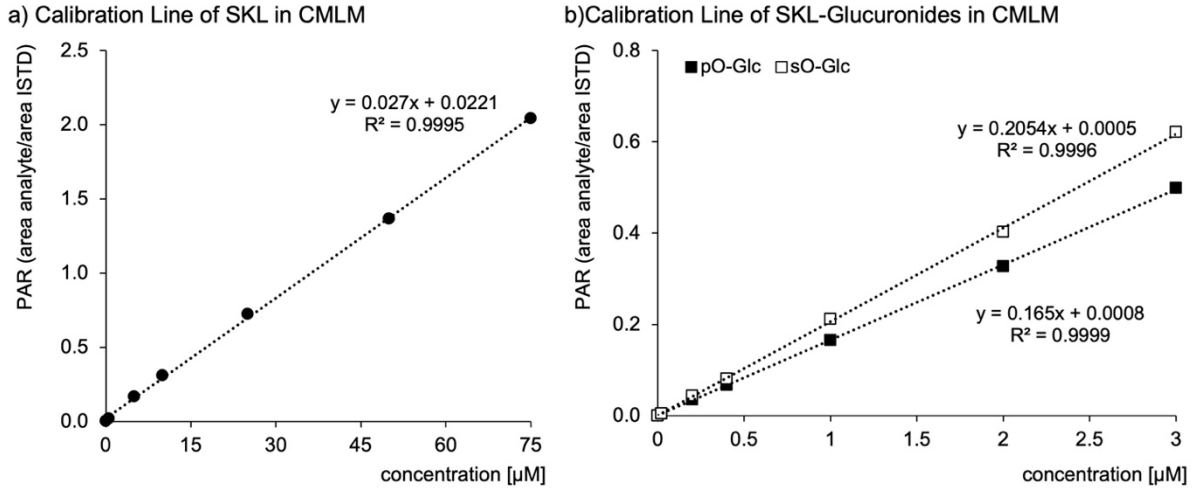


Fig. 102: Calibration lines for the determination of SKL (a) and its glucuronides pO-Glc and sO-Glc (b) in monkey LM to determine V_{max} and K_m .

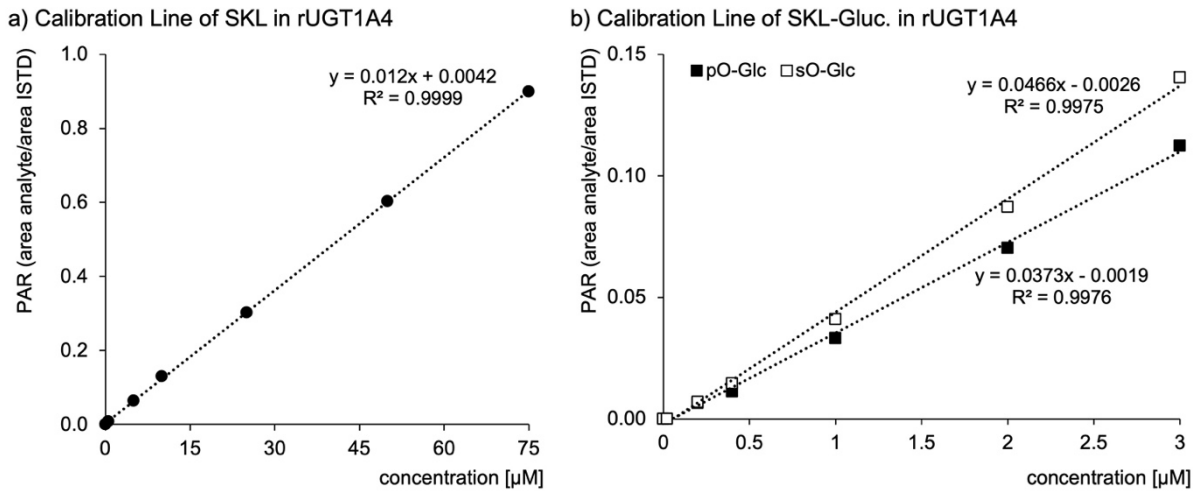


Fig. 103: Calibration lines for the determination of SKL (a) and its glucuronides pO-Glc and sO-Glc (b) in rUGT1A4 to determine V_{max} and K_m .

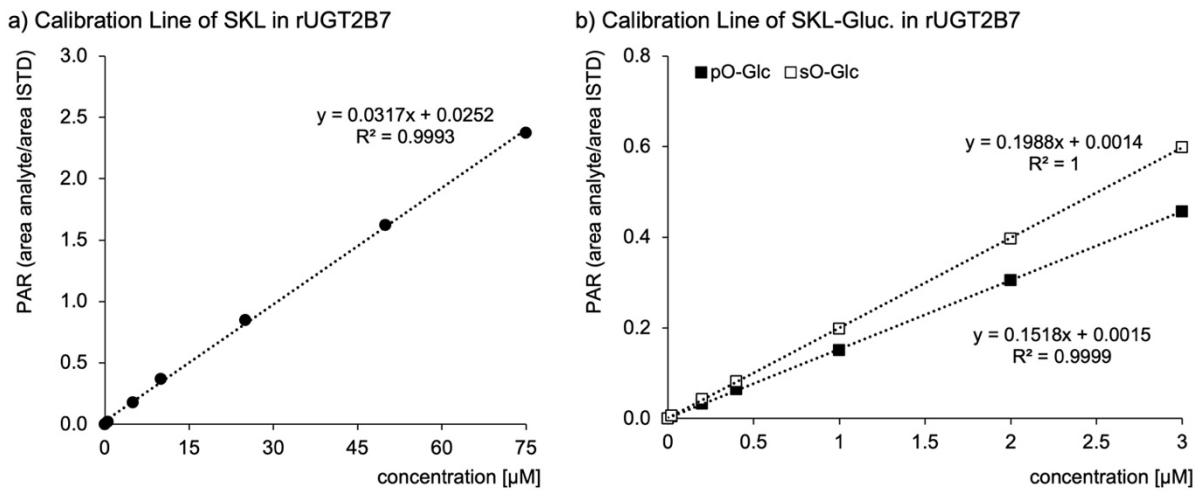


Fig. 104: Calibration lines for the determination of SKL (a) and its glucuronides pO-Glc and sO-Glc (b) in rUGT1A4 to determine V_{max} and K_m .

8. BIBLIOGRAPHY

1. Laufer, S., U. Holzgrabe, and D. Steinhilber, *Drug discovery: a modern decathlon*. *Angew Chem Int Ed Engl*, 2013. **52**(15): p. 4072-6.
2. Mohs, R.C. and N.H. Greig, *Drug discovery and development: Role of basic biological research*. *Alzheimers Dement (N Y)*, 2017. **3**(4): p. 651-657.
3. Prior, H., et al., *Reviewing the Utility of Two Species in General Toxicology Related to Drug Development*. *International Journal of Toxicology*, 2018. **37**(2): p. 121-124.
4. Fischer, T.W. and P. Elsner, *Good Clinical Practice Bedeutung für die klinische Forschung*. *Der Ophthalmologe*, 2002. **99**(1): p. 63-71.
5. Tonkens, R., *An overview of the drug development process*. *Physician Exec*, 2005. **31**(3): p. 48-52.
6. Pillaiyar, T., et al., *A medicinal chemistry perspective of drug repositioning: Recent advances and challenges in drug discovery*. *Eur J Med Chem*, 2020. **195**: p. 112275.
7. DiMasi, J.A., H.G. Grabowski, and R.W. Hansen, *Innovation in the pharmaceutical industry: New estimates of R&D costs*. *J Health Econ*, 2016. **47**: p. 20-33.
8. Hodgson, J., *ADMET--turning chemicals into drugs*. *Nat Biotechnol*, 2001. **19**(8): p. 722-6.
9. Derendorf, H., et al., *Pharmakokinetik Einführung in die Theorie und Relevanz für die Arzneimitteltherapie ; 29 Tabellen. 2., vollst. überarb. und erw. Aufl. ed.* 2002, Stuttgart: Wiss. Verl.-Ges. 336 S.
10. Gibaldi, M. and G. Levy, *Pharmacokinetics in clinical practice. I. Concepts*. *JAMA*, 1976. **235**(17): p. 1864-7.
11. Fan, J. and I.A. de Lannoy, *Pharmacokinetics*. *Biochem Pharmacol*, 2014. **87**(1): p. 93-120.
12. Paalzow, L.K., *Torsten Teorell, the father of pharmacokinetics*. *Ups J Med Sci*, 1995. **100**(1): p. 41-6.

-
13. Bulitta, J.B. and N.H. G. Holford, *Non-Compartmental Analysis*, in *Wiley StatsRef: Statistics Reference Online*.
 14. Yu, R.H. and Y.X. Cao, *A method to determine pharmacokinetic parameters based on andante constant-rate intravenous infusion*. *Sci Rep*, 2017. **7**(1): p. 13279.
 15. Zhang, Y., et al., *PKSolver: An add-in program for pharmacokinetic and pharmacodynamic data analysis in Microsoft Excel*. *Comput Methods Programs Biomed*, 2010. **99**(3): p. 306-14.
 16. Boxenbaum, H.G., S. Riegelman, and R.M. Elashoff, *Statistical estimations in pharmacokinetics*. *J Pharmacokinet Biopharm*, 1974. **2**(2): p. 123-48.
 17. Wagner, J.G., *Do You Need a Pharmacokinetic Model, and, If So, Which One*. *Journal of Pharmacokinetics and Biopharmaceutics*, 1975. **3**(6): p. 457-478.
 18. Grass, G.M. and P.J. Sinko, *Physiologically-based pharmacokinetic simulation modelling*. *Adv Drug Deliv Rev*, 2002. **54**(3): p. 433-51.
 19. Huang, W., S.L. Lee, and L.X. Yu, *Mechanistic approaches to predicting oral drug absorption*. *AAPS J*, 2009. **11**(2): p. 217-24.
 20. Atkinson, A.C., et al., *Optimum experimental designs for properties of a compartmental model*. *Biometrics*, 1993. **49**(2): p. 325-37.
 21. Toutain, P.L. and A. Bousquet-Melou, *Plasma terminal half-life*. *J Vet Pharmacol Ther*, 2004. **27**(6): p. 427-39.
 22. Smith, D.A., et al., *Volume of Distribution in Drug Design*. *J Med Chem*, 2015. **58**(15): p. 5691-8.
 23. Toutain, P.L. and A. Bousquet-Melou, *Plasma clearance*. *J Vet Pharmacol Ther*, 2004. **27**(6): p. 415-25.
 24. Kwan, K.C., *Oral bioavailability and first-pass effects*. *Drug Metab Dispos*, 1997. **25**(12): p. 1329-36.
 25. Lin, J.H. and A.Y. Lu, *Role of pharmacokinetics and metabolism in drug discovery and development*. *Pharmacol Rev*, 1997. **49**(4): p. 403-49.
 26. Toon, S. and M. Rowland, *Structure-pharmacokinetic relationships among the barbiturates in the rat*. *J Pharmacol Exp Ther*, 1983. **225**(3): p. 752-63.
 27. Caldwell, J., I. Gardner, and N. Swales, *An introduction to drug disposition: the basic principles of absorption, distribution, metabolism, and excretion*. *Toxicol Pathol*, 1995. **23**(2): p. 102-14.
 28. Smith, D.A., L. Di, and E.H. Kerns, *The effect of plasma protein binding on in vivo efficacy: misconceptions in drug discovery*. *Nat Rev Drug Discov*, 2010. **9**(12): p. 929-39.
 29. Bohnert, T. and L.S. Gan, *Plasma protein binding: from discovery to development*. *J Pharm Sci*, 2013. **102**(9): p. 2953-94.
 30. Kerns, E., E.H. Kerns, and L. Di, *Drug-like properties concepts, structure design and methods ; from ADME to toxicity optimization ; [metabolism, solubility, pharmacokinetics, permeability, CYP inhibition, toxicity, prodrugs]*. 2008, Amsterdam u.a.: Elsevier, Acad. Press. XIX, 526 S.
 31. Zeitlinger, M.A., et al., *Protein binding: do we ever learn?* *Antimicrob Agents Chemother*, 2011. **55**(7): p. 3067-74.
 32. Meyer, U.A., *Overview of enzymes of drug metabolism*. *J Pharmacokinet Biopharm*, 1996. **24**(5): p. 449-59.
 33. Benedetti, M.S., et al., *Drug metabolism and pharmacokinetics*. *Drug Metab Rev*, 2009. **41**(3): p. 344-90.

34. Zanger, U.M. and M. Schwab, *Cytochrome P450 enzymes in drug metabolism: regulation of gene expression, enzyme activities, and impact of genetic variation*. *Pharmacol Ther*, 2013. **138**(1): p. 103-41.
35. Almazroo, O.A., M.K. Miah, and R. Venkataramanan, *Drug Metabolism in the Liver*. *Clin Liver Dis*, 2017. **21**(1): p. 1-20.
36. Achour, B., J. Barber, and A. Rostami-Hodjegan, *Expression of hepatic drug-metabolizing cytochrome p450 enzymes and their intercorrelations: a meta-analysis*. *Drug Metab Dispos*, 2014. **42**(8): p. 1349-56.
37. Ortiz de Montellano, P.R., *Cytochrome P450 Structure, Mechanism, and Biochemistry*, in *SpringerLink Bücher*. 2005, Springer US: Boston, MA. p. Online-Ressource (XX, 689 p, digital).
38. Guengerich, F.P., *A history of the roles of cytochrome P450 enzymes in the toxicity of drugs*. *Toxicological Research*, 2021. **37**(1): p. 1-23.
39. Manikandan, P. and S. Nagini, *Cytochrome P450 Structure, Function and Clinical Significance: A Review*. *Curr Drug Targets*, 2018. **19**(1): p. 38-54.
40. Gordeziani, M.S., T.G. Varazi, and M.V. Pruidze, *Structural–functional organization of cytochrome P450 containing monooxygenase and some aspects of modeling*. *Annals of Agrarian Science*, 2016. **14**(2): p. 82-94.
41. Dvorak, Z. and P. Pavek, *Regulation of drug-metabolizing cytochrome P450 enzymes by glucocorticoids*. *Drug Metab Rev*, 2010. **42**(4): p. 621-35.
42. Regan, S.L., et al., *Acyl glucuronides: the good, the bad and the ugly*. *Biopharm Drug Dispos*, 2010. **31**(7): p. 367-95.
43. Zhou, X., et al., *Enterohepatic circulation of glucuronide metabolites of drugs in dog*. *Pharmacol Res Perspect*, 2019. **7**(4): p. e00502.
44. De Groot, M.J., D.F.V. Lewis, and S. Modi, *Molecular Modeling and Quantitative Structure–Activity Relationship of Substrates and Inhibitors of Drug Metabolism Enzymes*, in *Comprehensive Medicinal Chemistry II*, J.B. Taylor and D.J. Triggle, Editors. 2007, Elsevier: Oxford. p. 809-825.
45. Testa, B., *Comprehensive medicinal chemistry 5 ADME-tox approaches / vol. ed.: Bernard Testa*. [2. ed. 2007, Amsterdam u.a.: Elsevier. XXIX, 1152 S.
46. Oda, S., et al., *A comprehensive review of UDP-glucuronosyltransferase and esterases for drug development*. *Drug Metab Pharmacokinet*, 2015. **30**(1): p. 30-51.
47. Mackenzie, P.I., et al., *Nomenclature update for the mammalian UDP glycosyltransferase (UGT) gene superfamily*. *Pharmacogenet Genomics*, 2005. **15**(10): p. 677-85.
48. Miners, J.O., P.I. Mackenzie, and K.M. Knights, *The prediction of drug-glucuronidation parameters in humans: UDP-glucuronosyltransferase enzyme-selective substrate and inhibitor probes for reaction phenotyping and in vitro-in vivo extrapolation of drug clearance and drug-drug interaction potential*. *Drug Metab Rev*, 2010. **42**(1): p. 196-208.
49. Yang, N., et al., *UDP-glucuronosyltransferases (UGTs) and their related metabolic cross-talk with internal homeostasis: A systematic review of UGT isoforms for precision medicine*. *Pharmacol Res*, 2017. **121**: p. 169-183.
50. Shargel, L., et al., *Applied biopharmaceutics & pharmacokinetics*. 6th. Ed. ed. 2012, New York u.a.: McGraw-Hill. XVIII, 811 S.
51. Barreto, E.F., T.R. Larson, and E.J. Koubek, *Drug Excretion*, in *Reference Module in Biomedical Sciences*. 2021, Elsevier.
52. Talevi, A. and C.L. Bellera, *Drug Excretion*, in *ADME Processes in Pharmaceutical Sciences: Dosage, Design, and Pharmacotherapy Success*, A.

-
- Talevi and P.A.M. Quiroga, Editors. 2018, Springer International Publishing: Cham. p. 81-96.
53. Cooper, G.M., *The cell a molecular approach*. 2. ed. 2000, Washington, DC u.a.Sunderland, Mass.: ASM Press u.a.Sinauer Associates. XXIV, 689 S.
 54. Michaelis, L., et al., *The original Michaelis constant: translation of the 1913 Michaelis-Menten paper*. Biochemistry, 2011. **50**(39): p. 8264-9.
 55. Punekar, N.S., *ENZYMES: Catalysis, Kinetics and Mechanisms*, in *SpringerLink Bücher*. 2018, Springer Singapore: Singapore. p. Online-Ressource (XXIII, 562 p. 263 illus., 76 illus. in color, online resource).
 56. Lineweaver, H. and D. Burk, *The Determination of Enzyme Dissociation Constants*. Journal of the American Chemical Society, 1934. **56**(3): p. 658-666.
 57. Nelson, D.L., et al., *Lehninger Biochemie mit 131 Tabellen*. 4., vollst. überarb. und erw. Aufl., Übers. der 5. amerikan. Aufl., korr. Nachdr. ed. Springer-Lehrbuch. 2011, Berlin Heidelberg: Springer. XLIII, 1667 S.
 58. Grimm, S.W., et al., *The conduct of in vitro studies to address time-dependent inhibition of drug-metabolizing enzymes: a perspective of the pharmaceutical research and manufacturers of America*. Drug Metab Dispos, 2009. **37**(7): p. 1355-70.
 59. Cooperman, B.S., *Allosteric Regulation*, in *Encyclopedia of Biological Chemistry (Second Edition)*, W.J. Lennarz and M.D. Lane, Editors. 2013, Academic Press: Waltham. p. 71-74.
 60. Tornio, A., et al., *Clinical Studies on Drug-Drug Interactions Involving Metabolism and Transport: Methodology, Pitfalls, and Interpretation*. Clinical pharmacology and therapeutics, 2019. **105**(6): p. 1345-1361.
 61. Dole, M., et al., *Molecular Beams of Macroions*. The Journal of Chemical Physics, 1968. **49**(5): p. 2240-2249.
 62. Dellisanti, C.D., *Electrospray makes molecular elephants fly*. Nature Methods, 2015. **12**(1): p. 15-15.
 63. Kostianen, R., et al., *Liquid chromatography/atmospheric pressure ionization-mass spectrometry in drug metabolism studies*. J Mass Spectrom, 2003. **38**(4): p. 357-72.
 64. Vaidyanathan, S., D.B. Kell, and R. Goodacre, *Selective Detection of Proteins in Mixtures Using Electrospray Ionization Mass Spectrometry: Influence of Instrumental Settings and Implications for Proteomics*. Analytical Chemistry, 2004. **76**(17): p. 5024-5032.
 65. Ho, C.S., et al., *Electrospray ionisation mass spectrometry: principles and clinical applications*. Clin Biochem Rev, 2003. **24**(1): p. 3-12.
 66. Lottspeich, F. and H. Zorbach, *Bioanalytik*. Spektrum Lehrbuch. 1998, Heidelberg Berlin: Spektrum Akad. Verl. XXI, 1035 S.
 67. Waters, *Micromass Quattro micro API Mass Spectrometer Operator's Guide*. 2002.
 68. Sung, H., et al., *Global Cancer Statistics 2020: GLOBOCAN Estimates of Incidence and Mortality Worldwide for 36 Cancers in 185 Countries*. CA: A Cancer Journal for Clinicians, 2021. **71**(3): p. 209-249.
 69. Llovet, J.M., et al., *Hepatocellular carcinoma*. Nature Reviews Disease Primers, 2021. **7**(1): p. 6.
 70. Thun, M.J., et al., *Schottenfeld and Fraumeni cancer epidemiology and prevention*. Fourth edition ed. 2018, New York, NY: Oxford University Press. xix, 1308 Seiten.

71. Helmberger, T., et al., *Lokoregionäre Therapie des HCC*. Der Nuklearmediziner, 2011. **34**(03): p. 157-164.
72. Tian, G., et al., *Comparative efficacy of treatment strategies for hepatocellular carcinoma: systematic review and network meta-analysis*. BMJ Open, 2018. **8**(10): p. e021269.
73. Keating, G.M. and A. Santoro, *Sorafenib: a review of its use in advanced hepatocellular carcinoma*. Drugs, 2009. **69**(2): p. 223-40.
74. Shibuya, M., *Vascular Endothelial Growth Factor (VEGF) and Its Receptor (VEGFR) Signaling in Angiogenesis: A Crucial Target for Anti- and Pro-Angiogenic Therapies*. Genes & cancer, 2011. **2**(12): p. 1097-1105.
75. Choi, W.-M., et al., *Regorafenib Versus Nivolumab After Sorafenib Failure: Real-World Data in Patients With Hepatocellular Carcinoma*. Hepatology Communications, 2020. **4**(7): p. 1073-1086.
76. Llovet, J.M., et al., *Sorafenib in advanced hepatocellular carcinoma*. N Engl J Med, 2008. **359**(4): p. 378-90.
77. Buonaguro, L., *Human Hepatocellular Carcinoma (HCC)*. Cancers (Basel), 2020. **12**(12).
78. Finn, R.S., et al., *Atezolizumab plus Bevacizumab in Unresectable Hepatocellular Carcinoma*. N Engl J Med, 2020. **382**(20): p. 1894-1905.
79. Buljan, M., et al., *Kinase Interaction Network Expands Functional and Disease Roles of Human Kinases*. Molecular Cell, 2020. **79**(3): p. 504-520.e9.
80. Wilson, L.J., et al., *New Perspectives, Opportunities, and Challenges in Exploring the Human Protein Kinome*. Cancer Research, 2018. **78**(1): p. 15.
81. Laufer, S., et al., *New Horizons in Drug Discovery - Understanding and Advancing Kinase Inhibitors*. Journal of Medicinal Chemistry, 2020. **63**(15): p. 7921-7922.
82. Roskoski, R., *Properties of FDA-approved small molecule protein kinase inhibitors: A 2021 update*. Pharmacological Research, 2021. **165**: p. 105463.
83. Edeline, J., et al., *Safety and Efficacy of Sorafenib in Renal Cell Carcinoma*. Cancer Growth and Metastasis, 2012. **5**: p. CGM.S7526.
84. Wilhelm, S.M., et al., *BAY 43-9006 Exhibits Broad Spectrum Oral Antitumor Activity and Targets the RAF/MEK/ERK Pathway and Receptor Tyrosine Kinases Involved in Tumor Progression and Angiogenesis*. Cancer Research, 2004. **64**(19): p. 7099-7109.
85. Zhu, Y.-j., et al., *New knowledge of the mechanisms of sorafenib resistance in liver cancer*. Acta Pharmacologica Sinica, 2017. **38**(5): p. 614-622.
86. Preiß, J. and J. Arends, *Taschenbuch Onkologie interdisziplinäre Empfehlungen zur Therapie 2014/15*. 17. Aufl. ed. 2014, Germering/München: Zuckschwerdt. XIV, 388 S.
87. Shimada, M., et al., *Monitoring Serum Levels of Sorafenib and Its N-Oxide Is Essential for Long-Term Sorafenib Treatment of Patients with Hepatocellular Carcinoma*. Tohoku J Exp Med, 2015. **237**(3): p. 173-82.
88. Tang, W., et al., *The mechanisms of sorafenib resistance in hepatocellular carcinoma: theoretical basis and therapeutic aspects*. Signal Transduct Target Ther, 2020. **5**(1): p. 87.
89. Clark, J.W., et al., *Safety and pharmacokinetics of the dual action Raf kinase and vascular endothelial growth factor receptor inhibitor, BAY 43-9006, in patients with advanced, refractory solid tumors*. Clin Cancer Res, 2005. **11**(15): p. 5472-80.

-
90. La Vine, D.B., et al., *Frequent dose interruptions are required for patients receiving oral kinase inhibitor therapy for advanced renal cell carcinoma*. *Am J Clin Oncol*, 2010. **33**(3): p. 217-20.
 91. Stadler, W.M., et al., *Safety and efficacy results of the advanced renal cell carcinoma sorafenib expanded access program in North America*. *Cancer*, 2010. **116**(5): p. 1272-80.
 92. Ghassabian, S., et al., *Role of human CYP3A4 in the biotransformation of sorafenib to its major oxidized metabolites*. *Biochem Pharmacol*, 2012. **84**(2): p. 215-23.
 93. Gillani, T.B., T. Rawling, and M. Murray, *Cytochrome P450-Mediated Biotransformation of Sorafenib and Its N-Oxide Metabolite: Implications for Cell Viability and Human Toxicity*. *Chem Res Toxicol*, 2015. **28**(1): p. 92-102.
 94. Gong, L., et al., *PharmGKB summary: sorafenib pathways*. *Pharmacogenetics and Genomics*, 2017. **27**(6): p. 240-246.
 95. Swift, B., et al., *Sorafenib Hepatobiliary Disposition: Mechanisms of Hepatic Uptake and Disposition of Generated Metabolites*. *Drug Metabolism and Disposition*, 2013. **41**(6): p. 1179-1186.
 96. Inaba, H., et al., *Phase I pharmacokinetic and pharmacodynamic study of the multikinase inhibitor sorafenib in combination with clofarabine and cytarabine in pediatric relapsed/refractory leukemia*. *J Clin Oncol*, 2011. **29**(24): p. 3293-300.
 97. Inaba, H., et al., *Sorafenib Population Pharmacokinetics and Skin Toxicities in Children and Adolescents with Refractory/Relapsed Leukemia or Solid Tumor Malignancies*. *Clin Cancer Res*, 2019. **25**(24): p. 7320-7330.
 98. Hussaarts, K., et al., *Influence of Probenecid on the Pharmacokinetics and Pharmacodynamics of Sorafenib*. *Pharmaceutics*, 2020. **12**(9).
 99. Boudou-Rouquette, P., et al., *Early sorafenib-induced toxicity is associated with drug exposure and UGT1A9 genetic polymorphism in patients with solid tumors: a preliminary study*. *PLoS One*, 2012. **7**(8): p. e42875.
 100. EMA, *Nexavar. INN-Sorafenib EPAR Scientific Discussion*. 2007. p. 49.
 101. Zhang, W. and H.T. Liu, *MAPK signal pathways in the regulation of cell proliferation in mammalian cells*. *Cell Research*, 2002. **12**(1): p. 9-18.
 102. Cuenda, A. and S. Rousseau, *p38 MAP-kinases pathway regulation, function and role in human diseases*. *Biochim Biophys Acta*, 2007. **1773**(8): p. 1358-75.
 103. Vlahopoulos, S.A., et al., *The role of ATF-2 in oncogenesis*. *Bioessays*, 2008. **30**(4): p. 314-27.
 104. Rudalska, R., et al., *In vivo RNAi screening identifies a mechanism of sorafenib resistance in liver cancer*. *Nat Med*, 2014. **20**(10): p. 1138-46.
 105. Kaminska, B., *MAPK signalling pathways as molecular targets for anti-inflammatory therapy--from molecular mechanisms to therapeutic benefits*. *Biochim Biophys Acta*, 2005. **1754**(1-2): p. 253-62.
 106. Walter, N.M., et al., *Design, Synthesis, and Biological Evaluation of Novel Type I(1)/2 p38alpha MAP Kinase Inhibitors with Excellent Selectivity, High Potency, and Prolonged Target Residence Time by Interfering with the R-Spine*. *J Med Chem*, 2017. **60**(19): p. 8027-8054.
 107. Müller, S., et al., *Donated chemical probes for open science*. *eLife*, 2018. **7**: p. e34311.
 108. Borst, O., et al., *Skepinone-L, a Novel Potent and Highly Selective Inhibitor of p38 MAP Kinase, Effectively Impairs Platelet Activation and Thrombus Formation*. *Cellular Physiology and Biochemistry*, 2013. **31**(6): p. 914-924.

109. Lee, J.K. and N.-J. Kim, *Recent Advances in the Inhibition of p38 MAPK as a Potential Strategy for the Treatment of Alzheimer's Disease*. *Molecules* (Basel, Switzerland), 2017. **22**(8): p. 1287.
110. Guenthoer, P., et al., *Evaluation of the therapeutic potential of the selective p38 MAPK inhibitor Skepinone-L and the dual p38/JNK 3 inhibitor LN 950 in experimental K/BxN serum transfer arthritis*. *Inflammopharmacology*, 2019. **27**(6): p. 1217-1227.
111. Koeberle, S.C., et al., *Skepinone-L is a selective p38 mitogen-activated protein kinase inhibitor*. *Nat Chem Biol*, 2011. **8**(2): p. 141-3.
112. Shimada, M., et al., *A quantitative HPLC-UV method for determination of serum sorafenib and sorafenib N-oxide and its application in hepatocarcinoma patients*. *Tohoku J Exp Med*, 2014. **233**(2): p. 103-12.
113. Gilar, M., A. Jaworski, and T.S. McDonald, *Solvent selectivity and strength in reversed-phase liquid chromatography separation of peptides*. *J Chromatogr A*, 2014. **1337**: p. 140-6.
114. Concha-Herrera, V., et al., *A comparative study of the performance of acetonitrile and methanol in the multi-linear gradient separation of proteic primary amino acids*. *Anal Chim Acta*, 2007. **582**(2): p. 250-8.
115. Yu, D. and X. Liang, *Fragmentation pathways and differentiation of positional isomers of sorafenib and structural analogues by ESI-IT-MS(n) and ESI-Q-TOF-MS/MS coupled with DFT calculations*. *J Mass Spectrom*, 2018. **53**(7): p. 579-589.
116. Services, U.S.D.o.H.a.H., *FDA Guidance for Industry - Bioanalytical Method Validation*. 2001.
117. ICH, *Validation of Analytical Procedures: Text and Methodology Q2 (R1)*, I.C.f.H.o.T.R.f.P.f.H. Use, Editor. 2005.
118. EMA, *Guideline on bioanalytical method validation*, C.f.M.P.f.H.U.C. European Medicines Agency, Editor. 2011. p. 23.
119. Ogawa, L.M. and E.J. Vallender, *Genetic substructure in cynomolgus macaques (*Macaca fascicularis*) on the island of Mauritius*. *BMC Genomics*, 2014. **15**: p. 748.
120. Iwasaki, K. and Y. Uno, *Cynomolgus monkey CYPs: a comparison with human CYPs*. *Xenobiotica*, 2009. **39**(8): p. 578-81.
121. Storch, K., *Untersuchungen zum Metabolismus und Pharmakokinetik neuer p38 α -MAP-Kinase-Inhibitoren [p38 α -Map-Kinase-Inhibitoren]*, in *Medicinal Chemistry*. 2014, Eberhard Karls University Tübingen: Tübingen. p. 189.
122. Sattar, A., et al., *Pharmacokinetics and Metabolism of Cyadox and Its Main Metabolites in Beagle Dogs Following Oral, Intramuscular, and Intravenous Administration*. *Front Pharmacol*, 2016. **7**: p. 236.
123. Khanna, C., et al., *The dog as a cancer model*. *Nature Biotechnology*, 2006. **24**(9): p. 1065-1066.
124. Smith, D.A., *Species differences in metabolism and pharmacokinetics: are we close to an understanding?* *Drug Metab Rev*, 1991. **23**(3-4): p. 355-73.
125. Lin, J.H., *Species similarities and differences in pharmacokinetics*. *Drug Metab Dispos*, 1995. **23**(10): p. 1008-21.
126. Kim, M.T., et al., *Critical evaluation of human oral bioavailability for pharmaceutical drugs by using various cheminformatics approaches*. *Pharm Res*, 2014. **31**(4): p. 1002-14.
127. Dressman, J.B., et al., *Estimating drug solubility in the gastrointestinal tract*. *Adv Drug Deliv Rev*, 2007. **59**(7): p. 591-602.

-
128. Taft, D.R., *Chapter 9 - Drug Excretion*, in *Pharmacology*, M. Hacker, W. Messer, and K. Bachmann, Editors. 2009, Academic Press: San Diego. p. 175-199.
 129. Karbownik, A., et al., *Pharmacokinetic Interaction between Sorafenib and Atorvastatin, and Sorafenib and Metformin in Rats*. *Pharmaceutics*, 2020. **12**(7).
 130. Jain, L., et al., *Population pharmacokinetic analysis of sorafenib in patients with solid tumours*. *Br J Clin Pharmacol*, 2011. **72**(2): p. 294-305.
 131. Takeda, H., et al., *Clinical features associated with radiological response to sorafenib in unresectable hepatocellular carcinoma: a large multicenter study in Japan*. *Liver Int*, 2015. **35**(5): p. 1581-9.
 132. Yamazoe, Y., et al., *A sex-specific form of cytochrome P-450 catalyzing propoxycoumarin O-depropylation and its identity with testosterone 6 beta-hydroxylase in untreated rat livers: reconstitution of the activity with microsomal lipids*. *J Biochem*, 1988. **104**(5): p. 785-90.
 133. Robertson, G.R., G.C. Farrell, and C. Liddle, *Sexually dimorphic expression of rat CYP3A9 and CYP3A18 genes is regulated by growth hormone*. *Biochem Biophys Res Commun*, 1998. **242**(1): p. 57-60.
 134. Tanaka, E., *Gender-related differences in pharmacokinetics and their clinical significance*. *J Clin Pharm Ther*, 1999. **24**(5): p. 339-46.
 135. Ma, B.L., et al., *Polyethylene glycol 400 (PEG400) affects the systemic exposure of oral drugs based on multiple mechanisms: taking berberine as an example*. *Rsc Advances*, 2017. **7**(5): p. 2435-2442.
 136. Shortt, J., et al., *The drug vehicle and solvent N-methylpyrrolidone is an immunomodulator and antimyeloma compound*. *Cell Rep*, 2014. **7**(4): p. 1009-19.
 137. Tompkins, L., et al., *Effects of Commonly Used Excipients on the Expression of CYP3A4 in Colon and Liver Cells*. *Pharmaceutical Research*, 2010. **27**(8): p. 1703-1712.
 138. Davies, N.M., et al., *Multiple peaking phenomena in pharmacokinetic disposition*. *Clin Pharmacokinet*, 2010. **49**(6): p. 351-77.
 139. Roberts, M.S., et al., *Enterohepatic circulation: physiological, pharmacokinetic and clinical implications*. *Clin Pharmacokinet*, 2002. **41**(10): p. 751-90.
 140. Kim, T.H., et al., *Population Pharmacokinetic Modeling of the Enterohepatic Recirculation of Fimasartan in Rats, Dogs, and Humans*. *AAPS J*, 2015. **17**(5): p. 1210-23.
 141. Ascenzi, P., et al., *Clinical relevance of drug binding to plasma proteins*. *Journal of Molecular Structure*, 2014. **1077**: p. 4-13.
 142. Tod, M., et al., *Functional and Clinical Evidence of the Influence of Sorafenib Binding to Albumin on Sorafenib Disposition in Adult Cancer Patients*. *Pharmaceutical Research*, 2011. **28**(12): p. 3199-3207.
 143. Wentsch, H.K., et al., *Optimized Target Residence Time: Type I1/2 Inhibitors for p38alpha MAP Kinase with Improved Binding Kinetics through Direct Interaction with the R-Spine*. *Angew Chem Int Ed Engl*, 2017. **56**(19): p. 5363-5367.
 144. Bossoni, G., et al., *Influence of species specificity on gastric emptying rate and blood levels of carisoprodol*. *Pharmacol Res Commun*, 1979. **11**(8): p. 693-702.
 145. McMaster, P.D., *Do Species Lacking a Gall Bladder Possess Its Functional Equivalent?* *J Exp Med*, 1922. **35**(2): p. 127-40.

146. Gardiner, P., R.J. Cox, and K. Grime, *Plasma Protein Binding as an Optimizable Parameter for Acidic Drugs*. Drug Metab Dispos, 2019. **47**(8): p. 865-873.
147. Ghassabian, S., et al., *Sorafenib N-Oxide Is an Inhibitor of Human Hepatic CYP3A4*. AAPS J, 2019. **21**(2): p. 15.
148. Berry, L.M., C. Li, and Z. Zhao, *Species differences in distribution and prediction of human V(ss) from preclinical data*. Drug Metab Dispos, 2011. **39**(11): p. 2103-16.
149. Curran, R.E., et al., *Control and measurement of plasma pH in equilibrium dialysis: influence on drug plasma protein binding*. Drug Metab Dispos, 2011. **39**(3): p. 551-7.
150. Scheife, R.T., *Protein binding: what does it mean?* DICP, 1989. **23**(7-8 Suppl): p. S27-31.
151. Villarroel, M.C., et al., *Plasma protein binding of sorafenib, a multi kinase inhibitor: in vitro and in cancer patients*. Invest New Drugs, 2012. **30**(6): p. 2096-102.
152. Yan, Z. and G. Caldwell, *Optimization in drug discovery : in vitro methods*. Methods in pharmacology and toxicology. 2004, Totowa, N.J.: Humana Press. xv, 418 p.
153. Fasinu, P., P.J. Bouic, and B. Rosenkranz, *Liver-based in vitro technologies for drug biotransformation studies - a review*. Curr Drug Metab, 2012. **13**(2): p. 215-24.
154. Baranczewski, P., et al., *Introduction to in vitro estimation of metabolic stability and drug interactions of new chemical entities in drug discovery and development*. Pharmacol Rep, 2006. **58**(4): p. 453-72.
155. Baur, B., et al., *Metabolically stable dibenzo[b,e]oxepin-11(6H)-ones as highly selective p38 MAP kinase inhibitors: optimizing anti-cytokine activity in human whole blood*. J Med Chem, 2013. **56**(21): p. 8561-78.
156. Zuber, R., E. Anzenbacherova, and P. Anzenbacher, *Cytochromes P450 and experimental models of drug metabolism*. J Cell Mol Med, 2002. **6**(2): p. 189-98.
157. Martignoni, M., G.M. Groothuis, and R. de Kanter, *Species differences between mouse, rat, dog, monkey and human CYP-mediated drug metabolism, inhibition and induction*. Expert Opin Drug Metab Toxicol, 2006. **2**(6): p. 875-94.
158. Komori, M., et al., *Molecular cloning of monkey liver cytochrome P-450 cDNAs: similarity of the primary sequences to human cytochromes P-450*. Biochim Biophys Acta, 1992. **1171**(2): p. 141-6.
159. Dear, G.J., et al., *Urinary metabolites of a novel quinoxaline non-nucleoside reverse transcriptase inhibitor in rabbit, mouse and human: identification of fluorine NIH shift metabolites using NMR and tandem MS*. Xenobiotica, 2000. **30**(4): p. 407-26.
160. Kobayashi, K., et al., *Substrate specificity for rat cytochrome P450 (CYP) isoforms: screening with cDNA-expressed systems of the rat*. Biochem Pharmacol, 2002. **63**(5): p. 889-96.
161. Hammer, H., et al., *Cross-species analysis of hepatic cytochrome P450 and transport protein expression*. Arch Toxicol, 2021. **95**(1): p. 117-133.
162. Okey, A.B., et al., *Induction of drug-metabolizing enzymes: mechanisms and consequences*. Clin Biochem, 1986. **19**(2): p. 132-41.

-
163. Mahfoudh, A.M., et al., *In vitro ex vivo assessment of Morinda citrifolia on drug metabolizing enzymes in spontaneously hypertensive rats*. *Pharmaceutical Biology*, 2009. **47**(12): p. 1108-1116.
 164. Soars, M.G., et al., *An assessment of udp-glucuronosyltransferase induction using primary human hepatocytes*. *Drug Metab Dispos*, 2004. **32**(1): p. 140-8.
 165. Monod, J., J. Wyman, and J.P. Changeux, *On the Nature of Allosteric Transitions: A Plausible Model*. *J Mol Biol*, 1965. **12**: p. 88-118.
 166. Waxman, D.J. and M.G. Holloway, *Sex differences in the expression of hepatic drug metabolizing enzymes*. *Mol Pharmacol*, 2009. **76**(2): p. 215-28.
 167. Shapiro, B.H., A.K. Agrawal, and N.A. Pampori, *Gender differences in drug metabolism regulated by growth hormone*. *Int J Biochem Cell Biol*, 1995. **27**(1): p. 9-20.
 168. Fisher, M.B., et al., *In vitro glucuronidation using human liver microsomes and the pore-forming peptide alamethicin*. *Drug Metabolism and Disposition*, 2000. **28**(5): p. 560-566.
 169. Heo, Y.A. and Y.Y. Syed, *Regorafenib: A Review in Hepatocellular Carcinoma*. *Drugs*, 2018. **78**(9): p. 951-958.
 170. Liu, S., et al., *Preclinical comparison of regorafenib and sorafenib efficacy for hepatocellular carcinoma using multimodality molecular imaging*. *Cancer Lett*, 2019. **453**: p. 74-83.
 171. Benoit-Biancamano, M.O., et al., *A pharmacogenetics study of the human glucuronosyltransferase UGT1A4*. *Pharmacogenet Genomics*, 2009. **19**(12): p. 945-54.
 172. Saber-Mahloogi, H., *Nexavar Pharmacology/Toxicology Review and Evaluation*. 2005, Food and Drug Administration - Center for Drug Evaluation and Research.
 173. Lathia, C., et al., *Lack of effect of ketoconazole-mediated CYP3A inhibition on sorafenib clinical pharmacokinetics*. *Cancer Chemother Pharmacol*, 2006. **57**(5): p. 685-92.
 174. Peer, C.J., et al., *Sorafenib is an inhibitor of UGT1A1 but is metabolized by UGT1A9: implications of genetic variants on pharmacokinetics and hyperbilirubinemia*. *Clin Cancer Res*, 2012. **18**(7): p. 2099-107.
 175. Buckley, D.B. and C.D. Klaassen, *Tissue- and gender-specific mRNA expression of UDP-glucuronosyltransferases (UGTs) in mice*. *Drug Metab Dispos*, 2007. **35**(1): p. 121-7.
 176. Shiratani, H., et al., *Species differences in UDP-glucuronosyltransferase activities in mice and rats*. *Drug Metab Dispos*, 2008. **36**(9): p. 1745-52.
 177. Yamamoto, K., et al., *Functional characterization of cynomolgus monkey UDP-glucuronosyltransferase 1A9*. *Eur J Drug Metab Pharmacokinet*, 2014. **39**(3): p. 195-202.
 178. Kilpatrick, G.J. and T.W. Smith, *Morphine-6-glucuronide: actions and mechanisms*. *Med Res Rev*, 2005. **25**(5): p. 521-44.
 179. Goettert, M., R. Graeser, and S.A. Laufer, *Optimization of a nonradioactive immunosorbent assay for p38alpha mitogen-activated protein kinase activity*. *Anal Biochem*, 2010. **406**(2): p. 233-4.
 180. Fura, A., *Role of pharmacologically active metabolites in drug discovery and development*. *Drug Discov Today*, 2006. **11**(3-4): p. 133-42.
 181. Miners, J.O., R.A. McKinnon, and P.I. Mackenzie, *Genetic polymorphisms of UDP-glucuronosyltransferases and their functional significance*. *Toxicology*, 2002. **181-182**: p. 453-6.

182. Guillemette, C., *Pharmacogenomics of human UDP-glucuronosyltransferase enzymes*. *Pharmacogenomics J*, 2003. **3**(3): p. 136-58.
183. Sawyer, M.B., et al., *A Uridine Glucuronosyltransferase 2B7 Polymorphism Predicts Epirubicin Clearance and Outcomes in Early-Stage Breast Cancer*. *Clin Breast Cancer*, 2016. **16**(2): p. 139-44 e1-3.
184. Xie, X.C., et al., *Associations of UDP-glucuronosyltransferases polymorphisms with mycophenolate mofetil pharmacokinetics in Chinese renal transplant patients*. *Acta Pharmacol Sin*, 2015. **36**(5): p. 644-50.
185. Stelzer, G., et al., *The GeneCards Suite: From Gene Data Mining to Disease Genome Sequence Analyses*. *Curr Protoc Bioinformatics*, 2016. **54**: p. 1 30 1-1 30 33.
186. Strassburg, C.P., et al., *Polymorphic expression of the UDP-glucuronosyltransferase UGT1A gene locus in human gastric epithelium*. *Mol Pharmacol*, 1998. **54**(4): p. 647-54.
187. Strassburg, C.P., et al., *Polymorphic gene regulation and interindividual variation of UDP-glucuronosyltransferase activity in human small intestine*. *J Biol Chem*, 2000. **275**(46): p. 36164-71.
188. Barbarino, J.M., et al., *PharmGKB summary: very important pharmacogene information for UGT1A1*. *Pharmacogenet Genomics*, 2014. **24**(3): p. 177-83.
189. Gall, W.E., et al., *Differential glucuronidation of bile acids, androgens and estrogens by human UGT1A3 and 2B7*. *J Steroid Biochem Mol Biol*, 1999. **70**(1-3): p. 101-8.
190. Kasteel, E.E.J., et al., *Human variability in isoform-specific UDP-glucuronosyltransferases: markers of acute and chronic exposure, polymorphisms and uncertainty factors*. *Arch Toxicol*, 2020. **94**(8): p. 2637-2661.
191. Caillier, B., et al., *A pharmacogenomics study of the human estrogen glucuronosyltransferase UGT1A3*. *Pharmacogenet Genomics*, 2007. **17**(7): p. 481-95.
192. Fujiwara, R., E. Yoda, and R.H. Tukey, *Species differences in drug glucuronidation: Humanized UDP-glucuronosyltransferase 1 mice and their application for predicting drug glucuronidation and drug-induced toxicity in humans*. *Drug Metab Pharmacokinet*, 2018. **33**(1): p. 9-16.
193. Williams, J.A., et al., *Drug-drug interactions for UDP-glucuronosyltransferase substrates: a pharmacokinetic explanation for typically observed low exposure (AUC_i/AUC) ratios*. *Drug Metab Dispos*, 2004. **32**(11): p. 1201-8.
194. Zhou, J., T.S. Tracy, and R.P. Remmel, *Glucuronidation of dihydrotestosterone and trans-androsterone by recombinant UDP-glucuronosyltransferase (UGT) 1A4: evidence for multiple UGT1A4 aglycone binding sites*. *Drug Metab Dispos*, 2010. **38**(3): p. 431-40.
195. Tukey, R.H. and C.P. Strassburg, *Human UDP-glucuronosyltransferases: metabolism, expression, and disease*. *Annu Rev Pharmacol Toxicol*, 2000. **40**: p. 581-616.
196. Jiang, L., et al., *Identifying and applying a highly selective probe to simultaneously determine the O-glucuronidation activity of human UGT1A3 and UGT1A4*. *Sci Rep*, 2015. **5**: p. 9627.
197. Lan, B., et al., *The Effect of Polymorphism in UGT1A4 on Clinical Outcomes of Adjuvant Tamoxifen Therapy for Patients With Breast Cancer in China*. *Clin Breast Cancer*, 2019. **19**(2): p. e370-e375.

-
198. Hu, D.G., et al., *Induction of human UDP-Glucuronosyltransferase 2B7 gene expression by cytotoxic anticancer drugs in liver cancer HepG2 cells*. Drug Metab Dispos, 2015. **43**(5): p. 660-8.
 199. Edavana, V.K., et al., *Fulvestrant up regulates UGT1A4 and MRPs through ERalpha and c-Myb pathways: a possible primary drug disposition mechanism*. Springerplus, 2013. **2**: p. 620.
 200. Lu, L., et al., *Drug-Metabolizing Activity, Protein and Gene Expression of UDP-Glucuronosyltransferases Are Significantly Altered in Hepatocellular Carcinoma Patients*. PLoS One, 2015. **10**(5): p. e0127524.
 201. Lv, X., et al., *Chemical Probes for Human UDP-Glucuronosyltransferases: A Comprehensive Review*. Biotechnol J, 2019. **14**(1): p. e1800002.
 202. Donato, M.T., et al., *Validated assay for studying activity profiles of human liver UGTs after drug exposure: inhibition and induction studies*. Anal Bioanal Chem, 2010. **396**(6): p. 2251-63.
 203. Miners, J.O., et al., *Inhibition of human UDP-glucuronosyltransferase enzymes by lapatinib, pazopanib, regorafenib and sorafenib: Implications for hyperbilirubinemia*. Biochem Pharmacol, 2017. **129**: p. 85-95.
 204. Karbownik, A., et al., *In vivo assessment of potential for UGT-inhibition-based drug-drug interaction between sorafenib and tapentadol*. Biomed Pharmacother, 2020. **130**: p. 110530.
 205. Giampa, M. and E. Sgobba, *Insight to Functional Conformation and Noncovalent Interactions of Protein-Protein Assembly Using MALDI Mass Spectrometry*. Molecules, 2020. **25**(21).
 206. Guo, J. and H.X. Zhou, *Protein Allosterity and Conformational Dynamics*. Chem Rev, 2016. **116**(11): p. 6503-15.
 207. Wu, B., et al., *First-pass metabolism via UDP-glucuronosyltransferase: a barrier to oral bioavailability of phenolics*. J Pharm Sci, 2011. **100**(9): p. 3655-81.
 208. Gao, L., et al., *An investigation of the metabolic activity, isozyme contribution, species differences and potential drug-drug interactions of PI-103, and the identification of efflux transporters for PI-103-O-glucuronide in HeLa1A9 cells*. RSC Advances, 2020. **10**(16): p. 9610-9622.
 209. Einav, T., L. Mazutis, and R. Phillips, *Statistical Mechanics of Allosteric Enzymes*. J Phys Chem B, 2016. **120**(26): p. 6021-37.
 210. Garza, A.Z., S.B. Park, and R. Kocz, *Drug Elimination*, in *StatPearls*. 2021: Treasure Island (FL).
 211. Ghibellini, G., E.M. Leslie, and K.L. Brouwer, *Methods to evaluate biliary excretion of drugs in humans: an updated review*. Mol Pharm, 2006. **3**(3): p. 198-211.
 212. Huang Foen Chung, J.W. and R. van Mastrigt, *Age and volume dependent normal frequency volume charts for healthy males*. J Urol, 2009. **182**(1): p. 210-4.
 213. Raab, W., *[Diagnostic value of the determination of urinary enzyme activities]*. Z Klin Chem Klin Biochem, 1971. **9**(2): p. 143-54.
 214. Ye, L., et al., *Sorafenib metabolism is significantly altered in the liver tumor tissue of hepatocellular carcinoma patient*. PLoS One, 2014. **9**(5): p. e96664.
 215. Zenser, T.V., V.M. Lakshmi, and B.B. Davis, *Human and Escherichia coli beta-glucuronidase hydrolysis of glucuronide conjugates of benzidine and 4-aminobiphenyl, and their hydroxy metabolites*. Drug Metab Dispos, 1999. **27**(9): p. 1064-7.

216. Ambrosius, W.T., *Topics in biostatistics*. Methods in molecular biology,. 2007, Totowa, N.J.: Humana Press. xii, 528 p.
217. Ratain MJ, P.W.J., *Principles of Pharmacokinetics*, in *Cancer Medicine*. 6th edition, M. Donald W Kufe, Raphael E Pollock, MD, PhD, Ralph R Weichselbaum, MD, Robert C Bast, Jr, MD, Ted S Gansler, MD, MBA, James F Holland, MD, ScD (hc), and Emil Frei, III, MD., Editor. 2003, BC Decker.
218. Rowland, M., Tozer, Thomas, *Clinical pharmacokinetics and pharmacodynamics : concepts and applications*. 4th ed. ed. 2010, United States: Philadelphia : Wolters Kluwer Health/Lippincott William & Wilkins, c2011.
219. Ludden, T.M., S.L. Beal, and L.B. Sheiner, *Comparison of the Akaike Information Criterion, the Schwarz criterion and the F test as guides to model selection*. J Pharmacokinet Biopharm, 1994. **22**(5): p. 431-45.
220. Argikar, U.A., *Saccharolactone: The History, the Myth, and the Practice*. Curr Drug Metab, 2018. **19**(4): p. 304-309.
221. Rowland, A., et al., *The "albumin effect" and drug glucuronidation: bovine serum albumin and fatty acid-free human serum albumin enhance the glucuronidation of UDP-glucuronosyltransferase (UGT) 1A9 substrates but not UGT1A1 and UGT1A6 activities*. Drug Metab Dispos, 2008. **36**(6): p. 1056-62.
222. Peng, Y., et al., *Atypical Kinetics and Albumin Effect of Glucuronidation of 5-n-Butyl-4-{4-[2-(1H-tetrazole-5-yl)-1H-pyrrol-1-yl]phenylmethyl}-2,4-dihydro-2-(2,6-dichlorophenyl)-3H-1,2,4-triazol-3-one, a Novel Nonpeptide Angiotensin Type 1 Receptor Antagonist, in Liver Microsomes and UDP-Glucuronosyltransferase*. Molecules, 2018. **23**(3).
223. Yuan, L., X. Sophia Xu, and Q.C. Ji, *Challenges and recommendations in developing LC-MS/MS bioanalytical assays of labile glucuronides and parent compounds in the presence of glucuronide metabolites*. Bioanalysis, 2020. **12**(9): p. 615-624.